Small Molecule Inhibition of Lipidated Proteins/Cargo Interaction

and

Synthesis of a Cinchona Alkaloid-derived Library as potent Autophagy Inhibitors

Dissertation

zur Erlangung des akademischen Grades eines

Doktors der Naturwissenschaften

(Dr. rer. nat.)

der Fakultät für Chemie und Chemische Biologie

der Technischen Universität Dortmund

vorgelegt von

M. Sc. Guillaume Garivet

Geboren am 16.07.1988

in Mont-de-Marsan, France

Dortmund 2017

Die vorliegende Arbeit entstand im Zeitraum von Oktober 2013 bis Dezember 2017 unter der Anleitung von Prof. Dr. Dr. h.c. Herbert Waldmann an der Fakultät für Chemie und Chemische Biologie der Technischen Universität Dortmund und dem Max-Planck-Institut für molekulare Physiologie Dortmund.

1. Gutachter: Prof. Dr. Dr. h.c. Herbert Waldmann

2. Gutachter: Prof. em. Dr. Alfred Wittinghofer

Teile dieser Arbeit wurden bereits in folgenden Beiträgen veröffentlicht:

Erwin N., Sperlich B., Garivet G., Waldmann H., Weise K., Winter R.* "Lipoprotein insertion into membranes of various complexity: lipid sorting, interfacial adsorption and protein clustering" *Phys. Chem. Chem. Phys.*, **2016**, *18*, 8954-8962

Mejuch T., Garivet G., Hofer W., Kaiser N., Fansa E.K., Ehrt C., Koch O., Baumann M., Ziegler S., Wittinghofer A., Waldmann H.* " Small Molecule Inhibition of the UNC119a/b-Cargo Interaction" *Angew. Chem. Int. Ed.,* **2017**, *56*, 6181 –6186

Dédiée à Monsieur Michel Garivet et

Madame Danièle Garivet.

ACKNOWLEDGEMENTS

TABLE OF CONTENTS

ABSTRACT

Src family tyrosine kinases are involved in cancer pathologies when misregulated. Interference with the signaling activity of the N-myristoylated nonreceptor protein tyrosine kinase Src is considered a viable approach in anti-cancer drug discovery. UNC119, a lipid binding protein able to accommodate myristoylated protein, has shown to be required for inducing the kinase activity of some Src family kinases.

Herein, a potent and specific inhibitor of the UNC119-Src interaction with a novel chemotype was identified using a Homogeneous Time Resolved Fluorescence screening. The selectivity of the compound was validated using a fluorescence polarization and cellular thermal shift assays. The structure-activity relationship for this compound class was based on a synthesized and purchased compound collection. Further investigations revealed binding of the selected compound to UNC119A and UNC119B in cells.

HTRF screening

Hit identification

IC_{50} = 109 ± 44 nM

Structure-activity relationship

I
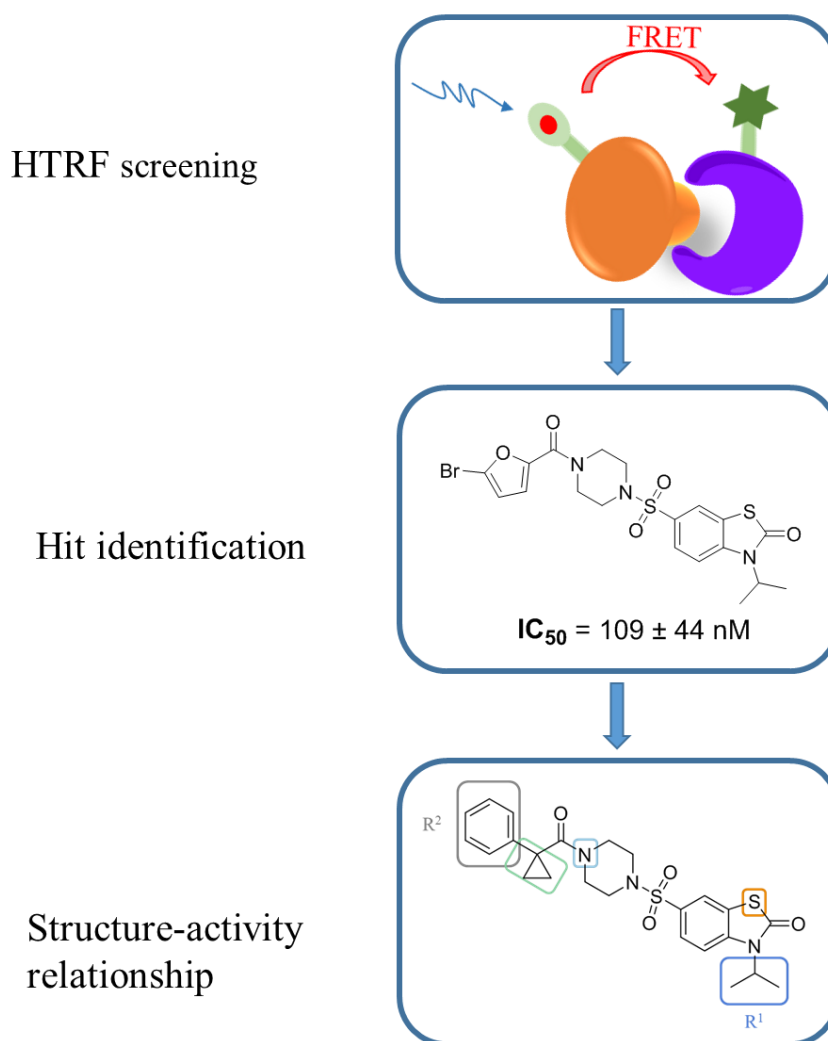
The compound induces reduction of activating Src-autophosphorylation on Y419, an important residue for the kinase activity. A decrease of 40% of the phosphorylation level on Y419 was measured using an In-cell western assay and showed the impact of the compound on the kinase activity. UNC119 inhibition in Src-dependent colorectal cancer (CRC) cells results in the specific reduction of cell growth and clonogenic potential. Using microscopy techniques, the disruption of the interaction was characterized in an in-vivo environment (by means of a fluorescence lifetime imaging microscopy of Förster resonance energy transfer experiment). These results demonstrate that small molecule interference with the dynamics of the Src spatial cycle may open up a novel opportunity to interfere with oncogenic Src-signaling.

Cinchona alkaloids are a privileged class of natural products used for the treatment of malaria as well as in organic chemistry for catalysis of organic reactions. In a phenotypic screen, a quinidine-based compound was identified during the optimization process of Oxautin-1, a potent autophagy inhibitor. The structure-activity studies of this compound needed to be evaluated. A collection of 50 molecules was synthesized using modern C-H activation chemistry. These different reactions permitted to decorate the scaffold at different positions.

Phenotypic screen

Hit identification

Autophagy IC$_{50}$
0.56 ± 0.15 µM

Structure-activity relationship
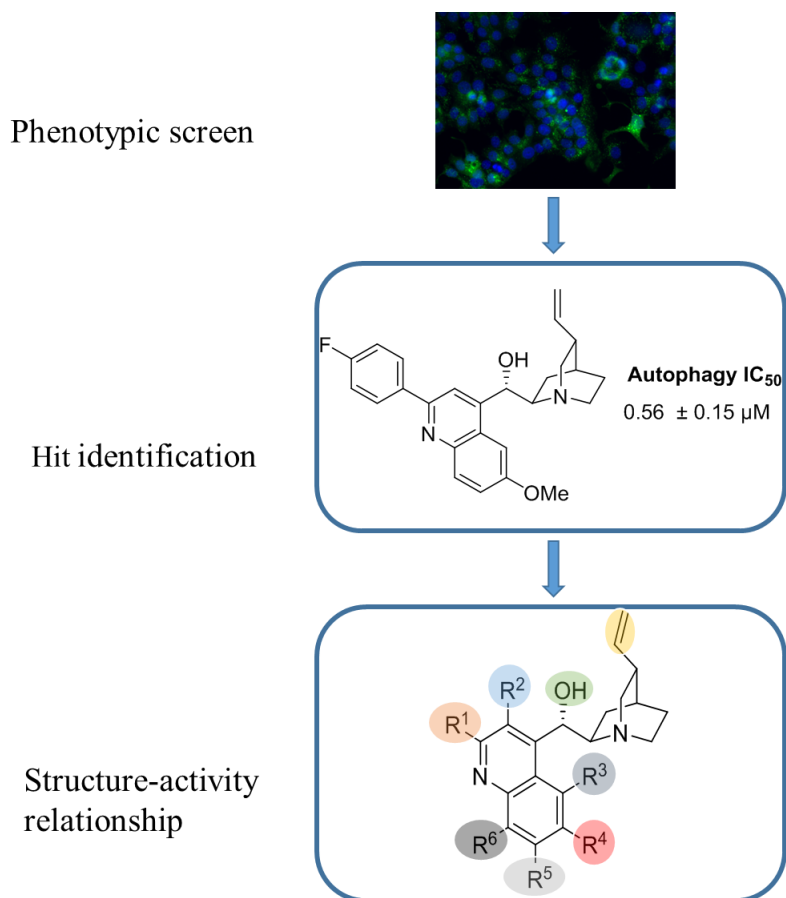
Using a cell- painting assay, the optimized compound Autoquin, was predicted as a lysosomotropic agent, where it showed similar morphological changes as known lysosomotropic agents. Using a cell-based and cell free acid ceramidase assay, the prediction was confirmed. Because this target did not explain the inhibition of autophagosome biogenesis, identification of a secondary target is currently under investigation.

KURZZUSAMMENFASSUNG

Tyrosinkinasen der Src-Familie sind bei Fehlregulation an Krebserkrankungen beteiligt. Die Inhibition der Signalübertragung durch die N-myristoylierte Nicht-Rezeptor Tyrosinkinase Src wird als vielversprechender Ansatz bei der Entwicklung von Krebsmedikamenten angesehen. UNC119, ein Protein, welches myristoylierte Proteine binden kann, wird zur Einleitung der Kinase-Aktivität von manchen Kinasen der Src-Familie benötigt.
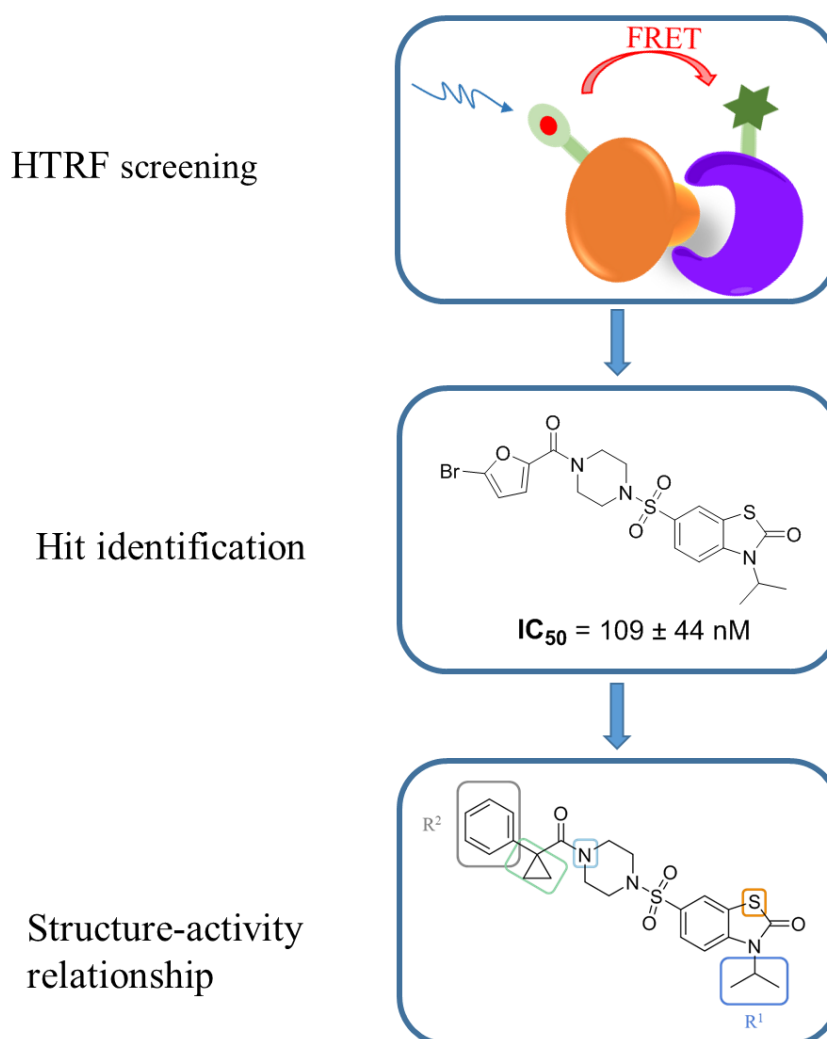
Im Rahmen dieser Arbeit wurde ein potenter und spezifischer Inhibitor der UNC119-Src-Interaktion mit neuem Chemotyp unter Verwendung des homogenen zeitaufgelösten Fluoreszenz-Screenings identifiziert. Die Selektivität der Verbindung wurde durch Fluoreszenzpolarisation und zelluläre Thermal Shift Assays validiert. Diese sekundären Assays werden zur Bestätigung der Ergebnisse genutzt. Die Struktur-Aktivitäts-Beziehung für die Verbindungsklasse wurde anhand einer synthetisierten und gekauften Verbindungssammlung

abgeleitet. Weitere Untersuchungen zeigten, dass das Molekül in Zellen an UNC119A und UNC119B bindet.

Die Verbindung induziert eine Reduktion der aktivierenden Src- Autophosphorylierung an Y419, einem wichtigen Rest für die Aktivität der Kinase. Die Abnahme des Phosphorylierungsgrades von Y419 um 40% wurde mit Hilfe eines In-cell Western Assays gemessen und zeigt die Auswirkung der Verbindung auf die Aktivität der Kinase. Die Hemmung von UNC119 in Src-abhängigen kolorektalen Krebszellen führt zu einer spezifischen Reduktion des Zellwachstums und des klonogenen Potenzials. Mittels Mikroskopie wurde die Störung der Interaktion in einem in-vivo System beschrieben (durch Fluoreszenzlebensdauer-Mikroskopie Förster-Resonanzenergietransfer Experiment). Die Ergebnisse zeigen, dass Interferenzen von kleinen Molekülen mit der Dynamik des Src-Spatial-Cyclus eine neuartige Möglichkeit eröffnen, mit dem onkogenen Src-Signaling zu interferieren.

Cinchona Alkaloide sind bevorzugte Grundgerüste sowohl in der medizinischen Chemie zur Behandlung von Malaria als auch in der organischen Chemie zur Katalyse organischer Reaktionen. Während des Optimierungsprozesses von Oxautin-1, einem wirksamen Autophagie-Inhibitor, wurde in einem phänotypischen Screening eine Chinidin-basierte Verbindung identifiziert.

Phenotypic screen

Hit identification

Autophagy IC$_{50}$
0.56 ± 0.15 μM

Structure-activity relationship
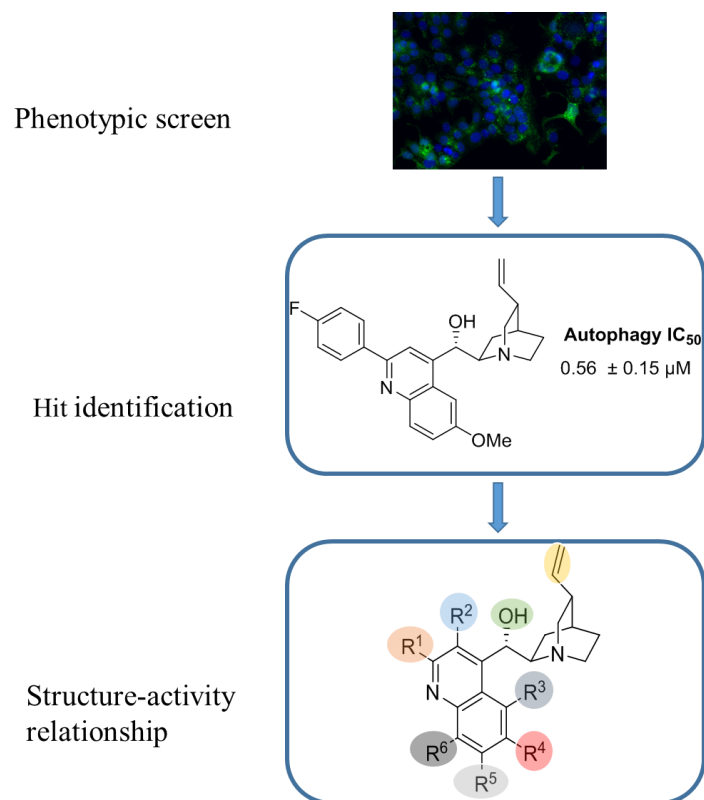
Die Struktur-Aktivitäts-Beziehungen für diese Substanzklasse mussten beurteilt werden. Eine Sammlung von 50 Molekülen wurde durch moderne C-H-Aktivierung synthetisiert. Diese verschiedenen Reaktionen erlauben es, das Grundgerüst an verschiedenen Positionen zu verändern. Mit Hilfe der Cell-Painting-Screen-Technologie wurde die optimierte Verbindung Autoquin als lysosomotropes Mittel vorhergesagt, da es ähnliche morphologische Änderungen wie schon bekannte Mittel aufweist. Ein zellbasierter und ein zellfreier Säure-Ceramidase Assay bestätigten die Vorhersage. Da das Zielprotein die Hemmung der Autophagosom Biogenese nicht aufgeklärt hat, wird ein zweites Zielprotein derzeit untersucht.

1. GENERAL INTRODUCTION

1.1. Chemical Genetics

Chemical genetics involves the use of small molecules to understand biological systems. Classical genetics uses mutagenesis to investigate the relationship between phenotypes and genes. By analogy, chemical genetics is related to classical genetics. This approach can be divided in two different approaches: forward and reverse chemical genetics (Figure 1).[1]
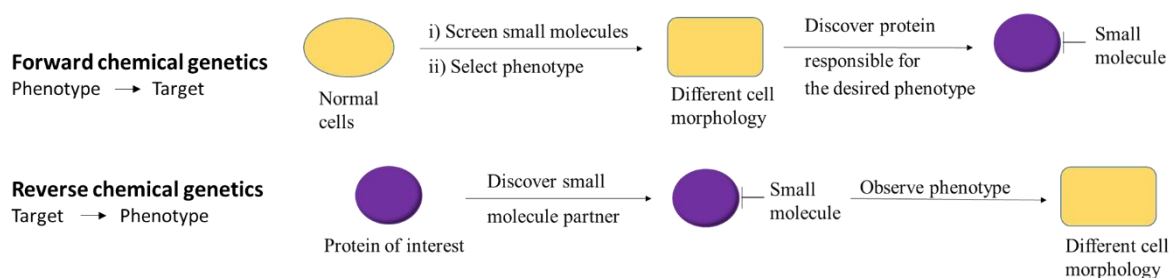
Figure 1. Schematic representation of forward and reverse chemical genetics. Adaptation from Spring.[2]

1.2. Forward Chemical Genetics

1.2.1. Definition

The first approach in Figure 1 is called forward chemical genetics by analogy to forward genetics. It operates from "phenotype to target".[3] In this approach, researchers employ small molecules to assess their potential effect on gene activity, cell behavior or cellular mechanisms.[4] Based on its potency for a specific phenotypic response, a small molecule is selected for target identification.

Optimization rounds, known as Structure Activity Relationship (SAR) studies, are an important and crucial step in the development of a tool compound.[5] The optimization of the different parameters of the selected compound, such as toxicity, solubility and potency, is a crucial step before further characterization and pharmacological development.[6,7] Ultimately, an optimized compound can lead to the identification of the mode-of-action (MOA).[8]

The target identification step in forward chemical genetics is a challenging and time-consuming step. Research laboratories around the world spend millions of dollars in projects involving the identification of targets of promising small molecules. For the development of a small molecule, it is important to find not only the primary target but also any additional targets the molecule might have. It has recently been shown that clinically approved small molecules can often have multiple biological targets which may lead to undesired and unpredictable side

1

effects when used as a therapeutic agent.[9] This issue is often a main drawback in the development of new drugs as these adverse effects may only be revealed in the later stages of development, when millions of dollars have already been spent into the development of this pharmaceutical agent.[10] Nevertheless, forward chemical genetics has proven to be a valuable tool in the field of new medicine.[5]

1.2.2. Screening Technologies and Limitations in Forward Chemical Genetics

In order to rapidly identify small molecules leading to a phenotypic response, multiple screening methods have been developed. High- and Medium-Throughput Screening (HTS and MTS, respectively) techniques are used extensively to screen medium to large libraries of compounds.[11] These methods are based on several different readouts such as fluorescence for marking a cellular protein of interest, or cell viability. Cell viability techniques compare the toxicity of a small molecule toward unhealthy cells (such as cancer cells) compared to healthy cells.[12–14] As a result of the recent developments in microscopy and instruments analyzing cell morphology and growth in real time, phenotypic HTS is now widely used for the identification of bioactive small molecules.

After the evaluation of the desired phenotype upon treatment of the cells or organisms with a library of small molecules, it is necessary to perform orthogonal and unbiased assays in order to confirm the identified hit molecule. This step is essential in order to rule out false positive or false negative compounds and can give crucial information for the selection of the lead.[15,16] Given that a toxic molecule can appear as a false positive hit in a phenotypic screen, a secondary assay looking at the selectivity or the toxicity of the compound toward healthy cell lines or a different cell line is important.[17] Secondary assays should be done during an early stage, in parallel to the SAR studies, to avoid the development of unselective or non-specifically toxic compounds.

1.3. Reverse Chemical Genetics

1.3.1. Definition

The classic workflow of reverse genetics is the following: an interesting gene is selected and manipulated to generate mutants. The difference in phenotype between the wild type and the mutant leads to the understanding of the gene function.[18] Analogously to the classical reverse genetics approach, reverse chemical genetics (RCG) operates from "target to phenotype".[1] In this approach, an interesting protein (or gene) is first selected, based on its connection to a certain disease or relevant biological response, and a library of small molecules is screened against it to identify a ligand that perturbs its function. When a specific ligand is selected and optimized (following the same approach used for forward chemical genetics), it is used on cells or an organism in order to study and characterize the triggered phenotypic response. The ligand, in this approach, is considered to mimic the genetic mutation.

In order to evaluate the phenotypic response, the selected compound can be modified with a linker coupled to a fluorophore or a solid phase. The modification allows the preparation of tools valuable for target identification and validation. For example, attachment of a fluorophore allows the use of compounds in techniques such as determination of fluorescence polarization to validate target binding biophysically. Functionalization of the small molecule with a linker (e.g. a biotinylated PEG linker) can be used for pulldown experiments to identify the target or the selectivity of the compound in a more complex environment. To be able to distinguish between on- and off-target responses, the probe needs to be carefully designed.[19] While designing a probe, the selection of a wrong modification site around the small molecule or the wrong fluorophore could lead to a complete loss of activity of the probe or can lead to false read-out and lead to wrong conclusions regarding the explored target.

1.3.2. Screening Technologies and Limitations in Reverse Chemical Genetics

As opposed to forward chemical genetics, which uses cells or organisms to observe a phenotypic response, reverse chemical genetics allows the study of the interaction between the small molecule and the protein of interest in an *in vitro* measurement. Screening techniques were developed and used in order to characterize compounds interacting with a selected protein.

Fluorescence techniques, for example, are based on the use of dyes to label a specific protein, small molecule or peptide, thereby enabling an easy readout that can be used in HTS.[20] Consequently, fluorescence techniques are commonly used in reverse chemical genetics by the

pharmaceutical industry as well as in academic laboratories.[21] For using a fluorescence-based screen, the selected protein (and in certain cases their binding partners) needs to be labelled with a fluorophore.[22]

The most challenging step in reverse chemical genetics is the identification of the phenotype. After development of a small molecule based on screening techniques, the identification of the biological response induced by the perturbation of the function of a selected proteins is often challenging. *In vitro* assays are a good starting point for the RCG approach. These assays allow the identification of compounds directly interacting with the protein of interest. However, the optimization of the identified compound is an important step. A non-optimized compound will generate a loss of time and resources in the phase of drug development.

An important parameter to evaluate before selecting a lead compound is the chemical structure of a hit. Pan-Assay Interference Compounds (PAINS), which contain structural motifs known to non-specifically interfere with assay read-outs, are repeatedly identified as hits in a large number of screens.[23] Nowadays, computational filters exist to remove PAINS from the screening results. Despite these efforts, PAINS continue to be reported as biologically active compounds which often leads to wrong conclusions and presents a major drawback in this field. In a typical academic library, PAINS represent 5–12% of the whole library.[24] This is also the case for commercially available libraries, such as the molecular libraries small molecule repository (MLSMR) and the library of pharmacologically active compounds (LOPAC®). These commercially available libraries are often starting point of a screen development because of their accessibility and the PAINS remaining compounds need to be carefully analyzed.

1.4. The Small-Molecule Approach

Using small molecules to study biological phenomena offers advantages over traditional genetics[25] and hence an attractive alternative. Small molecules generally induce their biological effect faster (in most of the cases within minutes) and the effects are reversible, thereby permitting *in vivo* studies in situations where deletion of a gene would be lethal.[2]

There are also limitations to the use of small molecules. While any gene can be manipulated by genetics, not yet every protein can be targeted by small molecules, and only a few proteins have known ligands. By continuing to explore chemical space, biologically active molecules can be designed to target proteins without known ligands.

The need to look for different chemical space to identify further bioactive small molecules has become a topic of interest in the last years.[26,27] However, the chemical space used for the development of small molecules over the past two decades is limited.[28] To date, only a small portion of chemical space has been explored, with considerable effort being made, mainly by academic laboratories, to counteract this problem.[29] Focusing on prevalidated scaffolds could open new opportunities for the design of small molecules. One interesting class of compounds is the so-called "dark matter",[30] i.e. compounds with interesting chemical structure that have never been identified as hits in any screen. As a result, once an activity for these compounds is identified, they are typically highly selective modulators.

1.5. High Throughput Screening
1.5.1. Introduction

Since the 1980s and particularly the 1990s, the pharmaceutical industry has extensively used HTS to screen small molecule libraries. The completion of the Human Genome project identified many new proteins. Thanks to this project, new targets could be screened leading to the fast development of HTS technology. Using HTS to screen large chemical libraries, companies hoped to accelerate the phase of lead identification.[11]

Target-to-lead efforts involve several steps, including target selection and characterization, assay development, compound screening and hit validation. In the pharmaceutical industry, such effort takes between two to three years and have a high cost. The development of HTS screens enables this process to be accelerated (and decrease the cost) of the compound screening steps. For example, it takes one week to screen a database of around 10,000 molecules and up to one month for a database of 1,000,000 compounds.[11] Without HTS technology, the evaluation of the activity of such big libraries will not be possible. HTS success rates are generally estimated to be $\approx 50\%$ and can reach up to 60%, as reported by some companies.[9]

HTS is widely used because of its unique advantage to be applicable to a broader range of targets. Other techniques, such as fragment-based screening, structure-based design and virtual screening, can be more limited and time-consuming. Virtual screening, for example, also has the limitation to be applicable only to targets with a 3-D-resolved structure, which is not always the case at the beginning of the development of a bioactive compound.

One of the most used technique for HTS are fluorescence-based screens. For the development of fluorescence-based screens, a protein's binding partner or substrate is often labelled with a fluorophore.[22] The choice of the fluorophore is one important parameter for the screen, as it needs to allow the identification of small perturbations thus delivering high signal-to-noise ratios. The read-outs can include changes in fluorescence intensity or polarization.

With the development of HTS technology and the access to large compound collections, the successful development of inhibitors based on screening methods has increased drastically.[11]

Dasatinib, an anticancer drug, developed by Bristol-Myers Squibb in 2006, was discovered using an HTS screening of their in-house library (Figure 2).[31] The screen used recombinant mouse or human lymphocyte-specific protein tyrosine kinase (Lck), a member of the Src FTKs, as the enzyme and enolase as substrate. An aminothiazole was identified and, after extensive SAR studies and hit optimization, Dasatinib was developed as a low nanomolar Src family kinase inhibitor. Dasatinib is currently used in the treatment of chronic myelogenous leukemia.[32,33]
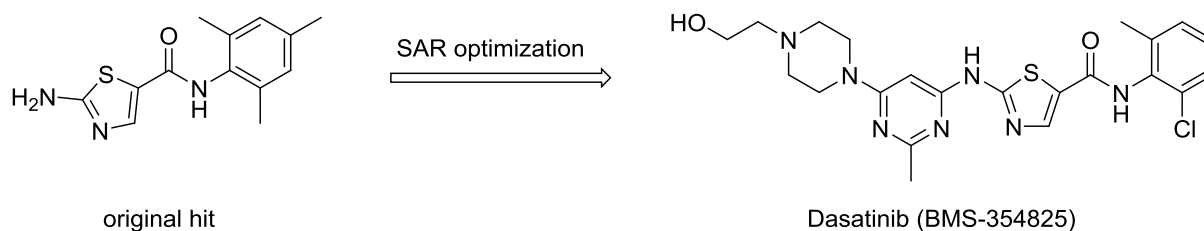
Figure 2. Example of the successful development of a drug using an HTS screening. Chemical structures of the original hit after screening the Bristol-Myers library and the optimized hit Dasatinib, a potent Src Kinase inhibitor.

1.5.2. Homogenous Time Resolved Fluorescence

Homogeneous time-resolved fluorescence (HTRF) is a frequently used technology to measure the interaction between a small molecule and a protein. The technology combines Förster resonance energy transfer (FRET) with time-resolved measurements. These features provide significant benefits such as assay flexibility, reliability and increased assay sensitivity, making this technique an ideal platform for HTS.[34]

HTRF screens have been successfully used for the identification of bioactive molecules. For example, this approach allowed the discovery of small molecules interacting with several G-protein coupled receptors (GPCRs), e.g. 5-HT$_4$,[35] 5-HT$_6$[36] and leukotriene receptor.[37] Furthermore, the HTRF technology has been applied to a high number of enzymatic activity assays, Protein-Protein interaction (PPI) assays and Protein-Peptide and Protein-DNA interaction assays.[38,39]

HTRF screens use rare-earth lanthanides. The principle behind the FRET signal is based on the energy transfer between two distinct fluorophores, a donor (long-lived fluorescence) and an acceptor (short-lived fluorescence) when in close proximity (Figure 3).[34] When a small molecule interacts with the donor, the distance between the donor and acceptor increases. This spatial distance increase leads to a decrease or an abolition of the FRET signal. The use of two different fluorophores makes this bioassay both sensitive and robust, and enables its miniaturization to 1536-well plates for the use in high-throughput mode.[40–42]
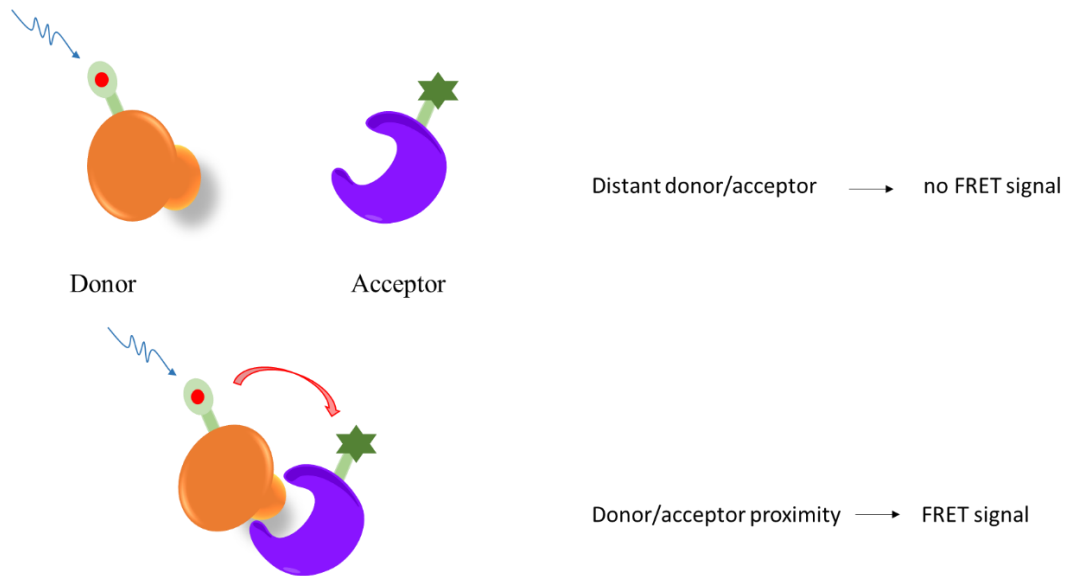
Figure 3. HRTF principle. Based on the energy transfer between a donor and an acceptor when in close proximity. Adaptation from Degorce et al.[34]

2. Small Molecule Inhibition of Lipidated Proteins/Cargo Interaction

2.1. Introduction

Tyrosine phosphorylation is an important cellular event mediated by protein tyrosine kinases (PTK), which regulates several biological responses such as cell migration, proliferation, differentiation and cell survival.[43] Current evidence shows that different families of tyrosine kinases regulate additional cellular complexity, resulting from extensive cross-talk between pathways.

2.1.1. Src Family Kinases

One important family of PTKs, the Src PTKs, is able to communicate with a large number of receptors. The Src PTK were first identified as the transforming protein of the oncogenic retrovirus (v-Src). The nine different members of the Src PTKs have high sequence homology and similar structural features. This family includes Src, Fyn, Yes, Yrk (only found in chicken), Blk, Fgr, Hck, Lck, Lyn and the Frk subfamily proteins Frk/Rak and Iyk/Bsk whose N-terminal sequences are shown in Figure 4.[44]
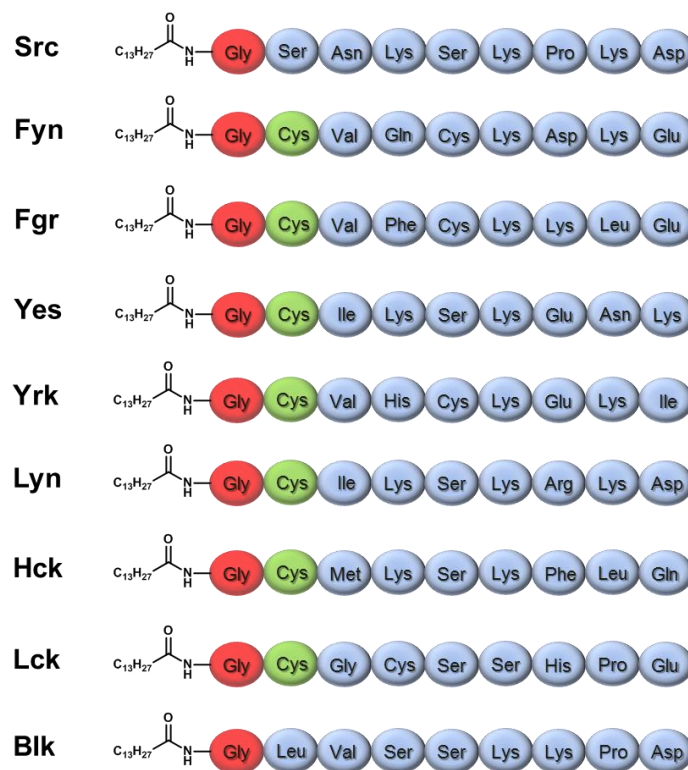
Figure 4. N-terminal sequences of the Src PTKs family members. The last nine amino acids after the myristoylated group showed high similarity in structure and sequence.

All family members show similar domain arrangement (Figure 5). Src family kinases are 52–60 kDa proteins composed of six distinct functional regions: The Src homology (SH) 4 domain, the unique region, the SH3 domain, the SH2 domain, the catalytic domain and a short regulatory tail.[43] The SH4 domain, a 15-amino acids sequence, contains the signal for the lipid modification. The 50-amino acid long SH3 domain, directs specific association with a proline rich motif related to the (X= PXXP) consensus sequence. The 100-amino acids long SH2 domain provides interaction with phosphotyrosine motifs. The catalytic domain is essential for the enzymatic activity (Figure 5).
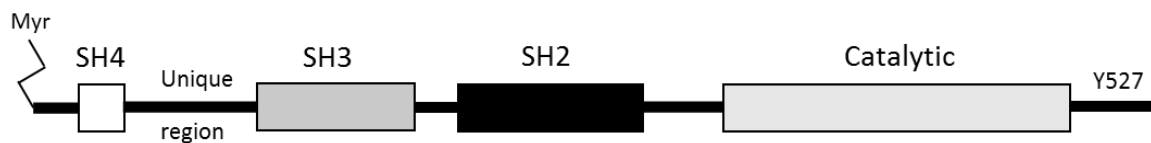
Figure 5. Domains of protein tyrosine kinase Src. Adaptation from Thomas et al.[45]

SH2 and SH3 domains play a crucial role in the regulation of the activity of the protein kinase.[46] High-resolution crystal structures of several Src PTKs showed how this regulation takes place: intramolecular interactions of the SH3 and SH2 domains stabilize the inactive conformation of these kinases. Both domains are on the opposite side of the catalytic domain and repress the kinase activity by interaction with a few amino acids inside the catalytic domain (Figure 6).

When tyrosine 527 (Y527) is phosphorylated, a conserved arginine in the SH2 domain interacts with the phosphorylated tyrosine via an electrostatic interaction. This interaction forces the enzyme into a closed conformation, rendering it inactive (Figure 6).[47]

The SH3 domain of the Src protein kinase is responsible for regulating its kinase activity through an intramolecular interaction with specific adaptors. Interaction with the RXXPXXP motif of the ligand induces a conformational change of the enzyme, preventing the small and the large lobes of the kinase domain from closing.[45]
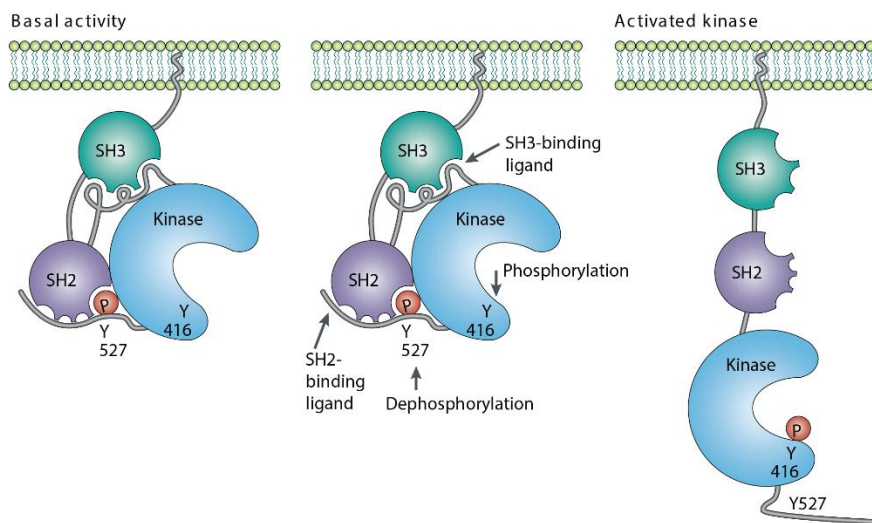
Figure 6. Activation of Src FKs through phosphorylation of Tyrosine 527. Reproduced from Martin et al.[47]

Biochemical studies suggest that the autophosphorylation of the tyrosine 416 (Y416) (inside the catalytic domain) is also important for the regulation of the kinase activity.[48] This site, not phosphorylated in the inactive wild type, is constitutively activated in oncogenic Src mutants. Altogether, these findings show that there is more than one way to activate Src tyrosine kinases. Often more than one mechanism is involved in response to a stimulus. Through all of the SH domains, Src FKs are able to communicate with a diverse group of proteins.

Src has been associated with multiple roles in cancer progression.[49] In breast cancer, Src promotes growth of tumor cells via interaction with human epidermal growth factor receptor 2 (HER2). This interaction is thought to be responsible for the high metastatic potential of HER2-overexpressing cancers. Src has also been associated with lung cancer, for which an increase of c-Src protein and kinase activity has been reported in 50–80% of the patients.[48] In prostate cancer and in colon cancer, the Src protein promotes proliferation of cancer cells.[48] Recently, Src has been identified as a binding partner of UNC119, a lipid binding protein which may be a chaperone. The link between the two proteins and the biological relevance of this interaction remains unclear.

2.1.2. UNC119: a Myristoyl Binding Molecular Chaperone

Protein N-myristoylation refers to the attachment of a myristoyl group, a saturated fatty acid chain of 14 carbons, to the N-terminus of a protein. This lipidation is involved in many biological processes and is generally an irreversible protein modification, which promotes reversible protein membrane and protein-protein interactions.[50–52]

UNC119, a protein able to recognize and accommodate a myristoylated protein, is a member of a lipid-binding protein family with two different paralogs generated by an ancestral gene. First discovered in *C. elegans* due to a spontaneous mutation resulting in a defect of chemosensation, locomotion and feeding behavior, UNC119 was also identified in an independent cloning and called Human retina-specific gene 4 (HRG4, a human orthologue).[53–55] UNC119 has been identified in plants and all animals. This lipid-binding protein participate in the localization and the trafficking of lipidated proteins. It has been shown that UNC119 act as "GDI-like" solubilizing factor for lipidated cargo.[56,57]

UNC119 is a 27 kDa protein, which exists as two isoforms, UNC119A and UNC119B. They share a sequence homology of 60% and no biological difference between these two isoforms has been characterized so far. At a cellular level, UNC119 has been identified in the mouse photoreceptor sensory cilium complex, in the neurons of *C. elegans* and in the flagellar rootlet of *Naegleria*.[54,58] UNC119A is responsible for ciliary delivery of myristoylated cargo. A link between UNC119 and myristoylated Src family kinases was investigated.
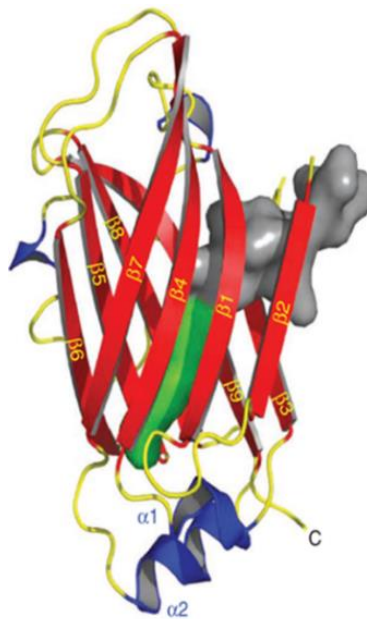
Figure 7. Co-crystal structure of human UNC119 (retina gene 4) and an N-terminal Transducin-alpha mimicking peptide. UNC119 is represented in red as cartoon. Extracted from the PDB file: 3RBQ.[59]

Zhang and coworkers solved a high-resolution crystal structure of UNC119A in 2011 (Figure 7).[59] The 1.95 Å crystal structure reveals an immunoglobulin-β-like-sandwich forming a hydrophobic cavity able to accommodate a lipid moiety. The co-crystal structure of UNC119 in complex with a lauroyl and six residues of the Gα peptide (Lau-GAGASAEEKH) showed that the binding site easily accommodates a lauroyl (C12) moiety.

UNC119 shares a 24% amino acid sequence identity with PDE6δ and 10% with RhoGDI. Sequence homology between the hydrophobic cavities of these molecules is higher. For example, the similarity with PDE6δ increases to 56%. RhoGDI and PDE6δ are also lipid binding proteins, and are able to accommodate geranylgeranyl and farnesyl chains.[60,61] Remarkably, UNC119 is only able to accommodate lauroyl and myristoyl lipid moieties (Figure 8).[62] Although UNC119 has a high affinity to these specific lipid moieties, several studies show that the sequence of the target protein is also necessary for the specificity of UNC119 binding. UNC119A and UNC119B have been described to be critical for trafficking myristoylated proteins into cilia. UNC119A and UNC119B recognized several myristoylated proteins including few ciliary proteins and were link to ciliopathy nephronopthisis.[63]
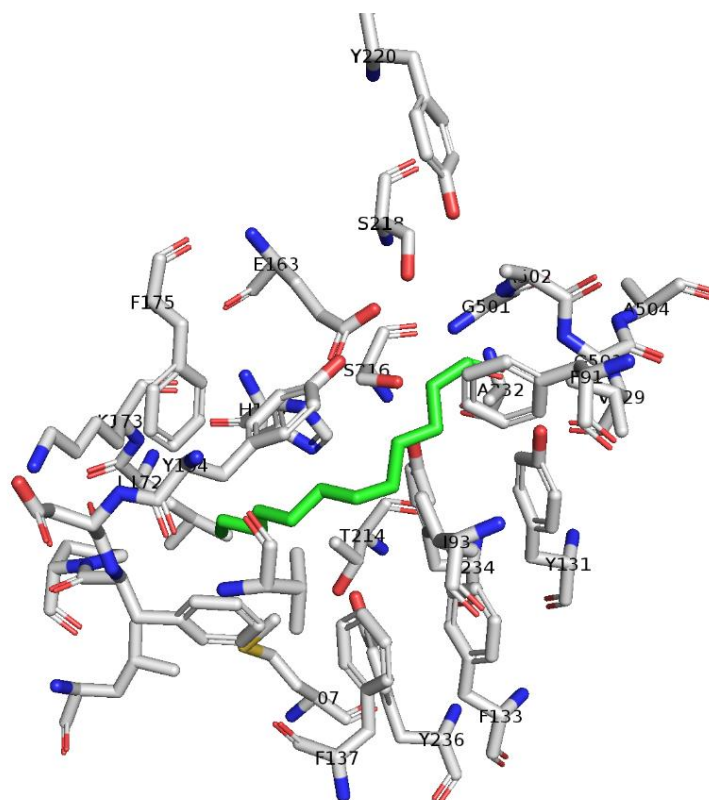
Figure 8. Co-crystal structure of human UNC119 (retina gene 4) and an N-terminal Transducin-alpha mimicking peptide. Sequence and 3D structure of the hydrophobic cavity of UNC119A are shown in grey with labelled amino acids. Peptide is shown in green. Picture performed with Pymol®. PDB file: 3RBQ.[59]

In mammals, UNC119 has been detected in leukocytes, T-cells, lung fibroblasts, the adrenal glands and kidney. UNC119 has been shown to interact with several biologically relevant proteins including the Arf-like GTPases ARL2[64] and ARL3[65], the Ca^{2+}-binding protein CaBP4[66] and the synaptic ribbon component of photoreceptors.[67] Given its important function in protein transportation and localization, deletion experiments were performed. Zhang and coworkers showed that deletion in mouse and *C. elegans* of UNC119 led to G protein mislocalization.[59] Deletion of the UNC119 in mouse leads to partial retention of transducin in the inner segment even after complete dark adaptation.

2.1.3. Interaction Between UNC119 and Src Family Kinase

UNC119 has shown to be crucial for the trafficking of myristoylated proteins. Baehr *et al.*, based on its ability to accommodate lauroyl- and myristoyl-lipidated proteins and their studies of the 3-D conformation of the protein, postulated that UNC119A interacted with the SH2 and SH3 domains of Src FKs (Figure 9).[62]
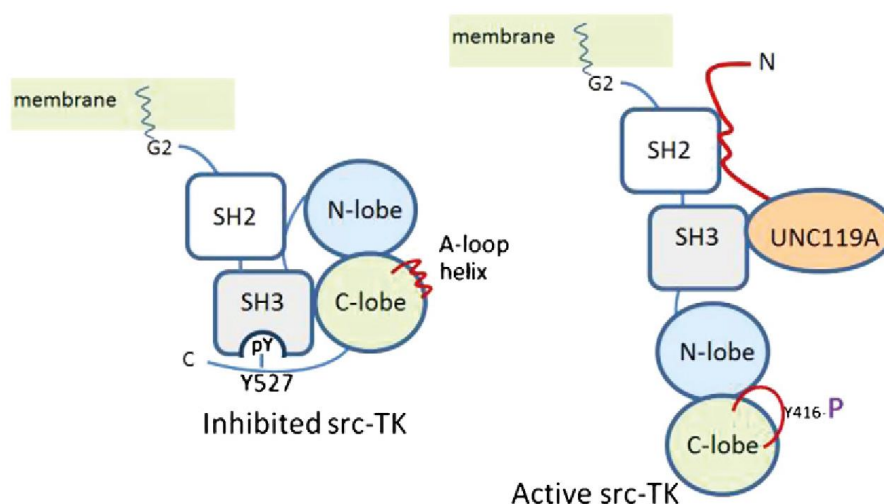
Figure 9. Model of the Src TKs activation by UNC119. Reproduced from Constantine et al.[62]

Alam and coworkers showed that UNC119 regulates myofibroblast differentiation through the activation of Fyn.[68] The same group had shown earlier that UNC119 was an activator of the Lck/Fyn and that this activator was essential for T cell activation and for immunological synapse formation.[69–71] Also based on the crystal structure analysis, they postulated that UNC119 induces the catalytic activity of these kinases through interaction with the SH2 and SH3 domains of Lck and Fyn, which supports the model of Constantine *et al.* (Figure 9).

2.1.4. Arl-3 and UNC119 Regulate Transport of Myristoylated Ciliary Cargo of Src FKs.

Arl2 and Arl3 are proteins known to regulate prenylated cargo release,[57,65] suggesting that these two small G proteins are involved in the regulation of the transport and release of Src family kinase by UNC119. Arl proteins are guanosine triphosphate (GTP) binding proteins.[56] Arl2 and Arl3 were identified as regulators of the transport of K-ras4B by PDE6δ.[56] Based on the analogy of structure and the similarity of functions between UNC119 and PDE6δ, the regulation of the cargo release by Arl2 and Arl3 was investigated.

Wittinghofer and coworkers showed, based on the high-resolution crystal structure of UNC119 in complex with Arl2 or Arl3, allosteric binding between UNC119 and the small G proteins (Figure 10). They were also able to show that surprisingly only Arl3 increases the release of cargo by three orders of magnitude.[72,73] Later, they also investigated the molecular function of Arl13B, another small G protein, acting as GEF for Arl3 and elucidated its crucial role in the cilia maintenance.[74,75]

The mechanism of cargo release was also studied. Contrary to the analogy with PDE6δ, for which the binding leads to a closing of the binding pocket[65], the small G protein binds to UNC119A leading to an opening of the binding pocket. The release of the cargo is not only dependent on the small nucleotide but also the localization in the cilia (Figure 10).[72]
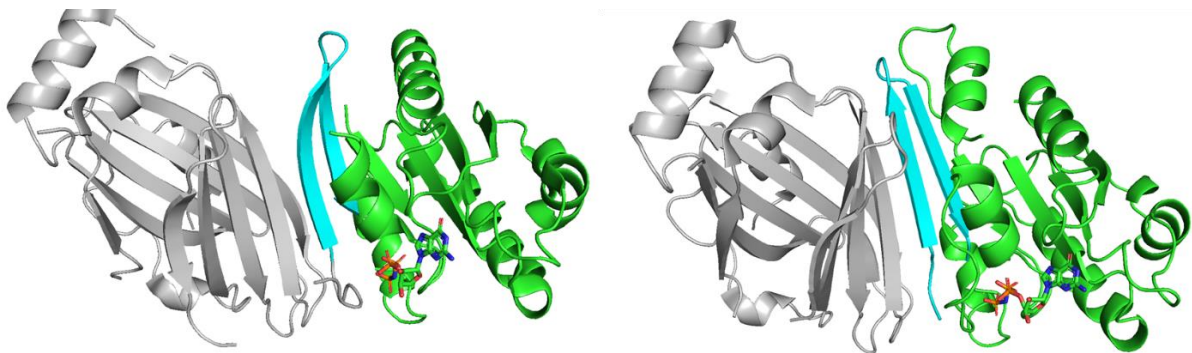
Figure 10. Ribbon representation of overall structure of UNC119A in complex with Arl2 (left) and Arl3 (right). UNC119A in grey, Arl2 and Arl3 in green. GppNHp showed as ball and stick. PDB files: 4GOK (UNC119A/Arl2) and 4GOJ (UNC119A/Arl3).[72]

Wright *et al.* showed that Arl3 and UNC119B are required for nephrocystin-3 (NPHP3) ciliary targeting.[63] They were able to demonstrate that this targeting is controlled by the binding of Arl3-GTP, which serves as release factor for the cargo between myristoylated-NPHP3 and UNC119B.

2.1.5. Small Molecule Inhibitors of Src Family Kinases

It has been shown that Src activity increases with diseases such as solid tumors and leukemia progression and is an indicator of poor clinical prognosis. Therefore, the development of Src inhibitors targeting the kinase activity of the protein is considered a potential anti-cancer therapy. Recently, Src has become an active target for drug development. A number of Src inhibitors, such as Dasatinib (BMS-354825)[76], Bosutinib (SKI-606)[77] and Sarcatinib (AZD0530),[78] are at various stages of clinical development (Table 1).

Dasatinib (see Chapter **1.5.1** for structure and screening information), developed by Bristol-Myers Squibb in 2006, is currently under evaluation as a therapeutic agent for various cancers (Table 1). It has been shown that Dasatinib also interacts with Abelson murine leukemia (ABL) kinase as a secondary target, leading to several off-target effects.[33]

Table 1. Selected current trials for Src family kinases inhibitors (Dasatinib, Bosutinib and Sarcatinib).*

Drug	Trial setting	Phase
Dasatinib	Patients with stage III or IV or recurrent non-small-cell lung cancer	II
Dasatinib	Metastatic pancreatic cancer	II
Dasatinib	Advanced solid tumors	I
Dasatinib	Advanced breast cancer	I
Bosutinib	Advanced metastatic breast cancer	II
Bosutinib	Advanced malignant solid tumors	I
Sarcatinib	Prostate and breast cancer patients with metastatic bone disease	II
Sarcatinib	Advanced solid malignancies	I
Sarcatinib	Extensive stage small-cell lung cancer	II

*Data obtained from www.clinicaltrials.org and Kim *et al.*[49]

All three compounds have off-target effects, most likely arising from their dual selectivity. These ATP-competitive Src inhibitors lack specificity and induce cytotoxicity. Because of this issue, novel approaches for the design of Src family kinase inhibitors are required.[46]

The Ras family GTPases bind with very high affinity to guanosine nucleotides and hydrolyze guanosine triphosphate (GTP) to guanosine diphosphate (GDP). These proteins regulate important processes such as growth and differentiation.[79] Mutations leading to the locked GTP form are associated with cancer development.[80] Similarly to the Src FKs, all Ras isoforms are also farnesylated. PDE6δ, the characterized binding partner of K-Ras4B, has a

high amino acid sequence homology with UNC119.[57] Selective inhibitors targeting PDE6δ binding pocket with nanomolar affinity were recently developed.[81–84] These inhibitors directly target the lipid binding pocket and offered a novel approach for targeting lipid binding protein involve in the transport and localization of oncogenic modulators.[81]

A similar approach to the one used for PDE6δ/Kras can be employed for targeting Src FKs, i.e., interfering with the interaction of myristoylated Src with UNC119. Targeting the lipid-binding site of UNC119 is therefore a novel approach for the design of Src FKs inhibitors and potentially for the development of compounds with lower side effects than those previously developed.

2.2. Aims

Src family tyrosine kinases are involved in cancer pathologies when misregulated. Therefore, the development of new tool compounds for better understanding the mechanism and the biological relevance of this target is in high demand.

The main goal of the project was to develop a small molecule disrupting the interaction between UNC119 and Src family kinases. A target-based screen from the Compound Management Screening facility permitted a screening of an in-house chemical library. This screening could lead to the characterization of inhibitors of the interaction between UNC119 and Src family kinases. After a careful selection of the scaffold based on the chemical structure, a compound collection needed to be synthesized (Figure 11). This compound collection was necessary to understand the structure activity relationship of the identified compounds. Further investigation of the biological response while disrupting this interaction could help to gain knowledge about the disruption of this interaction on a cellular level. Because of the importance of the phosphorylation of the Y416 for the kinase activity of the Src PTKs, the phosphorylation level of this specific residue should be evaluated upon treatment with new inhibitor.

The purpose was to offer a novel approach for targeting the UNC119/cargo interaction and evaluate the impact of the disruption of this interaction at a cellular level. Identifying the biological response of this disruption could give insight into this mechanism and the relevance of this cargo over the development of diseases such as colorectal cancer.

original hit, 34

IC_{50} = 109 ± 44 nM
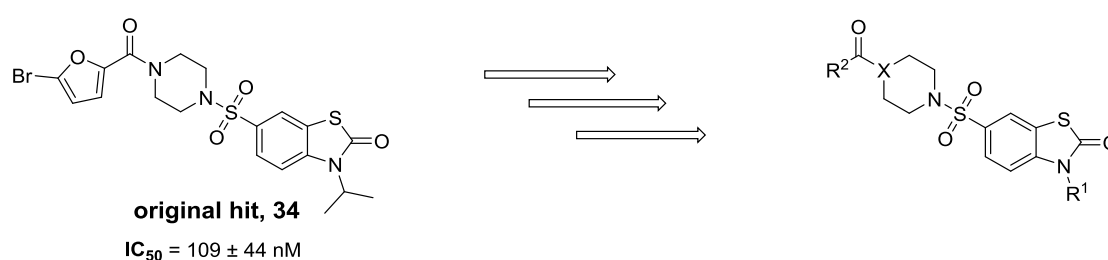
Figure 11. Structure activity relationship optimization of the initial hit from the screening.

2.3. Results and discussion

2.3.1. Identification of a Benzothiazolone Inhibiting UNC119/Src cargo

The interaction between UNC119 and Src FKs has shown to be relevant and involved in diseases. Current ATP-competitive inhibitors of the Src FKs possess many side effects and new therapeutics are necessary.[48] At the beginning of this project, no inhibitors of the Src/UNC119 interaction were reported. Targeting this interaction may represent a valuable tool for studying the biological relevance of Src FKs and gaining knowledge to develop new therapeutic agents for the treatment of cancer.

2.3.1.1. Homogenous Time Resolved Fluorescence Screen for the Identification of the Scaffold

Screen performed at the Compound Management and Screening Center.

As described in Chapter **1.5.3.**, lanthanides and especially europium can be used for the development of screening methods, due to their lack of toxicity compared to other metals and remarkable luminescence properties. In order to identify promising inhibitors of the UNC119/Src interaction, an HTRF screen was developed by the Compound Management and Screening Center, using an anti-GST-Eu3+ cryptate bound to a GST-labeled UNC119A protein as donor and a streptavidin-d2 attached to a myristoylated-Src-PEG-biotin peptide as acceptor (Figure 12). A FRET signal is emitted when UNC119A and Myr-Src are in close spatial proximity. Inhibitors of this interaction increase the distance between the donor and acceptor. Consequently, no signal transfer can occur, leading to a decrease in the FRET signal.
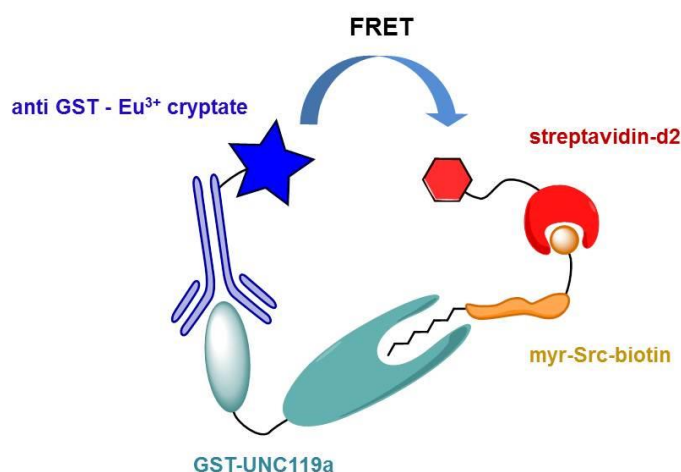
Figure 12. UNC119 HTRF screening using an Anti-GST-Eu3+ cryptate/GST-UNC119A as a donor and Myr-Src-biotin/Streptavidin-d2 as an acceptor. A FRET signal is emitted when UNC119A and Src-Myr are in spatial proximity. While treatment with a small molecule interacting with UNC119A, the distance between the acceptor and the donor increases leading to a decrease of the FRET signal. Screen performed at the Compound Management and Screening Center.

2.3.1.2. Synthesis of Lipidated Peptides as Tools

The successful use of peptides for mimicking lipid-binding proteins has been reported.[81] Furthermore, lipidated peptides were required for the development of the HTRF screen as well as to study the interaction between UNC119/Src FK in secondary assays such as fluorescence polarization (FP) for validation. Therefore, several building blocks were prepared before the preparation of the peptides.

2.3.1.2.1. Building Block Synthesis

Following already published methods, two different building blocks were prepared for the synthesis of the myristoylated-Src biotinylated peptide and for the synthesis of the K-Ras peptide analogs. The latter were necessary for the counter screen of the chemical library and PDE6δ.

The first required building block was an Fmoc-Lys(NH-Boc)-OAll. This building block is required for the attachment on the resin and for the orthogonal coupling with the lipidated residue on the resin (Allyl group orthogonal to Fmoc group). Starting from the commercially available free carboxylic acid **1**, the building block was synthesized following a standard procedure (Figure 13).[85] Treating the carboxylic acid with cesium carbonate in methanol (MeOH) for 10 minutes, followed by the addition of allyl-bromide in DMF for 1.5 h led to the desired building block **2** in good yield (87%).
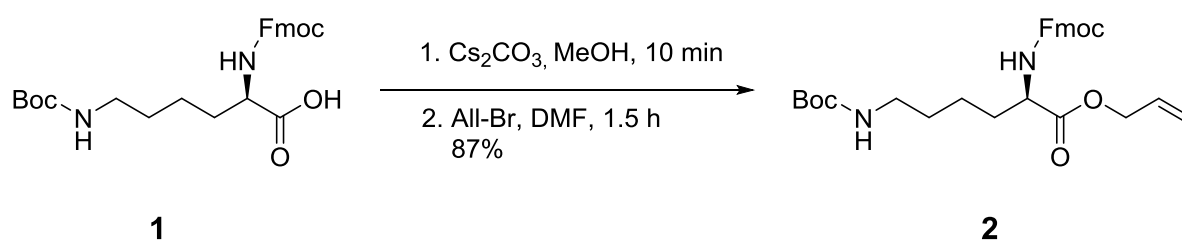
Figure 13. Synthesis of the Fmoc-Lys(NH-Boc)-OAll building block.

Another important building block required was the farnesylated cysteine for the preparation of the Ras derivatives peptides (Figure 14). Treating the commercially available NH$_2$-Cys(SH)-OMe with 7 N ammonia in MeOH, followed by farnesylated bromide at 0 °C for 3 h and 1 h more at room temperature (rt) afforded the desired compound in 80% yield.[86]
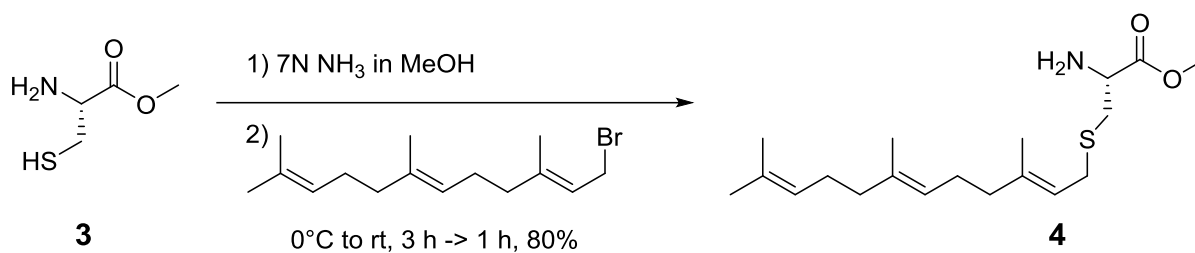
Figure 14. Synthesis of the farnesylated cysteine building block.

With these building blocks in hand, the synthesis of the desired modified peptides could be performed.

2.3.1.2.2. UNC Family Peptides

Nine different proteins compose the Src FKs. The Src protein was selected as the lipidated partner of UNC119 in the assay to be developed. It is one important member of the Src FKs and was already linked to pathology. As shown in Chapter **2.3.1.1.**, a biotinylated, myristoylated Src peptide was needed for the development of the HTRF screening.

After coupling of the building block **1** to the Wang resin, the OAll-group was removed selectively. Extension of the peptidic backbone was performed using 20% piperidine in dimethyl formamide (DMF) as an Fluorenylmethyloxycarbonyl (Fmoc) deprotection strategy followed by peptide coupling using the amino acid (AA), (2-(6-Chlor-1H-benzotriazol-1-yl)-1,1,3,3-tetramethylaminium-hexafluorophosphate (HCTU) and N,N-diisopropylethylamine (DIPEA) in DMF (Figure 15).[87] The biotinylated, myristoylated Src peptide was obtained in 8% overall yield. The purity was controlled by electrospray ionization mass spectrometry (ESI-MS) technique.
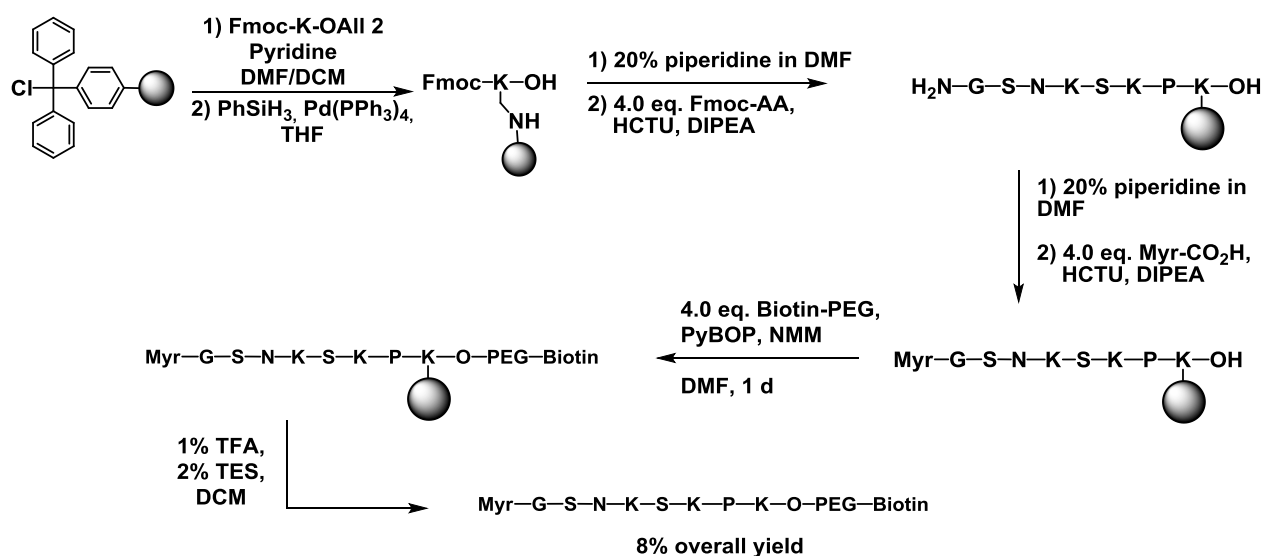
Figure 15. Synthesis of the biotin-PEG-Src-Myr peptide using SPPS. Chemicals: DCM: Dichloromethane, DMF: Dimethylforamide, HCTU: (2-(6-Chlor-1H-benzotriazol-1-yl)-1,1,3,3-tetramethylaminium-hexafluorophosphate), DIPEA: N,N-Diisopropylethylamine, NMM: N-Methylmorpholine, PEG: polyethylene glycol, PyBOP: Benzotriazol-1-yl-oxytripyrrolidinophosphonium hexafluorophosphate, TES: Triethylsilane and TFA: Trifluoroacetic acid.

With the biotinylated, myristoylated-Src peptide in hand, the screen was set up, enabling the identification of potential inhibitors of the UNC119/Src interaction.

2.3.1.2.3. Ras Family Peptides

Following already published protocols, three different Ras based peptides were synthesized using standard solid phase peptide synthesis (SPPS) techniques. The prepared Lys **2** was coupled to the Wang resin. The OAll- protecting group was selectively removed using Palladium (Pd). Coupling of the building block **4** was then performed before peptide elongation using Fmoc strategy (Figure 16). Three different peptide needed to be prepared to evaluate the COMAS library toward the PDE6δ/K-Ras4B cargo. Peptides containing different number of Lys were prepared. According to the protein sequence, the peptide containing the five lysine moiety should lead to a mutation in the sequence instead of an insertion which was predicted to have less of an effect on the protein.
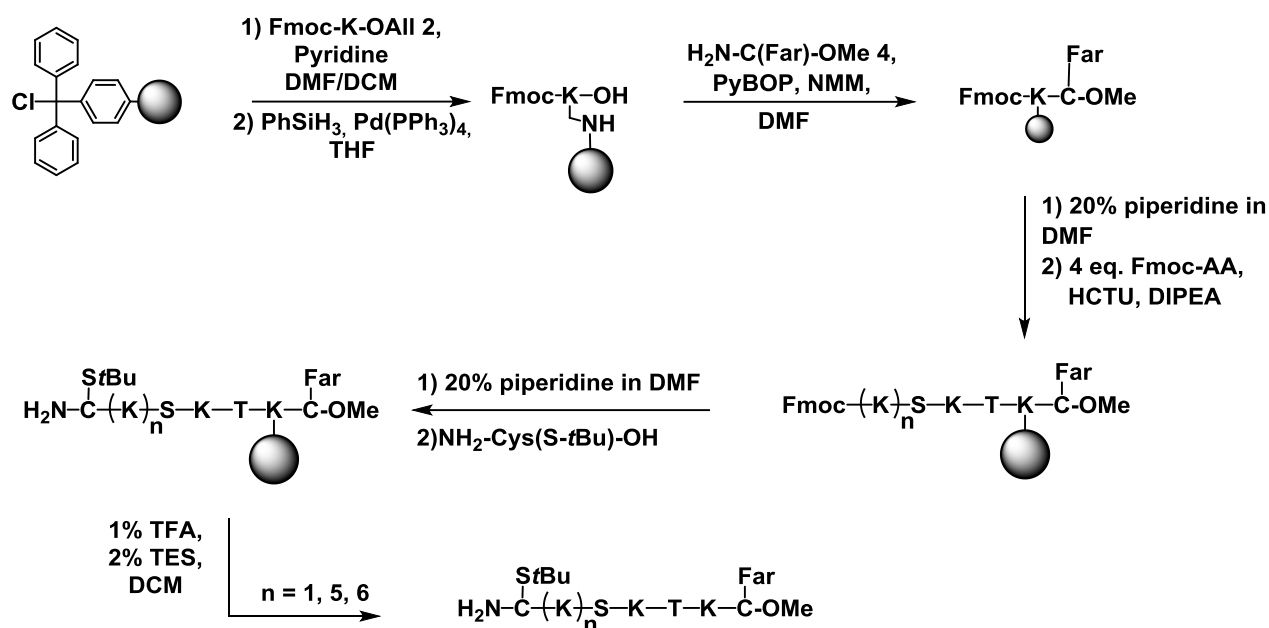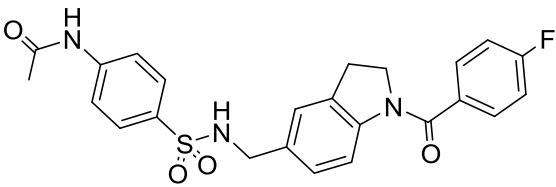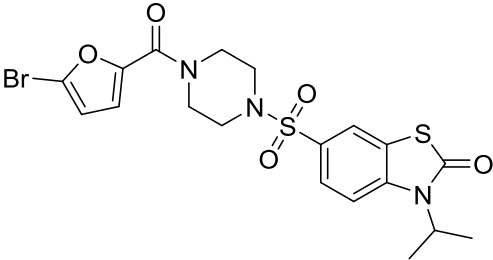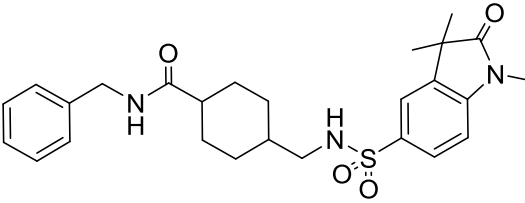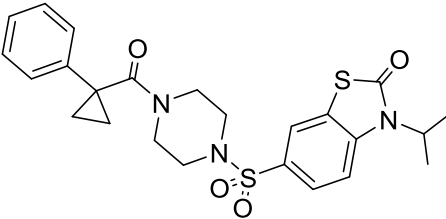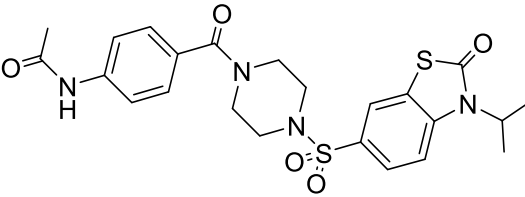
Figure 16. Synthesis of K-Ras analogs peptides using SPPS. Chemicals: DCM: Dichloromethane, DMF: Dimethylforamide, HCTU: (2-(6-Chlor-1H-benzotriazol-1-yl)-1,1,3,3-tetramethylaminium-hexafluorophosphate), DIPEA: N,N-Diisopropylethylamine, NMM: N-Methylmorpholine, PyBOP: Benzotriazol-1-yl-oxytripyrrolidinophosphonium hexafluorophosphate, TES: Triethylsilane and TFA: Trifluoroacetic acid.
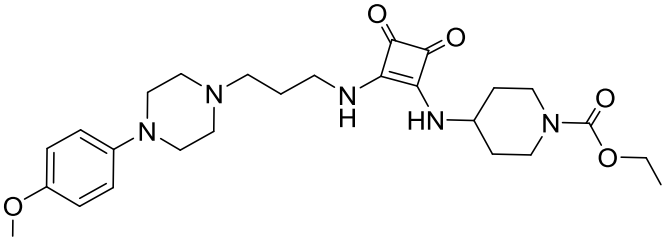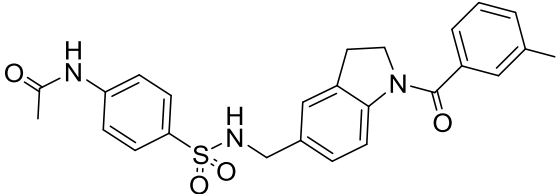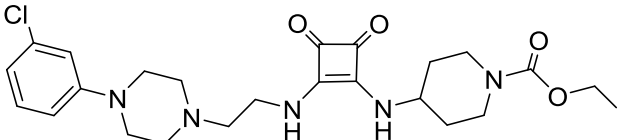
The three different analogs contained a varying number of Lys residues. The shorter analogs (n = 1 and 5) were obtained in an overall yield of 14% and 9%, respectively. The full-length K-Ras4B peptide (n = 6) was obtained in an acceptable overall yield of 8%, which was in accordance with the literature.[81] These peptides were designed for optimizing a screen in order to evaluate new inhibitors of the PDE6δ/K-Ras4B cargo.

2.3.1.3. Evaluation of Hits from the Initial HTRF Screen and Hit Selection

The in-house chemical library was screened and around 250,000 compounds were evaluated for the inhibition of the Src/UNC119 interaction. The next step was to filter the compounds according to their chemical structure in order to prioritize hits and remove undesirable compounds such as PAINS. This allowed the identification of more than 50 compounds with an IC_{50} below 1 µM (Table 2).

Table 2. Selected examples of UNC119A/Src cargo inhibitors after the first HTRF screening.*

Entry	Compound ID	Structure	IC_{50} (µM)
1	260890		0.20
2	199464 (Inhibitor **1**)		0.11
3	213701		0.58
4	199467		0.43
5	199469		0.41

6	203645		0.36
7	260796		0.29
8	203646		< 0.075

The promising 50 molecules, identified during the screen, were clustered and three compound classes, based on a benzothiazolone, a squaramide and an indoline scaffold, were selected for further characterization and SAR studies (Figure 17).
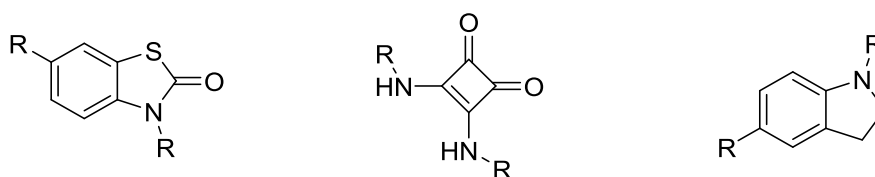
Figure 17. Promising scaffolds selection after the initial screen of the in-house library.

2.3.2. Synthesis of a Benzothiazolone-Based Compound Collection

The HTRF screen allowed the identification of three promising compound classes for disrupting the UNC/Src cargo interaction. For the benzothiazolone-based compound class, a compound collection needed to be prepared in order to optimize the properties and thereby obtain a potent inhibitor of the UNC119/Src cargo.

2.3.2.1. Retrosynthesis Evaluation

In order to establish a feasible synthesis route, a retrosynthetic analysis of the benzothiazolone compounds was performed (Figure 18). The first disconnection led to an already reported chlorosulfonylated benzothiazolone scaffold. The preparation of the chlorosulfonylated benzothiazolone derivatives is already known and can be achieved using chlorosulfonic acid as a reagent. The functionalization of the nitrogen of the benzothiazolone core could be performed using a nucleophilic substitution involving an alkane chain with a leaving group such as iodide or bromide.
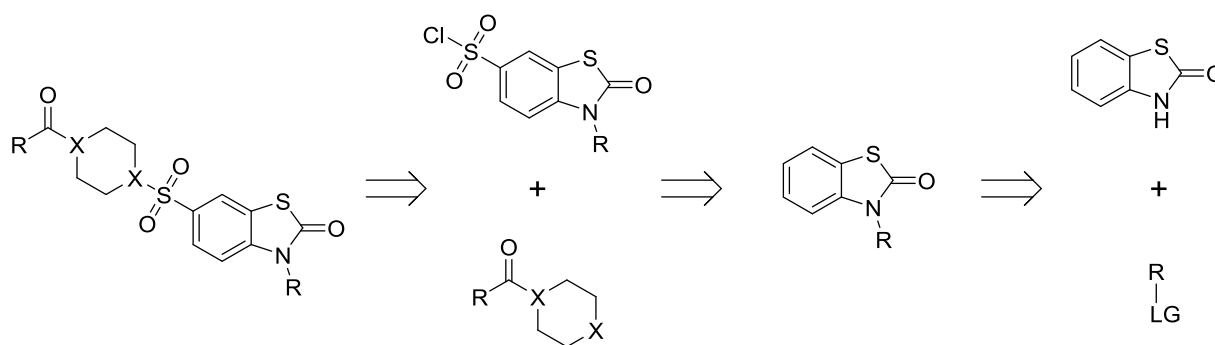
Figure 18. Retrosynthetic analysis of the benzothiazolone scaffold.

2.3.2.2. Synthesis of Benzothiazolone Derivatives

The synthesis of benzothiazolone-based compounds was achieved following the optimized route shown in Figure 19. The screening of different conditions was necessary for the coupling of the isopropyl moiety to the nitrogen of the benzothiazolone core. The best condition was the use of 2-iodopropane in DMF with sodium hydride as a base for 3 h yielding the core scaffold **5** in 69%.
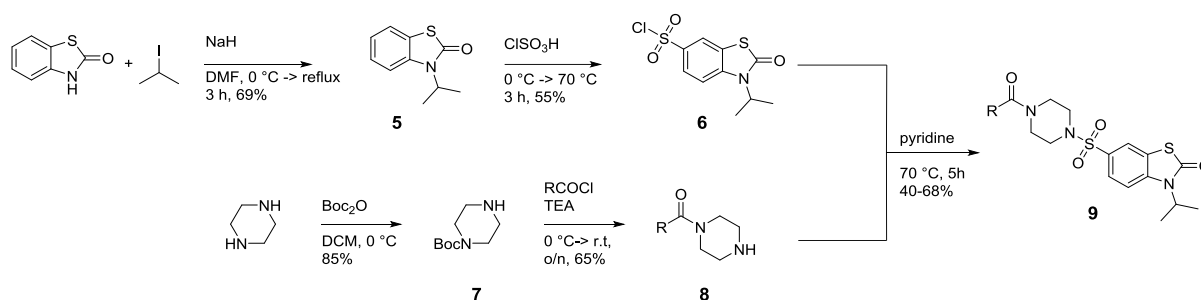
Figure 19. Optimized synthetic route of the benzothiazolone scaffold. Chemicals: Boc₂O: Boc anhydride, ClSO₃H: chlorosulfonic acid, DMF: dimethyl formamide, NaH: sodium hydride and TEA: triethylamide.

The chlorosulfonylation of **5** was performed following a reported procedure.[88] The functionalized piperidine fragment **8** was prepared in three steps: mono Boc-protection of piperidine (**7**), subsequent acylation and final removal of the Boc group. The final step was performed by mixing both fragments in pyridine at 70°C for 5 h leading to the target compounds **9**.

2.3.3. Structure-Activity Relationship for the Benzothiazolone-Based Compound Collection

Studying the structure-activity relationship (SAR) of a compound class is an important step in the development of a potent inhibitor. Certain modifications of the molecule could lead to an increase of the potency and enhance the biophysical parameters.

Analyzing the activity of compound series with only one individual modification is an important criterion for SAR studies, as this enables a correlation between each substitution and the changes in activity. The information obtained gives precious information for the design of optimized inhibitors. The different modification points examined are shown in Figure 20.
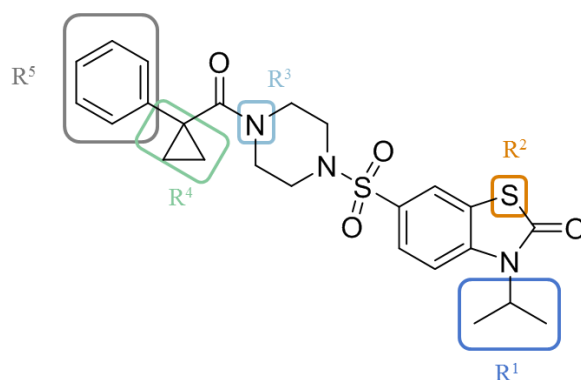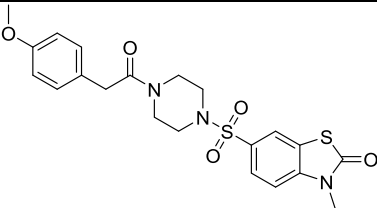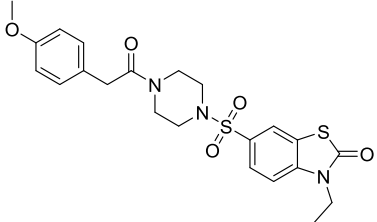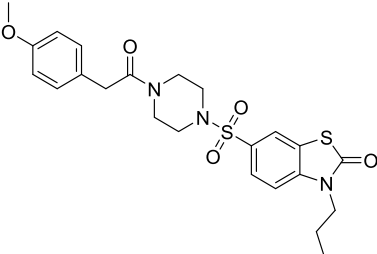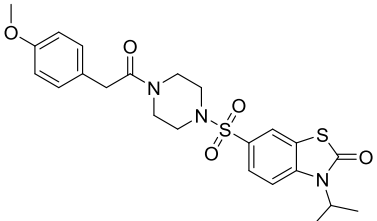
Figure 20. Chemical structure of the hit of the original screen and functional group modifications for a SAR study.

2.3.3.1. Relevance of the Isopropyl Group (R^1)

A preliminary SAR from the few analogs already present in the COMAS library showed that the substitution of the nitrogen in the benzothiazolone scaffold significantly impacts activity. Because this substitution is the first step in the synthesis of the compound collection, this point was the first one to be studied (Table 3).

Table 3. Substitution of the R^1 position of the benzothiazolone scaffold.
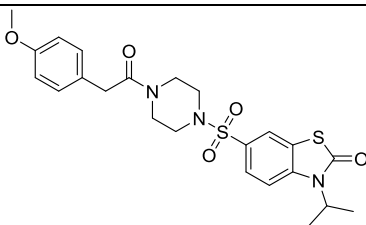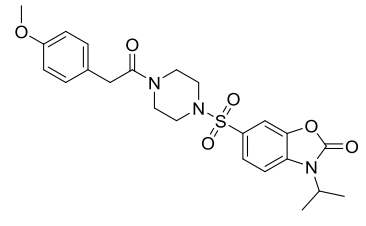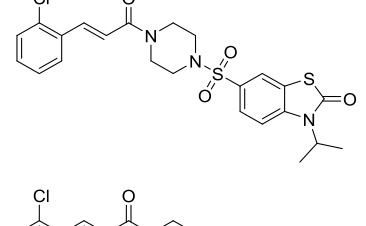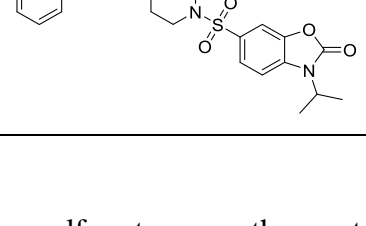
Entry	Structure		IC$_{50}$ (nM)
1		(10)	Inactive
2		(11)	555 ± 66
3		(12)	96 ± 5
4		(13)	74 ± 9

Based on this family of inhibitors, the substitution around the nitrogen of the benzothiazolone scaffold is poorly accessible. Whereas the methyl (Table 3, Entry 1) and ethyl (Entry 2) substitutions lead to a decrease of the potency, the isopropyl (Entry 4) delivered the best activity. Bigger and smaller group than isopropyl led to a decrease of potency.

2.3.3.2. Relevance of the Benzothiazolone Core Structure (R^2)

Because of the similarity between the indoline-based scaffold and the benzothiazolone-based scaffold, the importance of the sulfur of the benzothiazolone moiety needed to be investigated. Given that a few derivatives in the chemical library with an indoline and indole scaffold also showed activity in the primary screen, the impact of introducing other heteroatoms such as oxygen or nitrogen was evaluated (Table 4).

Table 4. Relevance of the sulfur atom of the benzothiazolone scaffold.
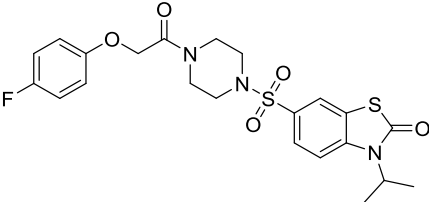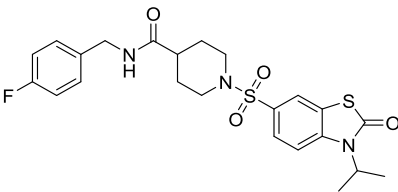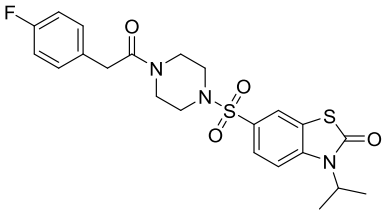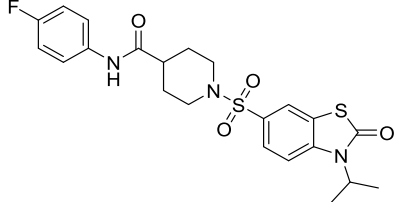
Entry	Structure		IC_{50} (nM)
1		(13)	74 ± 9
2		(14)	129 ± 9
3		(15)	35 ± 10
4		(16)	38 ± 3

The compound with a sulfur atom was the most active (Table 4, Entry 1). Substitution with an oxygen leads to a slight decrease of the activity (Table 4, Entry 2). Comparing compound **15** and **16** (Table 4, Entries 3 and 4), no evident conclusion was possible at that stage. Because few compounds in the original hits were based on the benzothiazolone scaffold, the compound collection was prepared using this scaffold.

2.3.3.3. Relevance of the Piperazine Functionality (R^3)

After exploring the benzothiazolone core scaffold, studying the influence of the substitution of the nitrogen atom and the relevance of the sulfur atom, the substitution of the piperazine moiety was examined. Most of the compounds in the library used for the primary screen contained a piperazine ring. In order to study the effect of this nitrogen atom, several compounds with a piperidine moiety were also investigated (Table 5).

Table 5. Structure activity relationship of the piperazine moiety.

Entry	Structure		IC$_{50}$ (nM)
1		(17)	28 ± 3
2		(18)	9 ± 4
3		(19)	50 ± 2
4		(20)	86 ± 40

When comparing Entry 1 and Entry 2 (Table 5), a three-fold increase in activity was observed when the piperazine moiety was substituted by a piperidine. However, because the two compounds have more than one modification, it was difficult to reach a conclusion regarding the importance of the piperazine moiety. However, compound **18** showed a good potency (Table 5, Entry 2). While comparing Entries 3 and 4, the piperazine derivative seems to be slightly more potent. Nevertheless, in both cases, the potency is similar, indicating that this part of the molecule could be varied without significant losses in activity.
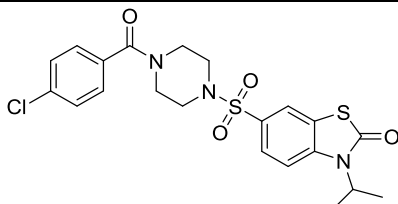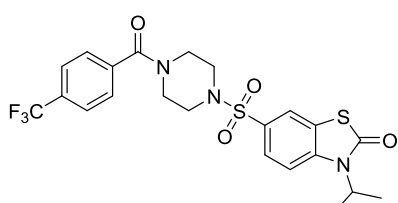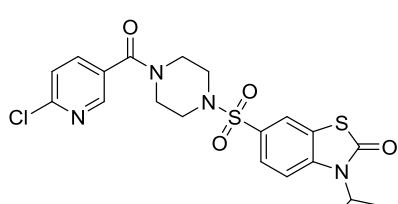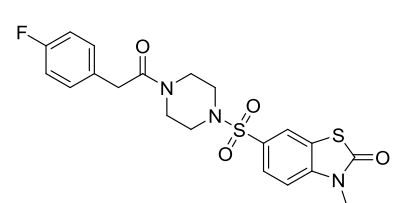
2.3.3.4.   Relevance of the Linker (R⁴)
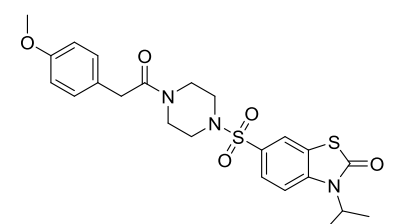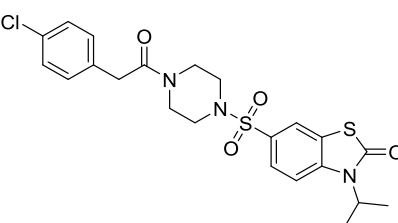
The molecular weight and the size of a molecule are two important parameters to consider while optimizing a lead compound. Therefore, the length of the spacer between the piperazine moiety and the phenyl group R⁵ was studied next. For this purpose, alkane chains, conjugated double bonds, ethers and amines were investigated.

2.3.3.4.1.   Influence of the Alkyl Chain Size

Investigating the effect of the space length between the piperazine and the phenyl group was interesting for several reasons. Potentially increasing the potency of the molecule was one, as well as evaluating the impact of the spacer size. This could be interesting for the design of a biological probe (Table 6).

Table 6. SAR of the alkane chain length.

Entry	Structure		IC$_{50}$ (nM)
1		(21)	73 ± 13
2		(22)	164 ± 10
3		(23)	50 ± 3
4		(19)	50 ± 2
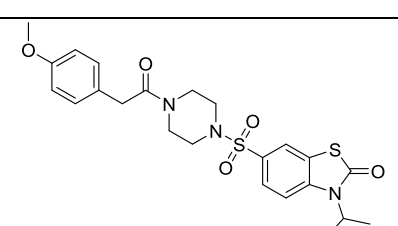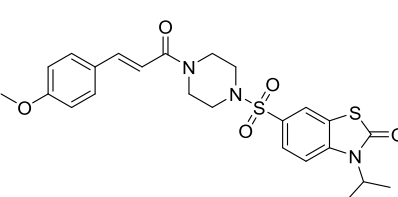
| 5 | | **(13)** | 74 ± 9 |

| 6 | | **(24)** | 40 ± 2 |

Molecules with the phenyl group directly attached to the carbonyl (Table 6, Entries 1-3) were compared to molecules with one more carbon spacer between R^5 and the carbonyl group (Table 6, Entries 4-6). Based on the potency of these six inhibitors, no evident correlation between the length of the alkane chain and the potency was observed. The molecules showed in entries 5 and 6 are slightly more potent which could indicate that an extension of the distance between the carbonyl function and the benzyl group leads to more potent compounds. However because substituents on the phenyl ring are different, the results indicated that modification are tolerated in this part of the molecule.

2.3.3.4.2. Influence of a Conjugated Functionality

The compound collection included several conjugated compound between the piperazine moiety and the benzyl group R^5. Compared to the alkane chains in the previous section, the 1,4-conjugated compounds have an additional carbon spacer (Table 7).

Table 7. SAR of the conjugated double bond derivatives.

Entry	Structure		IC$_{50}$ (nM)
1		**(13)**	74 ± 9
2		**(25)**	19 ± 2

| 3 | | (26) | 9 ± 2 |
| 4 | | (9a) | 61 ± 21 |

Optimization of the inhibitor was based on the *para*-O methoxy derivatives identified early on during the initial screen and with a good potency (Entry 1). Using the conjugated system based on this original hit, we identified a four-fold more potent inhibitor (Entry 2). Other derivatives bearing this 1,4-conjugated double bond showed an even higher potency (9 nM, Entry 3), reaching the detection limit of the screening set up.
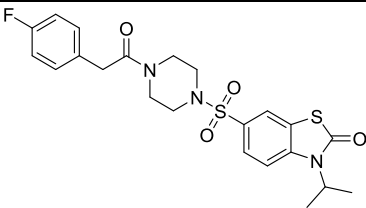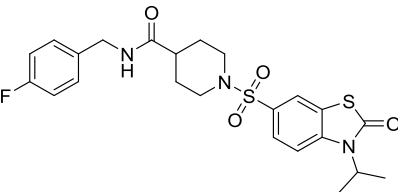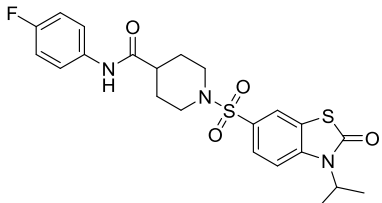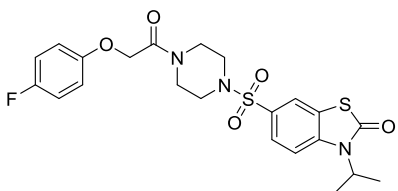
Conjugated double bonds, often used for covalent inhibitors, are often avoided in the design of non-covalent inhibitor. Because of their reactivity these compounds can behave as Michael acceptors and can give false positive results. As they are considered PAINS, these types of molecules are typically avoided in most lead optimization efforts. In order to investigate if the compound behaved as a Michael acceptor, a naphthalene derivative was evaluated (Entry 4). The naphthalene moiety should serve as a bioisostere of the conjugated system.[89]

The naphthalene derivative showed remaining good potency compare to a phenyl derivative (Table 7, Entries 3 and 4). This indicated that a 1,4-conjugated system is not only required for high potency. These results suggested that inhibitor **26** does not covalently bind to the target. Further MS measurements with the purified protein will be necessary to draw a final conclusion.

2.3.3.4.3. Influence of Heteroatomic Groups

The introduction of a spacer length of two to three atoms delivered the most potent inhibitors. After looking at different alkanes (Chapter **3.4.4.1**) and conjugated moieties (Chapter **3.4.4.2**), an ether and amide functionality were evaluated. Amide bonds are ubiquitous in peptides and proteins, which makes them an interesting modification in the optimization of a screening hit.

Table 8. SAR studies of the ether and amide bond derivatives.
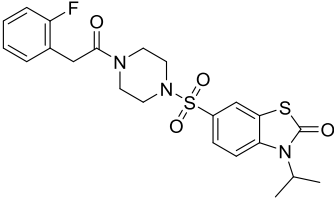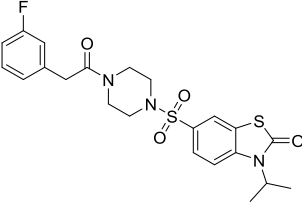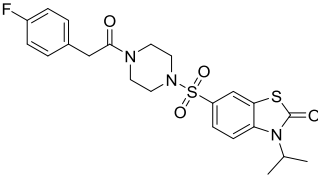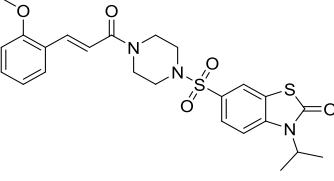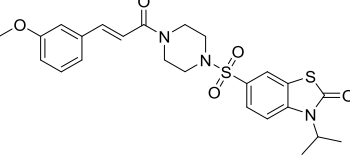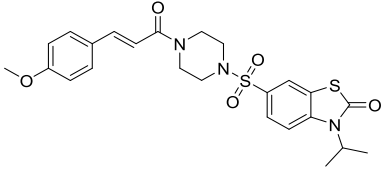
Entry	Structure		IC$_{50}$ (nM)
1		(19)	50 ± 2
2		(18)	9 ± 3
3		(20)	86 ± 40
4		(17)	28 ± 3

In Table 8, several analogs of the *para*-F substitution (Entry 1) are presented. The amide bond derivatives showed a five-fold increase in activity and hence afforded a low nanomolar potent compound (Entry 2). When shortening the spacer by one carbon, a decrease in activity was observed, which is consistent with the finding in Chapter **2.3.4.4.1.** (Entry 3). Introducing an ether bond instead of an amide bond showed a slight decrease in activity (Table 8, Entries 2 and 4).

2.3.3.5.   Relevance of the Phenyl Functionality (R^5)

The last interesting position to investigate was the substitution around the phenyl group R^5. The substitution pattern around the phenyl group (*ortho*, *meta* and *para*) was investigated (Table 9). For this purpose, we selected two different families of the top compounds, containing either alkane with one carbon (Entries 1–3) or the 1,4-conjugated system (Entries 4–6) as a spacer.

Table 9. SAR around the phenyl group R^5.

Entry	Structure		IC$_{50}$ (nM)
1		(27)	142 ± 6
2		(28)	65 ± 4
3		(19)	50 ± 2
4		(29)	79 ± 5
5		(30)	57 ± 8
6		(25)	19 ± 2

The *ortho*-fluorine substitution afforded a potent compound (Table 9, Entry 1). The *meta*-fluorine substitution (Table 9, Entry 2) resulted in a two-fold increase in potency and the *para*-substitution an even slightly more potent compound (Table 9, Entry 3). The same substitution pattern was observed for the compounds bearing a conjugated double bond at R^5 (Table 9, Entries 4–6). Generally the potencies are very similar, which suggests that modifications are well tolerated at this site.

2.3.3.6. Relevance of Additional Modifications

During the SAR study, other positions and substituents were investigated. For example, heterocycles and substitution of the side chains in alpha to the carbonyl were also interesting in order to fully understand the SAR. A summary of these modifications is shown in Table 10.

Table 10. Additional substitutions and positions evaluated in the SAR study of benzothiazolone scaffold.

Entry	Structure		IC$_{50}$ (nM)
1		(31)	95 ± 20
2		(32)	125 ± 16
3		(13)	74 ± 9
4		(33)	454 ± 8
5		(34)	109 ± 44

Introduction of a heterocycle, such as an indole (Table 10, Entry 1) or a 1,3-benzodioxiole (Table 10, Entry 2) did not improve the activity of the compound. Substitution of the aliphatic chain (Table 10, Entry 4) leads to a seven-fold decrease of the activity (compare with Entry 3). Introduction of small heterocycles such as furan leads to a slight decrease of the activity (Table 10, Entry 5).

2.3.3.7. Conclusion

A SAR study was performed on the promising benzothiazolone scaffold identified during the initial HTRF screening and is summarized in Figure 21.
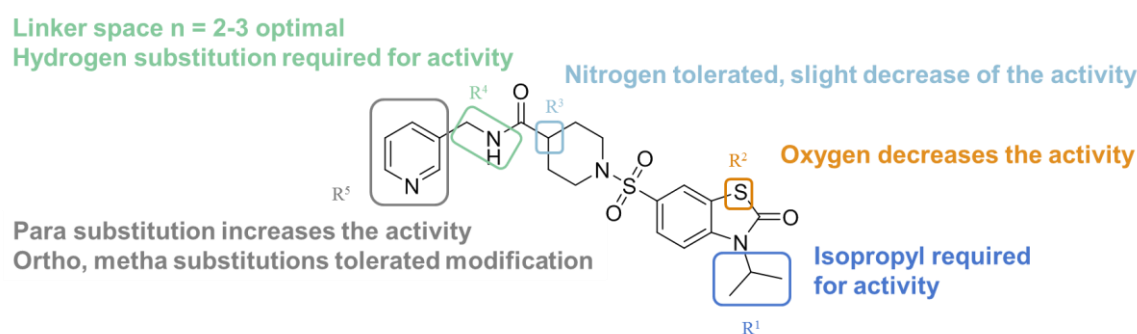
Figure 21. SAR summary of the benzothiazolone scaffold.

The substitutions around the benzothiazolone core were barely tolerated. The isopropyl group on the nitrogen R^1 was best for the potency of the molecule. Substitution of the sulfur R^2 by an oxygen or nitrogen delivered marginally less potent inhibitors. The substitution of the nitrogen (R^3) of the piperazine moiety led to slightly more potent inhibitors. Spacer length between the carbonyl group and the aromatic ring proved to be tunable: Linker size between two and three were optimal regardless of the amide substitution or the conjugated double bond. The substitution around the aromatic ring showed the *para-* position to be the most favorable.

The HTRF screening and the different rounds of optimization enabled the identification of a low nanomolar inhibitor interacting with the UNC119A and myristoylated-Src (**18**, Figure 22) and the understanding of the SAR around the scaffold.
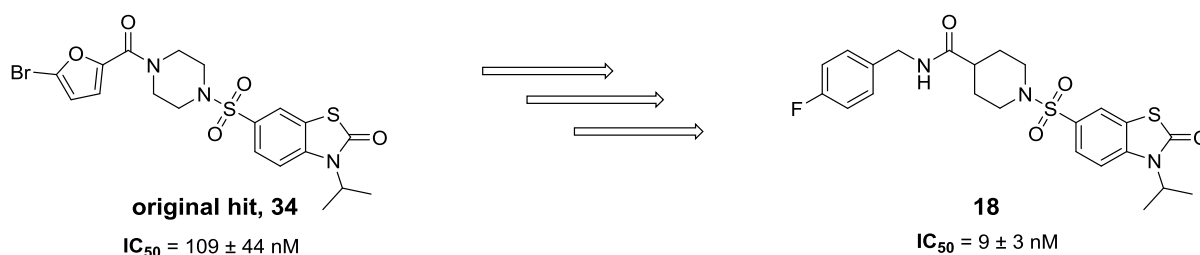
*Figure 22. Summary of the round optimization leading to the low nanomolar inhibitor **18**.*

2.3.4. Bio-Physical Evaluation of the Benzothiazolone Inhibitors

Further characterization of the best inhibitors, before phenotypic investigations, is a crucial step. Important parameters such as selectivity, solubility and toxicity toward cell growth need to be evaluated. A low nanomolar inhibitor with a poor solubility for example will not be a useful tool compound for studying the biological impact of a small molecule.

2.3.4.1. Selectivity of the Inhibitor Towards Lipid Binding Proteins

This experiment was performed by Dr. Eyad Fansa.

As described in Chapter **2.1.2**, UNC119 is a lipid-binding protein able to accommodate lauroylated and myristoylated proteins. The selected compound was evaluated against a panel of lipid binding proteins. PDE6δ[61], Calmodulin[90] and AILP1[91] which are able to accommodate a farnesylated protein, as well as a RhoGDI[60] which is able to accommodate a geranylgeranyled protein were selected (Figure 23). Because of the ability of the compound to disrupt the interaction between UNC119A and Src, it was necessary to evaluate his selectivity toward lipid binding protein able to accommodate similar lipidated proteins.

The selectivity towards the lipid binding proteins was measured by means of a FP assay. In this assay, fluorescently-labeled peptides representative for the respective cargo were chosen. These are the myristoylated Src-peptide for UNC119A, S-farnesylated Rheb-peptide for PDE6δ, AIPL1 and Calmodulin or a geranylgeranylated Rab peptide for RhoGDI. Binding to the specific binding partner leads to an increase of the fluorescence polarization signal. Competitive binding of the small molecule ligand induces release of bound peptide and thereby reduction of the polarization signal.
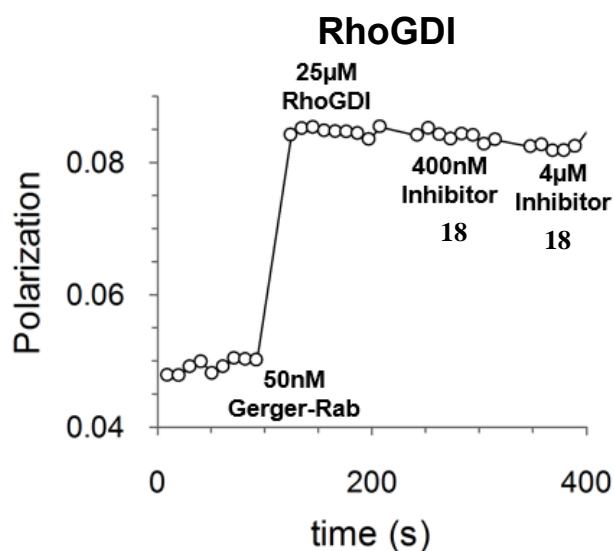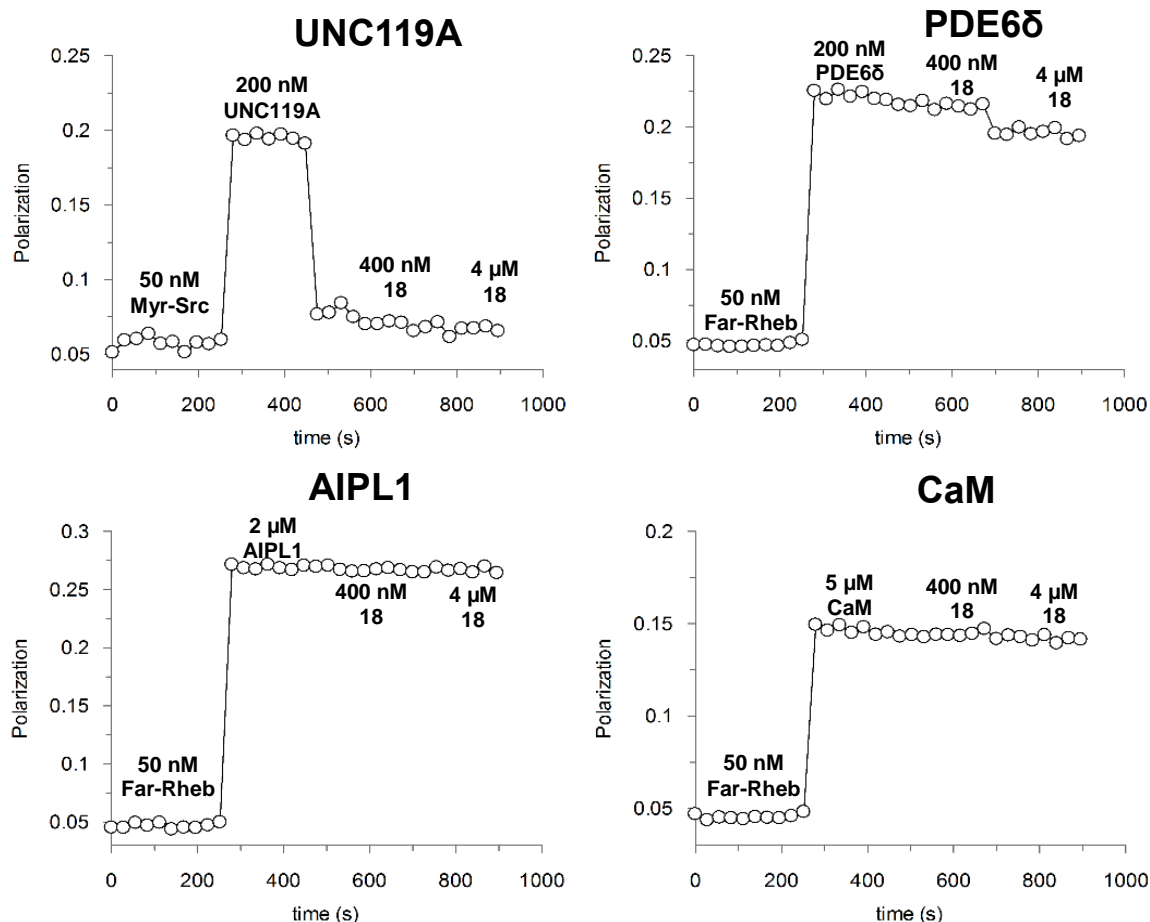
*Figure 23. Fluorescence polarization assay to determine selectivity of compound **18**. Fluorescently labeled lipidated peptides (Myr-Src, Far-Rheb and GerGer-Rab) were incubated with the respective binding partner (UNC119A, PDE6δ, AIPL1, CaM and RhoGDI). Upon addition of lipid binder, polarization increased due to the increase of mass. After addition of inhibitor, polarization decreases indicating release of bound peptide. Experiments performed by Dr. Eyad Fansa.*
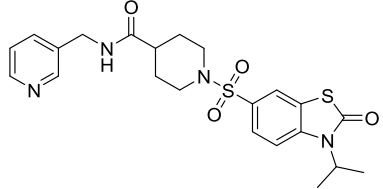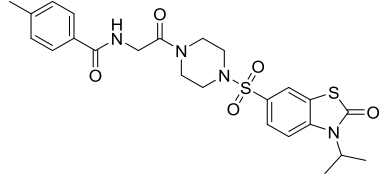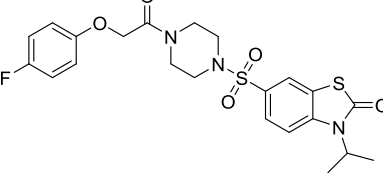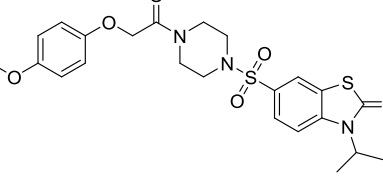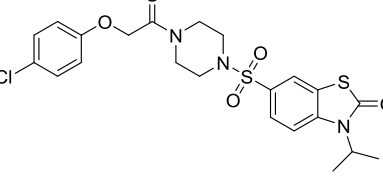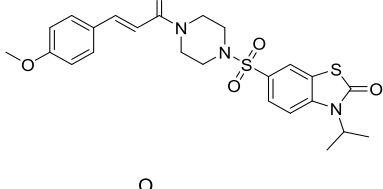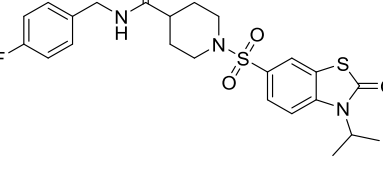
Figure 23 shows that an excess of compound selectivity releases the N-myristoylated Src-peptide from UNC119 whereas no displacement of the lipidated cargo from the farnesyl binding proteins PDE6δ, Calmodulin and AIPL1 was detected. In addition, no displacement of a geranylgeranylated peptide from the geranylgeranyl protein binding RhoGDI was observed. The optimized compounds selectively targets UNC119A.

2.3.4.2. Solubility Determination

The next important parameter to evaluate was the solubility of the most potent compounds. This measurement was performed using kinetic solubility experiments. The relative kinetic solubility of test compounds in aqueous buffer was calculated by measuring the spectrophotometric absorbance between 250 and 500 nm and comparing the recorded absorbance value to a 50% organic solution in acetonitrile as a high control.

During the several rounds of SAR analysis, the kinetic solubility of several hits was evaluated (Table 11).

Table 11. Kinetic solubility determination of the top hits.* n.d. Not determined.

Entry	Structure		IC$_{50}$ (nM)	Kinetic solubility (µM)
1		(35)	12 ± 5	$375.9 \pm$ n.d.
2		(36)	18 ± 2	38.5 ± 1.5
3		(17)	28 ± 3	25.9 ± 1.5
4		(37)	15 ± 1	24 ± 5.9
5		(38)	24 ± 4	12.8 ± 0.8
6		(25)	19 ± 2	10.1 ± 11.5
7		(18)	9 ± 4	$4.9 \pm$ n.d.

| 8 | | **(26)** | 9 ± 2 | 4 ± 1.1 |

*Experiment performed by the Lead Discovery Center (LDC).

The most potent compounds (lowest IC$_{50}$) were poorly soluble (Entries 7 and 8). Introduction of hydrogen bonding functions or heteroatoms are known to improve solubility. The compounds with the ether linkage as spacer (Entries 3-5) were further evaluated. These compounds, still low nanomolar inhibitors, showed a slightly increased solubility.

A compound with an amide bond (Entry 2) was also tested. Nevertheless, the solubility of this compound was in the same range as the one with the ether bond linkage (Entries 2 and 3).

Introduction of heterocycles may improve solubility. Introduction of a pyridine moiety (Entry 1) improved the solubility ten-fold compare to the most potent compound (compare Entries 1 and 8) whilst remaining very potent. This compound, **35**, was selected for the further biological experiments.

2.3.4.3.   Evaluation of the Toxicity for Inhibitor 35

After solubility evaluation, the toxicity of compound **35** toward cancer cells was evaluated. Using the Incucyte® live-cell microscope, the cancer cell line MDA-MB-231 was treated with **35** at different concentrations and their relative growth compared to the DMSO control was evaluated (Figure 24). The M.D. Anderson-Metastatic Breast-231 (MDA-MB-231) is a human triple negative breast cancer cell line.[92]

*Figure 24. Evaluation of the toxicity of the selected compound **35** toward MDA-MB-231 triple breast cancer cell line. DMSO was used as negative control and Dasatinib as positive control. N = 3, representative experiment shown.*

Compared to Dasatinib, used as a positive control, inhibitor **35** was less toxic to the MDA-MB-231 cells. This cell line was used based on the report for the development of Dasatinib. Treating the cells at different concentrations (1.1, 3.3 and 10 µM) did not show any difference. The confluency of the cells treated with inhibitor **35** was comparable to the DMSO treated cells (used as negative control). This data showed that this small molecule is not toxic toward this cell line.

2.3.4.4. Determination of Target Engagement using a Cellular Thermal Shift Assay

This experiment was performed by Nadine Kaiser.

Target engagement of compound **35** was determined in a complex cellular environment by means of a cellular thermal shift assay (CETSA).[93,94] This assay monitors the thermal stabilization of proteins upon binding to the ligand. Cell lysates are incubated with an unmodified hit compound and heated at different temperatures leading to partial denaturation. The abundance of peptides at each temperature can be used to construct a melting curve, which can be compared to the DMSO control curve. Tandem MS-MS analysis revealed stabilization of UNC119A and UNC119B in Jurkat cell lysate upon treated with compound **35** (Figure 25).
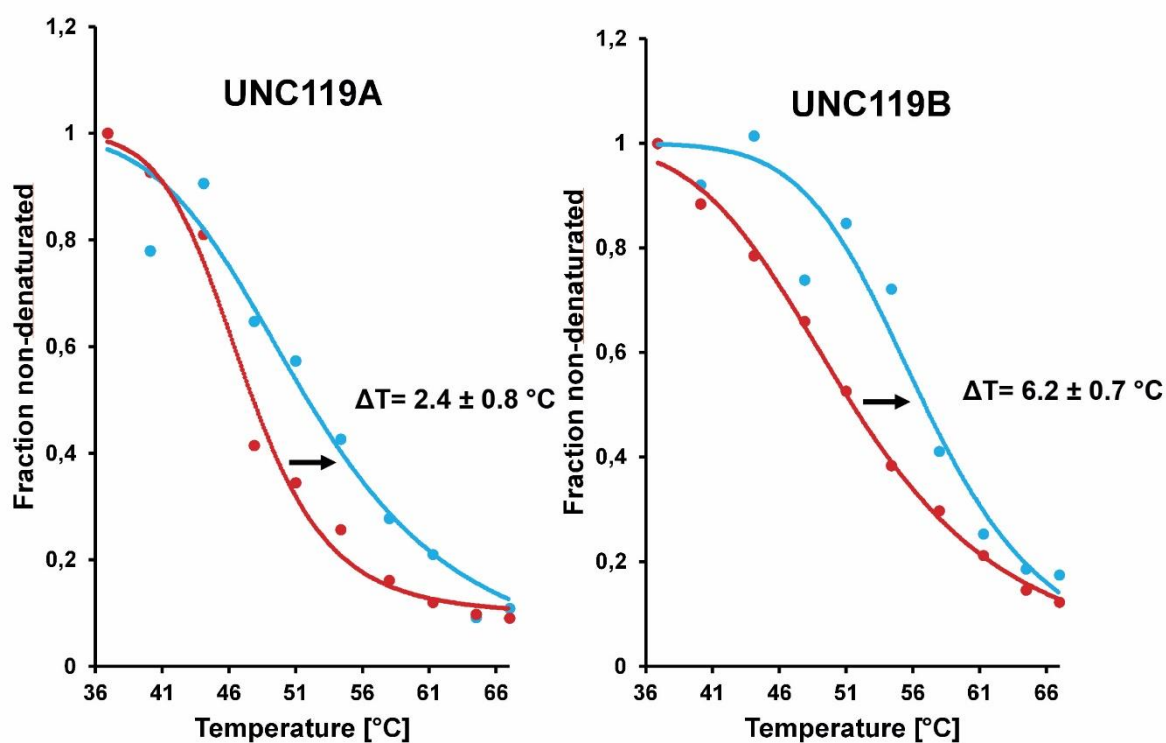
*Figure 25. Cellular thermal shift assay of UNC119 proteins upon treatment with DMSO control (red) and compound **35** (blue). Lysates from Jurkat cells were treated with compound 3 at 1 μM concentration, and thermal stabilization of the proteins was identified and quantified by means of tandem MS-MS analysis. Performed by Nadine Kaiser.*

Significant thermal shifts of $\Delta T = 2.4 \pm 0.8$ °C for UNC119A and $\Delta T = 6.2 \pm 0.7$ °C for UNC119B were measured. A stabilization or destabilization of PDE6δ under these conditions could not be observed, which confirms again selectivity of **35** for both UNC119 isoforms.

2.3.4.5. Conclusion

After the design and the evaluation of the potency of several low nanomolar inhibitors of the interaction between UNC119 and myristoylated Src peptide, several biophysical data were evaluated. The optimized compound interacted with UNC119A but did not interact with other lipid binding proteins such as PDE6δ, Calmodulin, AIPL1 and RhoGDI.

Solubility evaluation permitted to select the compound with the best activity: solubility ratio in order to perform further biological experiments. This evaluation showed that the most potent compounds were poorly soluble whilst the optimized pyridine derivative, which is known to improve solubility, was still highly active and showed the best solubility. Due to these results, inhibitor **35** was selected for further biological experiments.

Further evaluation and real time imaging of the growth of the triple negative breast cancer cell line (MDA-MB-231) was performed. Compared to Dasatinib, no effect towards the cells growth and no toxicity were observed.

A CETSA experiment showed target engagement with the small molecule for both isoforms of UNC119 and not for other lipid binding proteins. This confirmed the selectivity data observed and showed engagement in a more complex biological system for the desired targets.

2.3.5. Phenotypic Evaluation of Inhibitor 35

Using low nanomolar inhibitor **35**, further biological experiments were performed. The phenotypic response of targeting the UNC119 binding pocket was investigated. Because of it's important biological relevance for the kinase activity, the phosphorylation of Src at Y416 was monitored first.

2.3.5.1. In-Cell Western Assay

The In Cell Western assay (ICW) was developed to quantify intracellular signaling in whole cells. The In-Cell Western is an immune cytochemical assay performed in microplate format. Target-specific primary antibodies and infrared-labeled secondary antibodies are used to detect target proteins in fixed cells, and fluorescent signal from each well is quantified. The unique advantages of infrared fluorescence allow In-Cell Westerns to provide extremely sensitive and quantitative analysis of cellular signaling pathways in cultured cells in a higher throughput manner. In-Cell Westerns simultaneously detect two targets at 700 and 800 nm using two spectrally distinct dyes which allow the detection of two target proteins in their cellular environment. ICW has already been used to visualize tissue factors in human monocytes.[95]

As reported in Chapter **2.1.,** myristoylation and membrane localization of Src are two critical parameters for the kinase activity.[96] Inactive Src is phosphorylated at the regulatory tyrosine Y527 while phosphorylation of Y416 is required for activity. Dephosphorylation of Y527 leads to a conformational change and activate the kinase. The impact of the small molecule on the level of phosphorylation of Y416 using ICW was evaluated.

The conditions of the ICW protocol were initially optimized. Several parameters were then optimized such as primary and secondary antibody (Ab) concentrations. For this optimization, cells were treated with different concentrations of primary and secondary antibody and the phosphorylation level for MDA-MB-231 cells treated with the known kinase inhibitor Dasatinib was measured (Figure 26).
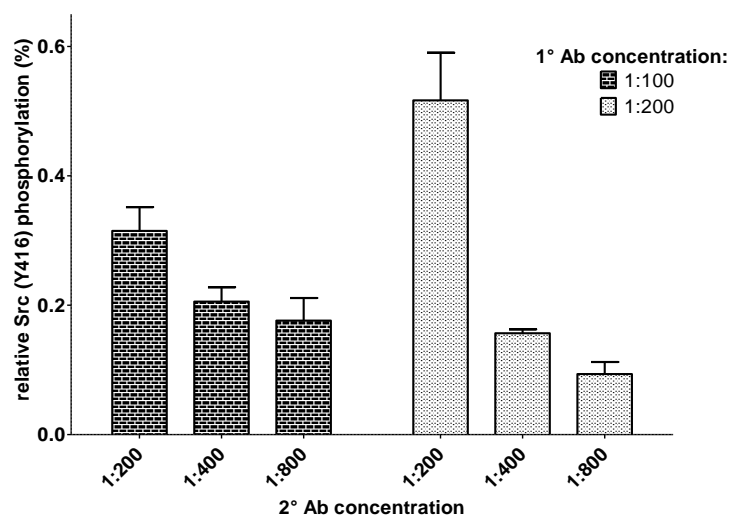
Figure 26. Primary and secondary antibody optimization of the ICW. MDA-MB-231 cells (1500 cells/well) were treated with a fixed concentration of Dasatinib (1.0 μM) and then treated with different concentration of primary (1:100 and 1:200) and secondary (1:200, 1:400 and 1:800) antibodies. Signal was normalized to the amount of total DNA. The data are expressed as mean ± SD, the experiment was repeated three times as a quadruplicate.

After treating MDA-MB-231 with a fixed concentration of a known Src family kinases inhibitor and several concentrations of primary and secondary antibodies, optimal conditions for the detection of the phosphorylation level of Y416 in the Src kinase were selected. For further experiments, 1:200 dilution for the primary antibody and 1:400 for the secondary antibody were selected for the assay. With an optimized protocol, Dasatinib was evaluated in the ICW assay in order to see the response of a known and characterized compound (Figure 27).
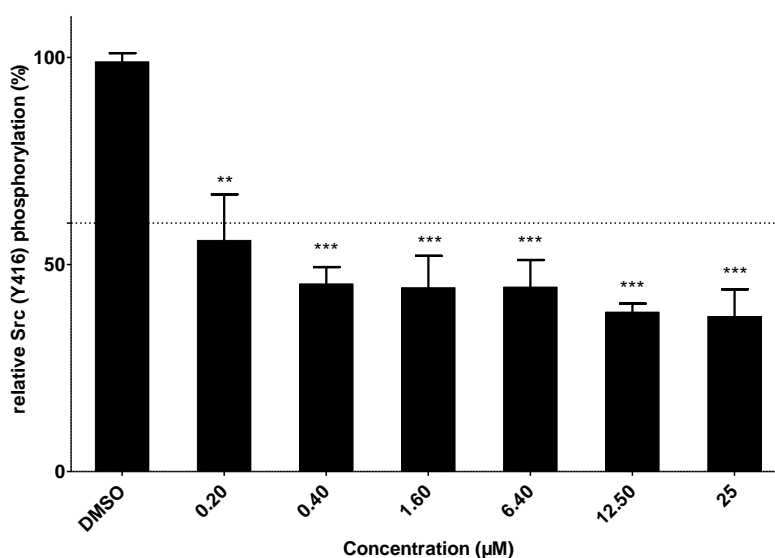
Figure 27. Impact on the phosphorylation of the Y416 while treatment with Dasatinib. MDA-MB-231 cells were treated for 24h at different concentration of Dasatinib. Signal was normalized to the amount of total Src in the cells. The data are expressed as mean ± SD, the experiment was repeated three times as a quadruplicate. The data significantly different from untreated DMSO controls (*** indicates $p < 0.001$, ** indicates $p < 0.01$, ns: non-significant) by Student's t-test.

Because of the residual signal present while treating cells with primary and secondary antibodies, the signal was always normalized to the residual signal. This background signal was the limit of detection of the ICW experiment. A strong impact of Dasatinib on the phosphorylation level of Y416 was observed. At 200 nM, a decrease of more than 50% of the phosphorylation level was observed. This result correlated with the known activity and the potency of Dasatinib toward this cell line.[76,97]

Compound **35** was then evaluated in the same conditions for the ICW (Figure 28). While treating the cells for 24 h at different concentrations of **35**, decrease of the phosphorylation level of the Y416 could not be measured. A slight decrease was observed for high concentrations such as 25 and 50 µM.
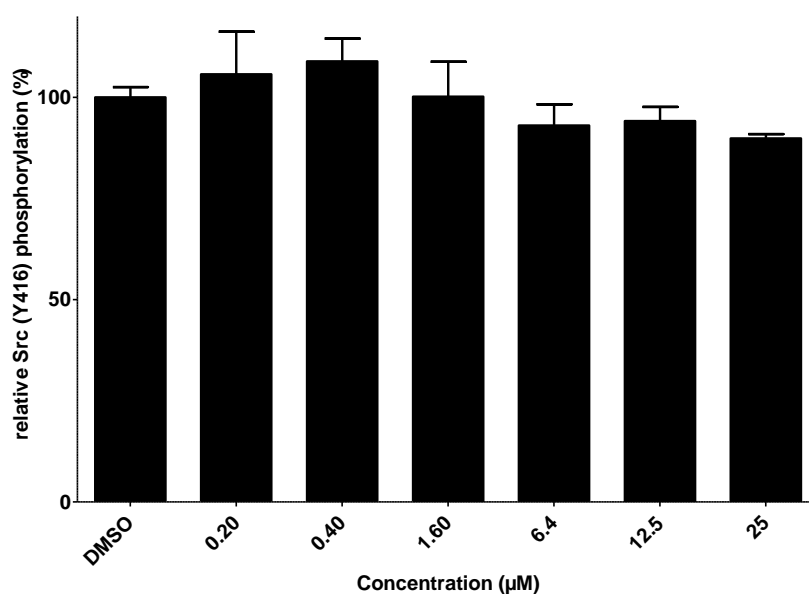
*Figure 28. Impact on the phosphorylation of the Y416 while treatment with compound **35**. MDA-MB-231 cells were treated for 24h at different concentration of Dasatinib. Signal was normalized to the amount of total Src in the cells. The data are expressed as mean ± SD, the experiment was repeated three times as a quadruplicate.*

Because of the small decrease of the Y416 phosphorylation level with compound **35,** an optimization of the parameters was necessary. Phosphorylation events are known to be fast in a cellular context.[98,99] For this reason, different time points were selected and the phosphorylation level of Y416 was determined. Initially, Dasatinib was investigated as the positive control (Figure 29).
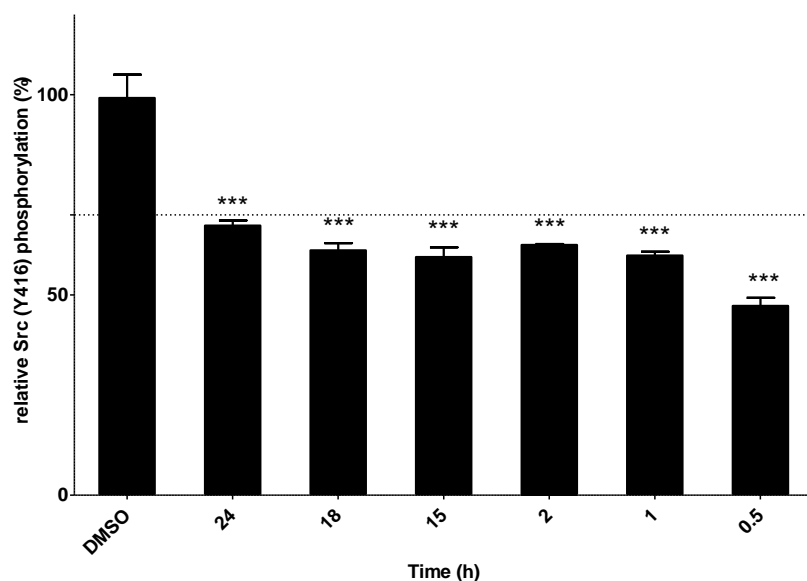
Figure 29. Impact on the phosphorylation of the Y416 while treatment with Dasatinib. MDA-MB-231 cells were treated at different time points using a fixed concentration of Dasatinib (3 µM). Signal was normalized to the amount of total Src in the cells. The data are expressed as mean ± SD, the experiment was repeated three times as a quadruplicate. The data significantly different from untreated DMSO controls (*** indicates $p < 0.001$, ** indicates $p < 0.01$, ns: non-significant) by Student's t-test.

The 24 h time point showed similar data than the previous ICW experiment. While the impact of the Y416 phosphorylation was not dramatically different, at 0.5 h the greatest decrease in phosphorylation was observed. It was then decided to re-measure compound **35** with the same time points in order to determine the best time to observed the impact of this compound on the phosphorylation level (Figure 30).
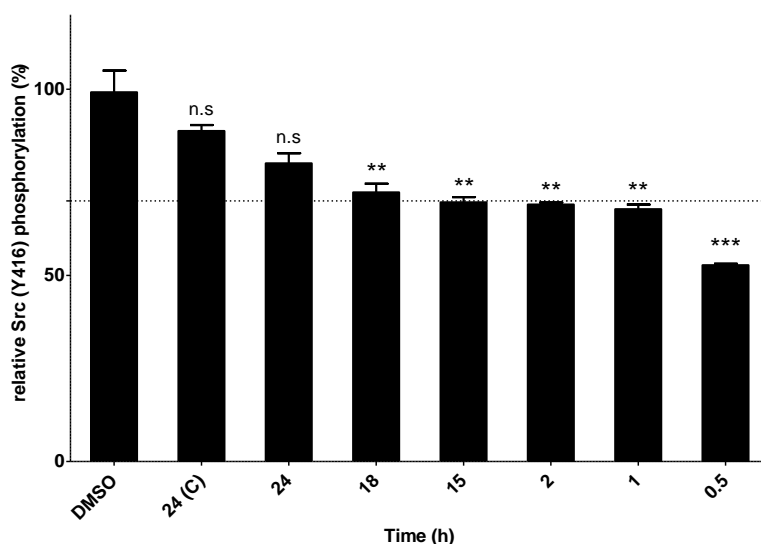
*Figure 30. Impact on the phosphorylation of the Y416 while treatment with compound **35**. MDA-MB-231 cells were treated at different time points using a fixed concentration of the small molecule (3 µM). Signal was normalized to the amount of total Src in the cells. The data are expressed as mean ± SD, the experiment was repeated three times as a quadruplicate. The data significantly different from untreated DMSO controls (*** indicates $p < 0.001$, ** indicates $p < 0.01$, ns: non-significant) by Student's t-test.*

The same tendency was observed for **35**. Although a slight difference could be observed while treating the cells for 18, 15, 2 and 1 hour, the most significant effect was observed after 30 min treatment. With this data in hand and the reference compound showing the same profile, the experiment was performed with 30 min treatment by the small molecule. The impact of Dasatinib was then re-measured and **35** in a dose dependent manner and evaluated the impact on the phosphorylation level of Y416 (Figure 31).
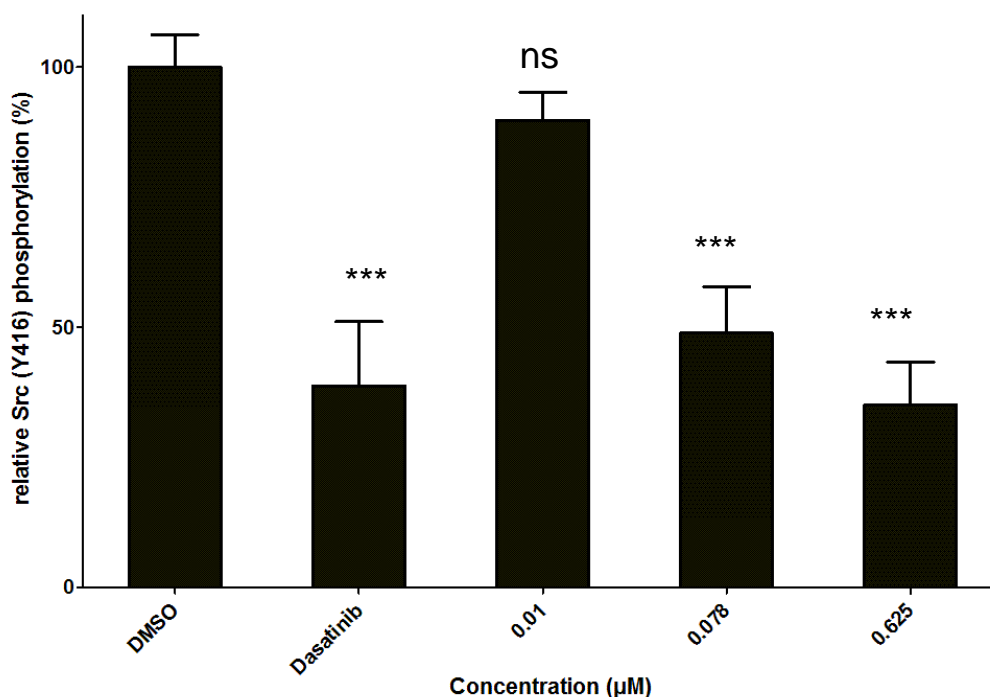
*Figure 31. Concentration dependence of treatment with compound **35** on the phosphorylation level of Src (Y416). The MDA-MB-231 cells were treated with DMSO (1%), **35** (625 nM, 78 nM and 10 nM) or Dasatinib (78 nM). The amounts of phosphorylated Src were normalized to the total protein. The data are expressed as mean ± SD, the experiment was repeated three times as a quadruplicate. The data significantly different from untreated DMSO controls (*** indicates $p < 0.001$, ** indicates $p < 0.01$, ns: non-significant) by Student's t-test.*

While treating the MDA-MB-231 cells with increasing concentrations of compound **35** for 30 min, the phosphorylation of Src (Y416) was reduced by 40% at 78 nM. The ICW experiment was carried out for two more scaffolds also identified using the HTRF screen and the data were consistent for the three compound classes.[100]

In the cellular context, phosphorylation may be partially controlled or rescued by other pathways and disrupting the interaction between UNC119 and Src may not be sufficient to completely abrogate the phosphorylation of Y416 and therefore the entire kinase activity.

2.3.5.2. Cell Migration

This experiment was performed by Walter Hofer.

Src signaling has been implicated in migration and metastasis, so interfering with this process might affect cell migration. To evaluate the impact of the compound on cell migration, a scratch assay was used to determine the effects of a treatment on cell migration parameters (speed, persistence and polarity).[101] MDA-MB-231 cells are grown to confluency and a thin "wound" introduced by scratching. Cells at the wound edge polarize and migrate into the wound space. Looking at the behavior of the cells upon treatment, this assay can deliver valuable information (Figure 32).
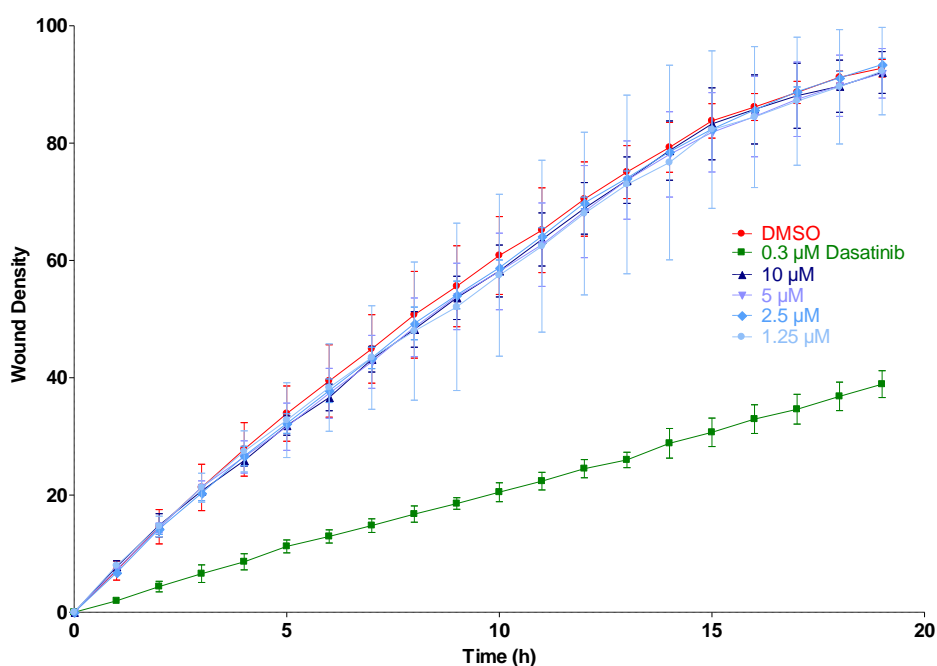
Figure 32. Wound density assay for compound 35. The data are expressed as mean ± SD, the experiment was repeated four times. Experiment performed by Walter Hofer.

Dasatinib, the reference compound, showed a decrease of wound density compared to the DMSO control. This showed that Dasatinib inhibited cell migration. Even at low concentrations (0.3 µM), the effect was significant. However, cells treated with **35** did not show any effect. Even at higher concentrations such as 10 µM, the migration of the cells was not affected.

2.3.5.3. Clonogenic Assay

This experiment was performed by Walter Hofer.

A clonogenic assay monitors the survival and proliferation of the cells after compound treatment as reflected in the colony size and colony number, respectively.[102] Since direct Src inhibition is known to lead to a reduction in cell growth in triple negative MDA-MB-231 breast cancer cells, this cell line was chosen for the clonogenic assay (Figure 33).[103]
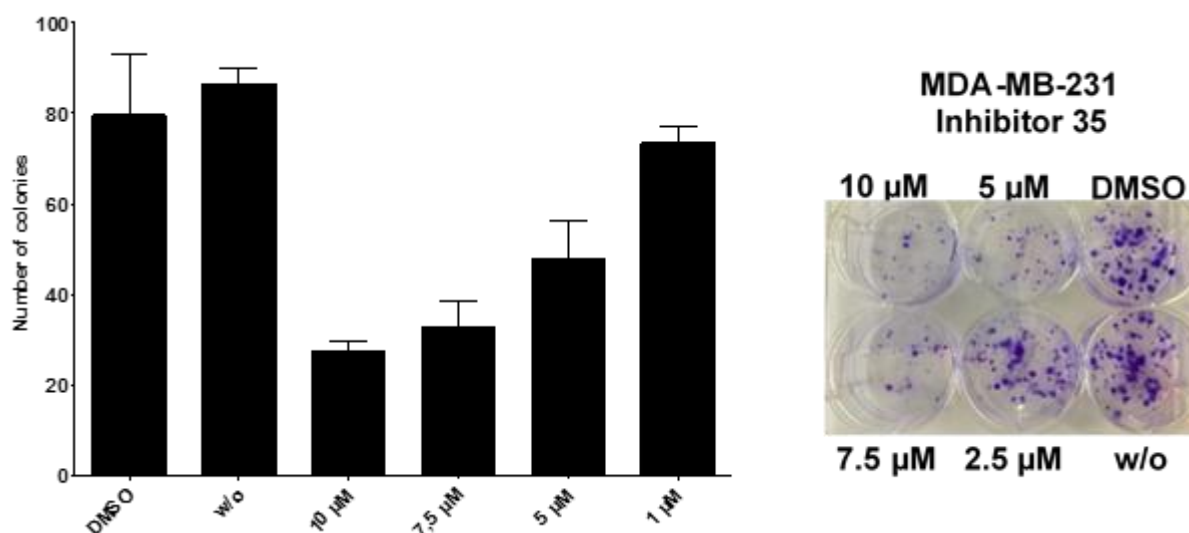
*Figure 33. Clonogenic assay. MDA-MB-231 cells were treated with indicated amount of inhibitor **35** (left). Images after treatment with **35** (right). Performed by Walter Hofer.*

Treatment of MDA-MB-231 cells with different concentrations of the inhibitor **35** for ten days led to a significant and dose dependent reduction in colony number and colony size, which is indicative of the impact of compound **35** towards cell survival.

2.3.5.4. Dynamic Src Localization

This experiment was performed by Dr. Antonios Konitsiotis.

Disrupting the interaction between cargo and lipid binding proteins in a living system was the target of the project. The interaction between myristoylated Src protein and UNC119 in live cells was characterized by means of fluorescence lifetime imaging microscopy of Förster resonance energy transfer (FLIM-FRET).

Similar experiments had previously been carried out for the characterization of an inhibitor blocking the interaction between PDE6δ and K-Ras4B farnesylated protein.[81] We sought to gain direct evidence of the disruption of UNC119 and myristoylated Src protein in a cellular environment, by compound **35**.

HeLa cells were transiently transfected with a mutant Src protein in which the C-terminal stretch are fused to mCitrine (Src6Q-mCit) and with UNC119A or UNC119B C-terminally fused to mCherry (UNC119A-mCh and UNC119B-mCh, respectively). The Src6Q-mCit mutant distributed to all membranes in the cell due to its rapid exchange between membrane surfaces. However, upon co-expression of both UNC119-mCh variants it exhibited a homogenous interacting fraction and solubilisation in the cytoplasm.[104] This facilitates the detection of small-molecule effects on the interaction between myristoylated Src proteins and UNC119 (Figure 34).
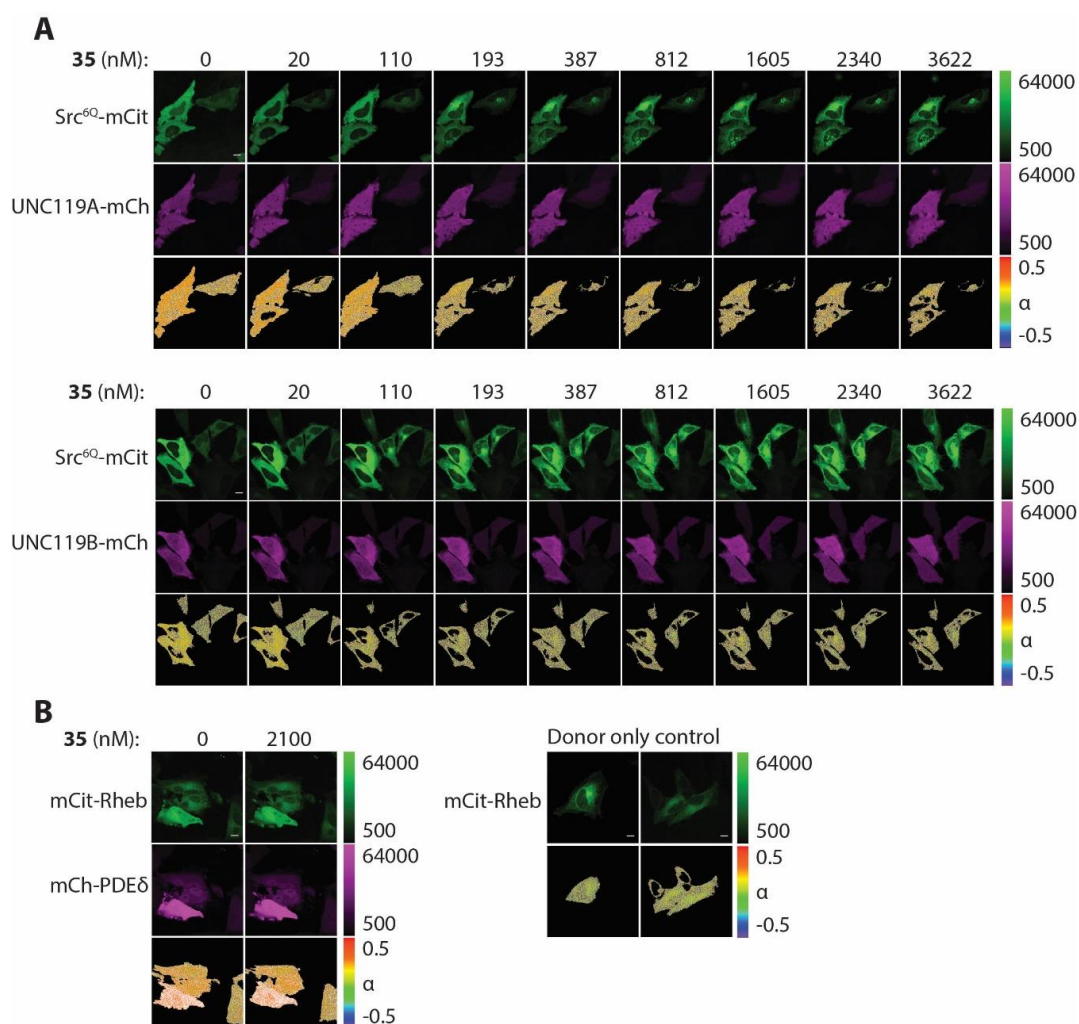
*Figure 34. **A**. Inhibition of the interaction between Src and UNC119 proteins in cells by compound **35** resulting in relocalization to endomembranes. FRET-FLIM of the interaction between Src6Q-mCit and UNC119A-mCh (top) or UNC119B-mCh (bottom) in HeLa cells with increasing concentrations of **35**. For each sample, the fluorescence intensity of Src6Q-mCit (donor), the fluorescence intensity of UNC119-mCh (acceptor) and the molar fraction of interacting molecules (α) are shown per the false-color look-up tables. Inhibitor concentrations are indicated above each image in nM. Dose response graphs on the right: fit of averaged dose-response of multiple cells (n=19 cells per condition) yielded an "in-cell" K_d of 111.3 ± 0.2 nM and 134.3 ± 4.1 nM UNC119A and UNC119B, respectively, for treatment with **35**. (n = 24 at least 3 independent experiments, data are mean ± S.E.M.), Scale bars, 10 μM. **B**. Representative FLIM measurements of the mCit-Rheb and mCh-PDEδ interaction with 2100 nM of 3. Upper and middle rows: fluorescence intensity of mCit-Rheb and mCh-PDEδ respectively. Lower rows: molar fraction α of interacting mCit-Rheb and mCh-PDEδ molecules. Inhibitor concentrations are indicated above each image in nM. n = 19 cells. (n= at least 2 independent experiments, data are mean ± S.E.M.). Scale bars, 10 μM. Performed by Dr. Antonios Konitsiotis.*

Increasing concentrations of **35** resulted in a reduced interaction of Src6Q-mCit with UNC119-mCh. Dose-dependent measurements permitted to determine the equilibrium dissociation constant (K_d), a ratio of k_{off}/k_{on}, between the two proteins of interest. This experiment yielded an 'in-cell' K_d for UNC119A of 111.3 ± 0.2 nM and an 'in-cell' K_d for UNC119B of 134.3 ± 4.1 nM for compound **35**. These values were 10-fold higher than the in vitro determined IC_{50}s. This difference is possibly due to competing membrane binding of the compound in cells.

2.3.5.5. Conclusion

The phenotypic response of disrupting the interaction between UNC119 and myristoylated protein was characterized. This interaction and the biological relevance of this protein was already known but not fully understood.

The optimized inhibitor engaged with UNC119A and UNC119B in a cellular lysate context and was less toxic toward triple breast cancer cells than the known inhibitor Dasatinib.

The activity of the Src FKs is highly correlated to the phosphorylation of tyrosine Y416. We showed, using an ICW assay that the small molecule influences the level of phosphorylation and leads to a decrease of around 40%.

Nevertheless, no influence was observed after treatment with the small molecule on the kinetics of the cell migration. However, a dose-dependent influence of compound **35** toward colony size and colony number was observed.

Using fluorescent-labelled UNC119-mCh and Src-mCit in a FLIM-FRET experiment, the interaction between UNC119 and myristoylated Src could be observed. A dose dependent disruption of this interaction led to the determination of K_d values. Upon treatment with the inhibitor, for the first time, the disruption of the interaction using a small molecule in live cells could be shown.

2.4.Summary

The need to investigate the biological relevance of the Src FKs and the link between Src FKs and cancer progression is in high demand. Clinically approved drugs and those in clinical trials are ATP competitive and showed several side effects. There is a great demand for the development of new small molecules for potential therapeutics or as tools to further understand the biological relevance Src FKs.

An HTRF screen was developed and the COMAS library was screened. A benzothiazolone scaffold was identified as a promising scaffold. An SAR study on this benzothiazolone scaffold led to a low nanomolar compound. A collection of 50 molecules was bought and synthesized to perform the structure activity relationship analysis.

Different parameters were evaluated to further characterize the most potent inhibitors. Selectivity was measured using a fluorescence polarization experiment and showed high selectivity for the most potent compounds to UNC119A (regarding to others lipid biding proteins). Solubility of the best compounds was evaluated and the compound **35** with a pyridine substitution showed appreciable solubility (375.9 µM) and remaining potency with an IC_{50} of 12 nM.

Target engagement of the compound **35** was determined in a CETSA experiment using Jurka cell lysate. The compound showed a significant increase of the melting temperature of both UNC119A and UNC119B. No interaction with others lipid binding proteins was observed.

The inhibitor binds to UNC119 in cells and induce reduction of activating Src-autophosphorylation on Y419. UNC119 inhibition in Src-dependent colorectal cancer cells results in the specific reduction of cell growth and clonogenic potential. The results demonstrate that small molecules interference with the dynamics of the Src spatial cycle may open up a novel opportunity to interfere with oncogenic Src-signaling.

Using fluorescence lifetime imaging microscopy with fluorescence labelled UNC119A and Myr-Src, the impact of the compound **35** was evaluated. Dose dependent disruption of the interaction between UNC119 and Myr-Src upon treatment with the small molecule allowed to determined 'in-cell' K_d values (111.3 nM for UNC119A and 134.5 nM for UNC119B).

3. Part B: Synthesis of a Cinchona Alkaloid derived Library as Potent Autophagy Inhibitors

3.1. Introduction

Alkaloid-containing plants have been used for 4,000 years and their applications are diverse, ranging from medicinal to psychotropic. Alkaloids are one of the most diverse groups of secondary metabolites. Whereas they are mainly isolated from plants, alkaloids can also be found in various organisms such as animals, insects and marine invertebrates.[105]

3.1.1. History of Alkaloid Natural Products

Early on, alkaloids have shown relevance in the treatment of various pathologies. The first alkaloid of importance was isolated in the early 19th century as an opium extract (from *Papaver somniferum*).[105] This plant has been used for centuries as analgesic. Morphine was first isolated in 1805 and Sertürner recognized its alkaline nature.[106] Following this finding, a number of biologically relevant molecules were isolated between the years 1817 and 1820. These alkaloids, such as strychnine, emetine, caffeine, quinine, cinchonine and colchicine, are still relevant today due to their broad applications (Figure 35). Some of them are still used for medical applications.[107]

Emetine   **Morphine**   **Strychnine**   **Quinine**

Cinchonine   **Colchinine**   **Chloroquine**   **Caffeine**
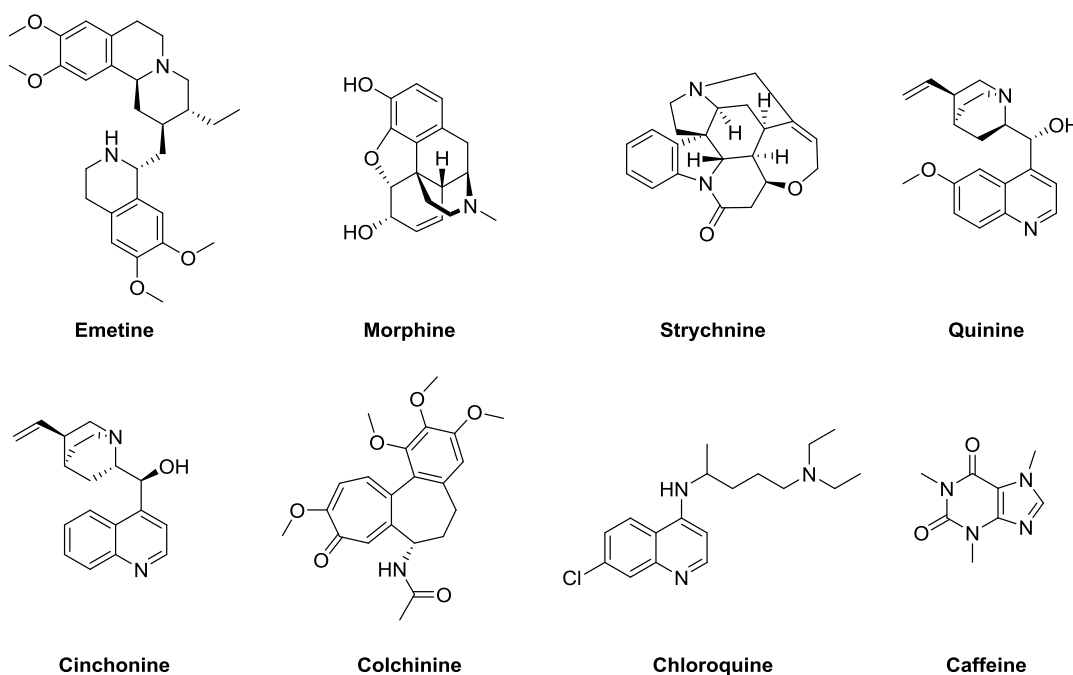
Figure 35. Structure of biologically relevant alkaloids.

The number of isolated and characterized alkaloids has increased over the 20th century. In 1939, only 200 alkaloids were structurally identified. By 2017, more than 270,000 alkaloids were listed in the Dictionary of Natural Products (DNP).[107]

3.1.2. Classification of Alkaloids

In 1983, Pelletier suggested a simple and general definition of an alkaloid: "An alkaloid is a cyclic compound containing nitrogen in a negative oxidation state which is of limited distribution in living organisms."[108] The whole class can be divided in three categories:

- True alkaloids (deriving from amino acids and containing a heterocyclic ring with nitrogen)
- Protoalkaloids (compounds in which the nitrogen atom is derived from an amino acid not part of the heterocycle)
- Pseudoalkaloids (the basic carbon skeleton is not derived from amino acids)

3.1.3. Use of Alkaloids in Medicine

Alkaloids were used as early as 2000 BCE to treat animals and humans as well as sources of poison for hunting and enemies. Based on their early use in history, one could expect that alkaloids were and are widely used in the development of drugs. However, only 53 alkaloids are currently used for pharmaceutical purposes (Table 12), which represents only 0.002% of all the discovered alkaloids. This small number can be explained by the toxic properties of this family of molecules (most of the alkaloids hit ion channels and show high toxicity) and the poor prediction of the drug-likeness by the widely used rule of five (RO5) proposed by Lipinski.[109] These rules were made for development of small molecules and most of the natural products often fall outside of these rules but still make good drugs.

Table 12. Examples of the 52 alkaloids used for pharmaceutical applications.

Alkaloid	Synonyms	Applications	Example Product
Cinchonidine	Cinchonan-9-ol	Increases reflexes, convulsions	Quinimax™, Paluject™
Caffeine		Neonatal apnea, atopic dermatitis	Agevis™, Anlagen™, Thomapyrine™
Cocaine		Local anesthetic	Used in highly regulated clinical environment
Morphine		Pain relief, diarrhea	Diastat™, Duromorph™
Quinidine	Conquinine, Conchinine, Pitayine	Ventricular and supraventricular arrhythmias, malaria, cramping	Cardioquin™, Duraquin™, Quindex™, Rhythomochin™
Quinine	6'-Methoxycinchonan-9-ol, Chinin	Malaria, babesiosis, myotonic disorders	Acticarbine™, Opdensit™, Pameion™, Vasocalm™

Data adaptation from Amirkia *et al.*[107]

3.1.4. Natural Product-Based Libraries

The design of suitable tools and probes for studying biological phenomena are in high demand. These molecules need to be selective and well designed to perturb only one particular protein function. Using proteins and amino acids combined, nature designed a limited amount of biologically active small molecules and explored only a small amount of the chemical space available.[110]

Using modern chemistry and with the increase of protein structures available in databases such as the Protein Data Bank (PDB), chemical biologists try to design molecules based on natural scaffolds to explore the remaining chemical space and analyze the fragments from the natural molecules. For this purpose, a method was created called Biology Oriented Synthesis (BIOS), which analyzes the structural conservatism and diversity in nature.[110] This analysis is based on the structural information of proteins and small molecules together.

To have access to the information provided by the BIOS analysis, a chemical tree was designed.[110] This chemical tree regroups the main sister molecule derivatives from most natural products and known drugs. For clarity, scaffolds were grouped by heteroatom and ring size (Figure 36).
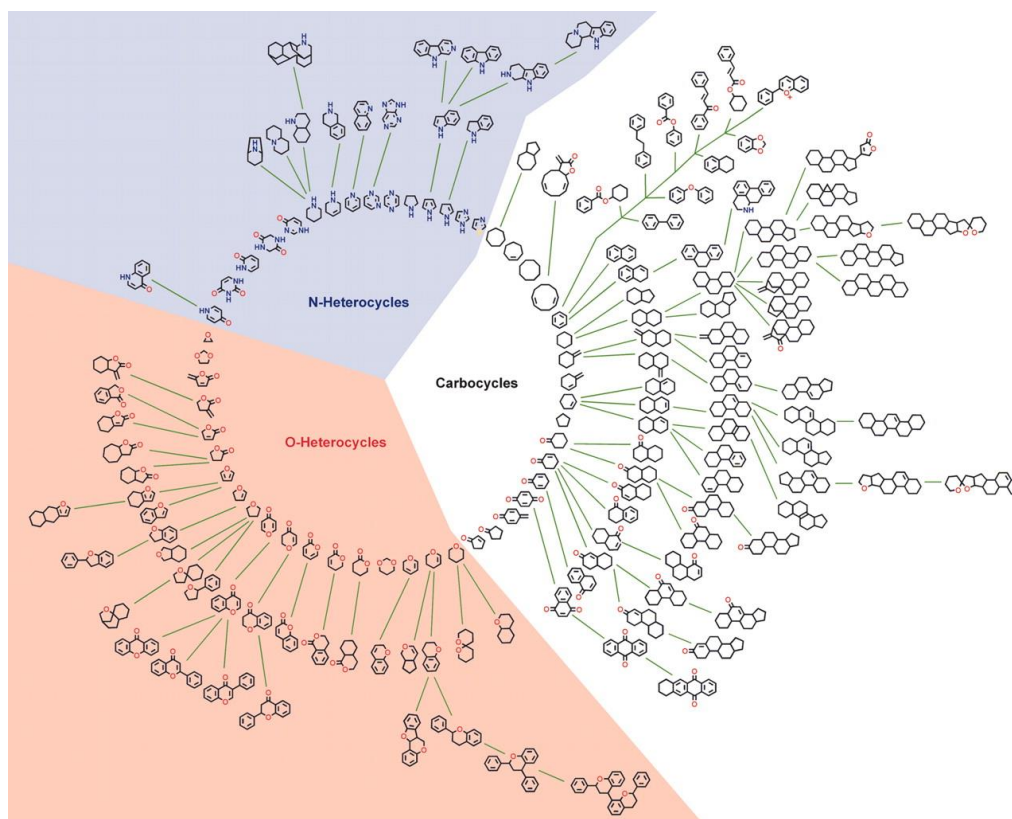
Figure 36. Scaffold tree representation.[111]

The difficulty to isolate new natural products leads to an increased use of small molecules. The need of new therapeutics from treating resistant pathogen or new diseases is in high demand. With the development of BIOS and the scaffold tree, the exploration of the chemical space and development of chemical library has improved.[17,112,113] Recurrent small scaffolds appearing in many natural products and drugs were a good starting point for the development of biological relevant molecules. Many biology-oriented compound collection have been synthesized and screened to develop new small molecules with high biological impact.

3.1.5. Cinchona Alkaloid Scaffold

Cinchona alkaloids are privileged scaffolds.[114] Privileged scaffolds are defined as fragments able to interact with more than one target and highly represented in the overall bioactive compound population,[115] which makes these fragments of great interest in the development of new therapeutic agents.

3.1.5.1. Use of Quinoline in Medicinal Chemistry

Cinchona alkaloids were first isolated from the plant (*Cinchona bark*) in 1810 by Gomez.[116] Few years after, Pelletier and Caventou isolated quinine and cinchonine (Figure 37). The determination of the exact structure and the chemical synthesis of these alkaloids became a great challenge for chemists during the 19th century.[117]

R = H, Cinchonidine
R = OMe, Quinine

R = H, Cinchonine
R = OMe, Quinidine
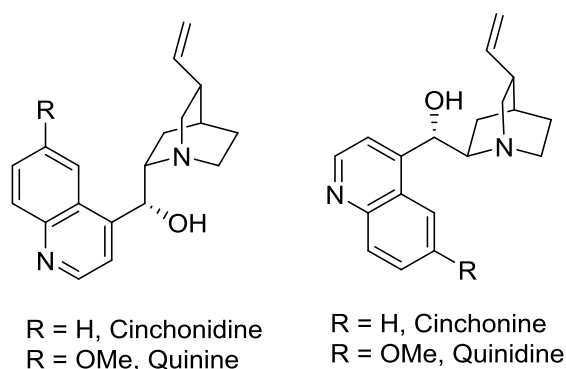
Figure 37. Cinchona alkaloids scaffolds and related names.

Because of the structural complexity of quinine, a synthetic route was not possible for large-scale synthesis and hence commercialization of the product. Quinine, which was the first antimalarial drug, was used as an extract from the cinchona tree. Chloroquine (CQ) (Figure 35), another quinoline-derived molecule, was first synthesized in 1934 and CQ replaced quinine for the treatment of malaria after the Second World War, as it possesses fewer side

effects than quinine. Because of these interesting properties and its strong therapeutic potential in the treatment of malaria, other quinoline-based molecules were widely studied to solve the resistance developed by the parasites spreading malaria. Extensive studies over quinoline allowed biosynthetic pathway of quinine to be proposed, starting from strictosidine (Figure 38).[118]
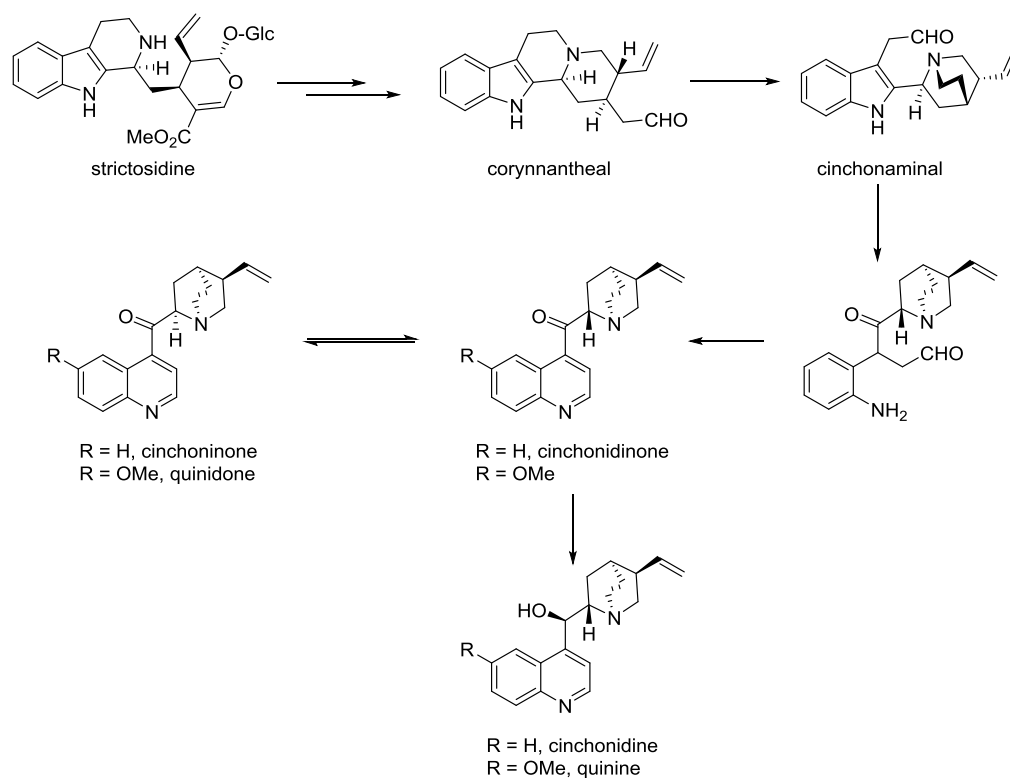
Figure 38. Proposed biosynthetic pathway of quinine.

3.1.5.2. Use of Cinchona Alkaloid in Organic Chemistry

Despite their use in medicinal chemistry, cinchona alkaloids are also recognized as a privileged compound class in asymmetric synthesis. With the development of the catalysis concept to access novel chemical transformations and the need of new non-metallic catalysts, quinine and quinidine represented attractive candidates for the catalysis of organic reactions.[119] The key feature responsible for their successful utility in catalysis is that they possess diverse chiral skeletons, are easily tunable, commercially available and inexpensive. The presence of the 1,2-aminoalcohol subunit containing the highly basic and bulky quinuclidine, which complements the proximal Lewis acidic hydroxyl function, is primarily responsible for their catalytic activity. The presence of the quinuclidine base functionality makes them effective ligands for a variety of metal-catalyzed processes.

The first example of the use of cinchonidine as a catalyst was reported by Fiske *et al.* in 1912 for the hydrocyanation of aldehydes.[119] Nowadays, quinine-catalyzed reactions are widely used in the organic synthesis. For example, quinine-based catalysts are used in organic synthesis such as the one-pot asymmetric synthesis of β-amino acids (Figure 39),[120] intramolecular aldol reactions to form β-lactone[121] and asymmetric dihydroxylation.[122]
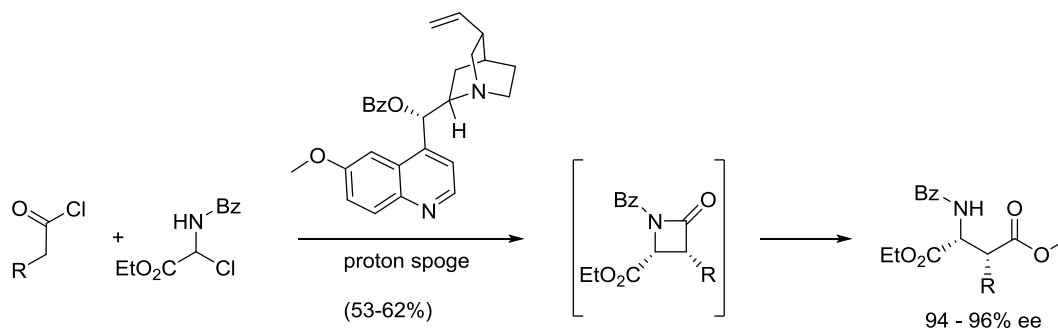
Figure 39. One-pot asymmetric synthesis of β-amino acids.[120]

The ammonium salt of quinine and quinidine have also been used for specific transformations. Because of the reactivity of the nitrogen, the use of the corresponding salt presented different reactivity. For example, cinchonidinium bromide was used as a catalyst in the asymmetric alkylation of glycine under phase transfer as a key step in the total synthesis of belactosin A, an antitumor antibiotic (Figure 40).[123]
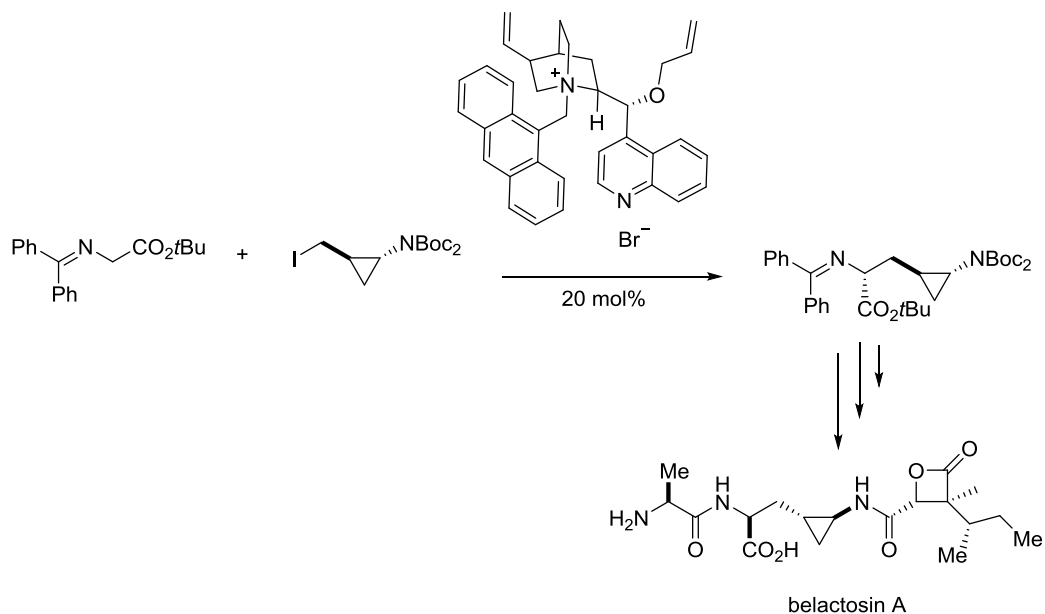
Figure 40. Synthesis of belactosin A using the asymmetric alkylation of a glycine derivative.

Extensive studies have been carried out to understand how this class of catalyst behaves during organic reactions. Using nuclear magnetic resonance (NMR) spectroscopic data and computational techniques, it was possible to identify the different conformations adopted by the catalyst and better understand its mode of action.[124,125]

With all the data and the already reported techniques, different catalysts based on this privileged family, such as a Thiourea cinchona alkaloid, were designed and successfully employed in a wide range of transformations.

In order to increase the basicity and nucleophilicity of cinchona alkaloids for catalyst design purposes, the synthesis of cyclized cinchona alkaloids, β-isocupreidines ("oxazatwistanes"), was of particular interest. The designed β-cupreidine (β-ICD) showed, a limited conformational flexibility and an increased basicity and nucleophilicity, compared to quinidine. This difference is mainly due to the reduced steric hindrance of the quinuclidine nitrogen center and the increased ring strain of its tricyclic framework (Figure 41).[126]

a) Cinchona alkaloids

R = H, cinchonidine
R = OMe, Quinine

R = H, cinchonine
R = OMe, Quinidine

b) Oxazatwistanes

β-isocupreidine (β-ICD)
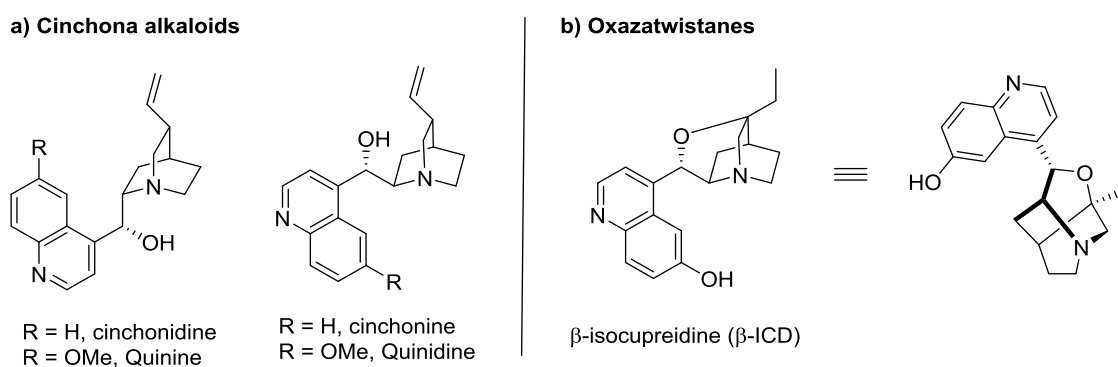
Figure 41. Oxazatwistane scaffolds compared to the natural cinchona alkaloids. A) Natural based scaffold of quinine and quinidine derivatives. B) Non-natural analog of quinine: β-isocupreidine.

The first report of the use of β-ICD was for the Morita-Baylis-Hillman asymmetric reaction by Hatakeyama and coworkers.[127] To date, oxazatwistane derivatives have shown great importance in catalysis. Numerous different reactions have been catalyzed by the β-ICD family, making these compounds valuable tools for organic chemists. β-ICD catalysts have proven to be highly efficient for systems with an aromatic moiety next to a five-membered ring such as indole, indenonem and isatin.[126]

Surprisingly, no biological data has ever been reported for the oxazatwistane scaffold and derivatives. Given its strained ring system and increased basicity it could be predicted to have diverse biological activity compared to the natural products that it derives from.

3.1.6. Autophagy

Autophagy is an essential cellular mechanism whose role is, under normal physiological conditions, to remove long-lived, aggregated and/or misfolded proteins and to clear damaged organelles, thereby regulating cell growth and aging.[128]

The first step in autophagy is the autophagosome formation. There are two distinct modes: selective and non-selective autophagy. In non-selective autophagy, no cargo is selected. In selective autophagy, the cargo is selected before autophagosome formation. Then the autophagolysosome formation and degradation takes place (Figure 42). All these steps are crucial for the process to take place successfully. If one of this step is disrupted, the whole machinery is impacted.[129]

Phagophore

Lysosome (acidic)

Chloroquine
Bafilomycin

Autophagolysosome

Autophagosome

(eGFP)-LC3-I   (eGFP)-LC3-II   Phosphatidyl ethanolamine   p62   Degradative Enzymes
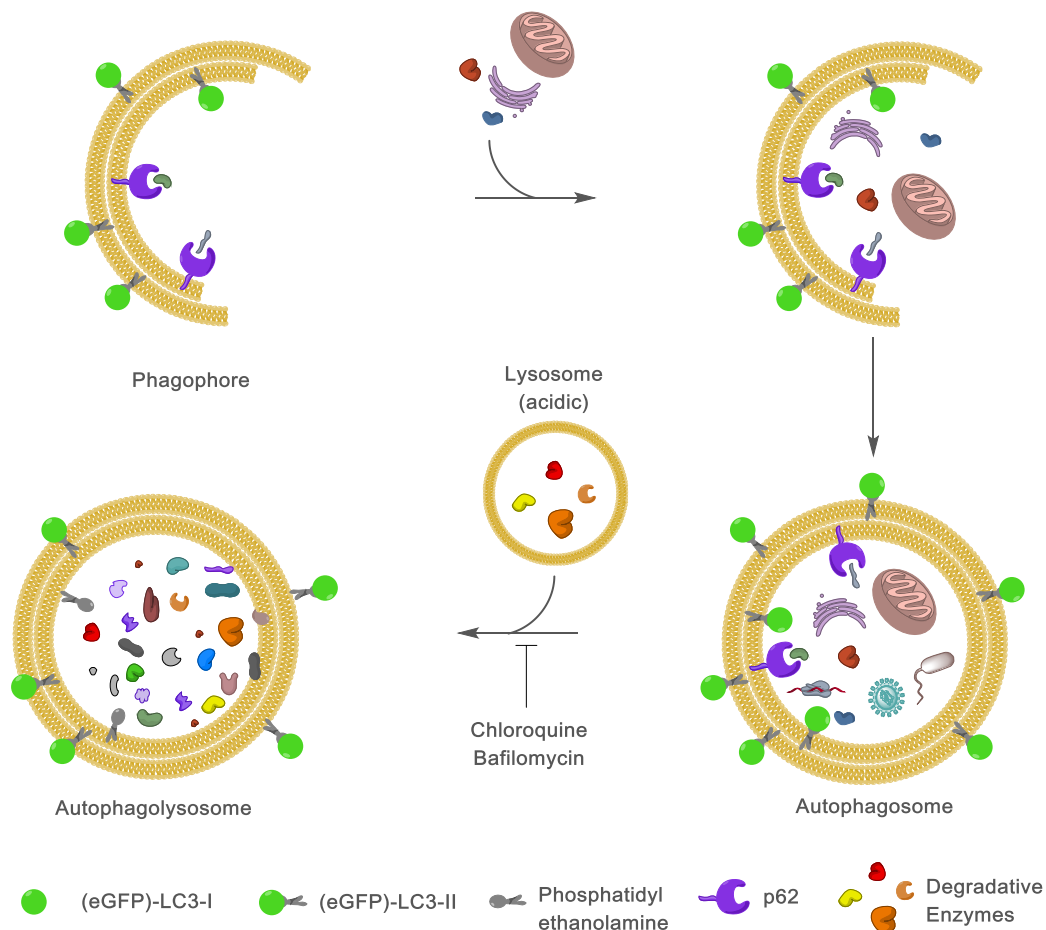
Figure 42. Autophagy machinery process.

Macroautophagy is initiated by the formation of autophagosome. The role of this step is to deliver the protein aggregates and other target materials to the lysosome for degradation.[128] This process is divided in three distinct parts: autophagosome initiation, elongation and nucleation. Each steps of this process is regulated by a number of proteins.

One important protein involved in the autophagosome initiation is the mammalian target of rapamycin (mTOR).[130] This protein is a serine/threonine kinase that forms two different complexes: mTORC1 and mTORC2 and acts as a central regulator of cell growth. It was shown that mTOR plays a key role at the interface of the pathways that regulate the balance between cell growth and autophagy.[131] In most cases, autophagy takes place in an mTOR-dependent manner.[130] At the end of the process, the autophagosome fuses with early and late endosomes to form amphisome.

3.1.6.1.   Role and Regulation of Autophagy in Diseases

The link between autophagy deficiency and disease was postulated early on. Cancer was the first disease to be linked to impaired autophagy.[132] However, the therapeutic application and drugs interfering with this vital biological process is controversial, and the understanding of autophagy and tumor development is still not clear. Nevertheless, increasing evidence shows that autophagy might be necessary for tumor progression.

3.1.6.2.   Forward Chemical Genetics in Autophagy

As described in the Chapter **1**, FCG is a valuable method to develop tool compounds for studying biological pathways. Mizushima and coworkers carried out the first HTS to identify autophagy modulators.[133] This cell-based assay used a Green fluorescent protein (GFP)-labelled Light Chain 3 (LC3) to analyze autophagy *in vivo*. Later, Balgi and coworkers established the first phenotypic screen in human cells. This screening lead to the identification of numerous autophagy modulators.[134]

Despite the extensive study of the mechanism of autophagy over the past years, few molecules have entered clinical trials. This could be explained by the poor understanding of the different steps and the proteins involved in this biological process. One important class of small molecules is CQ and its derivatives such as hydroxychloroquine. These quinoline-based modulators are autophagy flux inhibitors acting via the inhibition of the autophagosome-lysosome fusion (Figure 42) and are the only autophagy inhibitors in advanced clinical trials.

Because of the few autophagy modulators entering clinical trials, there is a strong need for the development of new autophagy inhibitors. Tool compounds inhibiting the different steps of the process are required for further understanding of the autophagic machinery. New targets or potent therapeutics could lead to new therapeutic agents.

3.2. Aims

Developing new modulators to understand and interfere with biologically relevant processes are in high demand. Autophagy, a vital process for the cells, was already extensively studied but is still not fully understood. The need for new tool compounds for a better understanding of this machinery is required. In 2017, an oxazatwistane-based scaffold was identifed as potent autophagy inhibitor.

The aim of the thesis was to synthesize a library directly based on *Cinchona* alkaloid scaffolds to explore the structure activity relationship. Using modern state of the art C-H functionalization and metal cross coupling reactions, a large variety of modifications on this scaffold can be access (Figure 43). Using this compound class and/or designed probes, the biological target(s) could be identified. The identification of new proteins involved in the autophagic response might be useful to gain knowledge about this machinery.
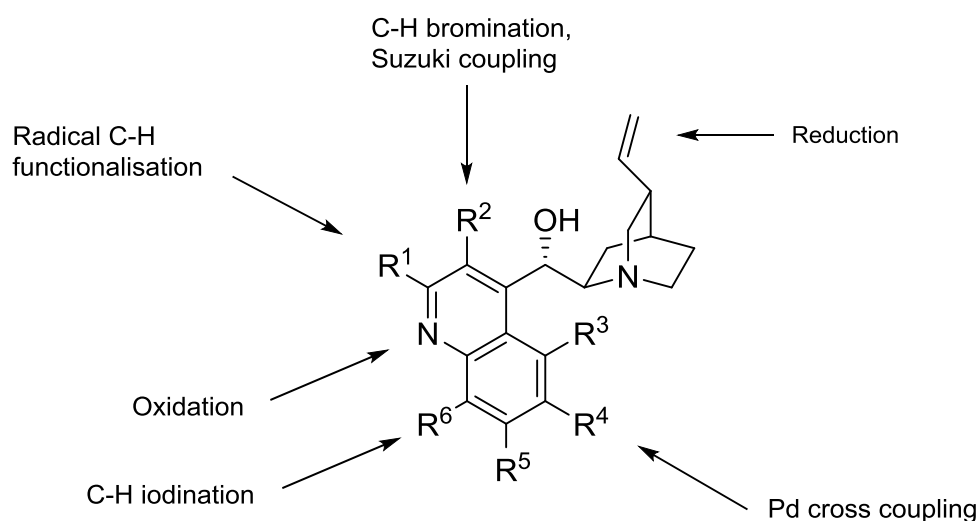
Figure 43. Quinidine scaffold and chemistry involved for different functionalization.

3.3. Result and discussion

3.3.1. Identification of a Quinidine-Based Autophagy Inhibitor

3.3.1.1.   Phenotypic Screen for the Identification of Autophagy Modulators

The screen was performed at COMAS.

In order to identify autophagy modulators, a technique was used based on the observation that LC3-I, upon activation of autophagy, is conjugated to PE, thereby generating LC3-II, and then inserted into the isolation membrane. Under normal conditions, eGFP-tagged LC3-I is distributed in the cytoplasm leading to distribution of the fluorescence signal. When the autophagic response is activated, such as under starvation conditions or by the direct inhibition of mTOR by rapamycin, eGFP-LC3-II accumulates at the autophagosome and green fluorescence puncta can be detected (Figure 44).[133]

Figure 44. Autophagy phenotypic screen for the identification of novel inhibitors. LC3-I, upon activation of autophagy, is conjugated to PE, thereby generating LC3-II, and then inserted into the isolation membrane. Under normal conditions, LC3-I is distributed through the cytoplasm leading to distribution of the fluorescence signal. Therefore, when the autophagic response is active, GFP-LC3-II accumulates to the autophagosome and green fluorescence puncta can be detected.

The need for new autophagy modulators to investigate and further understand the whole process is important. This screening set-up permitted the evaluation of the COMAS library and the identification of new autophagy inhibitors.

3.3.1.2. Oxazatwistanes Derivatives and Quinidine-Based Scaffold Identification

Using the cell-based autophagy screening, the 250,000 compounds of the COMAS library were screened. An interesting oxazatwistane scaffold was identified and further analogs were synthesized. A library of compounds based on that oxazatwistane scaffold leads to the identification of Oxautin-1, a low micromolar autophagy inhibitor (Figure 45).[135] Oxautin-1 inhibits both autophagosome biogenesis and autophagosome maturation. Using a gfp-WIPI2b cell line to monitor PI3P puncta as a marker for autophagosome biogenesis, it was shown that Oxautin-1 was able to inhibit the autophagosome biogenesis and showed that the compound is not only a fusion inhibitor.
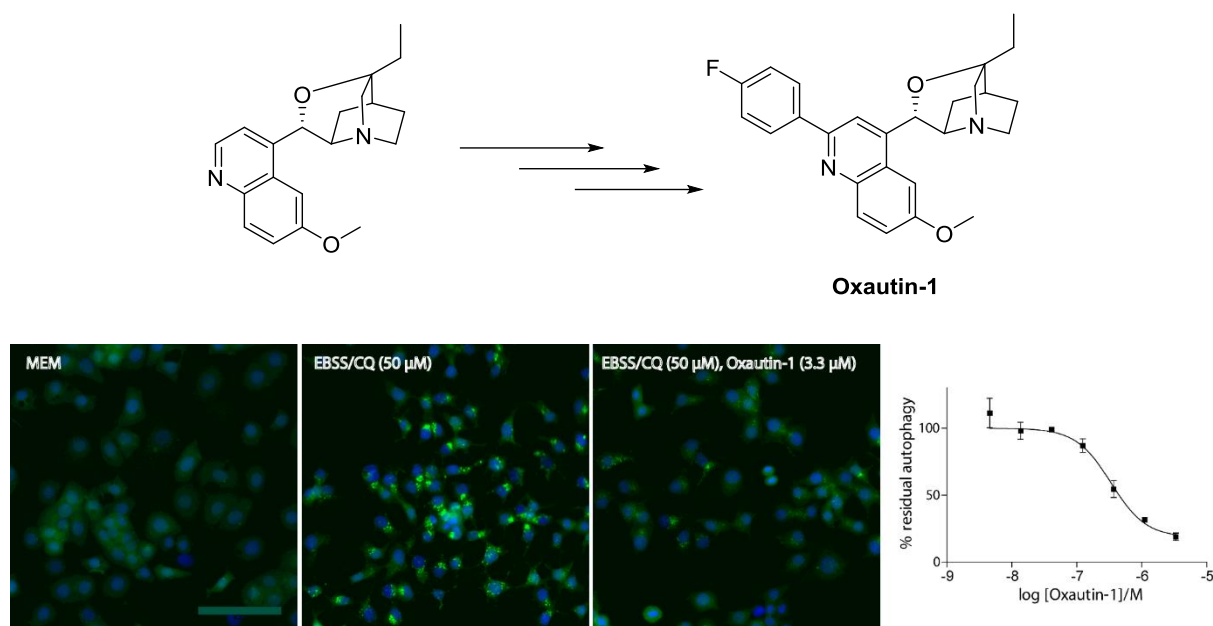
Oxautin-1

Figure 45.Chemical structure and screening evaluation of Oxautin 1. The compound dose-dependently inhibits the accumulation of eGFP-LC3-II in MCF7-LC3 cells. Reproduced from Laraia et al.[135]

During the SAR studies of the oxazatwistane compound class, the uncyclised quinuclidine derivative **100** was synthesized (Figure 46). This compound remained potent in the autophagy screen. Because of its simpler synthesis and potential for additional diversifications at the alcohol and alkene sites, the scaffold was selected and the synthesis of a new compound collection was carried out to optimize this newly identified autophagy modulator.
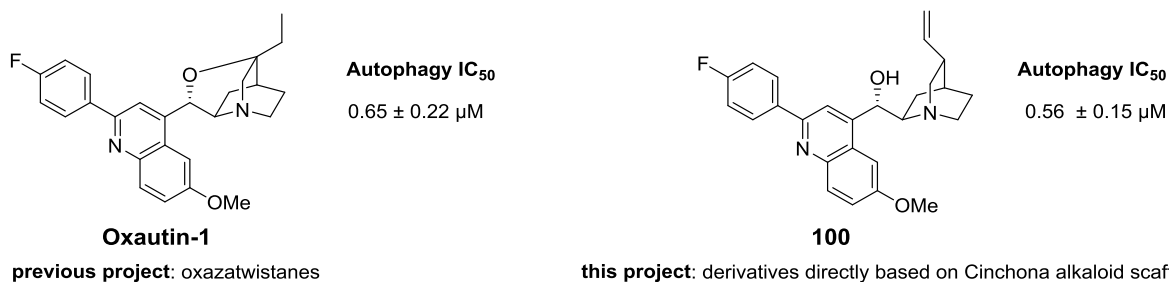
Figure 46. Identification of a new natural product-based scaffold during the process of optimization of oxazatwistane-based inhibitors.

3.3.1.3.   Validation of the Quinidine-Based Inhibitor

This experiment was performed by Dr. Luca Laraia.

Because GFP-based phenotypic screens possess some limitations, it is necessary to confirm the activity using a different assay. For example, GFP is a target for proteasomal degradation and can affect the function of LC3 because of its size.[136] That is why an independent analysis of LC3 levels is necessary in parallel to the phenotypic screen. By measuring the level of LC3-II by immunoblotting, the activity of the compound can be validated. The level of LC3-II should increase upon activation of autophagy and increase further with compound treatment, as compounds of this class were previously shown to inhibit the autophagosome-lysosome fusion. The second marker of autophagic flux is the ubiquitin-binding protein p62, which is degraded when the autophagic response is active. For this reason, the level of p62 upon compound treatment should decrease. The western blot analysis confirmed that the quinidine-based compound induces the accumulation of lipidated LC3 and the degradation of p62 in amino acid-starved cells in a dose dependent manner (Figure 47).
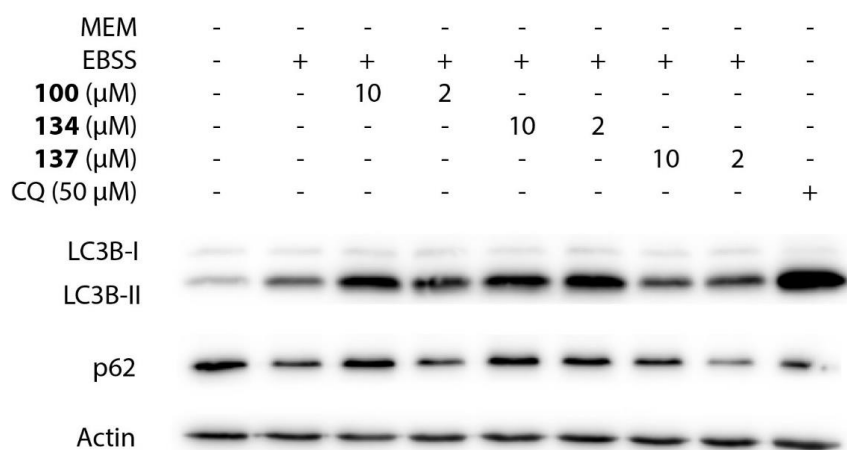
Figure 47. Quinidine-based inhibitor **100** inhibits the autophagy-induced accumulation of LC3-II and degradation of p62 in MCF7-eGFP-LC3 cells, similarly to the known fusion inhibitor Chloroquine (CQ). Compound **134** and **135** were also evaluated. MCF7 cells stably expressing eGFP-LC3 were incubated with either MEM, EBSS, or EBSS and compound for 3 h and lysed with Laemmli buffer. n = 3, representative image shown. Performed by Dr. Luca Laraia

68

3.3.2. Synthesis of a Quinidine-Based Compound Collection

An interesting natural product-based scaffold was identified in a phenotypic screen as a potent autophagy inhibitor. A compound collection was synthesized to optimize the compound and use it as a tool to further characterize the phenotypic response.

3.3.2.1.   Forward Synthetic Analysis of Quinidine

At first, an analysis of the quinidine-based hit was performed to select modification points around the scaffold. The starting materials, are inexpensive and commercially available. This enabled the rapid investigation of compounds based on the four natural products quinine, quinidine, cinchonine and cinchonidine.
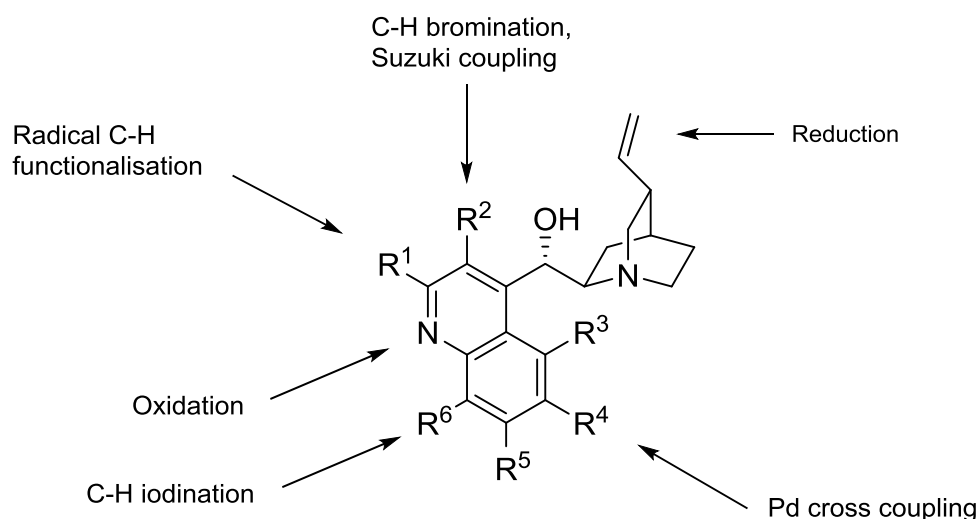
Figure 48. Different points of modifications on the cinchona alkaloid scaffolds

Using modern C-H activation chemistry, several positions could be modified around the quinidine scaffold (Figure 48). Using oxidation and reduction, modifying around the double bond of the quinuclidine ring as well as investigating the role of the alcohol functionality was planned.

3.3.2.2. Synthesis of C2-Functionalized Quinidine

Based on recently reported conditions developed by Phil Baran and coworkers, the C2 position of the scaffold was investigated.[137] Using commercially available starting material, in presence of boronic acid, trifluoroacetic acid and silver(I) nitrate in a DCM/H_2O mixture the desired C2 functionalized product was obtained. This reaction allowed to readily diversify this position in one step and with moderate yields (Figure 49).
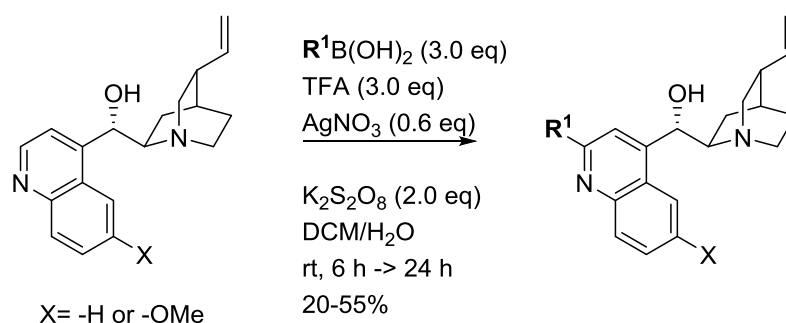
Figure 49. C2 functionalization of quinidine using the Borono-Minisci reaction.

However, the reaction was limited to certain boronic acids. The use of electron deficient boronic acids such as 3,5-dimethoxyphenylboronic acid or 4-pyridinylboronic acid did not yield the target compounds. Using this chemistry, a compound collection of 20 analogs was prepared and evaluated in the phenotypic screen. Compounds based on all four scaffolds (quinidine, quinine, cinchonine and cinchonidine) were prepared at first to investigate the influence of the stereochemistry of the natural product core and the methoxy substituent on the quinoline ring.

3.3.2.3. Synthesis of C3-Functionalized Quinidine

Using conditions reported by Jaric *et al.*, functionalization at the C3 position of the quinidine scaffold was possible.[138] They reported the possibility of either functionalizing the C2 position using a bulky protected group on the alcohol (TBDMS) or the position C3 using MeLi and TMPMg.LiCl in complex in the presence of an electrophile. This is a two-step reaction where first the alcohol is blocked with a Li^+ counter-anion followed by transmetallation leading to the halogenated C3 intermediates **102** (X = Br) and **103** (X = I). Suzuki coupling of these intermediates using boronic acids and a Pd catalyst lead to the desired C3-functionalized compounds (Figure 50).

70
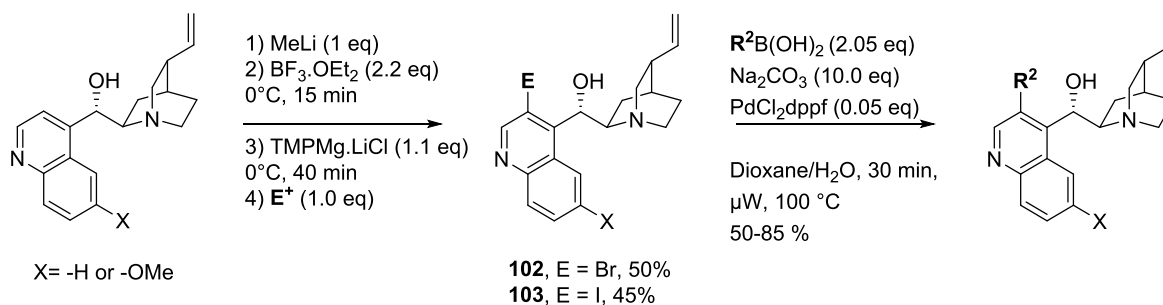
Figure 50. Chemical synthesis for the C3 functionalization. $E^+ = I_2$ or $Cl_4Br_2C_2H_2$.

These conditions were successfully used to functionalize the selected quinidine scaffold to investigate the activity of the C3 substituted analogs. Compare to the C2 functionalization, the C3 is more robust. The second step, a Suzuki coupling, allowed the functionalization with electron deficient boronic acid such as CF_3-, NO_2-. A compound collection of approximately 15 molecules was synthesized and screened.

3.3.2.4. Synthesis of Additional Analogs of Quinidine

The effect of varying other positions, including the double bond or the alcohol functionality was also investigated (Figure 51).
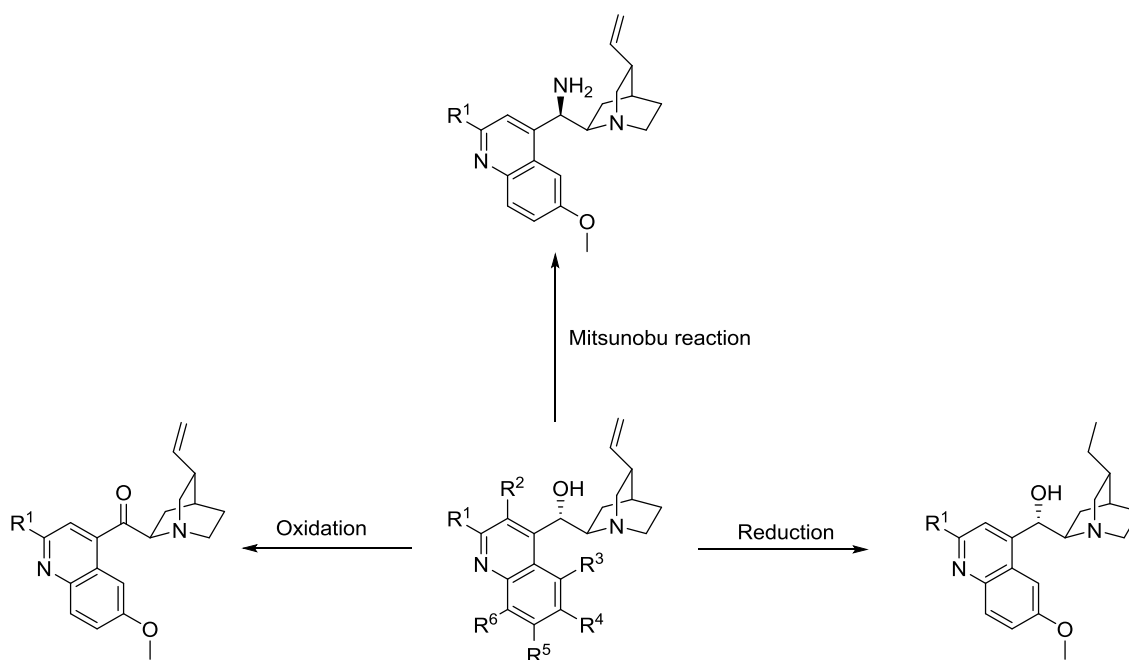
Figure 51. Others modifications around the quinidine scaffold.

Compounds with different modification (such as reduction of the double bond, exchange of the alcohol function with an amine function and a ketone-derivative) were synthesized according to literature conditions for similar substrates.[139,140]

3.3.3. Structure-Activity Studies of a Quinidine-Based Compound Collection

A compound collection of 60 small molecules was synthesized. An SAR analysis was subsequently carried out to identify the importance of each substituent, hopefully improve potency, and determine a suitable attachment point for immobilization of the compound onto solid phase for target identification studies.
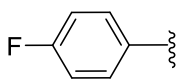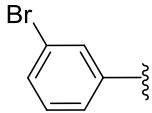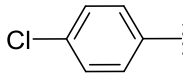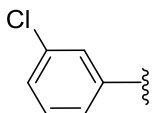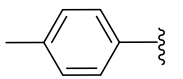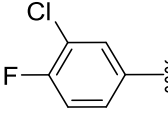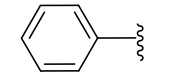
3.3.3.1. Relevance of the Phenyl Functionality (R^1)

The original hit identified during the Oxautin-1 development, inhibitor **100**, was originally functionalized with a 4-fluorophenyl moiety in position C2. Because of the potency of the inhibitor in the autophagy screen, 30 molecules with different C2 substituents were synthesized. For clarity purposes, the compounds will be grouped according to their starting alkaloid scaffold.

3.3.3.1.1. Relevance of R^1 on Quinidine-Based Compounds

Seven examples were prepared based on the quinidine starting material (Table 13).

Table 13. Structures and activities for the quinidine based analogs of R^1 position (Figure 50, R^1).

Entry	R^1	IC$_{50}$ (µM)	Entry	R^1	IC$_{50}$ (µM)
1	F—phenyl— **(100)**	0.56 ± 0.15	5	Br-phenyl **(104)**	7.48 ± 0.70
2	Cl—phenyl— **(101)**	2.44 ± 1.01	6	Cl-phenyl **(105)**	5.70 ± 0.39
3	CH$_3$—phenyl— **(102)**	2.31 ± 0.07	7	Cl,F-phenyl **(106)**	inactive
4	phenyl **(103)**	inactive			

Substitution with a *para*-fluorophenyl showed good potency with an IC$_{50}$ around 500 nM (Entry 1). Entry 1 showed the compound originally identified from the screen of the oxazatwistane derivatives. Replacement of the *para*-fluoro by a *para*-chloro group (Table 13, Entries 1 vs. 2) showed a four-fold decrease of potency. Exchanging the fluoride by a methyl
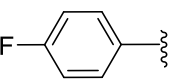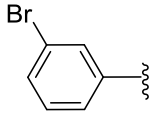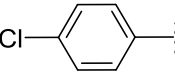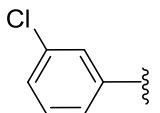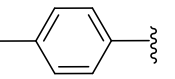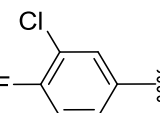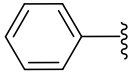
group showed a similar decrease of potency (Entry 1 vs. 3). While removing the substituent on the phenyl ring, the compound become completely inactive (Entry 4).

Substitution in *meta-* instead of *para-* position (Entry 2 vs. 6) led to a three-fold decrease of activity. 3-chloro,4-fluorophenyl substitution led to complete loss of activity (Entry 7).

3.3.3.1.2. Relevance of R^1 on Quinine-Based Compounds

Seven examples were prepared based on the quinine starting material (Table 14). In order to compare with the compounds prepared with quinidine (Table 13), the same substituents were used. This allowed to study the impact of the 3-D chemical structure on the autophagy activity.

Table 14. Structures and activities for the quinine based analogs of R^1 position (Figure 50, R^1).
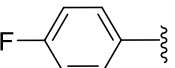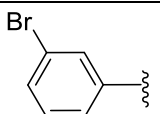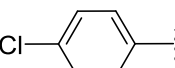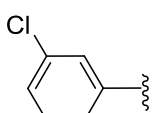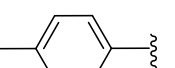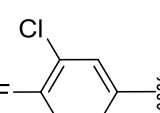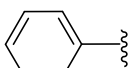
Entry	R^1		IC$_{50}$ (μM)	Entry	R^1		IC$_{50}$ (μM)
1	F—⬡—‌	(107)	3.30 ± 1.60	5	Br—⬡—‌	(111)	2.72 ± 1.319
2	Cl—⬡—‌	(108)	2.70 ± 1.30	6	Cl—⬡—‌	(112)	-
3	—⬡—‌	(109)	inactive	7	Cl,F—⬡—‌	(113)	-
4	⬡—‌	(110)	inactive				

For the quinine scaffold, the results differed when compared to those observed for the quinidine. The compound with the same substitution pattern as identified for the quinidine (Table 13, Entry 1) was also prepared for the quinine (Table 14, Entry 1). A six fold decrease in potency was observed by changing the configuration of the starting material. Replacement with *para*-chlorophenyl lead to a slight increase of potency similar to the *para*-fluoro compound (Table 14, Entries 1 and 2). A compound with a substitution in *meta-* position showed similar activity than the *para*-substituted compounds (Table 14, Entries 1, 2 and 5). Di-substitution and *meta*-chloro compounds (Entries 6 and 7) were not isolated with a good purity from the reaction mixture.

3.3.3.1.3. Relevance of R^1 on Cinchonine-Based Compounds

After investigation of quinine and quinidine series, the cinchonine starting material was used for synthesizing the next series of compounds (Table 15). This permitted to study and understand the impact of the methoxy group on the activity.

Table 15. Structures and activities for the cinchonine-based analogs of R^1 position (Figure 50, R^1).

Entry	R^1	IC$_{50}$ (µM)	Entry	R^1	IC$_{50}$ (µM)
1	F—⬡— (114)	1.62 ± 0.19	5	Br-phenyl (118)	inactive
2	Cl—⬡— (115)	toxic	6	Cl-phenyl (119)	5.43 ± 0.13
3	—⬡— (116)	inactive	7	Cl, F-phenyl (120)	inactive
4	⬡— (117)	inactive			

Interestingly, the *para*-fluorophenyl compound (Entry 1) remained active independently of the starting material used (quinine, quinidine and cinchonine). However, the *para*-chloro substitution leads to a toxic compound (Entry 2). Substitutions with a methyl group (Entry 3), a phenyl ring (Entry 4), *meta*-bromophenyl (Entry 5) and di-substitutedphenyl (Entry 7) lead inactive compounds in the autophagy screen.

3.3.3.1.4. Conclusion
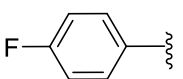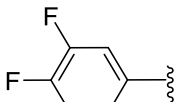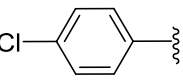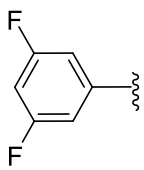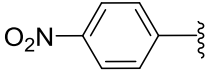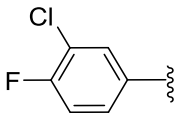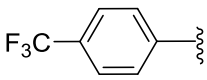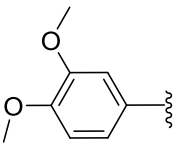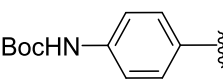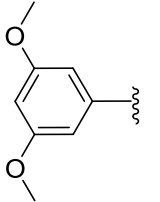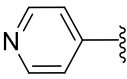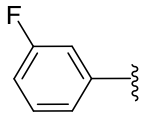
The influence of the C2 substitution on the phenyl ring was investigated for three of the natural cinchona alkaloids derivatives. The quinidine scaffold was most promising, leading to the discovery of an autophagy inhibitor with low micromolar potency. Analyzing the result for the quinine and cinchonine compound classes showed a loss of potency or toxic compounds in most cases.

Based on these results, the quinidine scaffold was selected for further functionalization whilst only one or two examples for each of the other families were prepared in order to confirm the initial assumption.

3.3.3.2. Relevance of the Phenyl Functionality (R^2)

After the synthesis of analogs at the C2 position, the C3 position was investigated for the quinidine scaffold. Only the quinidine scaffold was prepared based on the SAR results from the C2 position. Following the chemistry reported by Jaric et al.,[138] 14 compounds were prepared (Table 16).

Table 16. Structures and activities for the quinidine based analogs of R^2 position (Figure 50, R^2).

Entry	R^2		IC$_{50}$ (μM)	Entry	R^2		IC$_{50}$ (μM)
1	F—⟨⟩—	(121)	inactive	8	F,F—⟨⟩—	(128)	inactive
2	Cl—⟨⟩—	(122)	inactive	9	F,F—⟨⟩—	(129)	inactive
3	O$_2$N—⟨⟩—	(123)	3.87 ± 0.69	10	Cl,F—⟨⟩—	(130)	inactive
4	F$_3$C—⟨⟩—	(124)	3.52 ± 0.69	11	O,O—⟨⟩—	(131)	inactive
5	BocHN—⟨⟩—	(125)	-	12	O,O—⟨⟩—	(132)	inactive
6	N⟨⟩—	(126)	inactive	13	Br—⟨	(133)	inactive
7	F—⟨⟩—	(127)	inactive				

The compounds with the same substitution pattern as **100** and **101** (Table 13, Entries 1 and 2) lead to complete inactive compounds in position C3 (Table 16, Entries 1 and 2). Compound decorated with a nitro- and trifluoromethyl- groups (Table 16, Entries 3 and 4) showed activity, but with a six-fold decrease of potency. Introduction of heteroatoms led to complete inactive compound (Table 16, Entry 6). Surprisingly, the NH-Boc protected boronic

acid did not lead to any product formation (Entry 5). Other substitution pattern in C3, including di-substituted moieties (Entries 8-13) were completely inactive in the phenotypic assay. The intermediate with a bromide in position C3 (compound **102**) was also tested and showed no activity towards autophagy.

3.3.3.3.   Relevance of Additional Modifications

Several other positions were investigated of the new discovered autophagy modulator **100**. Studies on the influence of the double bond, the role of the oxygen function, the substitution by an amine function and the reduction to the ketone were also investigated.

3.3.3.3.1.   Relevance of the Double Bond

The importance of the double bond for the activity towards autophagy inhibition was evaluated. Based on the most active compound, two derivatives were prepared (Figure 52).

	100	**134**	**135**
Autophagy IC$_{50}$	0.56 ± 0.15 μM	1.00 ± 0.15 μM	1.61 ± 0.15 μM
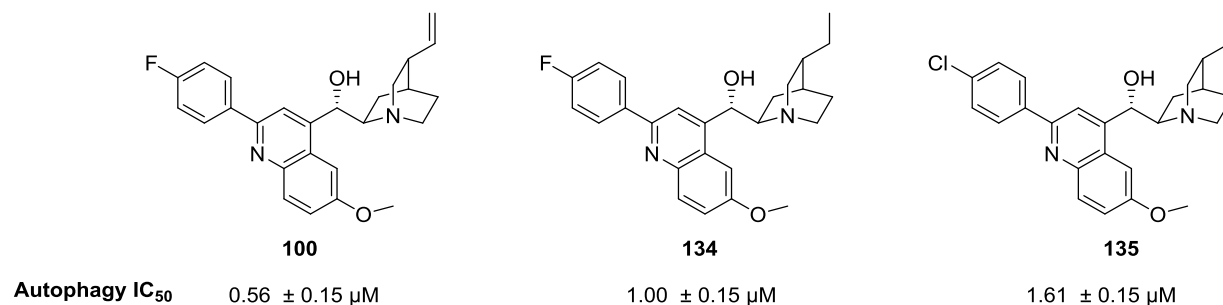
Figure 52. Biological relevance of the double bond for the autophagy activity.

A very slight decrease of potency was observed for the reduced compound **134**. This indicates that the double bond may play a small role in target binding. However, because compounds **134** and **135** retained good potencies, the double bond could be a site of choice for further functionalization and for the design of an active biological probe for target identification studies.

3.3.3.3.2.   Relevance of the Alcohol Moiety

Hydroxy groups offer a potential site for further functionalization and for the design of biological probes.[19] A ketone- and amine-containing derivatives were prepared and evaluated in the cell-based screen (Figure 53).

100	**136**	**137**
Autophagy IC$_{50}$ 0.56 ± 0.15 µM	inactive	inactive
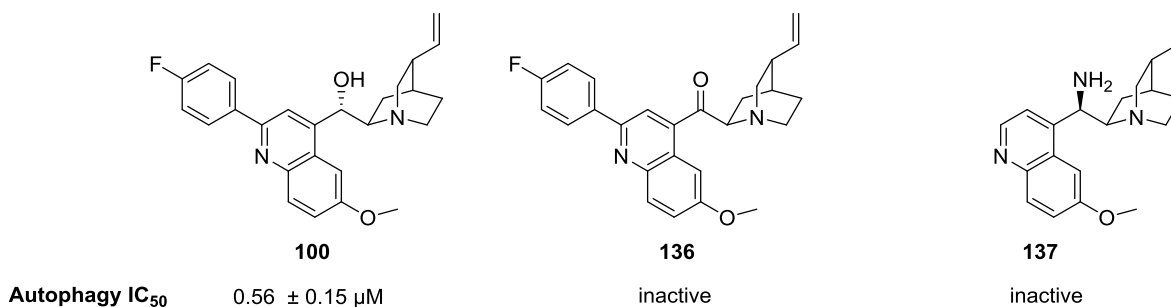
Figure 53. Biological relevance of the oxygen function for the autophagy activity.
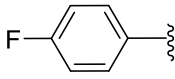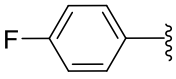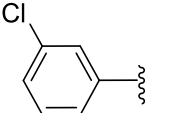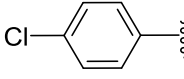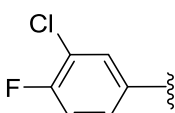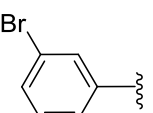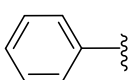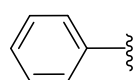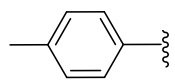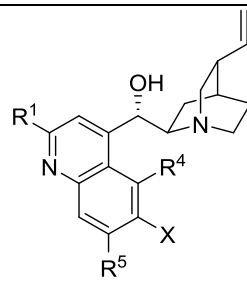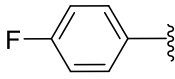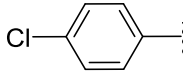
Oxidizing the alcohol to a ketone leads to a complete loss of activity. This could be explained by the different properties of the two chemical group (hydrogen bonding for example). The synthesis of the amine-derived compound with a C2-substituent on the quinoline ring proved to be more challenging than expected. Using an established method to prepare the NH$_2$-quinidine compound,[139] the functionalization of the C2 derivative failed. Protection of the nitrogen with different protecting group such as Acetyl and Boc- did not afforded the desired compound. The starting material (**137**) was measured and found to be inactive.

These results gave us insights for the preparation of a chemical probe. At first, the oxygen group was predicted to be a good attachment point for a linker. Because of the loss of activity and the reactivity of the scaffold, another part of the molecule needed to be selected for the synthesis of a probe.

3.3.3.3.3.   Relevance of Other Positions

The functionalization of the C2 position using Borono-Minisci chemistry afforded most of the desired compounds in good yield.[137] Interestingly, some side products were obtained during this one-pot reaction and permitted to explore others position around the quinidine scaffold (Table 17).

Entry	R^4 (X = OMe)		IC$_{50}$ (µM)	Entry	R^5 (X = H)		IC$_{50}$ (µM)
1	F—phenyl	(138)	inactive	8	F—phenyl	(145)	inactive
2	Cl (meta-phenyl)	(139)	inactive	9	Cl—phenyl	(146)	2.52 ± 0.32
3	Cl / F phenyl	(140)	5.40 ± 2.40	10	Br (meta-phenyl)	(147)	inactive
4	phenyl	(141)	inactive	11	phenyl	(148)	inactive
5	methyl—phenyl	(142)	non-isolated				
6§	F—phenyl	(143)	2.30 ± 0.50				
7§	Cl—phenyl	(144)	5.20 ± 1.02				

* Experiment performed by COMAS

Several molecules were obtained as a side product of the C2 functionalization. This observation had already been reported for the oxazatwistanes synthesis.[135] Any substitution in position R^4 lead to inactive compounds (Table 17, Entries 1-5). Only the di-substitution was slightly active but ten-fold less than the top compound **100** (Entry 3). When the same compounds were obtained from the reduced double bond scaffold (Entries 6 and 7), the *para*-fluoro and *para*-chloro remained active. This was an additional point in favor of using the double bond as modification point for the chemical probe preparation.

For the case of the cinchonidine scaffold (X = H, Entries 8-11), only the *para*-chloro substitution lead to an active compound (Entry 9).

3.3.3.4. Conclusion

A collection of 60 compounds was prepared using modern C-H activation chemistry. Despites the SAR studies and several rounds of synthesis, the initial hit (inhibitor **100**), remained the most active. This compound, named Autoquin, was selected for further biological investigation to determine the target(s) of this class of molecules.

3.3.4. Target Identification of Autoquin

A cell-based phenotypic screen permitted to identify Autoquin, a potent autophagy modulator. While the phenotypic response was characterized, it was interesting to identify the target(s) involved in this phenotypic response for this new autophagy inhibitor.

3.3.4.1.   Cell Painting Assay

The assay was performed at COMAS.

To identify potential targets of a bioactive small molecule, a complex phenotypic profiling such as the cell painting assay (CPA) can be employed. The CPA was developed to maximize profile diversity and to increase the amount of data and the number of insights gained out of a phenotypic HTS.[141] The approach involves staining different cell compartments such as nucleus, mitochondria, endoplasmic reticulum and Golgi using five different fluorescent channels (Figure 54).
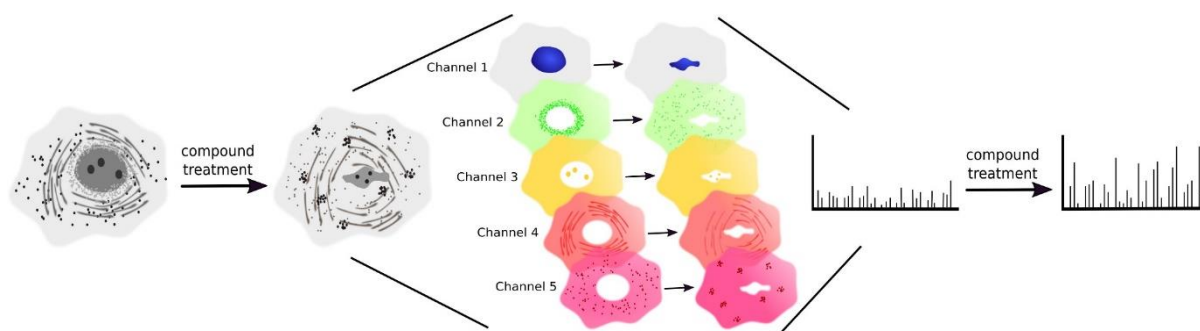
Figure 54. Cell painting assay workflow

Using this set up, the screen generates more complex data and allows the observation of different cellular compartments and processes. This is a significantly more complex system compared to the regular phenotypic screens.[142] An image-based analysis allows the evaluation of hundreds of parameters simultaneously for five different fluorescence channels. Reference compounds with known target or known phenotypic response were characterized in order to define a fingerprint for all known compounds. CPA permits unbiased monitoring of changes in numerous cellular features and biological processes. Screening a new compound and comparing the "fingerprint" to known bioactive compounds allows the identification of compounds that act by a similar mode-of-action and potentially through the same target. This screening method could be used as a tool for prediction of target or confirmation of an expected phenotypic response.

3.3.4.2.　Identification of the Lysosomotropic Agent Similarity

The CPA is based on the characteristic response by known compounds and the parameters change induced by these reference compounds. The COMAS possesses around thousand reference compounds with different targets and phenotypic effects. The fingerprint response (change in parameters such as cell and organelle morphology and size) was measured for several compounds from the cinchona alkaloid library, including Oxautin-1 and Autoquin (Figure 55).
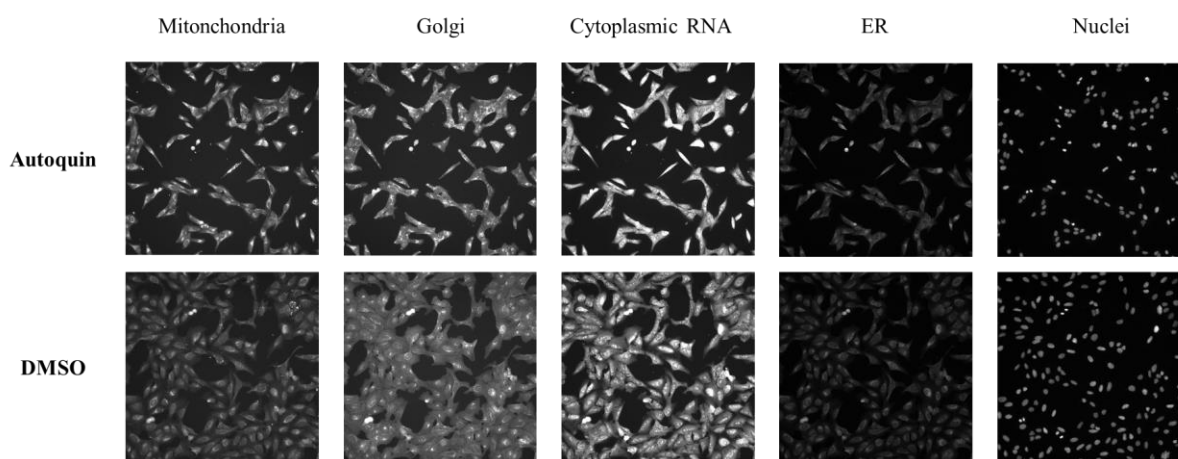
Figure 55. Picture analyzed for the cell-painting screen of Autoquin performed at COMAS. Pictures shown as example of the different compartments of the cell analyzed and the difference induced by the compound. Pictures on the top row correspond to cells treated with Autoquin. Those on the bottom row correspond to the DMSO control. ER: Endoplasmic reticulum.

The similarity of the fingerprint between the developed autophagy inhibitors and the known lysosomotropic agents was significant (60%) (Figure 56). Looking at the different cell compartments or cell morphological parameters, Autoquin showed a high similarity in its fingerprint with lysosomotropic agents such as Perhexiline and Astemizole.
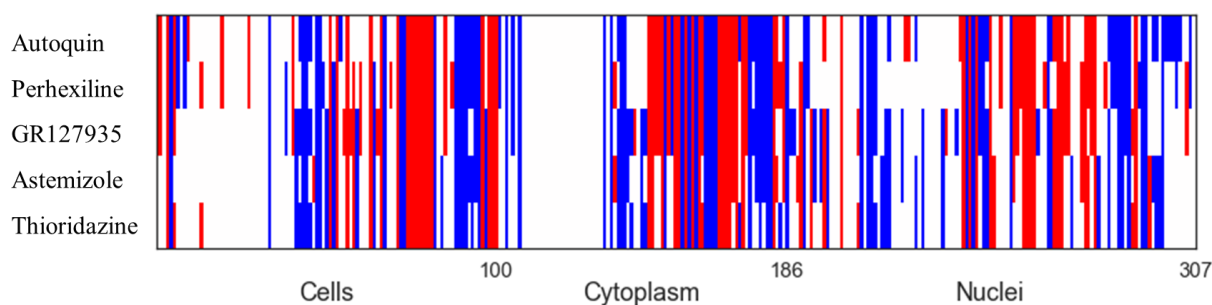
Figure 56. Fingerprints of Autoquin and known lysosomotropic agents. Figure by Dr. Axel Pahl.

The chemical structure of the lysosomotropic agents present inside the library are shown in Figure 57. Structure similarities between these compounds and Autoquin can be observed.

GR127935
Selective 5HT1B/D antagonist

Hits in antimalarial screen

Thioridazine
Dopamine receptor antagonist

Sertraline
5HT uptake inhibitor

Lidoflazine
Ca^{2+} channel activator

Perhexiline
Ca^{2+} blocking agent
vasodilator

Astemizole
H1 antagonist
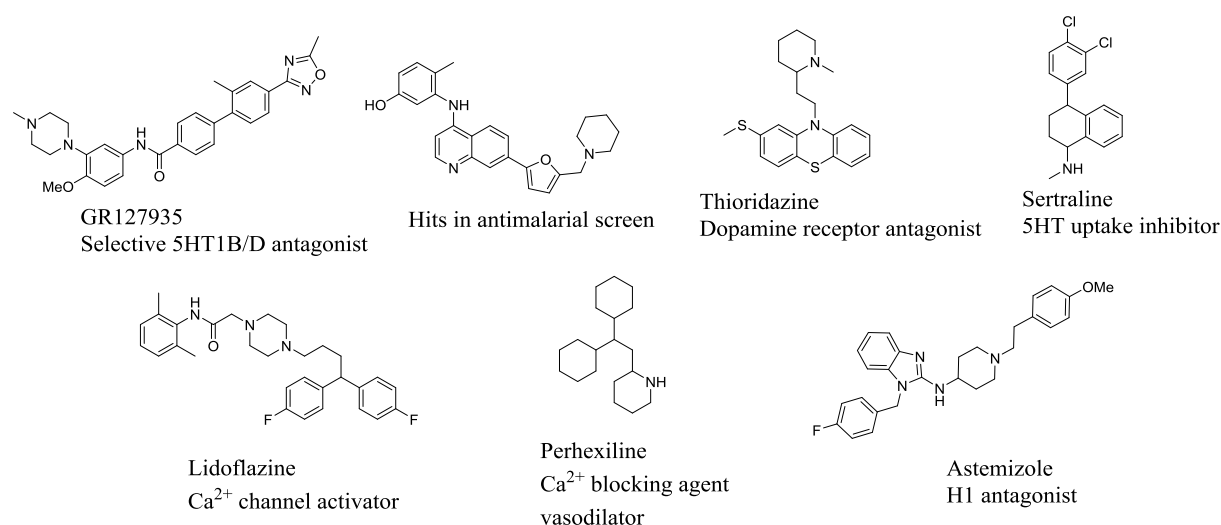
Figure 57. List of reference compounds known as lysosomotropic agents and known activities.

This data suggested that the synthesized compound act as lysosomotropic agents. However, CPA is useful to predict targets, complementary experiments to confirm the targets were necessary.

3.3.4.3. Validation of the Lysosomotropic Activity

Experiments performed by the Arenz Lab, Humboldt Universität zu Berlin.

Lysosomotropic agents are taken up selectively into lysosomes. This definition applies to every compounds irrespective of their chemical structure and of the mechanism of uptake (Figure 58). Lysosomes are involved in many biological processes and are required for the degradation of the cargo from the autophagosomes.[143]
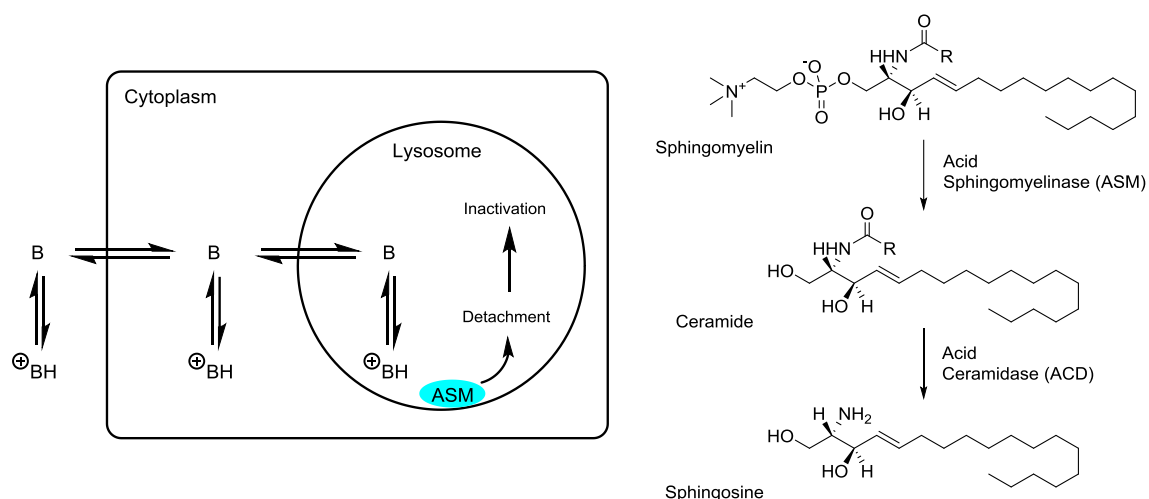
Figure 58. Mechanism of action for lysosomotropic agents.

The accumulation in the lysosomes sequesters bis-monoacylglycerophosphate (BMP) leading to detachment of sphingolipid hydrolases (including Acid sphingomyelinase, ASM) from the lysosomal membrane, leading to their degradation in the lysosomes. Sphingolipid hydrolases are required for autophagosome lysosome fusion, however the exact way this occurs is still unclear (Figure 58).[144]

The CPA of the compounds Oxautin-1 and Autoquin predicted that this compound could behave as lysosomotropic agents. In order to confirm this activity, the compounds were tested in two different assays monitoring activity of the sphingolipid hydrolase acid ceramidase (ACD) (Figure 59). ACD activity should be inhibited in a cell-based assay by lysosomotropic agents, which can accumulate in intact lysosomes. However, this should not occur in cell lysates, where lysosomes are no longer intact.
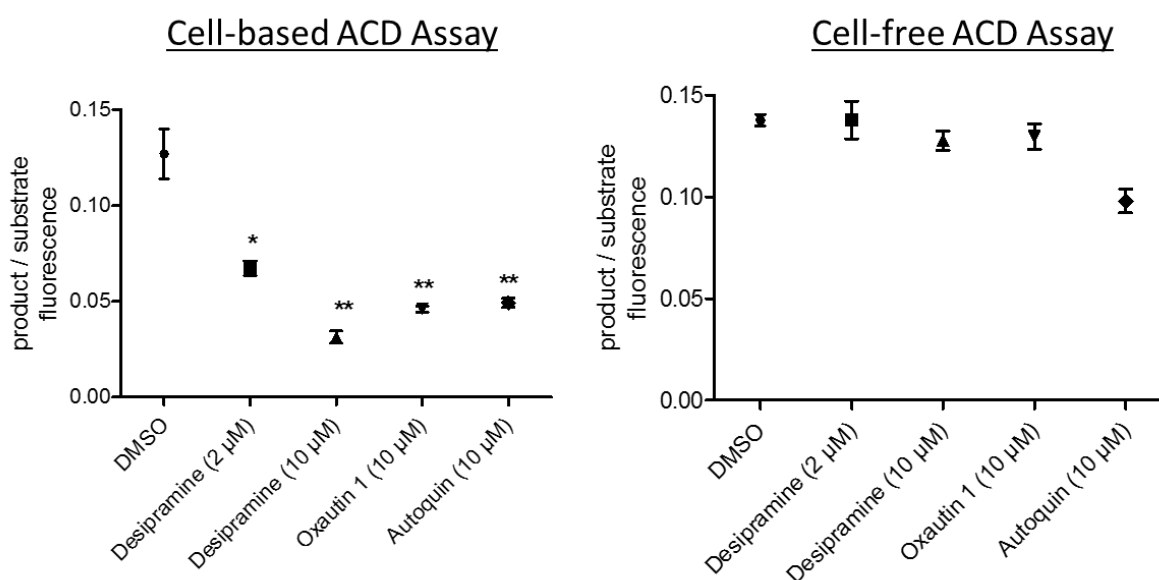
Figure 59. Cell based and cell-free ACD assay for Oxautin-1 and Autoquin. Experiment was performed twice. The data significantly different from untreated DMSO controls (*** indicates p < 0.001, ** indicates p < 0.01, ns: non-significant) by Student's t-test.

Both compounds, showed a significant decrease in ACD activity in the cell-based ACD assay. However, in a cell-free ACD assay, treatment the compounds did not inhibit the enzyme. These two experiments validated the CPA results and the compounds as lysosomotropic agents. Cinchona derivatives inhibit ASM and ACM indirectly. However, this experiment did not explain or characterized the main target responsible for inhibition of autophagosome biogenesis. This data suggested that Oxautin-1 and Autoquin have, at least, two targets.

3.3.4.4.   Calcitonin Gene-Related Peptide

Calcitonin Gene-Related Peptide (CGRP) receptors are composed of G protein-coupled receptor known as calcitonin-like receptor. CGRP exists as two form called α-CGRP and β- CGRP and are expressed by multiple cell types.[145,146] Daines *et al.* identified quinine analogs as non-peptide CGRP receptor antagonist.[147] Because of the structure similarity, Oxautin-1 and Autoquin were evaluated toward CGRP receptor as antagonist and agonist.

3.3.4.4.1. Cellular Agonist and Antagonist Effects toward CGRP Receptor

The assay was performed at Eurofins®. The compounds, Autoquin and Oxautin-1, were tested towards CGRP receptor in agonist and antagonist mode. Cellular agonist effect was calculated as a percentage of control response to a known reference agonist for each target and cellular antagonist effect was calculated as a percentage inhibition of control reference agonist response for each target (Figure 60). Details of the experiments can be found in the experimental part (chapter **4**).
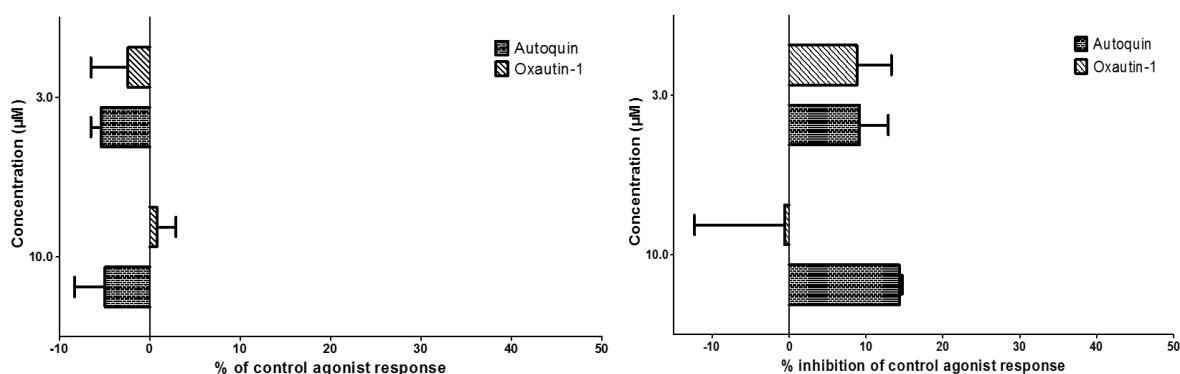
Figure 60. Evaluation of Oxautin and towards CGRP receptors. Agonist and antagonist effect were measured for both compounds at two different concentration (10 and 3 μM). Results showing a stimulation or an inhibition higher than 50% are considered to represent significant effects of the test compounds. A stimulation or an inhibition between 25% and 50% indicate weak to moderate effects. Results showing a stimulation or an inhibition lower than 25% are not considered significant.

We could not observe any significant impact of the compound Autoquin as well as Oxautin-1 as an agonist or antagonist of the CGRP receptors, and thus this target was devalidated.

3.3.4.4.2.   Calcium Assay

Calcium uptake is a vital event for the cells and is related to several dysfunction in cells.[148] The cell painting evaluation of the compound Autoquin (described in chapter **4.3.4.2**) revealed two similar compounds (Lidoflazine and Perhexiline) Ca^{2+} channel antagonist with a similarity of

61% in both cases. The impact of Autoquin was evaluated toward calcium uptake. This assay detects intracellular calcium mobilization using a cell permeable calcium-binding dye (Figure 61).
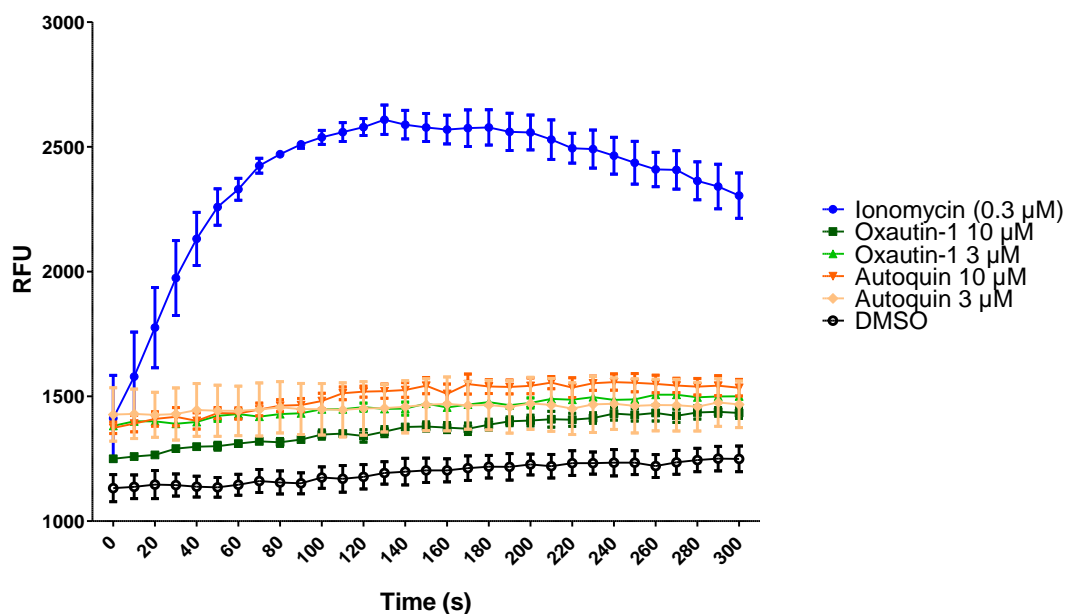
Figure 61. Calcium assay experiment of the Oxautin-1 and Autoquin in MCF7 cells. Ionomycin, a calcium ionophore, was used as a positive control and DMSO as a negative control. The experiment was repeated twice.

Because calcium uptake is a fast event, the experiment was measured during 300 s. The known compound promoting the calcium uptake in cells, Ionomycin, was used as a positive control.[149] We observed no increase in the calcium uptake while treating the cells with Oxautin-1 and Autoquin at two different concentrations (10µM and 3µM). It is still possible that these compounds may act as calcium channel uptake inhibitors, which would have to be evaluated using a different assay set-up.

3.3.4.5. Conclusion

Further investigations of Autoquin were performed in order to identify the biological target(s) involved in the autophagy response. A cell-painting assay revealed the similarity of the compound to lysosomotropic agents. A cell-based ACD assay was performed and confirmed the cell-painting screen prediction. However, this data did not explain the inhibition of autophagosome biogenesis.

Based on previous reports for similar compounds, CGRP receptors were tested but did not lead to any target identification. No impact of the calcium uptake was observed for Autoquin despites the prediction by the cell painting assay.

3.4. Summary

Autophagy is an essential cellular mechanism whose role is to remove long-lived, aggregated and/or misfolded proteins and to clear damaged organelles.[128] However, the process is not fully understood and the discovery of new tool compounds to study this process in greater detail is an active area of research.

Using a cell-based phenotypic screen, a low micromolar potent autophagy inhibitor, Autoquin, was identified. Several rounds of optimization were performed and a compound collection was synthesized. Autoquin was selected for further investigation of the potential target(s) involved in its mode-of-action.

Using a cell-painting assay, Autoquin showed a high similarity in its phenotypic fingerprint to lysosomotropic agents. Lysosomotropic activity is correlated to acid ceramidase level. Lysosomotropic agents should inhibit ACD in a cell-based assay. This mode-of-action was confirmed by a cell-based and cell-free ACD experiment, which showed that the enzyme was only inhibited in intact cells.

However, a second target was believed to be involved in the phenotypic response. Based on previous reports and structure similarity, several educated guesses were evaluated. Autoquin showed no activity toward CGRP in both agonist and antagonist mode.

Further biological experiments will be performed in a near future. A cellular thermal shift assay is currently ongoing and a pull-down will be performed as well. As described, the double bond was used as a site of choice for the probe synthesis (Figure 62). These experiments could, hopefully, guide us to the second target to further understand the link between Autoquin and the observed autophagy inhibition.
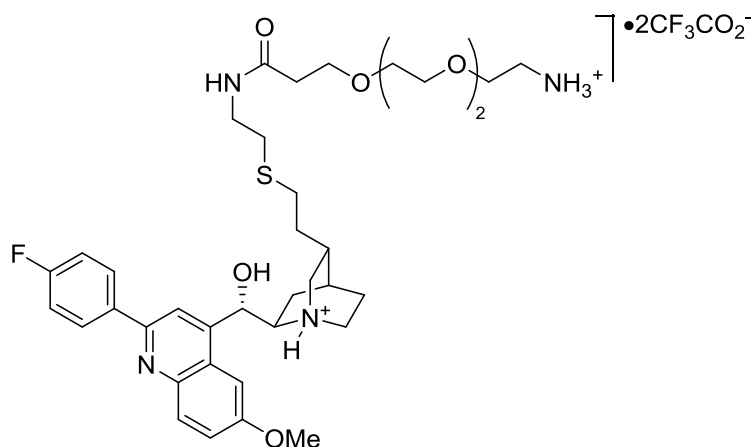
Figure 62. Active Pull down probe synthesized from the SAR study. Synthesis performed by Dr. Dan Foley

4. EXPERIMENTAL PART

4.1. Chemistry

4.1.1. General Directions

Unless otherwise noted, chemicals were obtained from Aldrich, Acros, TCI, or Alfa and were used without further purification. Dry solvents (DCM, THF and MeOH) were purchased and used without further purification unless stated otherwise. All other solvents or reagents were purified according to standard procedures or were used as received from Sigma Aldrich, Alfa Aesar, Acros, Fisher Scientific, Merck and TCI. Milli-Q grade water was used for all experiments. All reactions involving air or moisture sensitive reagents or intermediates were carried out following standard Schlenk line technique under an argon atmosphere and all the glassware were dried by heat gun under high vacuum prior to use. TLC was performed using pre-coated TLC Silica gel 60 F254 aluminum plates (Merck, Darmstadt), detection of compounds was performed by UV254 light and/or dipping into a solution of $KMnO_4$ (1.5 g in 400 mL H_2O, 5.0 g $NaHCO_3$) followed by heating with a heat gun. Column chromatography was performed using silica gel from Acros Organics (40–65 µm, 230–400 mesh). Flash master chromatography was performed using a Reveleris® X2 Flash System (Büchi) and GraceResolveTM cartridges.

4.1.1.1. Nuclear Magnetic Resonance

^1H and ^{13}C NMR spectroscopic data were recorded on a Varian Mercury VX 400, Bruker Avance DRX 400 or 500, Varian Unity Inova 600 at rt unless stated otherwise. NMR spectra were recorded using CD_3OD, $CDCl_3$, CD_2Cl_2 or DMSO-d_6 or as solvent. Chemical shift (δ) values are reported in ppm with the solvent resonance as internal standard (CD_3OD: $\delta = 3.31$ ppm for ^1H, $\delta = 49.00$ ppm for ^{13}C), ($CDCl_3$: $\delta = 7.26$ ppm for ^1H, $\delta = 77.16$ ppm for ^{13}C), (CD_2Cl_2: $\delta = 5.32$ ppm for ^1H, $\delta = 53.84$ for ^{13}C), (DMSO-d_6: $\delta = 2.50$ ppm for ^1H, $\delta = 39.52$ ppm for ^{13}C), multiplicities are indicated b.s (broadened singlet), s (singlet), d (doublet), t (triplet), q (quartet), m (multiplet), dd (doublet of doublet), dt (doublet of triplet), ddd (doublet of doublet of doublet), coupling constants (J) are given in Hertz (Hz). Unless stated otherwise all NMRs were measured at room temperature. Where possible, structural assignments were performed using standard 2-D NMR techniques (gCOSY, gHSQC, gHMBC) and using 3-D NMR technique (NOESY).

4.1.1.2. High Pressure Liquid Chromatography

Agilent HPLC (1100series) using a reversed phase column (C4 or C18, 5 μm, 250 x 4.6 mm) equipped with a Finnigan LCQ ESI spectrometer and an UV/VIS detector operating at 210 and 280 nm (flow rate: 1.0 mL/min, time: 15 min, solvents A: 0.1% HCOOH in water, B: 0.1% HCOOH in acetonitrile, 1 min 10% B, in 10 min to 100% B).

Preparative HPLC runs were performed on an Agilent HPLC (1100 series) using a reversed-phase C4 or C18 column (RP C4 or C18, solvents A: 0.1% TFA in water, B: 0.1% TFA in acetonitrile flow rate: 20.0 mL/min, for 5% B to 100% B over 55 min).

4.1.1.3. High Resolution Mass Spectrometry

HRMS-ESI were taken on an Accela HPLC-System (HPLC column 50/1 Hypersil GOLD1.9 μm) with an LTQ Orbitrap mass spectrometer from Thermo Scientific. (ESI)-MS were measured by using an Agilent 1100 series binary pump together with a reversed-phase HPLC column (Macherey-Nagel), ionization method: electron spray ionization.

4.1.1.4. Solid Phase Peptide Synthesis

Unless stated otherwise, the peptide synthesis was carried out on a 0.25 or 0.1 mmol scale using a CEM-Liberty peptide synthesizer with a CEM_Discover microwave. Each coupling was repeated twice and test cleavage of the peptide was performed at the end of each synthesis to ensure the desired peptide was obtained.

4.1.1.5. Optical Rotation Measurements

Optical rotations were measured using a Schmidt & Hänsch Polartronic polarimeter in cuvettes with a path length of 10 cm. Concentration and solvent used for the measurement are specified for each value.

4.1.2. Cargo Proteins and Lipidated Partners (Src and Kras)

4.1.2.1. Synthesis Building Blocks and Fluorophore

4.1.2.1.1. Building Blocks

allyl N2-(((9H-fluoren-9-yl)methoxy)carbonyl)-N6-(tert-butoxycarbonyl)-L-lysinate (2)
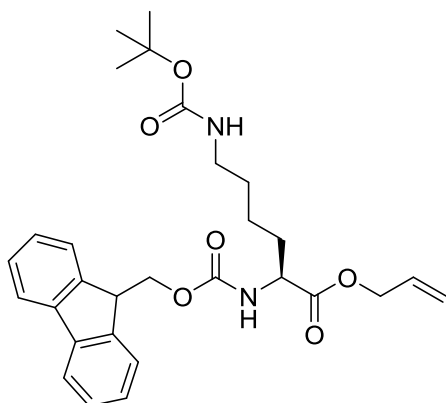
To a solution of Fmoc-Lys(Boc)-OH (10.0 g, 21.4 mmol, 1.0 eq) in dry methanol (66 mL) was slowly added caesium carbonate (3.48 g, 10.7 mmol, 0.5 eq). The solution was stirred for 10 min at r.t. The solvent was removed under reduced pressure and the residue coevaporated with Toluene. The solid residue was dissolved in dry DMF (66 mL). Then allyl bromide (17.6 mL, 0.21 mol, 10.0 eq) was added dropwise. The solution was stirred for 1.5 h. The crude was filtered through Celite® and the solvent was removed under reduced pressure. The obtained yellow oil was purified by flash chromatography using Ethyl acetate:cyclohexane (1:2 v/v) to furnish Fmoc-Lys(Boc)-OAll (9.48 g, 87%).

¹H NMR (400 MHz, CDCl$_3$): δ = 7.77 (d, J = 7.5 Hz, 2H), 7.61 (d, J = 6.8 Hz, 2H), 7.40 (t, J = 7.4 Hz, 2H), 7.32 (t, J = 7.4 Hz, 2H), 5.91 (qd, J = 12.0, 7.1 Hz, 1H), 5.30 (dd, J = 28.6, 13.7 Hz, 2H), 4.65 (d, J = 5.4 Hz, 2H), 4.54 (bs, 1H), 4.47 − 4.34 (m, 2H), 4.23 (dd, J = 11.0, 4.1 Hz, 1H), 3.11 (bs, 2H), 1.95 − 1.82 (m, 1H), 1.80 − 1.66 (m, 1H), 1.66 − 1.31 (m, 13H); **ESI-MS**: m/z = 509.90 [M + H]$^+$. Data in accordance with literature.[87]

methyl S-((2E,6E)-3,7,11-trimethyldodeca-2,6,10-trien-1-yl)-L-cysteinate) (4)
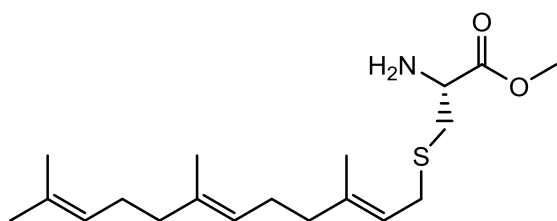
A solution of cysteine methyl ester (1.0 g, 5.83 mmol, 1.0 eq) in dry methanol (11 mL) was cooled down to 0 °C. A 7N ammonia solution (15.3 mL) was added slowly under vigorous stirring. Farnesyl bromide (1.58 mL, 5.83 mmol, 1.0 eq) was added to the prepared solution. The solution was stirred 3 h at 0 °C and 1 h at r.t. Solvent were removed under reduced pressure. The solid residue was dissolved in n-pentane (20 mL). The solution was filtered and the solvent were removed under reduced pressure. The crude product was purified using column chromatography on silica gel using a gradient of 0-3% methanol in DCM. A yellow oil was obtained (1.58 g, 80%).

^{1}H NMR (400 MHz, CDCl$_3$): δ = 5.15 (t, J = 7.4 Hz, 1H), 5.05 – 4.97 (m, 2H), 3.79 – 3.70 (m, 4H), 3.12 (ddd, J = 30.3, 13.1, 7.8 Hz, 2H), 2.89 (dd, J = 13.8, 4.6 Hz, 1H), 2.72 (dd, J = 13.8, 7.5 Hz, 1H), 1.99 (dt, J = 11.3, 6.8 Hz, 6H), 1.91 – 1.84 (m, 2H), 1.60 (s, 3H), 1.52 (s, 3H); **ESI-MS**: *m/z* = 340.71 [*M* + H]$^+$.

allyl N2-(((9H-fluoren-9-yl)methoxy)carbonyl)-N6-(Resin)-L-lysinate
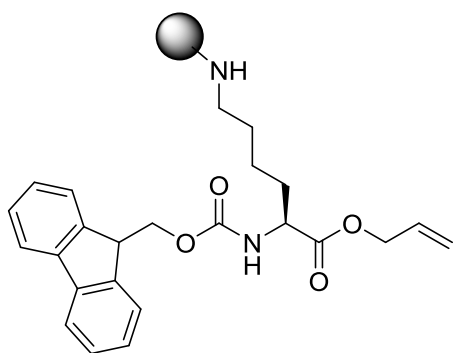
Fmoc-Lys(Boc)-OAll (0.5 eq) was dissolved in dry DCM (30 mL). TFA (30 mL) was added and the solution was stirred for 3 h at r.t. The solvent was coevaporated with toluene under reduced pressure and dried on high vacuum for 15 h. In a solid phase reactor, the 3-chlorotrytyl resin was dried on high vacuum for 12 h. Fmoc-Lys(OH)-OAll was dissolved in dry DCM (47 mL) and DIPEA (1.23 mL) was added dropwise. Dry DCM was added to the resin and gently shaken for 20 min under an inert atmosphere. The solvent was removed by filtration and the solution containing Fmoc-Lys(Boc)-OAll was added to the resin and mechanically stirred under Argon for 3.5 h. The solution was removed by filtration and the resin was washed with DCM/MeOH/DIPEA (17/2/1) to block the unreactive groups. The solution was removed and the resin was washed with DCM (3 x 10 mL), DMF (3 x 10 mL) and again DCM. Loading of the resin was calculated with a UV Fmoc test cleavage (l: 0.2-0.5 mmol/g).

ESI-MS: *m/z* = 409.11 [*M* + H]$^+$.

(Fmoc)HN-Lys-CO₂H:
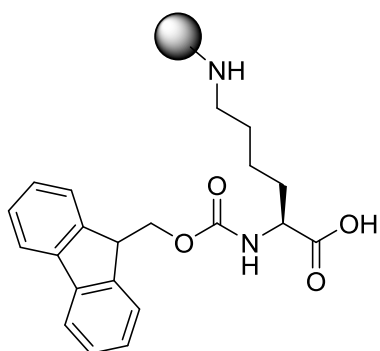
A solution containing PhSiH$_3$ (0.26 mL, 2.1 mmol, 14.0 eq), Pd(PPh$_3$)$_4$ (8.7 mg, 7.5 µmol, 0.05 eq) in THF (10 mL) was prepared. The solution was loaded to the resin and mechanically stirred under Argon during 12 h. The solution was removed by filtration and the resin was washed with THF (3 x 10 mL), DCM (3 x 10 mL), DMF (3 x 10 mL) and DCM. A test cleavage on 1.5 mg of the resin was performed to assure the completion of the reaction (DCM/0.5% TFA/2% TES).

ESI-MS: *m/z* = 369.09 [*M* + H]$^+$.

(Fmoc)HN-Lys-Cys(S-Far)-OMe:
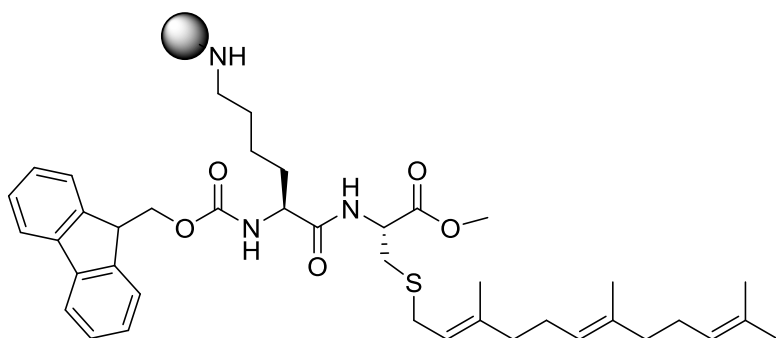
H-Cys(Far)-OMe (0.14 g, 0.40 mmol, 2.20 eq) and PyBOP (0.18 g, 0.33 mmol, 2.20 eq) were dissolved in a mixture of DMF/4-Methylmorpholine (0.08 mL, 0.69 mmol, 4.60 eq). The mixture was added to the resin (0.06 g, 0.15 mmol, 1.0 eq) and shaken overnight at r.t. The resin was extensively washed with DMF, DCM, DMF. The resin was dried under high vacuum for 3 h and a test cleavage was performed.

ESI-MS: *m/z* = 690.27 [*M* + H]$^+$.
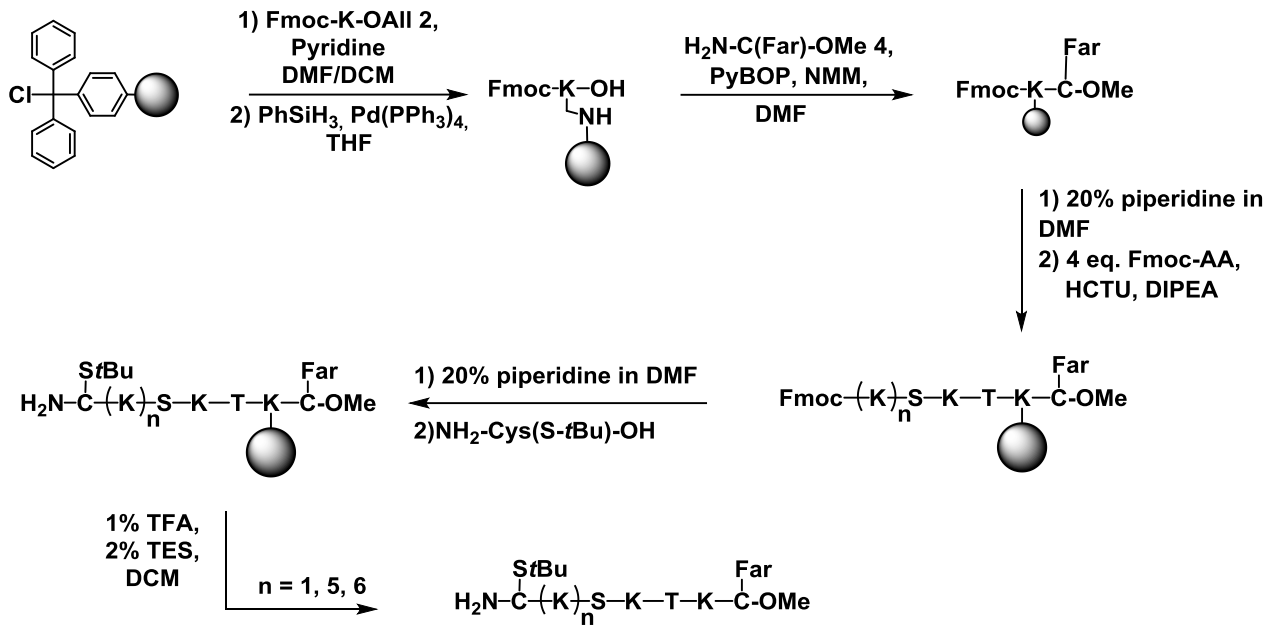
Figure 63. Scheme synthesis of the Ras family peptides.
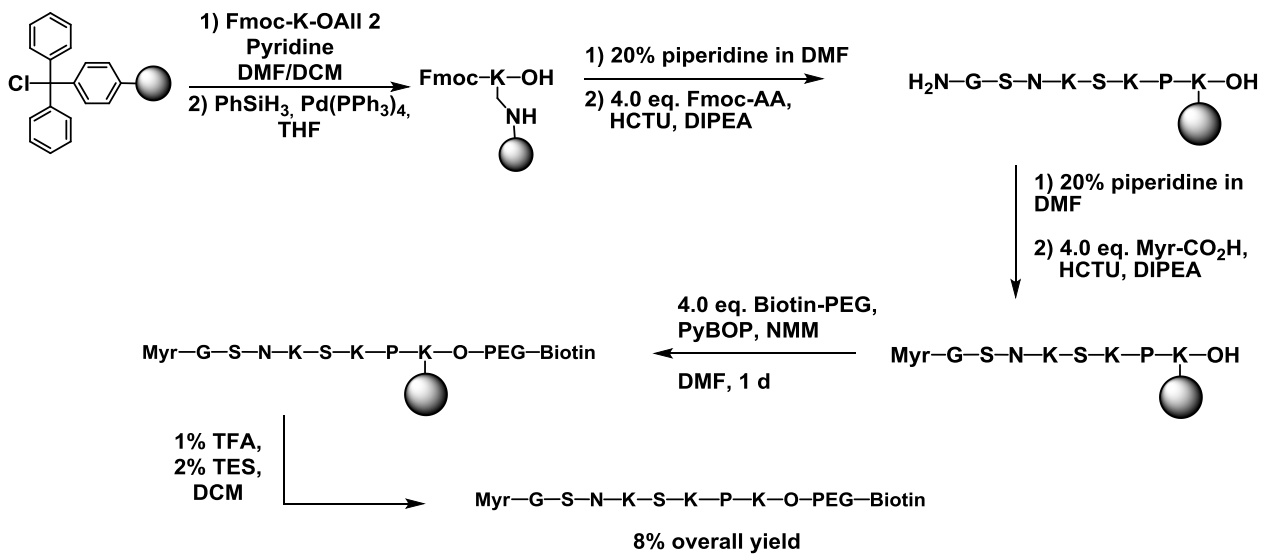
Figure 64. Scheme synthesis of the Src family peptides

4.1.2.2.   Lipid binding analogues peptides

K-Ras4B family peptides
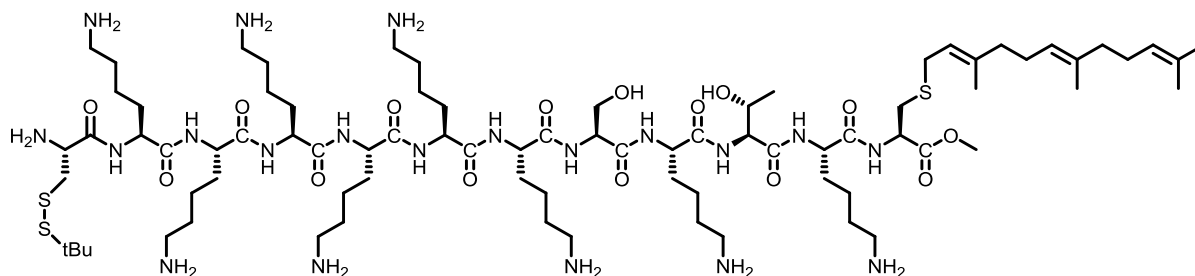
K-Ras4B peptide The C-terminal K-Ras4B peptide was synthesized by means of solid-phase peptide synthesis (scale: 0.1 mmol, loading: 0.4 mmol/g trityl resin) similar to a previously described procedure employing immobilized Fmoc-Lys-Cys-Far-OMe. Fmoc cleavage was achieved using 5 mL of 20% piperidine in DMF (2 x 10 min). Subsequently the resin was washed with DMF (5 x 10 mL). All amino acids were coupled using 4.0 eq amino acid, 4.0 eq HCTU and 8.0 eq DIPEA in 5 mL DMF. Double couplings were carried out at 60°C for 30 min each cycle. Cleavage of the resin from the solid support was performed by treating the resin with 10 mL of 1 % TFA in dry DCM containing 2 % TES for 1 hour, then with 1.5 % TFA for 1 hour and with 2 % TFA in DCM for an additional hour. After each treatment, the resin was washed with DCM/MeOH 1:1 and MeOH. Finally, toluene was added to the mixture and the solvents were evaporated under reduced pressure. The resulting crude product was dissolved in a minimal amount of MeOH and slowly added to an ice-cold solution of Et$_2$O. The precipitate was dissolved in DMSO and after purification by preparative HPLC using a C18 column, the peptide was obtained (10 mg, 9 %).

HR-ESI-MS: $m/z = 873.5573$ ([M + 2H]$^+$, calcd. for C$_{81}$H$_{154}$N$_{20}$O$_{15}$S$_3$$^+$: 1744.1143).

K-Ras4B analog 1 peptide The C-terminal K-Ras4B analog 1 peptide was synthesized by means of solid-phase peptide synthesis (scale: 0.05 mmol, loading: 0.4 mmol/g trityl resin) similar to a previously described procedure employing immobilized Fmoc-Lys-Cys-Far-OMe.[150] Fmoc cleavage was achieved using 5 mL of 20% piperidine in DMF (2 x 10 min). Subsequently the resin was washed 5 times with DMF. All amino acids were coupled twice employing 4.0 eq amino acid, 4.0 eq HCTU and 8.0 eq DIPEA in 5 mL DMF. Double coupling were carried out at 60 °C for 30 min each cycle. Cleavage of the resin from the solid support was performed by treating the resin with 10 mL of 1 % TFA in dry DCM containing 2 % TES for 1 h, then with 1.5 % TFA for 1 hour and with 2 % TFA in DCM for an additional hour. After each treatment the resin was washed with DCM/MeOH (1:1) and MeOH. Finally, toluene was added to the mixture and the solvents were evaporated under reduced pressure. The resulting crude product was dissolved in a minimal amount of MeOH and slowly added to an ice-cold solution of Et$_2$O. The precipitate was dissolved in DMSO and after purification by preparative HPLC using a C18 column, the peptide was obtained (7 mg, 14 %).

HR-ESI-MS: *m/z* = 888.5142 ([M + H]$^+$, calcd. for C$_{42}$H$_{78}$N$_7$O$_7$S$_3$$^+$: 888.5125). ($\Delta$ = 2.51 ppm)
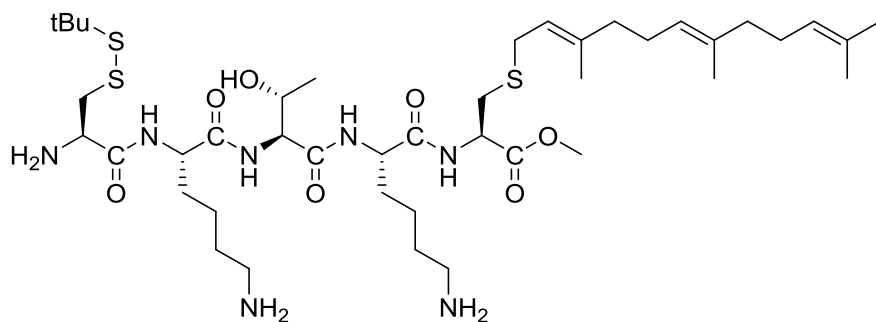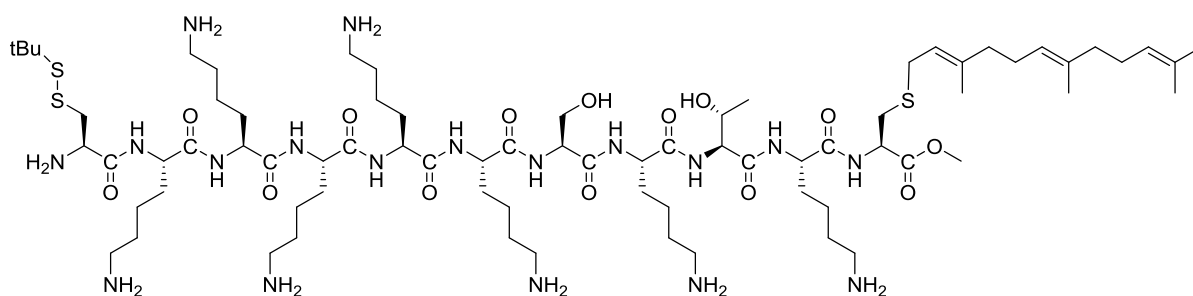
K-Ras4B analog 2 peptide The C-terminal K-Ras4B analog 2 peptide was synthesized by means of solid-phase peptide synthesis (scale: 0.1 mmol, loading: 0.4 mmol/g trityl resin) similar to a previously described procedure employing immobilized Fmoc-Lys-Cys-Far-OMe.[150] Fmoc cleavage was achieved using 5 mL of 20% piperidine in DMF (2 x 10 min). Subsequently the resin was washed with DMF (5 x 5 mL). All amino acids were coupled twice employing 4.0 eq amino acid, 4.0 eq HCTU and 8.0 eq DIPEA in 5 mL DMF. Double coupling were carried out at 60°C for 30 min each cycle. Cleavage of the resin from the solid support was performed by treating the resin with 10 mL of 1 % TFA in dry DCM containing 2 % TES for 1 h, then with 1.5 % TFA for 1 h and with 2 % TFA in DCM for an additional hour. After each treatment the resin was washed with DCM/MeOH 1:1 and MeOH. Finally, toluene was added to the mixture and the solvents were evaporated under reduced pressure. The resulting crude product was dissolved in a minimal amount of MeOH and slowly added to an ice-cold solution of Et$_2$O. The precipitate was dissolved in DMSO and after purification by preparative HPLC using a C18 column, the peptide was obtained (4 mg, 9 %).

HR-ESI-MS: m/z = 1616.0225([M + H]$^+$, calcd. for C$_{75}$H$_{144}$O$_{14}$N$_{18}$S$_3$$^+$: 1616.0188). ($\Delta$ = 2.39 ppm)

Src family peptides

Biotinylated Src-Myr peptide The C-terminal Src peptide was synthesized by means of solid-phase peptide synthesis (scale: 0.1 mmol, loading: 0.4 mmol/g trityl resin) using standard solid phase peptide synthesis. Fmoc cleavage was achieved using 5 mL of 20% piperidine in DMF (2 x 10 min). Subsequently the resin was washed with DMF (5 x 5 mL). All amino acids were coupled twice employing 4.0 eq amino acid, 4.0 eq HCTU and 8.0 eq DIPEA in 5 mL DMF. Double coupling were carried out at 60 °C for 30 min each cycle. The resulting N-terminal amino acid was coupled with 5 eq myristic acid at rt in DMF. The C-terminal amino acid was deprotected using PhSiH$_3$ (g, mmol, eq), Pd(PPh$_3$)$_4$ (g, mmol, eq) in THF. The Biotin-PEG Linker was coupled using Biotin-PEG (4.0 eq), PyBOP (4.0 eq), NMM (4.6 eq) in DMF. Cleavage of the resin from the solid support was performed by treating the resin with 10 mL of 2 % TFA in dry DCM containing 2 % TES for 1 h. The resin was washed with DCM/MeOH 1:1 and MeOH. Finally toluene was added to the mixture and the solvents were evaporated under reduced pressure. The resulting crude was dissolved in minimal amount of MeOH and after purification by preparative HPLC using a C18 column, the peptide was obtained (30 mg, 10 %).

HR-ESI-MS: m/z = 1483.9353 ([M + H]$^+$, calcd. for C$_{68}$H$_{124}$N$_{16}$O$_{17}$S$^+$: 1483.9286). (Δ = 4.91 ppm)

4.1.3. Small Molecules Compound Collection Blocking the UNC119/Src Interaction

4.1.3.1. Synthesis of Benzothiazolone-Based Analogs

3-isopropylbenzo[d]thiazol-2(3H)-one (5)

2(3*H*)-Benzothiazolone (1.0 g, 6.6 mmol, 1.0 eq) was dissolved in dry DMF (16 mL) under an argon atmosphere. 2-iodopropane (0.70 mL, 7.0 mmol, 1.1 eq) was added dropwise. The reaction mixture was cooled to 0 °C prior addition of NaH (0.37 g, 7.92 mmol, 1.2 eq). The reaction was stirred for 3 h at reflux. The resulting mixture was washed with brine and extracted three times with DCM. The organic phase was dried over Na_2SO_4, concentrated under high vacuum and purified by column chromatography using EtOAc/cyclohexane (1:1) (0.79 g, 60 %).

^{1}H NMR (400 MHz, CDCl$_3$): δ = 7.30 (d, J = 7.8 Hz, 1H), 7.21 (t, J = 7.8 Hz, 1H), 7.13 (d, J = 8.2 Hz, 1H), 7.04 (t, J = 7.6 Hz, 1H), 4.73 (dt, J = 13.8, 6.9 Hz, 1H), 1.50 (d, J = 7.0, 6H).

3-isopropyl-2-oxo-2,3-dihydrobenzo[d]thiazole-6-sulfonyl chloride (6)

To chlorosulfonic acid (12.0 eq.), 3-isopropylbenzo[d]thiazol-2(3H)-one (0.9 mmol, 1.0 eq) was added slowly at 0 °C under an argon atmosphere. The mixture was stirred at 0 °C for 20 min, and at 70 °C for 7 h. The mixture was carefully quenched onto ice (10 mL) under vigorous stirring. The precipitated crude was extracted with EtOAc (3 x 20 mL). The combined organic layers were dried over MgSO$_4$, filtered and concentrated under reduced pressure. The crude product was used without purification in the next step. Due to its poor stability in water, no ESI-MS data could be obtained.

tert-butyl piperazine-1-carboxylate (7)

To a solution of piperazine (2.4 g, 27.9 mmol, 1.0 eq) in dry DCM, was added dropwise a solution of di-*tert*-butyl dicarbonate, (3.0 g, 13.4 mmol, 0.5 eq) in dry DCM. The reaction mixture was stirred for 1 day until completion of the mono protected piperazine. The solution was washed with water and brine to extract the unreacted starting material. The solvent were removed under reduced pressure to afford the desired compound as a white solid (3.7 g, 72%). **^{1}H NMR (CDCl$_3$, 400 MHz)** δ 3.54 (t, 4H, J = 4.9 Hz), 3.03 (t, 4H, J = 4.7 Hz), 1.26 (s, 9H)**.**

naphthalen-2-yl(piperazin-1-yl)methanone (8a)

tert-butyl piperazine-1-carboxylate (3.7 g, 19.9 mmol, 1.0 eq) and 2-naphthoylchloride (5.7 g, 29.9 mmol, 1.5 eq) were mixed in dry DCM (15 mL). Then, Et$_3$N (4.2 mL, 29.9 mmol, 1.5 eq) was added dropwise at 0 °C. The reaction mixture was allowed to warm up to r.t and stirred o/n. The reaction mixture was washed with water and brine. The organic phase was dried under Na$_2$SO$_4$ and concentrated under reduced pressure. The crude compound was solved in a mixture of DCM/TFA 1:1 (50 mL). The reaction was stirred at r.t for 2 h until full deprotection of the starting material (monitored by TLC and ultra-HPLC). Toluene was added to the mixture and the solvents were co-evaporated under reduced pressure. The desired compound was obtained as an oil (2.88 g, 59 % over 2 steps) and used for the next step without further purification.

6-((4-(2-naphthoyl)piperazin-1-yl)sulfonyl)-3-isopropylbenzo[d]thiazol-2(3H)-one (9a)

Compound x (0.5 g, 2.10 mmol, 1.0 eq) and compound x (0.61 g, 2.10 mmol, 1.0 eq) were dissolved in pyridine (5 mL) and stirred at 70 °C for 5 h. The solvent were removed under high vacuum and the crude was purified by preparative HPLC to afford the desired compound as a xx solid? (150 mg, 75%).

^{1}H NMR (400 MHz, DMSO): δ = 8.14 (d, J = 1.8 Hz, 1H), 7.96 − 7.92 (m, 3H), 7.75-7.65 (m, 1H), 7.60 − 7.52 (m, 1H), 7.45 (dd, J = 8.6, 1.4 Hz, 1H), 7.27 − 7.21 (m, 1H), 7.18 − 7.10 (m, 2H), 4.88 − 4.79 (m, 1H), 3.54 (s, 4H), 3.02 (s, 4H), 1.50 (d, J = 6.9 Hz, 6H).

HR-ESI-MS: *m/z* = 496.1371 ([*M* + H]$^+$, calcd. for C$_{25}$H$_{26}$O$_4$N$_3$S$_2$$^+$: 496.1359).
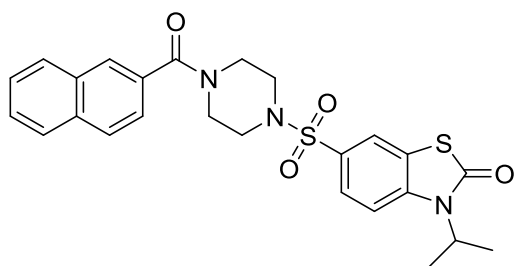
4.1.3.2.   Commercially Available Compounds

All the others compounds used for the UNC119/Src chemical library were purchased from ChemDiv®. The molecular weight and the UV traces of all the compounds were controlled by ESI-MS and the selected top compound was checked by ^{1}H NMR and HR-MS in house.
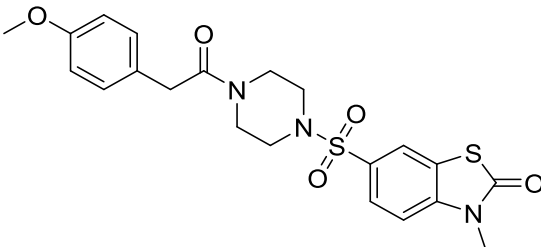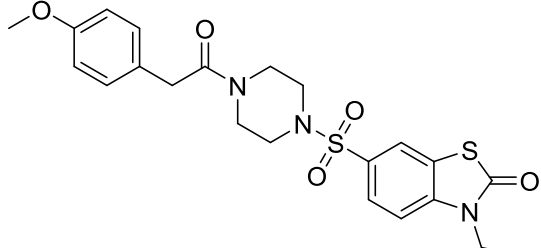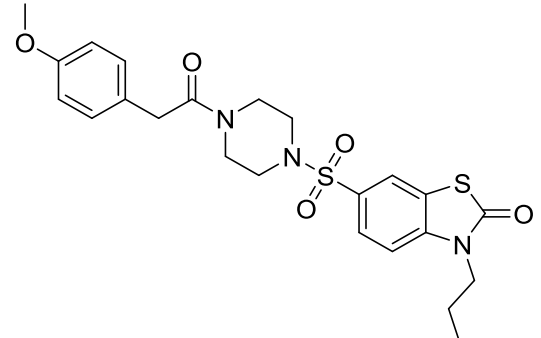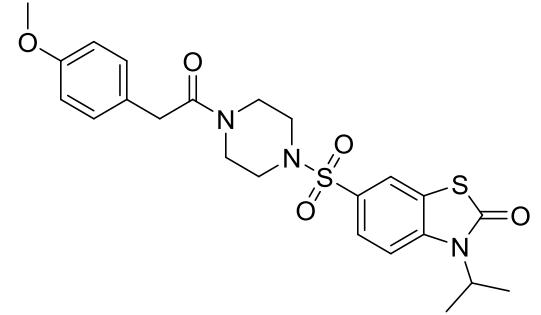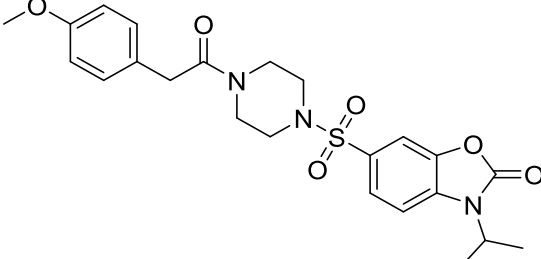
Compound ChemDiv® (catalog number: #L306_1198) (35)
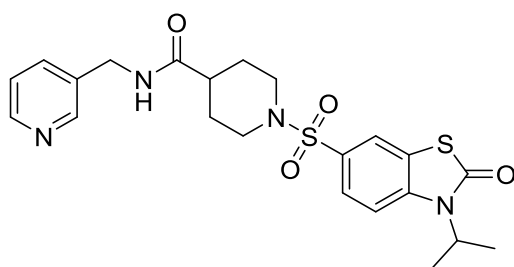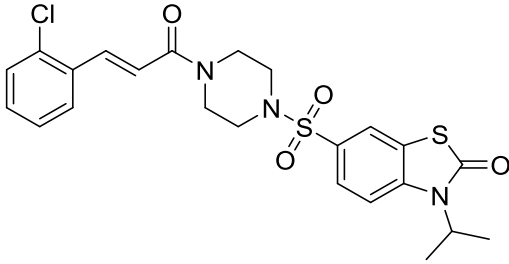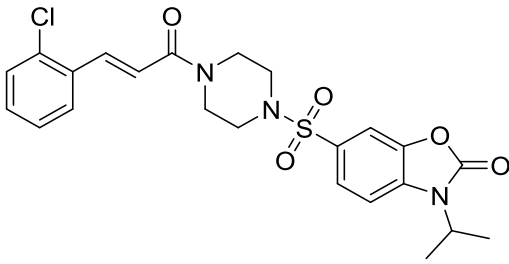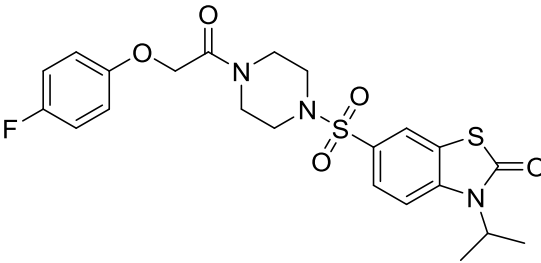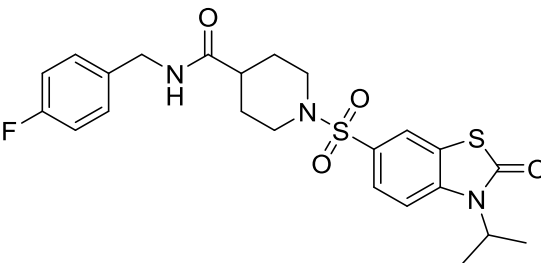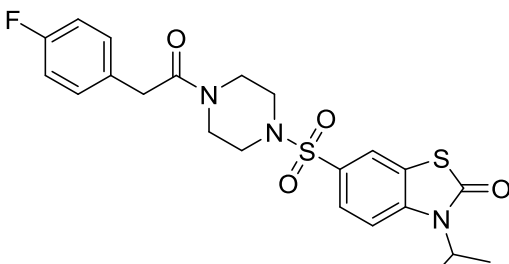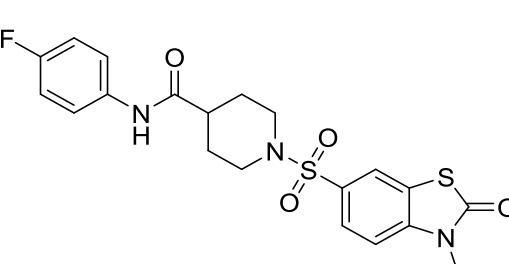
Compound **35** (5.3 mg) was obtained as a white powder from ChemDiv. Analytical data were verified in-house before screening and further biological evaluation.

HR-ESI-MS: *m/z* = 475.1465 ([*M* + H]$^+$, calcd. for C$_{22}$H$_{26}$N$_4$O$_4$S$_2$$^+$: 475.1468). (Δ = 0.59 ppm)

Table 18: Complete list of purchased compound from ChemDiv for disrupting the UNC119/Src interaction.

Compound	Catalogue Number #	Chemical structure	Molecular weight (g/mol^{-1})
10	L475-0214		461.55
11	L475-0363		475.58
12	L475-0666		489.61
13	L475-0835		489.61
14	L694-0363		473.54

15	L475-0816		506.04
16	L694-0344		489.97
17	L475-0915		493.57
18	L306-1319		491.61
19	L475-0830		477.57
20	L306-1238		477.58

21	L475-0851		**480.00**
22	L475-0923		**513.56**
23	L475-0885		**481.00**
24	L475-0855		**494.03**
25	L475-0833		**501.62**
26	L475-0837		**485.62**

27	L475-0866		477.57
28	L475-0876		477.57
29	L475-0916		501.62
30	L475-0834		501.62
31	L475-0832		498.62
32	L475-0839		489.56

33	L475-0887		**515.64**
34	L478-0814		**514.41**
35	L306_1198		**474.59**
36	L475-0803		**516.63**
37	L475-0914		**505.61**
38	L475-0859		**510.03**

39	L475-0880		**484.59**
40	L475-0781		**513.59**
41	L475-0907		**475.58**
42	L475-0883		**519.63**
43	L475-0886		**473.61**
44	L475-0908		**471.59**

45	L475-0910		473.61
46	L306-1210		494.04
47	L306-1348		480.65
48	L475-0760		502.60
49	L475-0783		492.58
50	L475-0898		446.55

| 51 | L475-0826 | | 519.63 |

| 52 | L475-0784 | | 516.63 |

4.1.4. Compound Collection Based on the Cinchona Alkaloid Scaffold

4.1.4.1. General Procedure

4.1.4.1.1. General Procedure IV: Borono-Minisci Reaction

$R^1B(OH)_2$ (3.0 eq)
TFA (3.0 eq)
$AgNO_3$ (0.6 eq)

$K_2S_2O_8$ (2.0 eq)
DCM/H_2O
rt, 6 h -> 24 h
20-55%

X= -H or -OMe

To a solution of the selected alkaloid (40 mg, 120 µmol) in DCM (1.25 mL) was added trifluoroacetic acid (28 µL, 370 µmol) followed by arylboronic acid (3.0 eq). Water (0.75 mL) was then added, followed by silver (I) nitrate (8 mg, 40 µmol) in water (0.50 mL). Potassium persulfate (100 mg, 370 µmol) was then added and the solution was stirred vigorously at rt. After 16 h the reaction was worked up by quenching with 3 mL of sat. NaHCO3 and diluting with 5 mL CH2Cl2. The organic layer was separated and the aqueous was washed with 3 x 5 mL iPrOH:CHCl3 (10%) mixture. The organic layers were combined, dried (Na2SO4) and filtered. The solvent was removed in vacuo and the mixture was purified by FC eluting 1–4 % (MeOH:CHCl3) or by mass-directed preparative HPLC.

4.1.4.1.2.   General Procedure V: Suzuki Coupling of Aryl Chloride

$R^2B(OH)_2$ (2.05 eq)
Na_2CO_3 (10.0 eq)
$PdCl_2dppf$ (0.05 eq)

Dioxane/H_2O, 30 min,
μW, 100 °C
50-85 %

E = Br or I
X = OMe or H

To a microwave tube charged with a solution of aryl bromide (25 mg, 65 µmol, 1.0 eq) and boronic acid (100 µmol, 1.5 eq) in dioxane (2 mL) was added a solution of Na_2CO_3 (69 mg, 0.65 mmol, 10 eq) in H_2O (1 mL) at rt. The reaction was degassed for 10 min with argon. Then, $PdCl_2dppf$ (13 mg, 15 µmol, 5 mol%) was added. The reaction mixture was stirred for 1 h at 100 °C in a CEM Discover microwave reactor. The reaction was cooled to room temperature, filtered through a pad of Celite® and the Celite washed with EtOAc (3 x 20 mL). The organic phase was washed with brine. The resulting aqueous phase was extracted with 2 x 20 mL 10% *i*PrOH in CHCl$_3$. Organic phases were dried (Na_2SO_4), filtered, and the solvent removed under reduced pressure. The crude was purified by preparative HPLC (ACN/H_2O + 0.1 % TFA) or a Reveleris® X2 Flash System (DCM/1-5% MeOH).

4.1.4.1.3.   C2 Substituted and Side Products Compound Collection

(S)-(2-(4-fluorophenyl)-quinolin-4-yl)((2R,4S,5R)-5-vinylquinuclidin-2-yl)methanol-trifluoroacetate (114)

The title compound was synthesized following **General Procedure IV** starting with cinchonine (40.0 mg, 136.0 µmol, 1.0 eq) and 4-Fluorophenylboronic acid (57.0 mg, 405 µmol, 3.0 eq). Purified using preparative HPLC (ACN/H$_2$O + 0.1 % TFA) to afford the product as an amorphous solid (23 mg, 38%).

^{1}H NMR (600 MHz, MeOD): δ = 8.31 (s, 1H), 8.29 (d, J = 8.4 Hz, 1H), 8.25 − 8.18 (m, 3H), 7.94 − 7.89 (m, 1H), 7.79 − 7.74 (m, 1H), 7.37 − 7.31 (m, 2H), 6.13 (s, 1H), 5.76 (ddd, J = 17.3, 10.5, 7.0 Hz, 1H), 5.12 (d, J = 17.2 Hz, 1H), 5.02 (d, J = 10.5 Hz, 1H), 4.31 − 4.25 (m, 1H), 3.75 (t, J = 8.9 Hz, 1H), 3.63 (dd, J = 13.0, 10.7 Hz, 1H), 3.38 − 3.31 (m, 2H), 2.82 (dd, J = 3.4, 1.7 Hz, 1H), 2.32 − 2.27 (m, 1H), 2.26 − 2.20 (m, 1H), 2.12 (dd, J = 5.9, 2.9 Hz, 1H), 2.01 − 1.94 (m, 1H), 1.62 (m, 1H); **^{13}C NMR** (151 MHz, MeOD): δ = 165.95 (d, J = 250.1 Hz), 162.29 (q, J = 36.1 Hz), 156.97, 151.69, 146.94, 139.15, 134.75, 132.58, 131.53 (d, J = 8.8 Hz), 129.31, 128.85, 125.28, 124.05, 118.58, 117.15 (d, J = 22.3 Hz), 68.74, 61.75, 55.58, 49.57, 45.49, 38.50, 28.21, 25.15, 19.43; **^{19}F NMR** (565 MHz, MeOD): δ = 77.03, -112.10; **HR-ESI-MS**: *m/z* = 389.2023 ([*M* + H]$^+$, calcd. for C$_{25}$H$_{26}$ON$_2$F$^+$: 389.2024) (Δ = 0.30 ppm)– No TFA visible; $[\boldsymbol{\alpha}]_{\mathbf{20}}^{\boldsymbol{D}}$ = + 71° (c = 1.0, MeOH).

(*R*)-(2-(4-fluorophenyl)-quinolin-4-yl)((2*S*,4*S*,5*R*)-5-vinylquinuclidin-2-yl)methanol-trifluoroacetate (149)

The title compound was synthesized following **General Procedure IV** starting with cinchonidine (40.0 mg, 136.0 µmol, 1.0 eq) and 4-Fluorophenylboronic acid (57.0 mg, 465 µmol, 3.0 eq). Purified using preparative HPLC (ACN/H$_2$O + 0.1 % TFA) to afford the product as an amorphous solid (19 mg, 32%).

^{1}H NMR (500 MHz, MeOD): δ = 8.27 (s, J = 9.3 Hz, 1H), 8.24 – 8.18 (m, 4H), 7.87 (t, J = 7.7 Hz, 1H), 7.72 (t, J = 7.7 Hz, 1H), 7.31 (t, J = 8.7 Hz, 2H), 6.06 (s, 1H), 5.75 (ddd, J = 17.3, 10.4, 7.1 Hz, 1H), 5.11 (d, J = 17.1 Hz, 1H), 5.02 (d, J = 10.5 Hz, 1H), 4.31 – 4.23 (m, 1H), 3.74 (t, J = 8.8 Hz, 1H), 3.62 (dd, J = 12.8, 10.8 Hz, 1H), 3.38 – 3.31 (m, 1H), 2.82 (s, 1H), 2.32 – 2.19 (m, 2H), 2.12 (t, J = 4.9 Hz, 1H), 1.96 (t, J = 9.7 Hz, 1H), 1.61 (dd, J = 13.3, 10.6 Hz, 1H), 1.36 – 1.17 (m, 1H); **^{13}C NMR** (126 MHz, MeOD): δ = 165.75 (d, J = 249.5 Hz), 162.38, 157.27, 150.32, 148.08, 139.14, 135.68, 132.03, 131.26 (d, J = 8.7 Hz), 129.88, 128.98, 125.18, 123.73, 118.25, 117.27, 117.02 (d, J = 22.1 Hz), 68.77, 61.79, 55.58, 49.63, 45.56, 38.53, 28.19, 25.16, 19.47; **^{19}F NMR** (565 MHz, MeOD): δ = -77.06, -111.82; **HR-ESI-MS**: *m/z* = 389.2025 ([*M* + H]$^+$, calcd. for C$_{25}$H$_{26}$ON$_2$F$^+$: 389.2024) (Δ = 0.26 ppm)– No TFA visible; $[\alpha]_{20}^{D}$ = - 34° (c = 1.0, MeOH).

(*R*)-(7-(4-fluorophenyl)-quinolin-4-yl)((2*S*,4*S*,5*R*)-5-vinylquinuclidin-2-yl)methanol-trifluoroacetate (145)

The compound was synthesized following **General Procedure IV**. Crude was purified using preparative HPLC (ACN/H_2O + 0.1 % TFA) to afford the pure compound (2 mg, 3%).

^{1}H NMR (500 MHz, MeOD): δ = 8.87 (d, J = 20.6 Hz, 1H), 8.31 − 8.19 (m, 1H), 8.16 − 8.04 (m, 1H), 7.98 (d, J = 7.4 Hz, 1H), 7.85 (dd, J = 12.5, 4.7 Hz, 1H), 7.76 (dd, J = 8.5, 5.3 Hz, 2H), 7.20 (dd, J = 11.5, 5.6 Hz, 2H), 5.98 (d, J = 25.2 Hz, 1H), 5.77 − 5.62 (m, 1H), 5.11 − 5.00 (m, 2H), 4.97 − 4.89 (m, 1H), 4.25 − 4.04 (m, 1H), 3.72 − 3.61 (m, 1H), 3.55 (dd, J = 23.6, 11.2 Hz, 1H), 2.74 (s, J = 6.9 Hz, 1H), 2.30 − 2.10 (m, 2H), 2.06 − 2.00 (m, 1H), 1.96 − 1.84 (m, 1H), 1.62 − 1.44 (m, 1H), 1.35 − 1.15 (m, 1H); **HR-ESI-MS**: *m/z* = 389.2024 ([*M* + H]$^+$, calcd. for $C_{25}H_{26}ON_2F^+$: 389.2024) − No TFA visible., $[\alpha]_{20}^{D}$= -38° (c = 1.0, MeOH) (Δ = 0.01 ppm).

(S)-(2-(4-fluorophenyl)-6-methoxyquinolin-4-yl)((2R,4S,5R)-5-vinylquinuclidin-2-yl)methanol- trifluoroacetate (100)

The title compound was synthesized following **General Procedure IV** starting with quinidine (40.0 mg, 120.0 µmol, 1.0 eq) and 4-Fluorophenylboronic acid (50.0 mg, 360 µmol, 3.0 eq). Purified using preparative HPLC (ACN/H$_2$O + 0.1 % TFA) to afford the product as an amorphous solid (19 mg, 32%).

^{1}H NMR (700 MHz, MeOD): δ = 8.16 (s, 1H), 8.07 − 8.03 (m, 3H), 7.50 (dd, J = 9.2, 1.9 Hz, 1H), 7.40 (d, J = 1.6 Hz, 1H), 7.25 (t, J = 8.6 Hz, 2H), 6.12 (s, 1H), 6.07 − 6.01 (m, 1H), 5.22 − 5.15 (m, 2H), 4.19 (ddd, J = 17.3, 10.4, 7.1 Hz, 1H), 3.95 (s, 3H), 3.64 (app t, J = 9.4 Hz, 1H), 3.45 (dd, J = 15.8, 7.3 Hz, 2H), 3.27 (dd, J = 21.0, 10.1 Hz, 1H), 2.67 (dd, J = 17.4, 8.5 Hz, 1H), 2.48 − 2.43 (m, 1H), 1.95 (s, 1H), 1.88 (t, J = 11.3 Hz, 1H), 1.79 (dd, J = 21.2, 10.8 Hz, 1H), 1.25 − 1.19 (m, 1H); **^{13}C NMR** (176 MHz, MeOD): δ = 164.13 (d, J = 249.3 Hz), 161.24 (q, J = 36.2 Hz), 159.44, 152.60, 149.33, 140.66, 136.75, 132.85, 129.95 (d, J = 8.7 Hz), 128.19, 125.30, 124.10, 118.77, 117.69, 117.19 (d, J=22.2 Hz), 100.98, 67.66, 59.82, 55.45, 49.09, 48.47, 36.97, 27.32, 22.63, 17.58; **^{19}F NMR** (565 MHz, MeOD): δ = -77.10, -111.59; **HR-ESI-MS**: m/z = 419.2127 ([M + H]$^+$, calcd. for C$_{26}$H$_{28}$O$_2$N$_2$F$^+$: 419.2129) (Δ = 0.66 ppm)− No TFA visible; $[\alpha]_{20}^{D}$ = + 62° (c = 1.0, MeOH).

(S)-(5-(4-fluorophenyl)-6-methoxyquinolin-4-yl)((2R,4S,5R)-5-vinylquinuclidin-2-yl)methanol- trifluoroacetate (138)

The compound was synthesized following **General Procedure IV**. Crude was purified using preparative HPLC (ACN/H$_2$O + 0.1 % TFA) to afford the pure compound (5 mg, 8%).

^{1}H NMR (600 MHz, MeOD): δ = 8.98 (d, J = 5.4 Hz, 1H), 8.36 (dd, J = 10.6, 7.4 Hz, 2H), 8.21 (dd, J = 27.1, 7.4 Hz, 1H), 8.05 (d, J = 9.4 Hz, 1H), 7.39 (td, J = 8.6, 2.7 Hz, 1H), 7.33 – 7.25 (m, 1H), 7.21 – 7.15 (m, 1H), 5.86 (ddd, J = 17.3, 10.5, 6.8 Hz, 1H), 5.24 – 5.14 (m, 2H), 4.08 (s, J = 9.7 Hz, 1H), 3.96 – 3.91 (m, 1H), 3.89 (s, 3H), 3.25 – 3.13 (m, 2H), 2.64 – 2.56 (m, 1H), 2.33 – 2.29 (m, 1H), 2.04 – 1.97 (m, 1H), 1.91 – 1.75 (m, 3H), 1.33 – 1.24 (m, 1H), 0.71 – 0.62 (m, 1H); **^{19}F NMR** (565 MHz, MeOD): δ = -76.50, -112.01; **HR-ESI-MS**: *m/z* = 419.2127 ([*M* + H]$^+$, calcd. for C$_{26}$H$_{28}$O$_2$N$_2$F$^+$: 419.2129) – No TFA visible., $[\alpha]_{20}^{D}$= +50° (c = 1.0, MeOH) (Δ = 0.50 ppm).

(*R*)-(2-(4-fluorophenyl)-6-methoxyquinolin-4-yl)((2*S*,4*S*,5*R*)-5-vinylquinuclidin-2-yl)methanol- trifluoroacetate (107)

The title compound was synthesized following **General Procedure IV** starting with quinidine (40.0 mg, 120.0 µmol, 1.0 eq) and 4-Fluorophenylboronic acid (50.0 mg, 360 µmol, 3.0 eq). Purified using preparative HPLC (ACN/H$_2$O + 0.1 % TFA) to afford the product as an amorphous solid (25 mg, 39%).

^{1}H NMR (700 MHz, MeOD): δ = 8.30 (s, J = 13.9 Hz, 1H), 8.21 – 8.11 (m, 3H), 7.60 (d, J = 9.2 Hz, 1H), 7.52 (s, 1H), 7.35 (t, J = 8.5 Hz, 2H), 6.15 (s, J = 23.4 Hz, 1H), 5.79 (ddd, J = 17.3, 10.4, 7.1 Hz, 1H), 5.14 (d, J = 17.1 Hz, 1H), 5.05 (d, J = 10.5 Hz, 1H), 4.29 (dd, J = 15.7, 7.2 Hz, 1H), 4.05 (s, J = 12.2 Hz, 3H), 3.77 – 3.70 (m, 1H), 3.70 – 3.63 (m, 1H), 3.40 – 3.32 (m, 2H), 2.84 (s, 1H), 2.31 (dd, J = 12.8, 7.6 Hz, 1H), 2.29 – 2.20 (m, 1H), 2.13 (d, J = 2.3 Hz, 1H), 1.99 (t, J = 10.2 Hz, 1H), 1.69 – 1.63 (m, 1H); **^{13}C NMR** (176 MHz, MeOD): δ = 165.70 (d, J = 250.12 Hz), 161.86 (d, J = 27.74 Hz), 160.80, 153.95, 151.03, 141.90, 139.24, 134.15, 131.27, 131.22, 129.51, 126.73, 125.50, 119.09, 117.23, 117.19 (d, J = 22.1 Hz), 102.46, 68.66, 61.31, 56.95, 55.58, 49.53, 45.36, 38.54, 28.30, 25.17, 19.43; **^{19}F NMR** (377 MHz, MeOD): δ = -76.85, -112.23; **HR-ESI-MS**: *m/z* = 419.2124 ([*M* + H]$^+$, calcd. for C$_{26}$H$_{28}$O$_2$N$_2$F$^+$: 419.2129) (Δ = 1.12 ppm)– No TFA visible; $[\alpha]_{20}^{D}$ = - 40° (c = 1.0, MeOH).

(S)-(2-(4-chlorophenyl)-quinolin-4-yl)((2R,4S,5R)-5-vinylquinuclidin-2-yl)methanol-trifluoroacetate (115)

The title compound was synthesized following **General Procedure IV** starting with cinchonine (40.0 mg, 135.0 µmol, 1.0 eq) and 4-Chlorophenylboronic acid (63.0 mg, 405 µmol, 3.0 eq). Purified using preparative HPLC (ACN/H$_2$O + 0.1 % TFA) to afford the product as an amorphous solid (30 mg, 48%).

^{1}H NMR (600 MHz, MeOD): δ = 8.23 (s, 1H), 8.19 – 8.14 (m, 4H), 7.83 (dd, J = 11.8, 4.5 Hz, 1H), 7.73 – 7.69 (m, 1H), 7.57 (d, J = 8.6 Hz, 2H), 6.14 (s, 1H), 6.13 – 6.08 (m, 1H), 5.25 (dd, J = 13.8, 9.2 Hz, 2H), 4.27 (ddd, J = 12.4, 8.4, 2.4 Hz, 1H), 3.73 (t, J = 9.5 Hz, 1H), 3.59 – 3.49 (m, 2H), 3.34 (ddd, J = 12.2, 10.1, 8.5 Hz, 1H), 2.74 (q, J = 8.6 Hz, 1H), 2.53 – 2.47 (m, 1H), 2.02 (s, 1H), 1.98 – 1.91 (m, 1H), 1.85 (ddd, J = 12.7, 10.2, 1.3 Hz, 1H), 1.31 – 1.25 (m, 1H); **^{13}C NMR** (151 MHz, MeOD): δ = 162.35 (d, J = 36.1 Hz), 157.17, 149.16, 149.00, 138.65, 138.07, 137.30, 131.59, 130.75, 130.32, 130.22, 128.83, 125.28, 123.60, 118.80, 117.71 (d, J = 9.4 Hz), 116.87, 69.05, 61.64, 50.55, 50.09, 49.85, 49.57, 38.38, 28.66, 23.97, 19.09; **HR-ESI-MS**: *m/z* = 407.1696 ([*M* + H]$^+$, calcd. for C$_{25}$H$_{26}$ON$_2$ ^{37}Cl$^+$: 407.1699) (Δ = 0.75 ppm) – No TFA visible; $[\boldsymbol{\alpha}]_{\mathbf{20}}^{\boldsymbol{D}}$= + 26° (c = 1.0, MeOH).
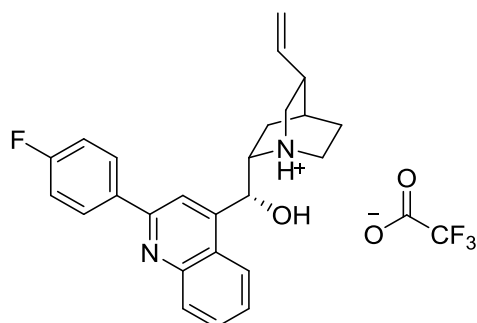
(S)-(7-(4-chlorophenyl)-quinolin-4-yl)((2R,4S,5R)-5-vinylquinuclidin-2-yl)methanol-trifluoroacetate (146)

The compound was synthesized following **General Procedure IV**. Crude was purified using preparative HPLC (ACN/H$_2$O + 0.1 % TFA) to afford the pure compound (5 mg, 8%).

^{1}H NMR (600 MHz, MeOD): δ = 9.01 (dt, J = 25.4, 6.2 Hz, 1H), 8.45 – 8.33 (m, 2H), 8.22 (d, J = 11.2 Hz, 1H), 8.05 – 7.98 (m, 1H), 7.89 – 7.80 (m, 2H), 7.60 – 7.50 (m, 2H), 6.31 – 6.19 (m, 1H), 6.13 – 6.06 (m, 1H), 5.31 – 5.22 (m, 2H), 3.79 – 3.68 (m, 1H), 3.62 – 3.47 (m, 2H), 2.74 (t, J = 13.4 Hz, 1H), 2.56 – 2.38 (m, 1H), 2.01 (dd, J = 16.0, 8.3 Hz, 2H), 1.97 – 1.90 (m, 2H), 1.89 – 1.79 (m, 2H); **HR-ESI-MS**: m/z = 407.1702 ([M + H]$^+$, calcd. for C$_{25}$H$_{26}$ON$_2$ ^{37}Cl$^+$: 407.1699) (Δ = 0.73 ppm) – No TFA visible; $[\alpha]_{20}^{D}$ = +69° (c = 1.0, MeOH).
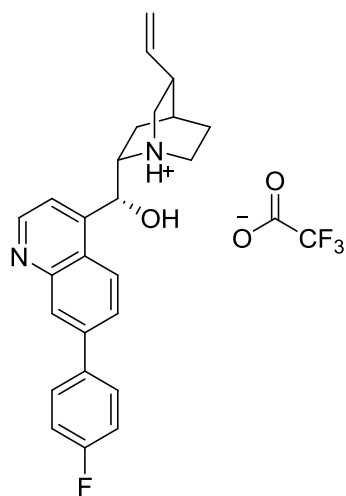
(S)-(2-(4-chlorophenyl)-6-methoxyquinolin-4-yl)((2R,4S,5R)-5-vinylquinuclidin-2-yl)methanol- trifluoroacetate (101)

The title compound was synthesized following **General Procedure IV** starting with quinidine (40.0 mg, 120.0 µmol, 1.0 eq) and 4-Chlorophenylboronic acid (56.0 mg, 360 µmol, 3.0 eq). Purified using preparative HPLC (ACN/H_2O + 0.1 % TFA) to afford the product as an amorphous solid (22 mg, 33%).

^{1}H NMR (700 MHz, MeOD): δ = 8.22 (s, 1H), 8.16 – 8.12 (m, 3H), 7.59 (d, J = 8.6 Hz, 2H), 7.54 (dd, J = 9.2, 2.6 Hz, 1H), 7.40 (d, J = 2.6 Hz, 1H), 6.16 (ddd, J = 17.5, 10.4, 7.3 Hz, 1H), 6.09 (d, J = 18.2 Hz, 1H), 5.32 – 5.27 (m, 2H), 4.30 (ddd, J = 12.4, 8.4, 2.4 Hz, 1H), 4.05 (s, 3H), 3.76 (app t, J = 9.4 Hz, 1H), 3.58 (dd, J = 16.5, 9.1 Hz, 2H), 3.25 – 3.20 (m, 1H), 2.79 (dd, J = 17.6, 8.6 Hz, 1H), 2.59 – 2.53 (m, 1H), 2.07 (s, J = 13.9 Hz, 1H), 2.03 – 1.97 (m, 1H), 1.92 (m, 1H), 1.38 – 1.29 (m, 1H); **^{13}C NMR** (176 MHz, MeOD): δ = 162.40 (d, J = 34.7 Hz), 160.36, 154.56, 147.86, 144.67, 138.57, 138.09, 136.96, 131.94, 130.13 (d, J = 21.0 Hz), 126.45, 124.04, 117.84 (d, J = 42.9 Hz), 102.05, 69.19, 61.42, 56.58, 50.51, 49.93, 49.53, 47.93, 38.37, 28.67, 24.02, 19.10; **HR-ESI-MS**: *m/z* = 437.1803 ([*M* + H]$^+$, calcd. for $C_{26}H_{28}O_2N_2$ $^{37}Cl^+$: 437.1804) (Δ = 0.24 ppm) – No TFA visible; $[\alpha]_{20}^{D}$= + 183° (c = 1.0, MeOH).
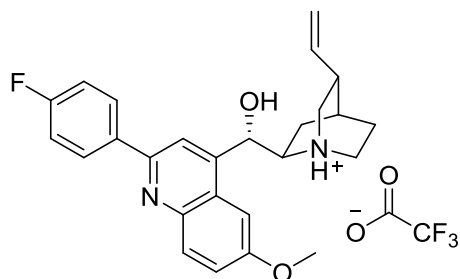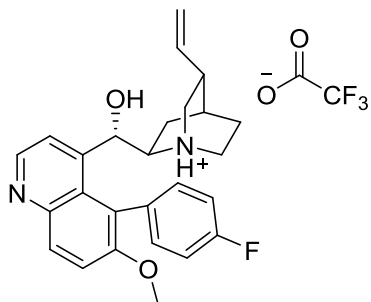
**(*R*)-(2-(4-chlorophenyl)-quinolin-4-yl)((2*S*,4*S*,5*R*)-5-vinylquinuclidin-2-yl)methanol-
trifluoroacetate (150)**

The title compound was synthesized following **General Procedure IV** starting with cinchonidine (40.0 mg, 135.0 µmol, 1.0 eq) and 4-Chlorophenylboronic acid (63.0 mg, 405 µmol, 3.0 eq). Purified using preparative HPLC (ACN/H$_2$O + 0.1 % TFA) to afford the product as an amorphous solid (25 mg, 40%).

^{1}H NMR (600 MHz, MeOD): δ = 8.27 (s, 1H), 8.20 (dd, J = 13.2, 8.4 Hz, 2H), 8.14 (d, J = 8.6 Hz, 2H), 7.87 (t, J = 7.7 Hz, 1H), 7.73 (t, J = 7.6 Hz, 1H), 7.58 (d, J = 8.6 Hz, 2H), 6.06 (d, J = 0.9 Hz, 1H), 5.74 (ddd, J = 17.3, 10.5, 7.1 Hz, 1H), 5.10 (d, J = 17.2 Hz, 1H), 5.00 (d, J = 10.5 Hz, 1H), 4.29 – 4.23 (m, 1H), 3.72 (t, J = 8.9 Hz, 1H), 3.61 (dd, J = 13.0, 10.7 Hz, 1H), 3.36 – 3.28 (m, 2H), 2.80 (s, J = 3.3 Hz, 1H), 2.30 – 2.19 (m, 2H), 2.10 (dd, J = 5.8, 2.9 Hz, 1H), 1.98 – 1.91 (m, 1H), 1.63 – 1.57 (m, 1H); **^{13}C NMR** (176 MHz, MeOD): δ = 162.31 (q, J = 35.7 Hz), 157.40, 149.97, 148.92, 139.37, 138.66, 137.68, 132.01, 130.71, 130.65, 130.49, 129.17, 125.52, 123.87, 118.23, 117.50, 69.01, 62.07, 55.85, 49.77, 45.80, 38.76, 28.43, 25.41, 19.74; **HR-ESI-MS**: *m/z* = 407.1697 ([*M* + H]$^+$, calcd. for C$_{25}$H$_{26}$ON$_2$ ^{37}Cl$^+$: 407.1699) (Δ = 0.50 ppm) – No TFA visible; $[\alpha]_{20}^{D}$= -16° (c = 1.0, MeOH).

(*R*)-(7-(4-chlorophenyl)-quinolin-4-yl)((2*S*,4*S*,5*R*)-5-vinylquinuclidin-2-yl)methanol-trifluoroacetate (151)

The compound was synthesized following **General Procedure IV**. Crude was purified using preparative HPLC (ACN/H$_2$O + 0.1 % TFA) to afford the pure compound (1 mg, 2%).

^{1}H NMR (700 MHz, MeOD): δ = 8.90 (d, J = 4.4 Hz, 1H), 8.20 (dd, J = 8.3, 1.3 Hz, 1H), 7.86 (d, J = 4.4 Hz, 1H), 7.85 – 7.78 (m, 2H), 7.61 – 7.58 (m, 2H), 7.52 – 7.49 (m, 2H), 6.05 (s, 1H), 5.81 (ddd, J = 17.3, 10.5, 7.0 Hz, 1H), 5.17 (d, J = 17.1 Hz, 1H), 5.07 (t, J = 10.1 Hz, 1H), 4.34 – 4.28 (m, 1H), 3.75 (t, J = 8.9 Hz, 1H), 3.67 (dd, J = 13.1, 10.7 Hz, 1H), 3.43 – 3.34 (m, 1H), 2.86 (s, 1H), 2.32 – 2.22 (m, 2H), 2.18 – 2.14 (m, 1H), 2.01 (dt, J = 15.8, 10.5 Hz, 1H), 1.63 (ddd, J = 13.5, 6.3, 3.2 Hz, 1H), 1.31 (d, J = 7.8 Hz, 1H); **HR-ESI-MS**: *m/z* = 407.1697 ([*M* + H]$^+$, calcd. for C$_{25}$H$_{26}$ON$_2$ ^{37}Cl$^+$: 407.1699) (Δ = 0.50 ppm) – No TFA visible; [*α*]$_{20}^{D}$= -° (c = 1.0, MeOH).
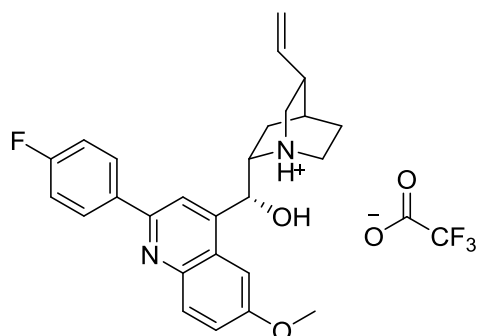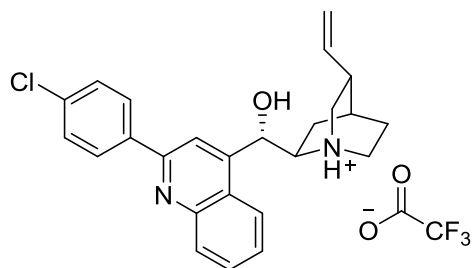
(R)-(2-(4-chlorophenyl)-6-methoxyquinolin-4-yl)((2S,4S,5R)-5-vinylquinuclidin-2-yl)methanol- trifluoroacetate (108)

The title compound was synthesized following **General Procedure IV** starting with quinine (40.0 mg, 120.0 µmol, 1.0 eq) and 4-Chlorophenylboronic acid (56.0 mg, 360 µmol, 3.0 eq). Purified using preparative HPLC (ACN/H₂O + 0.1 % TFA) to afford the product as an amorphous solid (15 mg, 22%).

¹H NMR (700 MHz, MeOD): δ = 8.27 (s, 1H), 8.16 – 8.10 (m, 3H), 7.61 – 7.55 (m, 3H), 7.46 (d, J = 2.5 Hz, 1H), 6.07 (s, 1H), 5.80 (ddd, J = 17.4, 10.5, 7.1 Hz, 1H), 5.15 (d, J = 17.1 Hz, 1H), 5.06 (d, J = 10.5 Hz, 1H), 4.34 – 4.25 (m, 1H), 4.05 (s, 3H), 3.79 – 3.71 (m, 1H), 3.66 (dd, J = 13.1, 10.7 Hz, 1H), 3.40 – 3.33 (m, 2H), 2.85 (b.s, 1H), 2.36 – 2.30 (m, 1H), 2.30 – 2.21 (m, 1H), 2.15 (m, 1H), 2.03 – 1.97 (m, 1H), 1.72 – 1.61 (m, 1H); **¹³C NMR** (176 MHz, MeOD): δ = 162.39 (q, J = 35.7 Hz), 160.53, 154.11, 149.10, 143.48, 139.08, 137.61, 137.22, 130.92, 130.16, 126.50, 124.48, 118.46, 117.15, 116.84, 102.13, 68.62, 61.29, 56.66, 55.47, 49.41, 45.31, 38.43, 28.15, 25.06, 19.38; **HR-ESI-MS**: m/z =437.1805 ([M + H]⁺, calcd. for C₂₆H₂₈O₂N₂ ³⁷Cl⁺: 437.1804) (Δ = 0.16 ppm) – No TFA visible; $[\alpha]_{20}^{D}$= -34° (c = 1.0, MeOH).
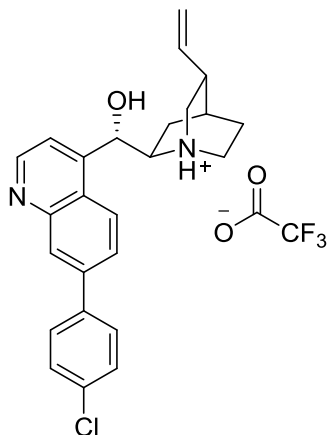
(S)-(2-(4-methylphenyl)-quinolin-4-yl)((2R,4S,5R)-5-vinylquinuclidin-2-yl)methanol-trifluoroacetate (116)

The title compound was synthesized following **General Procedure IV** starting with cinchonine (40.0 mg, 135.0 µmol, 1.0 eq) and 4-Methylphenylboronic acid (55.0 mg, 405 µmol, 3.0 eq). Purified using preparative HPLC (ACN/H$_2$O + 0.1 % TFA) to afford the product as an amorphous solid (14 mg, 23%).

^{1}H NMR (600 MHz, MeOD): δ = 8.27 (s, 1H), 8.21 (dd, J = 12.2, 8.4 Hz, 2H), 8.05 (d, J = 8.2 Hz, 2H), 7.89 (dd, J = 11.3, 4.1 Hz, 1H), 7.76 – 7.73 (m, 1H), 7.43 (d, J = 7.9 Hz, 2H), 6.17 (s, 1H), 6.16 – 6.09 (m, 1H), 5.30 (d, J = 10.4 Hz, 1H), 5.28 – 5.27 (m, 1H), 4.29 (tt, J = 15.1, 4.5 Hz, 1H), 3.77 (t, J = 9.5 Hz, 1H), 3.63 – 3.52 (m, 2H), 3.41 – 3.34 (m, 1H), 2.77 (q, J = 8.6 Hz, 1H), 2.52 (dd, J = 12.3, 10.7 Hz, 1H), 2.47 (s, 3H), 2.05 (s, 1H), 2.01 – 1.95 (m, 1H), 1.88 (dt, J = 11.3, 9.0 Hz, 1H), 1.32 (m, 1H); **^{13}C NMR** (151 MHz, MeOD): δ = 162.65 (d, J = 34.5 Hz), 158.40, 150.08, 147.87, 142.20, 138.04, 136.33, 132.03, 130.89, 129.52, 128.97, 128.83, 125.20, 123.73, 118.97, 118.32, 117.74, 117.04, 69.12, 61.62, 50.58, 50.12, 49.60, 38.34, 28.64, 23.96, 21.40, 19.12; **HR-ESI-MS**: m/z = 385.2264 ([M + H]$^+$, calcd. for C$_{26}$H$_{29}$ON$_2$$^+$: 385.2274) (Δ = 2.80 ppm) – No TFA visible; $[\alpha]_{20}^{D}$ = + 143° (c = 1.0, MeOH).

(*R*)-(2-(4-methylphenyl)-quinolin-4-yl)((2*S*,4*S*,5*R*)-5-vinylquinuclidin-2-yl)methanol-trifluoroacetate (152)
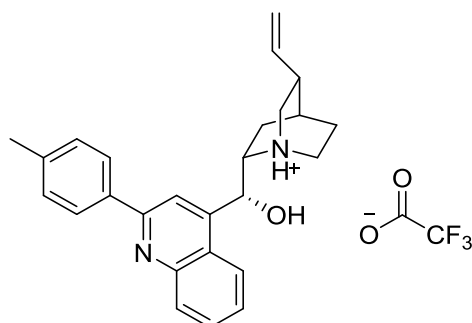
The title compound was synthesized following **General Procedure IV** starting with cinchonidine (40.0 mg, 135.0 µmol, 1.0 eq) and 4-Methylphenylboronic acid (55.0 mg, 405 µmol, 3.0 eq). Purified using preparative HPLC (ACN/H_2O + 0.1 % TFA) to afford the product as an amorphous solid (25 mg, 41%).

^{1}H NMR (700 MHz, MeOD): δ = 8.51 – 8.47 (m, 1H), 8.42 (d, J = 8.6 Hz, 1H), 8.14 (t, J = 7.8 Hz, 1H), 8.05 (d, J = 7.9 Hz, 2H), 7.98 (t, J = 7.7 Hz, 1H), 7.63 (d, J = 7.3 Hz, 1H), 7.56 (d, J = 7.9 Hz, 1H), 7.15 (d, J = 7.5 Hz, 1H), 6.27 (s, 1H), 5.78 (ddd, J = 17.2, 10.5, 6.8 Hz, 1H), 5.15 (d, J = 17.2 Hz, 1H), 5.06 (d, J = 10.6 Hz, 1H), 4.31 (dd, J = 15.0, 6.7 Hz, 1H), 3.78 (t, J = 8.8 Hz, 1H), 3.70 – 3.62 (m, 1H), 3.39 (m, 2H), 3.33 (s, 1H), 2.86 (s, 1H), 2.52 (s, 3H), 2.34 – 2.24 (m, 1H), 2.19 – 2.15 (m, 1H), 2.02 (t, J = 9.5 Hz, 1H), 1.69 – 1.62 (m, 1H); **^{13}C NMR** (176 MHz, MeOD): δ = 162.72 (q, J = 35.4 Hz), 156.96, 156.83, 145.13, 141.76, 141.47, 138.93, 135.07, 130.75, 129.98, 129.26, 125.34, 124.77, 124.25, 120.00, 118.64, 117.26, 68.76, 61.44, 55.55, 49.84, 45.46, 38.13, 27.89, 24.95 , 21.57, 19.28; **HR-ESI-MS**: *m/z* = 385.2268 ([*M* + H]$^+$, calcd. for $C_{26}H_{29}ON_2^+$: 385.2274) (Δ = 1.71 ppm) – No TFA visible; $[\alpha]_{20}^{D}$= - 85° (c = 1.0, MeOH).

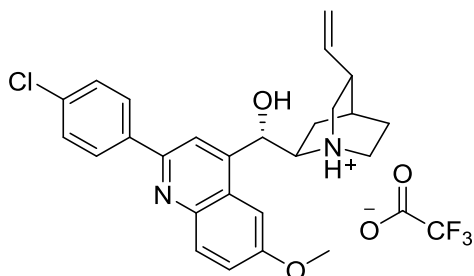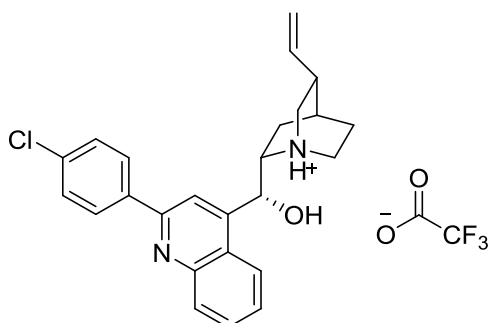**(S)-(2-(4-methylphenyl)-6-methoxyquinolin-4-yl)((2R,4S,5R)-5-vinylquinuclidin-2-yl)methanol- trifluoroacetate (102)**
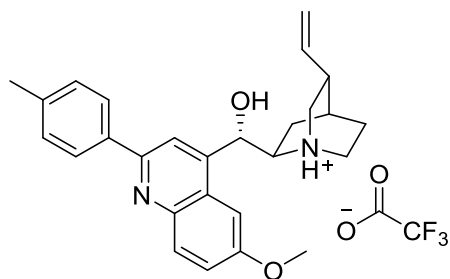
The title compound was synthesized following **General Procedure IV** starting with quinidine (40.0 mg, 120.0 µmol, 1.0 eq) and 4-Methylphenylboronic acid (49.0 mg, 360 µmol, 3.0 eq). Purified using preparative HPLC (ACN/H$_2$O + 0.1 % TFA) to afford the product as an amorphous solid (28 mg, 44%).

¹H NMR (700 MHz, MeOD): δ = 8.35 (s, 1H), 8.24 (d, J = 9.3 Hz, 1H), 7.98 (d, J = 7.8 Hz, 2H), 7.70 (d, J = 9.5 Hz, 1H), 7.61 (s, 1H), 7.50 (d, J = 7.8 Hz, 2H), 6.30 (s, J = 10.6 Hz, 1H), 6.14 (ddd, J = 16.6, 9.5, 7.3 Hz, 1H), 5.33 – 5.25 (m, 2H), 4.29 – 4.23 (m, 1H), 4.07 (s, 3H), 3.77 (t, J = 9.6 Hz, 1H), 3.56 (t, J = 11.5 Hz, 2H), 3.37 (dd, J = 21.4, 10.5 Hz, 1H), 2.77 (dd, J = 16.9, 8.3 Hz, 1H), 2.58 – 2.52 (m, 1H), 2.48 (s, 3H), 2.05 (s, 1H), 1.98 (t, J = 10.6 Hz, 1H), 1.90 – 1.85 (m, 1H); **¹³C NMR** (176 MHz, MeOD): δ = 162.68 (q, J = 35.6 Hz), 161.41, 154.11, 143.94, 138.12, 138.08, 131.34, 130.56, 130.11, 129.46, 129.31, 129.21, 127.07, 127.02, 126.77, 119.68, 117.71, 102.94, 69.05, 61.02, 57.12, 50.48, 49.76, 49.37, 38.34, 28.71, 24.00, 21.53, 18.89; **HR-ESI-MS**: m/z = 415.2369 ([M + H]$^+$, calcd. for C$_{27}$H$_{31}$O$_2$N$_2^+$: 415.2380) (Δ = 2.76 ppm) – No TFA visible; $[\alpha]_{20}^{D}$= + 115° (c = 1.0, MeOH).

(*R*)-(2-(4-methylphenyl)-6-methoxyquinolin-4-yl)((2*S*,4*S*,5*R*)-5-vinylquinuclidin-2-yl)methanol- trifluoroacetate (109)
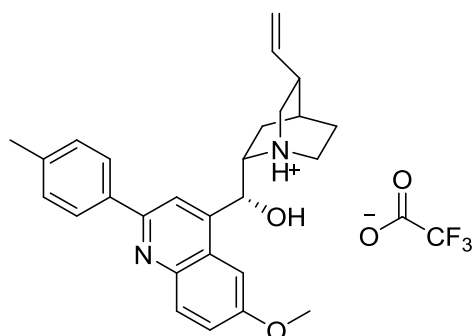
The title compound was synthesized following **General Procedure IV** starting with quinine (40.0 mg, 120.0 µmol, 1.0 eq) and 4-Chlorophenylboronic acid (49.0 mg, 360 µmol, 3.0 eq). Purified using preparative HPLC (ACN/H$_2$O + 0.1 % TFA) to afford the product as an amorphous solid (21 mg, 33%).

^{1}H NMR (600 MHz, MeOD): δ = 8.25 (s, 1H), 8.12 (d, J = 9.3 Hz, 1H), 7.92 (d, J = 8.2 Hz, 2H), 7.55 (dd, J = 9.3, 2.5 Hz, 1H), 7.47 (d, J = 2.2 Hz, 1H), 7.38 (d, J = 8.0 Hz, 2H), 6.11 (s, 1H), 5.73 (ddd, J = 17.4, 10.4, 7.2 Hz, 1H), 5.08 (d, J = 17.1 Hz, 1H), 4.98 (d, J = 10.4 Hz, 1H), 4.26 – 4.19 (m, 1H), 3.99 (s, 3H), 3.72 – 3.66 (m, 1H), 3.59 (dd, J = 12.9, 10.8 Hz, 1H), 3.29 (dt, J = 7.9, 6.3 Hz, 2H), 2.78 (s, 1H), 2.40 (s, J = 6.9 Hz, 3H), 2.27 – 2.14 (m, 2H), 2.07 (d, J = 2.8 Hz, 1H), 1.92 (t, J = 9.7 Hz, 1H), 1.60 – 1.55 (m, 1H); **^{13}C NMR** (126 MHz, MeOD): δ = 163.13 (q, J = 34.7 Hz), 160.77, 154.63, 151.63, 142.69, 140.78, 139.09, 134.04, 130.55, 1630.03, 129.86, 128.97, 128.42, 126.57, 125.65, 119.22, 117.06, 102.38, 68.40, 61.03, 56.82, 55.34, 45.13, 38.38, 28.14, 24.99, 21.45, 19.17; **HR-ESI-MS**: *m/z* = 415.2377 ([*M* + H]$^+$, calcd. for C$_{27}$H$_{31}$O$_2$N$_2$$^+$: 415.2380) (Δ = 0.66 ppm) – No TFA visible; $[\alpha]_{20}^{D}$ = - 61 °(c = 1.0, MeOH).

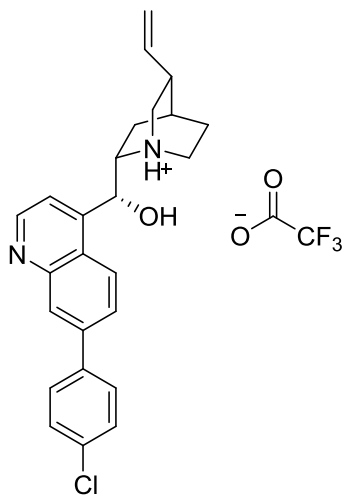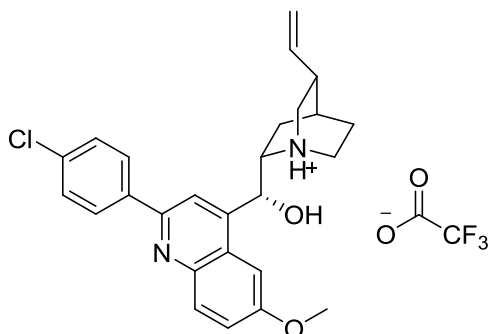**(S)-(2-phenyl-quinolin-4-yl)((2R,4S,5R)-5-vinylquinuclidin-2-yl)methanol-trifluoroacetate (117)**

The title compound was synthesized following **General Procedure IV** starting with cinchonine (40.0 mg, 135.0 µmol, 1.0 eq) and Phenylboronic acid (49.0 mg, 405 µmol, 3.0 eq). Purified using preparative HPLC (ACN/H_2O + 0.1 % TFA) to afford the product as an amorphous solid (16 mg, 27%).

^{1}H NMR (700 MHz, MeOD): δ = 8.29 (s, 1H), 8.25 (t, J = 7.3 Hz, 2H), 8.15 (dd, J = 5.2, 3.3 Hz, 2H), 7.92 – 7.89 (m, 1H), 7.78 – 7.75 (m, 1H), 7.61 (t, J = 7.3 Hz, 2H), 7.58 (t, J = 7.2 Hz, 1H), 6.22 (d, J = 1.4 Hz, 1H), 6.14 (ddd, J = 17.5, 10.4, 7.3 Hz, 1H), 5.32 – 5.26 (m, 2H), 4.30 (ddd, J = 12.6, 8.5, 2.4 Hz, 1H), 3.77 (t, J = 9.5 Hz, 1H), 3.63 – 3.53 (m, 2H), 3.41 – 3.35 (m, 1H), 2.77 (dd, J = 17.5, 8.6 Hz, 1H), 2.56 – 2.50 (m, 1H), 2.05 (s, 1H), 2.01 – 1.95 (m, 1H), 1.88 (ddd, J = 12.7, 10.3, 1.4 Hz, 1H), 1.35 – 1.31 (m, 1H); **^{13}C NMR** (176 MHz, MeOD): δ = 162.78 (q, J = 35.6 Hz), 158.95 , 158.39, 150.27, 147.95, 139.24, 138.07, 132.04, 131.48, 130.20, 129.65, 129.04, 128.99, 125.32, 123.86, 118.43, 117.71, 69.05, 61.61, 50.55, 50.05, 49.53, 38.34, 28.66, 23.97, 19.08; **HR-ESI-MS**: m/z = 371.2117 ([M + H]$^+$, calcd. for $C_{25}H_{27}ON_2^+$: 371.2118) (Δ = 0.19 ppm) – No TFA visible; $[\alpha]_{20}^{D}$= + 80° (c = 1.0, MeOH).
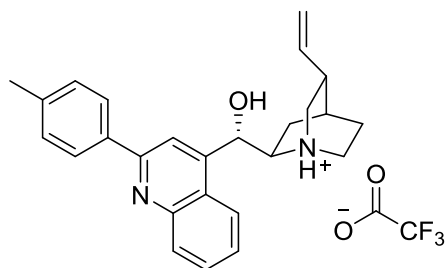
(*R*)-(2-phenyl-quinolin-4-yl)((2*S*,4*S*,5*R*)-5-vinylquinuclidin-2-yl)methanol-trifluoroacetate (153)

The title compound was synthesized following **General Procedure IV** starting with cinchonidine (40.0 mg, 135.0 µmol, 1.0 eq) and Phenylboronic acid (55.0 mg, 405 µmol, 3.0 eq). Purified using preparative HPLC (ACN/H_2O + 0.1 % TFA) to afford the product as an amorphous solid (19 mg, 33%).

^{1}H NMR (500 MHz, MeOD): δ = 8.30 (s, 1H), 8.27 − 8.22 (m, 2H), 8.11 (dt, J = 4.2, 2.3 Hz, 2H), 7.94 − 7.90 (m, 1H), 7.77 (ddd, J = 8.2, 7.0, 1.1 Hz, 1H), 7.63 − 7.57 (m, 3H), 6.19 (s, 1H), 6.11 (ddd, J = 17.5, 10.4, 7.3 Hz, 1H), 5.29 − 5.22 (m, 2H), 4.26 (ddd, J = 12.5, 8.4, 2.4 Hz, 1H), 3.75 (t, J = 9.5 Hz, 1H), 3.55 (dt, J = 22.5, 11.1 Hz, 2H), 3.39 − 3.31 (m, 1H), 2.74 (dd, J = 17.5, 8.6 Hz, 1H), 2.53 − 2.45 (m, 1H), 2.02 (s, 1H), 1.98 − 1.92 (m, 1H), 1.88 − 1.81 (m, 1H), 1.32 − 1.25 (m, 1H); **^{13}C NMR** (126 MHz, MeOD): δ = 162.28 (d, 35.98 Hz), 158.11, 151.63, 146.78, 138.26, 138.06, 132.67, 131.95, 130.34, 129.39, 129.25, 128.64, 125.40, 124.07, 118.77, 117.74, 69.09, 61.52, 50.54, 50.06, 49.63, 38.35, 28.65, 23.95, 19.05; **HR-ESI-MS**: *m/z* = 371.2118 ([*M* + H]$^+$, calcd. for $C_{25}H_{27}ON_2^+$: 371.2118) (Δ = 0.09 ppm) − No TFA visible; $[\alpha]_{20}^{D}$ = + 38° (c = 1.0, MeOH).

(*R*)-(7-phenyl-quinolin-4-yl)((2*S*,4*S*,5*R*)-5-vinylquinuclidin-2-yl)methanol-trifluoroacetate (148)

The compound was synthesized following **General Procedure IV**. Crude was purified using preparative HPLC (ACN/H$_2$O + 0.1 % TFA) to afford the pure compound (4 mg, 7%).

^{1}H NMR (500 MHz, MeOD): δ = 8.99 (dd, J = 26.5, 4.8 Hz, 1H), 8.40 − 8.33 (m, 1H), 8.22 (m, 1H), 8.14 (dd, J = 8.9, 1.6 Hz, 1H), 7.99 (t, J = 4.7 Hz, 1H), 7.82 (dd, J = 7.1, 5.5 Hz, 2H), 7.57 − 7.51 (m, 2H), 7.46 (dt, J = 14.9, 7.5 Hz, 1H), 6.24 − 6.16 (m, 1H), 6.16 − 6.05 (m, 1H), 5.31 − 5.23 (m, 2H), 4.32 − 4.24 (m, 1H), 4.03 − 3.96 (m, 1H), 3.79 − 3.69 (m, 1H), 3.63 − 3.47 (m, 1H), 3.36 (dd, J = 20.7, 10.4 Hz, 1H), 2.75 (s, 1H), 2.55 − 2.43 (m, 1H), 2.05 − 1.98 (m, 1H), 1.89 (ddd, J = 19.6, 16.2, 10.7 Hz, 2H), 1.34 − 1.19 (m, 1H); **HR-ESI-MS**: *m/z* = 371.2117 ([*M* + H]$^+$, calcd. for C$_{25}$H$_{27}$ON$_2$$^+$: 371.2118) (Δ = 0.28 ppm) − No TFA visible; $[\alpha]_{20}^{D}$ = + 45° (c = 1.0, MeOH).

(S)-(2-phenyl-6-methoxyquinolin-4-yl)((2R,4S,5R)-5-vinylquinuclidin-2-yl)methanol-trifluoroacetate (103)
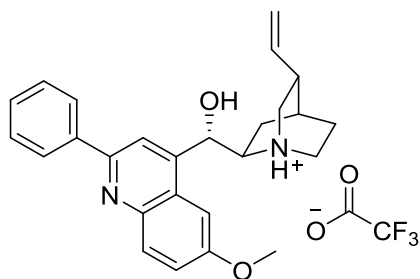
The title compound was synthesized following **General Procedure IV** starting with quinidine (40.0 mg, 120.0 µmol, 1.0 eq) and Phenylboronic acid (44.0 mg, 360 µmol, 3.0 eq). Purified using preparative HPLC (ACN/H$_2$O + 0.1 % TFA) to afford the product as an amorphous solid (27 mg, 44%).

^{1}H NMR (500 MHz, MeOD): δ = 8.31 (s, 1H), 8.19 (d, J = 9.3 Hz, 1H), 8.05 – 8.00 (m, 2H), 7.67 – 7.59 (m, 4H), 7.55 (d, J = 2.6 Hz, 1H), 6.26 (s, 1H), 6.10 (ddd, J = 17.5, 10.4, 7.3 Hz, 1H), 5.27 – 5.19 (m, 2H), 4.22 (ddd, J = 12.6, 8.4, 2.4 Hz, 1H), 4.02 (s, 3H), 3.72 (t, J = 9.5 Hz, 1H), 3.51 (dd, J = 12.2, 11.0 Hz, 2H), 3.36 – 3.28 (m, 1H), 2.72 (dd, J = 17.5, 8.6 Hz, 1H), 2.54 – 2.47 (m, 1H), 2.00 (s, 1H), 1.96 – 1.89 (m, 1H), 1.87-1.80 (m, 1H), 1.31 – 1.24 (m, 1H); **^{13}C NMR** (126 MHz, MeOD): δ = 162.39 (q, J = 35.8 Hz), 161.26, 154.03, 153.53, 139.15, 137.97, 135.49, 132.50, 130.45, 129.32, 127.05, 126.84, 118.83, 119.58, 117.54, 116.51, 102.59, 68.86, 60.83, 56.92, 50.27, 49.57, 38.19, 28.54, 23.83, 18.71; **HR-ESI-MS**: *m/z* = 401.2222 ([*M* + H]$^+$, calcd. for C$_{26}$H$_{29}$O$_2$N$_2$$^+$: 401.2224) (Δ = 0.47 ppm) – No TFA visible; $[\alpha]_{20}^{D}$ = + 118° (c = 1.0, MeOH).

(S)-(5-(phenyl)-6-methoxyquinolin-4-yl)((2R,4S,5R)-5-vinylquinuclidin-2-yl)methanol-trifluoroacetate (141)

The compound was synthesized following **General Procedure IV**. Crude was purified using preparative HPLC (ACN/H$_2$O + 0.1 % TFA) to afford the pure compound (6 mg, 10%).

^{1}H NMR (500 MHz, MeOD): δ = 8.92 (t, J = 7.2 Hz, 1H), 8.13 (d, J = 5.4 Hz, 1H), 8.07 (s, 1H), 7.60 (ddd, J = 7.7, 6.3, 5.3 Hz, 3H), 7.50 – 7.40 (m, 3H), 6.29 (s, J = 17.9 Hz, 1H), 6.10 (dddd, J = 17.6, 10.3, 7.3, 3.0 Hz, 1H), 5.32 – 5.21 (m, 2H), 4.26 (ddd, J = 12.4, 8.4, 2.2 Hz, 1H), 4.07 (s, J = 7.4 Hz, 3H), 3.76 (dd, J = 19.3, 9.7 Hz, 1H), 3.55 (t, J = 11.5 Hz, 2H), 3.43 – 3.32 (m, 1H), 2.76 (dd, J = 17.4, 8.5 Hz, 1H), 2.54 – 2.44 (m, 1H), 2.04 (s, 1H), 1.95 (dd, J = 14.4, 10.2 Hz, 1H), 1.92 – 1.83 (m, 1H), 1.27 (dtd, J = 13.4, 9.4, 3.9 Hz, 1H); **^{13}C NMR** (126 MHz, MeOD): δ = 162.54 (d, J = 37.0 Hz), 159.36, 153.89, 144.20, 141.63, 138.06, 137.36, 131.20, 130.62, 129.85, 129.45, 127.76, 126.08, 120.69, 117.75, 102.64, 68.99, 60.91, 57.37, 50.47, 49.80, 49.63, 38.28, 28.69, 23.96, 18.92; **HR-ESI-MS**: m/z = 401.2218([M + H]$^+$, calcd. for C$_{26}$H$_{29}$O$_2$N$_2$$^+$: 401.2224) (Δ = 1.36 ppm) – No TFA visible; $[\alpha]_{20}^{D}$= + 86° (c = 1.0, MeOH).
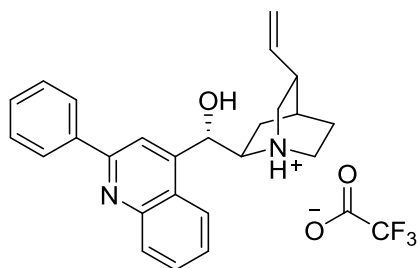
(*R*)-(2-phenyl-6-methoxyquinolin-4-yl)((2*S*,4*S*,5*R*)-5-vinylquinuclidin-2-yl)methanol-trifluoroacetate (110)
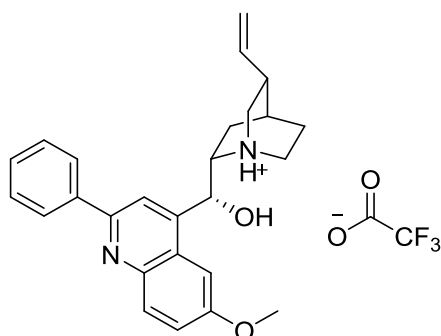
The title compound was synthesized following **General Procedure IV** starting with quinine (40.0 mg, 120.0 µmol, 1.0 eq) and Phenylboronic acid (44.0 mg, 360 µmol, 3.0 eq). Purified using preparative HPLC (ACN/H$_2$O + 0.1 % TFA) to afford the product as an amorphous solid (24 mg, 39%).

¹H NMR (500 MHz, MeOD): δ = 8.33 (s, 1H), 8.19 (d, J = 9.3 Hz, 1H), 8.07 – 8.03 (m, 2H), 7.65 – 7.59 (m, 4H), 7.54 (d, J = 2.5 Hz, 1H), 6.15 (s, 1H), 5.76 (ddd, J = 17.4, 10.4, 7.1 Hz, 1H), 5.10 (d, J = 17.1 Hz, 1H), 5.01 (d, J = 10.4 Hz, 1H), 4.28 – 4.19 (m, 1H), 4.03 (s, 3H), 3.75 – 3.69 (m, 1H), 3.62 (dd, J = 13.0, 10.7 Hz, 1H), 3.34 – 3.28 (m, 2H), 2.80 (d, J = 7.2 Hz, 1H), 2.31 – 2.17 (m, 2H), 2.09 (dd, J = 5.9, 2.9 Hz, 1H), 1.98 – 1.91 (m, 1H), 1.65 – 1.57 (m, 1H); **¹³C NMR** (126 MHz, MeOD): δ = 162.48 (q, J = 35.4 Hz), 161.12, 154.34, 152.72, 139.99, 139.08, 136.20, 132.20, 130.35, 129.20, 127.83, 126.98, 126.33, 119.65, 118.87, 117.09, 116.55, 102.53, 68.49, 61.02, 56.90, 55.38, 45.17, 38.38, 28.14, 24.99, 19.20; **HR-ESI-MS**: *m/z* = 401.2222 ([*M* + H]⁺, calcd. for C$_{26}$H$_{29}$O$_2$N$_2$⁺: 401.2224) (Δ = 0.44 ppm) – No TFA visible; $[\alpha]_{20}^{D}$ = + 27° (c = 1.0, MeOH).

(S)-(2-(3-bromophenyl)-quinolin-4-yl)((2R,4S,5R)-5-vinylquinuclidin-2-yl)methanol-trifluoroacetate (118)
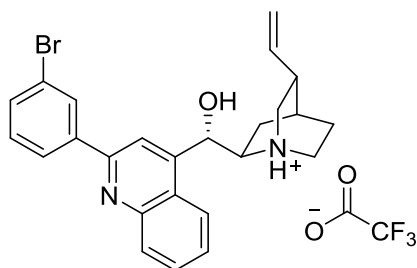
The title compound was synthesized following **General Procedure IV** starting with quinidine (40.0 mg, 120.0 µmol, 1.0 eq) and 3-Bromophenylboronic acid (72.0 mg, 360 µmol, 3.0 eq). Purified using preparative HPLC (ACN/H_2O + 0.1 % TFA) to afford the product as an amorphous solid (12 mg, 18%).

^{1}H NMR (700 MHz, MeOD): δ = 8.39 (t, J = 1.8 Hz, 1H), 8.25 (s, 1H), 8.23 (d, J = 7.9 Hz, 1H), 8.18 (d, J = 8.3 Hz, 1H), 8.16 – 8.14 (m, 1H), 7.87 (ddd, J = 8.3, 6.9, 1.1 Hz, 1H), 7.74 (ddd, J = 8.2, 6.9, 1.1 Hz, 1H), 7.70 (ddd, J = 8.0, 1.9, 0.8 Hz, 1H), 7.52 (t, J = 7.9 Hz, 1H), 6.19 – 6.12 (m, 2H), 5.32 – 5.27 (m, 2H), 4.30 (ddd, J = 12.5, 8.5, 2.4 Hz, 1H), 3.78 (t, J = 9.5 Hz, 1H), 3.58 (ddd, J = 32.1, 17.9, 11.0 Hz, 2H), 3.43 – 3.35 (m, 1H), 2.78 (dd, J = 17.6, 8.6 Hz, 1H), 2.58 – 2.51 (m, 1H), 2.06 (s, J = 12.8 Hz, 1H), 2.02 – 1.96 (m, 1H), 1.92 – 1.85 (m, 1H), 1.36 – 1.29 (m, 1H); **^{13}C NMR** (176 MHz, MeOD): δ = 162.33 (q, J = 36.2 Hz), 156.79, 149.31, 148.87, 142.46, 138.05, 133.83, 131.85, 131.79, 131.28, 131.15, 128.91, 127.45, 125.42, 124.12, 123.49, 117.90, 117.51, 69.16, 61.71, 50.58, 50.13, 49.53, 38.37, 28.63, 23.97, 19.18; **HR-ESI-MS**: m/z = 451.1199 ([M + H]$^+$, calcd. for $C_{25}H_{26}ON_2$ $^{81}Br^+$: 451.1203) (Δ = 0.75 ppm) – No TFA visible; $[\alpha]_{20}^{D}$= +69° (c = 1.0, MeOH).
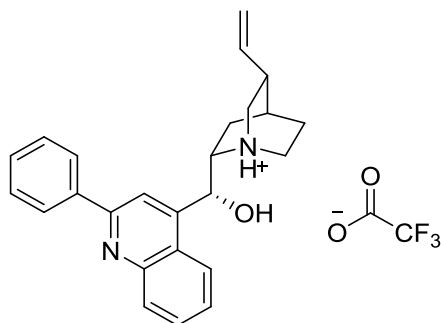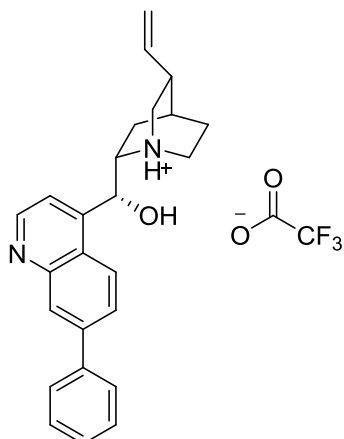
(*R*)-(2-(3-bromophenyl)-quinolin-4-yl)((2*S*,4*S*,5*R*)-5-vinylquinuclidin-2-yl)methanol-trifluoroacetate (154)
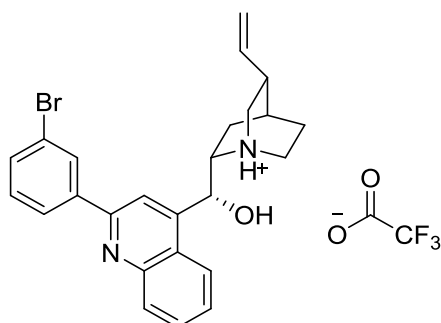
The title compound was synthesized following **General Procedure IV** starting with cinchonidine (40.0 mg, 120.0 µmol, 1.0 eq) and 3-Bromophenylboronic acid (81.0 mg, 405 µmol, 3.0 eq). Purified using preparative HPLC (ACN/H$_2$O + 0.1 % TFA) to afford the product as an amorphous solid (19 mg, 27%).

^{1}H NMR (700 MHz, MeOD): δ = 8.38 (s, 1H), 8.27 (s, 1H), 8.22 (t, J = 9.2 Hz, 2H), 8.15 (d, J = 7.8 Hz, 1H), 7.89 – 7.86 (m, 1H), 7.76 – 7.72 (m, 1H), 7.71 – 7.69 (m, 1H), 7.51 (t, J = 7.9 Hz, 1H), 6.08 (d, J = 1.4 Hz, 1H), 5.79 (ddd, J = 17.3, 10.5, 7.0 Hz, 1H), 5.15 (d, J = 17.2 Hz, 1H), 5.05 (d, J = 10.5 Hz, 1H), 4.34 – 4.28 (m, 1H), 3.79 – 3.75 (m, 1H), 3.65 (dd, J = 13.0, 10.7 Hz, 1H), 3.40 – 3.33 (m, 2H), 2.84 (dd, J = 3.4, 1.8 Hz, 1H), 2.34 – 2.24 (m, 2H), 2.15 (dd, J = 6.1, 3.0 Hz, 1H), 1.99 (tdd, J = 10.9, 5.2, 2.8 Hz, 1H), 1.67 – 1.61 (m, 1H); **^{13}C NMR** (176 MHz, MeOD): δ = 162.53 (q, J = 36.1 Hz), 156.99, 149.34, 149.07, 142.53, 139.38, 134.13, 131.88, 131.63, 131.60, 130.95, 129.21, 127.76, 125.65, 124.36, 123.81, 118.15, 117.50, 69.08, 62.10, 55.86, 49.77, 45.82, 38.77, 28.42, 25.41, 19.80; **HR-ESI-MS**: *m/z* = 451.1202 ([*M* + H]$^+$, calcd. for C$_{25}$H$_{26}$ON$_2$ ^{81}Br$^+$: 451.1203) (Δ = 0.18 ppm) – No TFA visible; $[\alpha]_{20}^{D}$ = -33° (c = 1.0, MeOH).

(S)-(2-(3-bromophenyl)-6-methoxyquinolin-4-yl)((2R,4S,5R)-5-vinylquinuclidin-2-yl)methanol- trifluoroacetate (104)
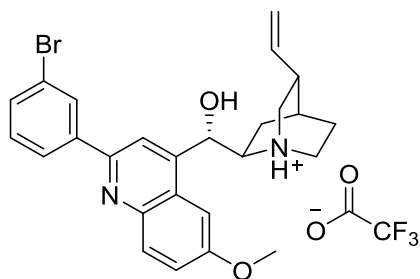
The title compound was synthesized following **General Procedure IV** starting with quinidine (40.0 mg, 120.0 µmol, 1.0 eq) and 3-Bromophenylboronic acid (72.0 mg, 360 µmol, 3.0 eq). Purified using preparative HPLC (ACN/H$_2$O + 0.1 % TFA) to afford the product as an amorphous solid (22 mg, 31%).

^{1}H NMR (700 MHz, MeOD): δ = 8.34 (t, J = 1.8 Hz, 1H), 8.20 (s, 1H), 8.14 (d, J = 9.2 Hz, 1H), 8.12 – 8.09 (m, 1H), 7.67 (ddd, J = 8.0, 1.9, 0.8 Hz, 1H), 7.54 (dd, J = 9.2, 2.6 Hz, 1H), 7.50 (t, J = 7.9 Hz, 1H), 7.38 (d, J = 2.6 Hz, 1H), 6.16 (ddd, J = 17.6, 10.5, 7.3 Hz, 1H), 6.07 (s, 1H), 5.30 (dd, J = 12.8, 5.5 Hz, 2H), 4.30 (ddd, J = 12.5, 8.4, 2.4 Hz, 1H), 4.04 (s, 3H), 3.77 (t, J = 9.5 Hz, 1H), 3.58 (dt, J = 18.9, 6.7 Hz, 2H), 3.43 – 3.36 (m, 1H), 2.79 (dd, J = 17.5, 8.6 Hz, 1H), 2.59 – 2.54 (m, 1H), 2.08 (s, 1H), 2.06 – 1.98 (m, 1H), 1.95 – 1.90 (m, 1H), 1.37 (ddt, J = 22.8, 13.9, 5.6 Hz, 3H), 1.32 – 1.29 (m, 2H); **^{13}C NMR** (176 MHz, MeOD): δ = 162.53 (d, J = 37.3 Hz), 160.34, 154.24, 147.27, 145.25, 142.58, 138.07, 133.41, 132.57, 131.79, 131.30, 127.16, 126.54, 124.08, 123.78, 117.85, 117.75, 101.96, 69.29, 61.49, 56.51, 50.53, 49.96, 49.53, 38.36, 28.63, 24.01, 19.17; **HR-ESI-MS**: m/z = 481.1305 ([M + H]$^+$, calcd. for C$_{26}$H$_{28}$O$_2$N$_2$ ^{81}Br$^+$:481.1308) (Δ = 0.67 ppm) – No TFA visible; $[\alpha]_{20}^{D}$= +70° (c = 1.0, MeOH).
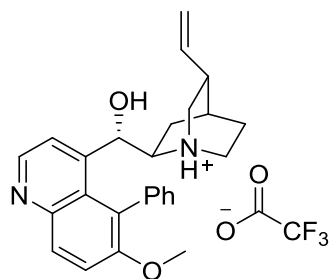
(*R*)-(2-(3-bromophenyl)-6-methoxyquinolin-4-yl)((2*S*,4*S*,5*R*)-5-vinylquinuclidin-2-yl)methanol- trifluoroacetate (111)
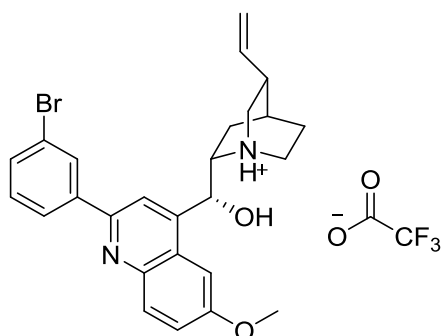
The title compound was synthesized following **General Procedure IV** starting with quinine (40.0 mg, 120.0 µmol, 1.0 eq) and 3-Bromophenylboronic acid (72.0 mg, 360 µmol, 3.0 eq). Purified using preparative HPLC (ACN/H$_2$O + 0.1 % TFA) to afford the product as an amorphous solid (17 mg, 24%).

^{1}H NMR (700 MHz, MeOD): δ = 8.32 (t, J = 1.8 Hz, 1H), 8.25 (s, J = 8.7 Hz, 1H), 8.14 (d, J = 9.2 Hz, 1H), 8.09 (d, J = 7.9 Hz, 1H), 7.70 − 7.67 (m, 1H), 7.55 (dd, J = 9.2, 2.6 Hz, 1H), 7.50 (t, J = 7.9 Hz, 1H), 7.46 (d, J = 2.6 Hz, 1H), 6.09 (d, J = 1.1 Hz, 1H), 5.80 (ddd, J = 17.3, 10.5, 7.1 Hz, 1H), 5.15 (dd, J = 17.1, 4.4 Hz, 1H), 5.06 (d, J = 10.5 Hz, 1H), 4.32 − 4.27 (m, 1H), 4.05 (s, 3H), 3.76 − 3.72 (m, 1H), 3.66 (dd, J = 13.1, 10.7 Hz, 1H), 3.35 (ddd, J = 13.1, 6.9, 3.1 Hz, 2H), 2.84 (dd, J = 3.4, 1.8 Hz, 1H), 2.34 − 2.30 (m, 1H), 2.29 − 2.23 (m, 1H), 2.15 (dd, J = 6.0, 3.0 Hz, 1H), 2.02 − 1.96 (m, 1H), 1.67 − 1.61 (m, 1H); **^{13}C NMR** (176 MHz, MeOD): δ = 162.33 (q, J = 35.3 Hz)), 160.81, 153.94, 149.02, 144.15, 141.74, 139.35, 133.91, 132.00, 131.87, 131.49, 128.33, 127.54, 126.87, 124.32 (d, J = 72.4 Hz), 118.44 117.23, 102.27, 68.87, 61.55, 56.95, 55.70, 49.65, 45.53, 38.67, 28.38, 25.30, 19.64; **HR-ESI-MS**: *m/z* = 481.1303 ([*M* + H]$^+$, calcd. for C$_{26}$H$_{28}$O$_2$N$_2$ ^{81}Br$^+$: 481.1308) (Δ = 1.12 ppm) − No TFA visible; $[\alpha]_{20}^{D}$= -11° (c = 1.0, MeOH).

(S)-(2-(3-chlorophenyl)-6-methoxyquinolin-4-yl)((2R,4S,5R)-5-vinylquinuclidin-2-yl)methanol- trifluoroacetate (105)
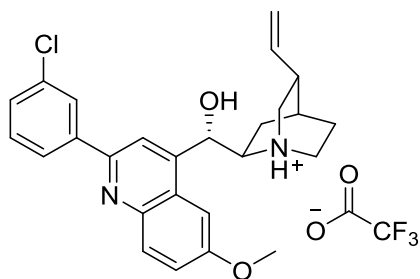
The title compound was synthesized following **General Procedure IV** starting with quinidine (40.0 mg, 120.0 µmol, 1.0 eq) and 3-Chlorophenylboronic acid (56.0 mg, 360 µmol, 3.0 eq). Purified using preparative HPLC (ACN/H$_2$O + 0.1 % TFA) to afford the product as an amorphous solid (20 mg, 30%).

^{1}H NMR (500 MHz, MeOD): δ = 8.16 (s, 1H), 8.13 (t, J = 1.6 Hz, 1H), 8.08 (d, J = 9.3 Hz, 1H), 8.01 (d, J = 7.6 Hz, 1H), 7.53 (d, J = 7.9 Hz, 1H), 7.51 − 7.46 (m, 2H), 7.34 (d, J = 2.4 Hz, 1H), 6.12 (ddd, J = 17.5, 10.5, 7.4 Hz, 1H), 6.05 (s, 1H), 5.27 − 5.22 (m, 2H), 4.29 − 4.22 (m, 1H), 3.99 (s, 3H), 3.71 (t, J = 9.4 Hz, 1H), 3.56 − 3.49 (m, 2H), 3.39 − 3.30 (m, 1H), 2.74 (dd, J = 17.4, 8.6 Hz, 1H), 2.55 − 2.48 (m, 1H), 2.01 (d, J = 10.7 Hz, 1H), 1.93 (dd, J = 7.5, 4.6 Hz, 1H), 1.90 − 1.81 (m, 1H), 1.29 (ddd, J = 12.4, 9.9, 6.7 Hz, 1H); **^{13}C NMR** (126 MHz, MeOD): δ = 160.38, 154.26, 147.55, 145.06, 142.23, 138.12, 136.09, 132.38, 131.59, 130.48, 128.37, 126.78, 126.58, 123.97, 117.91, 117.72, 101.89, 69.21, 61.40, 56.53, 50.48, 49.90, 38.39, 28.66, 24.01, 19.10; **HR-ESI-MS**: *m/z* = 437.1803 ([*M* + H]$^+$, calcd. for C$_{26}$H$_{28}$O$_2$N$_2$ ^{37}Cl$^+$:437.1804) (Δ = 0.20 ppm) – No TFA visible; $[\alpha]_{20}^{D}$= - 41° (c = 1.0, MeOH),

(S)-(5-(3-chlorophenyl)-6-methoxyquinolin-4-yl)((2R,4S,5R)-5-vinylquinuclidin-2-yl)methanol- trifluoroacetate (139)
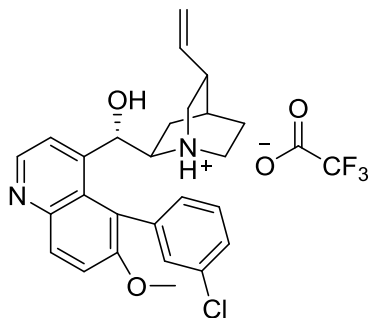
The compound was synthesized following **General Procedure IV**. Crude was purified using preparative HPLC (ACN/H$_2$O + 0.1 % TFA) to afford the pure compound (4 mg, 6%).

¹H NMR (500 MHz, MeOD): δ = 8.88 – 8.84 (m, 1H), 8.25 (dd, J = 9.4, 1.9 Hz, 1H), 8.15 (dd, J = 4.7, 2.0 Hz, 1H), 7.90 (d, J = 9.4 Hz, 1H), 7.79 (m, 1H), 7.54 (m, 3H), 7.18 (s, 1H), 7.09 (t, J = 8.8 Hz, 1H), 5.84 (ddd, J = 17.3, 10.5, 6.9 Hz, 1H), 5.14 (m, 3H), 3.96 – 3.88 (m, 1H), 3.84 (d, J = 7.4 Hz, 3H), 3.33 (m, 1H), 3.24 – 3.16 (m, 1H), 3.14 – 3.07 (m, 1H), 2.60 – 2.52 (m, 1H), 1.89 – 1.75 (m, 4H), 1.34 – 1.22 (m, 1H), 0.69 – 0.59 (m, 1H); **¹³C NMR** (126 MHz, MeOD): δ = 158.55, 150.88, 146.29, 140.43, 137.52, 135.37, 132.11, 131.77, 131.20, 130.72, 130.52, 130.30, 130.14, 126.54, 123.64, 122.84, 119.49, 117.70, 69.16, 60.09, 57.37, 51.07, 49.70, 37.92, 28.61, 23.30, 19.80; **HR-ESI-MS**: m/z = 437.1802 ([M + H]$^+$, calcd. for C$_{26}$H$_{28}$O$_2$N$_2$ ^{37}Cl$^+$:437.1804) (Δ = 0.46 ppm) – No TFA visible; $[\alpha]_{20}^{D}$ = + 12° (c = 1.0, MeOH).

(S)-(2-(3-chloro,4-fluorophenyl)-6-methoxyquinolin-4-yl)((2R,4S,5R)-5-vinylquinuclidin-2-yl)methanol- trifluoroacetate (106)
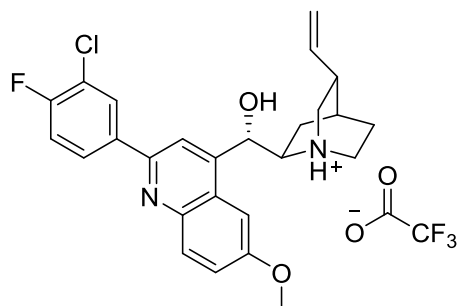
The title compound was synthesized following **General Procedure IV** starting with quinidine (40.0 mg, 120.0 µmol, 1.0 eq) and (3-Chloro,4-Fluoro)phenylboronic acid (56.0 mg, 360 µmol, 3.0 eq). Purified using preparative HPLC (ACN/H_2O + 0.1 % TFA) to afford the product as an amorphous solid (10 mg, 15%).

^{1}H NMR (500 MHz, MeOD): δ = 8.15 (s, 1H), 8.12 – 8.05 (m, 2H), 7.48 (dd, J = 9.3, 2.5 Hz, 1H), 7.40 (t, J = 8.8 Hz, 1H), 7.35 – 7.28 (m, 2H), 6.12 (ddd, J = 17.5, 10.4, 7.4 Hz, 1H), 6.02 (s, 1H), 5.28 – 5.22 (m, 2H), 4.29 – 4.20 (m, 1H), 3.99 (s, 3H), 3.72 (t, J = 9.4 Hz, 1H), 3.57 – 3.49 (m, 2H), 3.35 (m, 1H), 2.74 (dd, J = 17.4, 8.6 Hz, 1H), 2.57 – 2.48 (m, 1H), 2.04 – 1.99 (m, 1H), 1.99 – 1.91 (m, 1H), 1.91 – 1.82 (m, 1H), 1.35 – 1.23 (m, 1H); **^{13}C NMR** (176 MHz, MeOD): δ = 162.98 (q, J = 34.5 Hz), 160.91, 160.29, 159.48, 153.46, 147.09, 145.45, 138.12, 138.10, 132.77, 130.63, 128.68, 128.63, 126.40, 123.68, 122.55, 122.45, 118.16, 118.03, 117.72, 117.46, 101.93, 69.29, 61.50, 56.49, 50.53, 49.97, 49.53, 38.39, 28.66, 24.02, 19.18; **^{19}F NMR** (377 MHz, MeOD): δ = -77.05, -118.64; **HR-ESI-MS**: *m/z* = 455.1706 ([*M* + H]$^+$, calcd. for $C_{26}H_{27}O_2N_2$ $^{37}ClF^+$: 455.1710) (Δ = 0.88 ppm) – No TFA visible; $[\alpha]_{20}^{D}$= (c = 1.0, MeOH).

**(S)-(5-(3-chloro,4-fluorophenyl)-6-methoxyquinolin-4-yl)((2R,4S,5R)-5-vinylquinuclidin-2-yl)methanol- trifluoroacetate (140)**
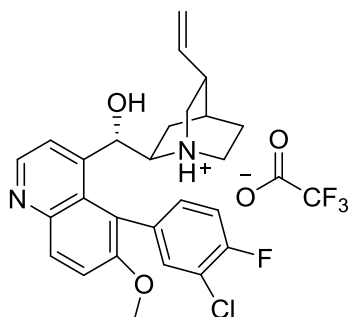
The compound was synthesized following **General Procedure IV**. Crude was purified using preparative HPLC (ACN/H_2O + 0.1 % TFA) to afford the pure compound (3 mg, 5%).

¹H NMR (500 MHz, MeOD): δ = 8.81 (dd, J = 4.7, 2.7 Hz, 1H), 8.22 (dd, J = 9.3, 2.4 Hz, 1H), 8.06 (dd, J = 9.2, 4.6 Hz, 1H), 7.83 (d, J = 9.4 Hz, 1H), 7.46 (t, J = 8.7 Hz, 1H), 7.38 – 7.33 (m, 1H), 7.29 – 7.24 (m, 1H), 5.90 – 5.79 (m, 1H), 5.20 – 5.05 (m, 3H), 4.09 – 3.92 (m, 2H), 3.88 – 3.81 (m, 3H), 3.23 – 3.07 (m, 2H), 2.59 (b.s, 1H), 1.82 (dd, J = 14.7, 8.4 Hz, 3H), 1.27 (ddd, J = 22.2, 10.7, 5.2 Hz, 2H), 0.60 (b.s, 1H); **¹³C NMR** (176 MHz, MeOD): δ = 163.18 (q, J = 35.0 Hz), 159.96, 158.55, 157.71, 148.02, 138.00, 137.03, 136.27, 135.56, 132.83, 131.10, 131.06, 130.60, 127.33, 121.57, 121.47, 120.75, 117.74, 117.59, 117.47, 115.45, 102.15, 69.15, 61.29, 56.95, 50.53, 49.97, 49.53, 38.30, 28.64, 23.99, 19.15.**¹⁹F NMR** (377 MHz, MeOD): δ = -77.21, -117.55; **HR-ESI-MS**: *m/z* = 455.1709 ([*M* + H]⁺, calcd. for $C_{26}H_{27}O_2N_2$ ³⁷ClF⁺: 455.1710) (Δ = 0.29 ppm) – No TFA visible; $[\alpha]_{20}^{D}$ = (c = 1.0, MeOH).

4.1.4.1.4. C3 Substituted Compound Collection

(S)-(3-bromo-6-methoxyquinolin-4-yl)((2R,4S,5R)-5-vinylquinuclidin-2-yl)methanol-trifluoroacetate (133)

A flame dry 50 ml Schlenk-tube was charged with a solution of (+)-Quinidine (1.0 g, 3.08 mmol, 1.0 eq) in THF. Methyl lithium (1.93 mL, 3.08 mmol, 1.0 eq) was added dropwise at 0°C. After addition, a white opaque solution was formed and the mixture was stirred for 1 h at rt. BF_3*OEt_2 (0.42 mL, 3.39 mmol, 1.1 eq) was added at 0°C and stirred for 15 min. A solution of TMPMgCl*LiCl (3.40 mL, 3.39 mmol, 1.1 eq) was added dropwise at 0°C and stirred for 40 min at 0 °C. Then, 1,2-Dibromo-1,1,2,2-tetrachloroethane (0.80 g, 4.62 mmol, 1.5 eq) was added to the reaction and the mixture was stirred 15 h at rt. The reaction was quenched with 15 mL NH_4Cl/NH_3 solution (9:1) and extracted with DCM (3 x 20 mL). The organic phase was dry over Na_2SO_4 and purified by flash chromatography (Al_2O_3 III, isohexane / ethyl acetate = 1:1) to afford the desired compound as an oil (65%).

^{1}H NMR (500 MHz, MeOD): δ = 8.78 (s, 1H), 8.51 (s, br, 1H), 7.97 (d, J = 9.2 Hz, 1H), 7.50 (dd, J = 9.2, 2.8 Hz, 1H), 6.11 − 6.01 (m, 2H), 5.39-5.32 (m, 2H), 5.01 (m, 1H), 3.98 (s, 3H), 3.85 (dd, J = 16.7, 8.1 Hz, 1H), 3.54 − 3.48 (m, 1H), 2.89 (dd, J = 13.6, 10.1 Hz, 1H), 2.66 − 2.58 (m, 1H), 2.54 − 2.47 (m, 1H), 2.33 (dd, J = 9.6, 5.1 Hz, 1H), 2.19 − 2.11 (m, 1H), 1.80 − 1.69 (m, 2H), 1.65 − 1.54 (m, 2H); **HR-ESI-MS**: *m/z* = 405.0994 ([*M* + H]$^+$, calcd. for $C_{20}H_{24}O_2N_2$ $^{81}Br^+$: 405.0995), (Δ = 0.35 ppm); $[\alpha]_{20}^{D}$ = + 82° (c = 1.0, MeOH). Data in accordance with the literature.[138]

(R)-(3-bromo-6-methoxyquinolin-4-yl)((2S,4S,5R)-5-vinylquinuclidin-2-yl)methanol-trifluoroacetate (155)
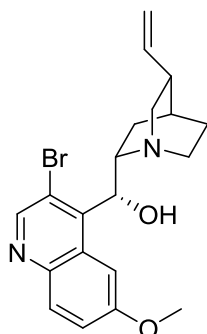
A flame dry 50 ml Schlenk-tube was charged with a solution of (-)-Quinine (1.0 g, 3.08 mmol, 1.0 eq) in THF. Methyl lithium (1.93 mL, 3.08 mmol, 1.0 eq)) was added dropwise at 0°C. After addition, a white opaque solution was formed and the mixture was stirred for 1 h at rt. BF₃*OEt₂ (0.42 mL, 3.39 mmol, 1.1 eq) was added at 0°C and stirred for 15 min. A solution of TMPMgCl*LiCl (3.40 mL, 3.39 mmol, 1.1 eq) was added dropwise at 0°C and stirred for 40 min at 0 °C. Then, 1,2-Dibromo-1,1,2,2-tetrachloroethane (0.80 g, 4.62 mmol, 1.5 eq) was added to the reaction and the mixture was stirred 15 h at rt. The reaction was quenched with 15 mL NH₄Cl/NH₃ solution (9:1) and extracted with DCM (3x20 mL). The organic phase was dry over Na₂SO₄ and purified by flash chromatography (Al₂O₃ III, isohexane / ethyl acetate = 1:1) to afford the desired compound as an oil (59%).

¹H NMR (500 MHz, MeOD): δ = 8.65 (s, 1H), 8.08 (s, br, 1H), 7.87 (d, J = 9.2 Hz, 1H), 7.37 (dd, J = 9.2, 2.8 Hz, 1H), 5.96 – 5.85 (m, 1H), 5.56 (d, J = 9.0 Hz, 1H), 5.03-5.01 (m, 2H), 4.06 (q, J = 7.1 Hz, 1H), 3.90 (s, 3H), 3.73 (dd, J = 16.7, 8.1 Hz, 1H), 3.45 – 3.38 (m, 1H), 2.89 (dd, J = 13.6, 10.1 Hz, 1H), 2.66 – 2.58 (m, 1H), 2.54 – 2.47 (m, 1H), 2.33 (dd, J = 9.6, 5.1 Hz, 1H), 2.19 – 2.11 (m, 1H), 1.80 – 1.69 (m, 2H), 1.65 – 1.54 (m, 2H); **HR-ESI-MS**: *m/z* = 405.0994 ([*M* + H]⁺, calcd. for C₂₀H₂₄O₂N₂ ⁸¹Br⁺: 405.0995), (Δ = 0.35 ppm); $[\alpha]_{20}^{D}$ = - 33° (c = 1.0, MeOH). Data in accordance with the literature.[138]

(S)-(3-iodo-6-methoxyquinolin-4-yl)((2R,4S,5R)-5-vinylquinuclidin-2-yl)methanol-trifluoroacetate (156)
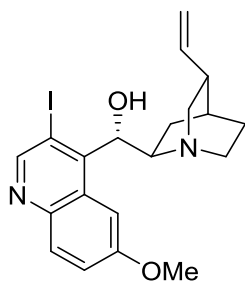
A flame dry 50 ml Schlenk-tube was charged with a solution of (+)-Quinidine (1.0 g, 3.08 mmol, 1.0 eq) in THF. Methyl lithium (1.93 mL, 3.08 mmol, 1.0 eq)) was added dropwise at 0°C. After addition, a white opaque solution was formed and the mixture was stirred for 1 h at rt. BF$_3$*OEt$_2$ (0.42 mL, 3.39 mmol, 1.1 eq) was added at 0°C and stirred for 15 min. A solution of TMPMgCl*LiCl (3.40 mL, 3.39 mmol, 1.1 eq) was added dropwise at 0°C and stirred for 40 min at 0 °C. Then, Iodine (1.17 g, 4.62 mmol, 1.5 eq) was added to the reaction and the mixture was stirred 15 h at rt. The reaction was quenched with 15 mL NH$_4$Cl/NH$_3$ solution (9:1) and extracted with DCM (3x20 mL). The organic phase was dry over Na$_2$SO$_4$ and purified by flash chromatography (Al$_2$O$_3$ III, isohexane / ethyl acetate = 1:1) to afford the desired compound as an oil (60%).

^{1}H NMR (500 MHz, MeOD): δ =8.80 (s, 1H), 8.10 (s, br, 1H), 7.85 (d, J = 9.2 Hz, 1H), 7.27 (dd, J = 9.0, 2.9 Hz, 1H), 5.82-5.73 (m, 1H), 5.51-5.44 (m, 1H), 5.00 (d, J = 1.4 Hz, 1H), 4.98 (dt, J = 7.2, 1.3 Hz, 1H), 3.89 (s, 3H), 3.62-3.47 (m, 1H), 2.95-2.84 (m, 1H), 2.70-2.60 (m, 2H), 2.31-2.25 (m, 1H), 1.90-1.83 (m, 2H), 1.77-1.69 (m, 2H), 1.55-1.48 (m, 2H); **HR-ESI-MS**: m/z = 451.0868 ([M + H]$^+$, calcd. for C$_{20}$H$_{24}$O$_2$N$_2$I$^+$: 451.0877), (Δ = 1.95 ppm); $[\alpha]_{20}^{D}$= + 39° (c = 1.0, MeOH). Data in accordance with the literature.[138]

(S)-(3-(4-fluorophenyl)-6-methoxyquinolin-4-yl)((2R,4S,5R)-5-vinylquinuclidin-2-yl)methanol- trifluoroacetate (121)
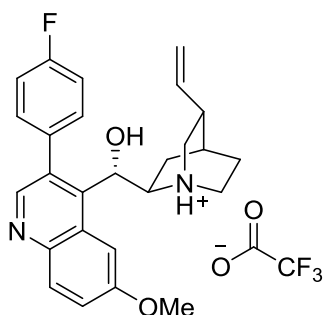
The compound was synthesized following **General Procedure V** starting with (R)-(3-bromo-6-methoxyquinolin-4-yl)((2S,4S,5R)-5-vinylquinuclidin-2-yl)methanol). Purified using preparative HPLC (ACN/H_2O + 0.1 % TFA) to afford the pure compound (22 mg, 63%).

^{1}H NMR (600 MHz, MeOD): δ = 8.65 (s, 1H), 8.23 (d, J = 2.6 Hz, 1H), 8.08 (d, J = 9.2 Hz, 1H), 7.61 (ddd, J = 12.0, 9.0, 4.0 Hz, 3H), 7.37 (dd, J = 16.5, 7.9 Hz, 2H), 5.91 (ddd, J = 17.1, 10.5, 6.5 Hz, 1H), 5.51 (d, J = 8.4 Hz, 1H), 5.18 (dd, J = 30.4, 13.8 Hz, 2H), 4.02 (s, J = 6.9 Hz, 3H), 3-38-3.31 (m, 1H), 3.00 – 2.94 (m, 1H), 2.91 (dd, J = 11.6, 5.1 Hz, 1H), 2.84 (ddd, J = 16.3, 9.5, 6.4 Hz, 1H), 2.72 (d, J = 3.5 Hz, 1H), 2.28 – 2.21 (m, 1H), 2.12 (d, J = 2.9 Hz, 1H), 2.04 (dd, J = 14.2, 7.3 Hz, 1H), 1.86 – 1.79 (m, 1H), 1.79 – 1.71 (m, 1H), 1.37 – 1.28 (m, 1H); **^{13}C NMR** (151 MHz, MeOD): δ = 161.85 (d, J = 38.2 Hz), 160.27, 148.84, 139.02, 136.04, 134.17, 133.17 (d, J = 8.3 Hz), 130.37, 129.15, 128.00, 124.58, 117.25, 117.00, 116.46 (d, J = 23.1 Hz), 106.02, 71.94, 61.67, 56.36, 55.24, 49.57, 44.06, 37.86, 36.01, 27.62, 27.30, 24.79, 24.51, 17.11; **^{19}F NMR** (565 MHz, MeOD): δ = -77.13, -113.94; **HR-ESI-MS**: m/z = 419.2127 ([M + H]$^+$, calcd. for $C_{26}H_{28}O_2N_2F^+$: 419.2129) (Δ = 0.64 ppm) – No TFA visible; $[\alpha]_{20}^{D}$= + 24° (c = 1.0, MeOH).

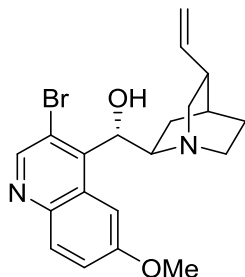**(S)-(3-(4-chlorophenyl)-6-methoxyquinolin-4-yl)((2R,4S,5R)-5-vinylquinuclidin-2-yl)methanol- trifluoroacetate (122)**

The compound was synthesized following **General Procedure V** starting with (R)-(3-bromo-6-methoxyquinolin-4-yl)((2S,4S,5R)-5-vinylquinuclidin-2-yl)methanol (25.0 mg, mmol, 1.0 eq). Purified using preparative HPLC (ACN/H$_2$O + 0.1 % TFA) to afford the pure compound (26 mg, 72%).

^{1}H NMR (700 MHz, MeOD): δ = 8.60 (s, 1H), 8.19 (d, J = 2.6 Hz, 1H), 8.08 (d, J = 9.2 Hz, 1H), 7.65 (d, J = 8.1 Hz, 2H), 7.60 − 7.54 (m, 3H), 5.92 (ddd, J = 17.1, 10.5, 6.5 Hz, 1H), 5.49 (d, J = 8.3 Hz, 1H), 5.23 (d, J = 10.5 Hz, 1H), 5.17 (d, J = 17.2 Hz, 1H), 4.02 (s, 3H), 3.35 (t, J = 6.8 Hz, 1H), 2.97 (ddd, J = 13.1, 4.8, 2.2 Hz, 1H), 2.94 − 2.88 (m, 2H), 2.74 (d, J = 3.6 Hz, 1H), 2.29 − 2.21 (m, 1H), 2.14 (d, J = 2.9 Hz, 1H), 2.06 (dd, J = 14.3, 7.2 Hz, 1H), 1.87 − 1.75 (m, 2H), 1.33 (dd, J = 19.8, 12.6 Hz, 1H); **^{13}C NMR** (176 MHz, MeOD): δ = 162.51 (d, J = 36.2 Hz), 159.97, 149.82, 145.19, 140.87, 138.98, 137.21, 136.20, 135.64, 132.62, 131.80, 130.59, 128.66, 123.78, 117.27, 105.83, 72.00, 61.73, 56.27, 55.34, 49.53, 44.11, 37.88, 31.12, 27.30, 24.78, 24.52; **HR-ESI-MS**: *m/z* =437.1806 ([M + H]+, calcd. for C$_{26}$H$_{28}$O$_2$N$_2$ ^{37}Cl$^+$: 437.1804) (Δ = 0.17 ppm) – No TFA visible; $[\alpha]_{20}^{D}$= + 19° (c = 1.0, MeOH).

(S)-(3-(4-nitrophenyl)-6-methoxyquinolin-4-yl)((2R,4S,5R)-5-vinylquinuclidin-2-yl)methanol- trifluoroacetate (123)

The compound was synthesized following **General Procedure V** starting with (R)-(3-bromo-6-methoxyquinolin-4-yl)((2S,4S,5R)-5-vinylquinuclidin-2-yl)methanol (25.0 mg, mmol, 1.0 eq). Purified using preparative HPLC (ACN/H_2O + 0.1 % TFA) to afford the pure compound (9 mg, 25%).

^{1}H NMR (700 MHz, MeOD): δ = 8.64 (d, J = 4.5 Hz, 2H), 8.25 (dd, J = 9.0, 2.1 Hz, 2H), 7.72 (dd, J = 9.6, 2.8 Hz, 1H), 7.44 (d, J = 2.6 Hz, 1H), 7.33 (d, J = 2.6 Hz, 1H), 6.08 − 5.98 (m, 1H), 5.97 (s, 1H), 5.18 (t, J = 14.0 Hz, 2H), 4.23 − 4.17 (m, 1H), 3.97 (s, 3H), 3.64 (t, J = 9.4 Hz, 1H), 3.51 − 3.42 (m, 2H), 3.33 − 3.27 (m, 1H), 3.11 (dd, J = 14.7, 7.2 Hz, 1H), 2.94 (dd, J = 14.5, 7.1 Hz, 1H), 2.68 (dd, J = 17.5, 8.7 Hz, 1H), 2.45 − 2.39 (m, 1H), 1.98 − 1.86 (m, 1H), 1.85 − 1.78 (m, 1H), 1.28 − 1.16 (m, 1H); **^{13}C NMR** (176 MHz, MeOD): δ = 159.40, 148.78, 148.49, 147.22, 146.42, 142.60, 142.27, 138.04, 132.75, 128.05, 124.00 (d, J = 11.6 Hz), 120.65, 117.72, 102.68, 80.43, 69.08, 61.37, 56.61, 50.53, 49.99, 49.53, 38.34, 35.36, 28.66, 24.02, 19.15; **HR-ESI-MS**: m/z = 446.2071 ([M + H]$^+$, calcd. for $C_{26}H_{28}O_4N_3^+$: 446.2074) (Δ = 0.76 ppm) – No TFA visible; $[\alpha]_{20}^{D}$= - 18° (c = 1.0, MeOH).

(S)-(3-(4-trifluoromethylphenyl)-6-methoxyquinolin-4-yl)((2R,4S,5R)-5-vinylquinuclidin-2-yl)methanol- trifluoroacetate (124)

The compound was synthesized following **General Procedure V** starting with (R)-(3-bromo-6-methoxyquinolin-4-yl)((2S,4S,5R)-5-vinylquinuclidin-2-yl)methanol (25.0 mg, mmol, 1.0 eq). Purified using preparative HPLC (ACN/H$_2$O + 0.1 % TFA) to afford the pure compound (11 mg, 29%).

^{1}H NMR (600 MHz, MeOD): δ = 8.63 (s, 1H), 8.31 (s, 1H), 8.08 (d, J = 9.2 Hz, 1H), 7.94 (d, J = 7.6 Hz, 2H), 7.79 (s, 2H), 7.58 (dd, J = 9.2, 2.7 Hz, 1H), 5.75 – 5.67 (m, 1H), 5.52 (d, J = 6.9 Hz, 1H), 5.09 (dd, J = 10.7, 0.7 Hz, 1H), 4.74 (dd, J = 17.4, 0.7 Hz, 1H), 4.02 (s, 3H), 3.96 (q, J = 8.3 Hz, 1H), 3.15 – 3.06 (m, 3H), 2.91 – 2.85 (m, 1H), 2.68 – 2.61 (m, 1H), 2.20 – 2.13 (m, 1H), 2.06 (s, 1H), 2.02 – 1.87 (m, 3H); **^{13}C NMR** (151 MHz, MeOD): δ = 161.77 (d, J = 35.6 Hz), 160.09, 148.73, 144.38, 142.65, 142.04, 137.77, 135.41, 132.13, 131.59, 130.89, 129.92, 128.93, 128.19, 126.40, 124.59, 124.49, 116.91, 106.37, 72.82, 62.12, 57.62, 56.31, 50.89, 49.57, 37.14, 27.61, 24.20, 23.66; **^{19}F NMR** (565 MHz, MeOD): δ = -64.17, -77.22; **HR-ESI-MS**: m/z = 469.2098 ([M + H]$^+$, calcd. for C$_{27}$H$_{28}$O$_2$N$_2$F$_3^+$: 469.2097) (Δ = 0.12 ppm) – No TFA visible; $[\alpha]_{20}^{D}$= - 57° (c = 1.0, MeOH).

(S)-(3-(4-*tert*-butyloxycarbonylaminophenyl)-6-methoxyquinolin-4-yl)((2R,4S,5R)-5-vinylquinuclidin-2-yl)methanol- trifluoroacetate (125)

The compound was synthesized following **General Procedure V** starting with (R)-(3-bromo-6-methoxyquinolin-4-yl)((2S,4S,5R)-5-vinylquinuclidin-2-yl)methanol (25.0 mg, mmol, 1.0 eq). Purified using preparative HPLC (ACN/H$_2$O + 0.1 % TFA) to afford the pure compound (11 mg, 25%).

^{1}H NMR (500 MHz, MeOD): δ = 8.65 (s, 1H), 8.32 (d, J = 2.6 Hz, 1H), 8.07 (d, J = 9.3 Hz, 1H), 7.70 (d, J = 8.3 Hz, 2H), 7.56 (dd, J = 9.3, 2.7 Hz, 1H), 7.51 (d, J = 8.8 Hz, 2H), 5.77 − 5.68 (m, 1H), 5.64 (d, J = 7.8 Hz, 1H), 5.13 (d, J = 10.6 Hz, 1H), 4.78 (d, J = 17.5 Hz, 1H), 4.03 (s, 3H), 3.13 − 3.00 (m, 3H), 2.83 − 2.76 (m, 1H), 2.65 (d, J = 6.7 Hz, 1H), 2.17 − 1.98 (m, 4H), 1.93 (s, 1H), 1.58 (s, 9H), 1.39 − 1.30 (m, 1H); **^{13}C NMR** (126 MHz, MeOD): δ = 172.98, 159.96, 157.10, 155.11, 149.11, 147.06, 142.14, 141.77, 137.77, 136.77, 131.72, 131.53, 130.39, 129.17, 127.61, 124.18, 120.27, 117.00, 106.37, 101.40, 72.63, 62.09, 61.54, 56.26, 50.93, 49.63, 37.06, 28.65, 27.54, 24.73, 23.75, 20.86, 14.47; **HR-ESI-MS**: *m/z* = 516.2853 ([*M* + H]$^+$, calcd. for C$_{31}$H$_{38}$O$_4$N$_3^+$: 516.2857) − No TFA visible., (Δ = 0.78 ppm); $[\boldsymbol{\alpha}]_{\mathbf{20}}^{\boldsymbol{D}}$= + 72° (c = 1.0, MeOH).

(S)-(3-(3-fluorophenyl)-6-methoxyquinolin-4-yl)((2R,4S,5R)-5-vinylquinuclidin-2-yl)methanol- trifluoroacetate (127)

The compound was synthesized following **General Procedure V** starting with (R)-(3-bromo-6-methoxyquinolin-4-yl)((2S,4S,5R)-5-vinylquinuclidin-2-yl)methanol (25.0 mg, mmol, 1.0 eq). Purified using preparative HPLC (ACN/H_2O + 0.1 % TFA) to afford the pure compound (26 mg, 75%).

^{1}H NMR (600 MHz, MeOD): δ = 8.66 (s, 1H), 8.37 (s, J = 25.8 Hz, 1H), 8.08 (d, J = 9.3 Hz, 1H), 7.66 (dd, J = 14.0, 7.7 Hz, 1H), 7.60 (dd, J = 9.3, 2.7 Hz, 1H), 7.41 (d, J = 6.2 Hz, 2H), 7.34 (td, J = 8.5, 2.2 Hz, 1H), 5.79 – 5.72 (m, 1H), 5.61 (d, J = 7.0 Hz, 1H), 5.15 (d, J = 10.6 Hz, 1H), 4.83 (s, 1H), 4.03 (s, 3H), 3.99 – 3.92 (m, 1H), 3.16 – 3.07 (m, 3H), 2.98 – 2.91 (m, 1H), 2.70 – 2.61 (m, 1H), 2.23 – 2.16 (m, 1H), 2.07 (s, 1H), 2.03 – 1.88 (m, 3H); **^{13}C NMR** (151 MHz, MeOD): δ = 161.53 (q, J = 36.8 Hz), 160.21, 148.11, 143.26, 143.09, 140.28, 137.76, 135.65, 129.94, 129.91, 129.27, 129.21, 127.09, 126.42, 124.94, 118.44, 118.04, 117.04, 106.53, 72.77, 62.17, 56.61, 50.53, 49.57, 37.20, 27.67, 24.13, 23.66; **^{19}F NMR** (565 MHz, MeOD): δ = -77.10, -115.83. **HR-ESI-MS**: *m/z* = 419.2126 ([*M* + H]$^+$, calcd. for $C_{26}H_{28}O_2N_2F^+$: 419.2129) (Δ = 0.92 ppm) – No TFA visible; $[\alpha]_{20}^{D}$= ° (c = 1.0, MeOH).
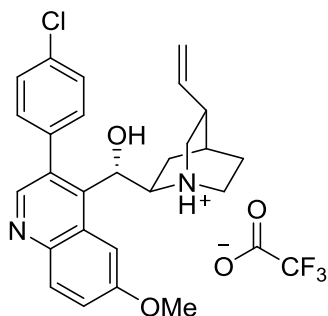
(S)-(3-(3,4-difluorophenyl)-6-methoxyquinolin-4-yl)((2R,4S,5R)-5-vinylquinuclidin-2-yl)methanol- trifluoroacetate (128)

The compound was synthesized following **General Procedure V** starting with (R)-(3-bromo-6-methoxyquinolin-4-yl)((2S,4S,5R)-5-vinylquinuclidin-2-yl)methanol (25.0 mg, mmol, 1.0 eq). Purified using preparative HPLC (ACN/H$_2$O + 0.1 % TFA) to afford the pure compound (18 mg, 50%).

^{1}H NMR (600 MHz, MeOD): δ = 8.77 (d, J = 4.7 Hz, 1H), 7.88 (d, J = 4.6 Hz, 1H), 7.56 − 7.50 (m, 2H), 7.45 (d, J = 2.6 Hz, 1H), 7.43 − 7.34 (m, 2H), 6.18 − 6.09 (m, 2H), 5.29 (t, J = 13.4 Hz, 2H), 4.30 (ddd, J = 12.3, 8.4, 2.3 Hz, 1H), 4.07 (s, 3H), 3.74 (t, J = 9.4 Hz, 1H), 3.56 (q, J = 11.0 Hz, 2H), 3.44 − 3.35 (m, 1H), 2.78 (q, J = 8.5 Hz, 1H), 2.55 − 2.48 (m, 1H), 2.06 (s, 1H), 2.02 − 1.96 (m, 1H), 1.90 (dt, J = 11.4, 9.0 Hz, 1H), 1.36 − 1.24 (m, 1H); **^{13}C NMR** (151 MHz, MeOD): δ = 162.98 (d, J = 34.9 Hz), 159.72, 148.00, 147.56, 141.88, 138.04, 128.12, 127.98, 127.91, 124.19, 120.79, 120.67, 120.57, 118.10, 117,98, 117.72, 102.13, 69.02, 61.29, 56.80, 50.51, 49.93, 49.85, 49.57, 38.32, 28.67, 24.00, 19.08; **^{19}F NMR** (565 MHz, MeOD): δ = -76.84, -141.05, -141.93; **HR-ESI-MS**: *m/z* = 437.2036 ([*M* + H]$^+$, calcd. for C$_{26}$H$_{27}$O$_2$N$_2$F$_2^+$: 437.2035) (Δ = 0.28 ppm) – No TFA visible; $[\alpha]_{20}^{D}$= + 91° (c = 1.0, MeOH).
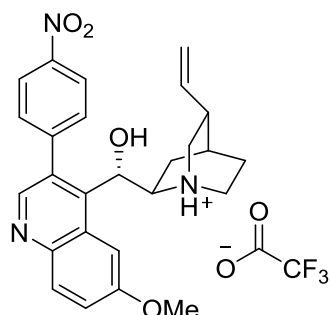
(S)-(3-(3,5-difluorophenyl)-6-methoxyquinolin-4-yl)((2R,4S,5R)-5-vinylquinuclidin-2-yl)methanol- trifluoroacetate (129)
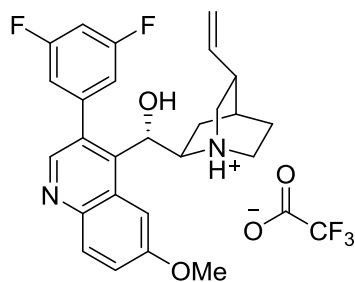
The compound was synthesized following **General Procedure V** starting with (R)-(3-bromo-6-methoxyquinolin-4-yl)((2S,4S,5R)-5-vinylquinuclidin-2-yl)methanol (25.0 mg, mmol, 1.0 eq). Purified using preparative HPLC (ACN/H$_2$O + 0.1 % TFA) to afford the pure compound (24 mg, 67%).

^{1}H NMR (500 MHz, MeOD): δ = 8.73 (d, J = 4.6 Hz, 1H), 7.81 (d, J = 4.5 Hz, 1H), 7.48 (d, J = 2.6 Hz, 1H), 7.37 (d, J = 2.6 Hz, 1H), 7.15 (tt, J = 10.2, 5.2 Hz, 2H), 7.01 (tt, J = 9.2, 2.3 Hz, 1H), 6.09 (ddd, J = 17.5, 10.4, 7.3 Hz, 1H), 6.02 (s, 1H), 5.33 – 5.19 (m, 2H), 4.26 (ddd, J = 12.4, 8.4, 2.3 Hz, 1H), 4.02 (s, 3H), 3.70 (t, J = 9.5 Hz, 1H), 3.53 (dd, J = 21.3, 10.6 Hz, 2H), 3.44 – 3.33 (m, 1H), 2.74 (dd, J = 17.4, 8.3 Hz, 1H), 2.48 (dd, J = 12.3, 10.6 Hz, 1H), 2.15 (dd, J = 15.1, 7.4 Hz, 1H), 2.05 – 1.91 (m, 2H), 1.91 – 1.83 (m, 1H); **^{13}C NMR** (151 MHz, MeOD): δ =165.03 (d, J = 11.5 Hz), 163.39 (d, J = 11.5 Hz), 159.83, 149.06, 145.43, 142.14, 141.27, 137.81, 134.37, 131.63, 128.66, 124.09, 118.16, 117.11, 106.33, 105.15 (t, J = 25.5 Hz), 101.24, 72.91, 62.39, 56.23, 50.87, 49.85, 37.31, 27.76, 23.66, 23.61; **^{19}F NMR** (377 MHz, MeOD): δ = -76.87, -112.64; **HR-ESI-MS**: *m/z* = 437.2025 ([*M* + H]$^+$, calcd. for C$_{26}$H$_{27}$O$_2$N$_2$F$_2^+$: 437.2035) (Δ = 2.26 ppm) – No TFA visible; $[\alpha]_{20}^{D}$= + 73° (c = 1.0, MeOH).
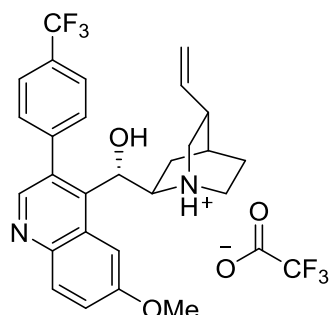
(S)-(3-(3-chloro,4-fluorophenyl)-6-methoxyquinolin-4-yl)((2R,4S,5R)-5-vinylquinuclidin-2-yl)methanol- trifluoroacetate (130)
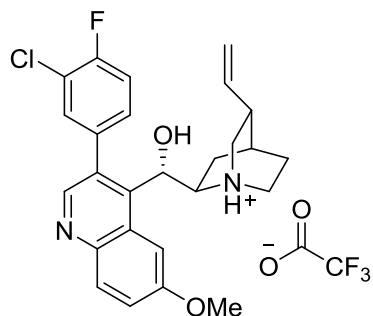
The compound was synthesized following **General Procedure V** starting with (R)-(3-bromo-6-methoxyquinolin-4-yl)((2S,4S,5R)-5-vinylquinuclidin-2-yl)methanol (25.0 mg, mmol, 1.0 eq). Purified using preparative HPLC (ACN/H$_2$O + 0.1 % TFA) to afford the pure compound (13 mg, 35%).

^{1}H NMR (500 MHz, MeOD): δ = 8.53 (s, 1H), 8.30 (s, 1H), 8.01 (d, J = 9.2 Hz, 1H), 7.73 (b.s, 1H), 7.52 – 7.43 (m, 2H), 7.20 – 7.07 (m, 1H), 5.87 – 5.73 (m, 1H), 5.50 (b.s, 1H), 5.16 (d, J = 10.6 Hz, 1H), 4.98 – 4.88 (m, 1H), 3.97 (s, 3H), 3.19 – 3.06 (m, 3H), 2.71 – 2.58 (m, 1H), 2.34 – 2.20 (m, 2H), 2.05 (s, 1H), 2.02 – 1.75 (m, 2H), 1.43 – 1.17 (m, 2H); **^{13}C NMR** (151 MHz, MeOD): δ = 159.80, 149.49, 145.40, 141.42, 137.84, 137.82, 134.37, 133.18, 131.64, 131.45, 131.40, 128.72, 123.96, 122.72, 117.04, 106.30, 73.00, 62.35, 56.22, 50.87, 49.85, 49.57, 37.27, 27.73, 23.60, 1.79; **^{19}F NMR** (377 MHz, MeOD): δ = -76.74, -117.93; **HR-ESI-MS**: m/z = 455.1705 ([M + H]$^+$, calcd. for C$_{26}$H$_{27}$O$_2$N$_2$ ^{37}ClF$^+$: 455.1710) – No TFA visible., (Δ = 1.16 ppm); $[\alpha]_{20}^{D}$= - 2° (c = 1.0, MeOH).
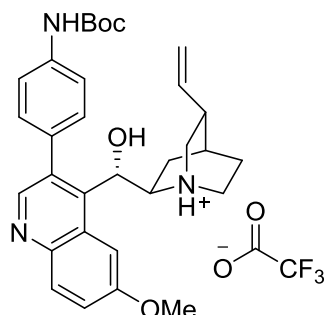
(S)-(3-(3,4-dimethoxyphenyl)-6-methoxyquinolin-4-yl)((2R,4S,5R)-5-vinylquinuclidin-2-yl)methanol- trifluoroacetate (131)
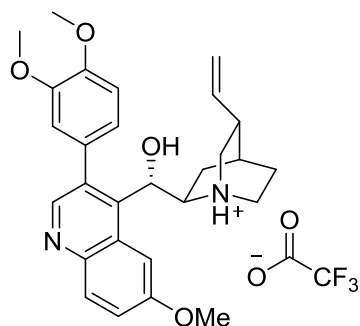
The compound was synthesized following **General Procedure V** starting with (R)-(3-bromo-6-methoxyquinolin-4-yl)((2S,4S,5R)-5-vinylquinuclidin-2-yl)methanol (25.0 mg, mmol, 1.0 eq). Purified using preparative HPLC (ACN/H$_2$O + 0.1 % TFA) to afford the pure compound (15 mg, 40%).

^{1}H NMR (700 MHz, MeOD): δ = 8.81 (d, J = 5.2 Hz, 1H), 8.14 (d, J = 5.1 Hz, 1H), 7.62 (dt, J = 8.9, 4.6 Hz, 2H), 7.22 – 7.11 (m, 3H), 6.39 (s, 1H), 6.15 (ddd, J = 17.5, 10.4, 7.3 Hz, 1H), 5.31 (dd, J = 19.6, 13.8 Hz, 2H), 4.30 (ddd, J = 12.2, 8.4, 2.2 Hz, 1H), 4.13 (d, J = 17.7 Hz, 3H), 3.97 – 3.93 (m, 3H), 3.90 (s, 3H), 3.78 (dd, J = 16.5, 6.9 Hz, 1H), 3.59 (dd, J = 21.2, 10.0 Hz, 2H), 3.44 – 3.36 (m, 1H), 2.81 (dd, J = 17.4, 8.5 Hz, 1H), 2.59 – 2.51 (m, 1H), 2.07 (d, J = 19.0 Hz, 1H), 2.06 – 1.97 (m, 1H), 1.91 (dt, J = 11.5, 9.3 Hz, 1H), 1.37 – 1.28 (m, 1H); **^{13}C NMR** (176 MHz, MeOD): δ = 163.24 (d, J = 35.2 Hz), 160.90, 151.39, 150.77, 144.64, 138.05, 130.14, 129.01, 127.01, 123.88, 120.88, 117.75, 115.00, 113.33, 106.52, 101.94, 68.94, 61.03, 57.36, 56.92, 56.60, 56.31, 50.51, 49.80, 49.53, 38.29, 28.71, 24.49, 23.99, 18.93; **HR-ESI-MS**: *m/z* = 461.2439 ([*M* + H]$^+$, calcd. for C$_{28}$H$_{33}$O$_4$N$_2$$^+$: 461.2435) (Δ = 0.91 ppm) – No TFA visible; $[\alpha]_{20}^{D}$= - 69° (c = 1.0, MeOH).
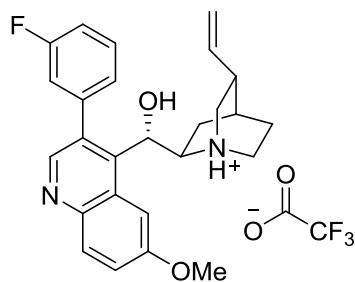
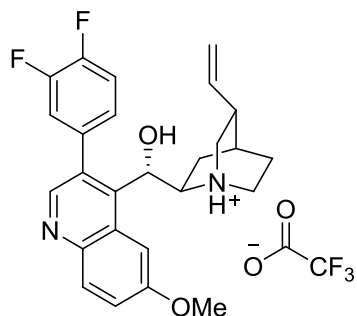**(S)-(3-(3,5-dimethoxyphenyl)-6-methoxyquinolin-4-yl)((2R,4S,5R)-5-vinylquinuclidin-2-yl)methanol- trifluoroacetate (132)**

The compound was synthesized following **General Procedure V** starting with (R)-(3-bromo-6-methoxyquinolin-4-yl)((2S,4S,5R)-5-vinylquinuclidin-2-yl)methanol (25.0 mg, mmol, 1.0 eq). Purified using preparative HPLC (ACN/H$_2$O + 0.1 % TFA) to afford the pure compound (9 mg, 24%).

^{1}H NMR (700 MHz, MeOD): δ = 8.72 (s, 1H), 8.40 (d, J = 2.7 Hz, 1H), 8.11 (d, J = 9.2 Hz, 1H), 7.64 (dd, J = 9.3, 2.7 Hz, 1H), 6.71 (t, J = 2.2 Hz, 2H), 6.52 (d, J = 2.3 Hz, 1H), 5.77 (ddd, J = 17.4, 10.7, 5.6 Hz, 1H), 5.72 (d, J = 7.6 Hz, 1H), 5.17 (ddd, J = 10.7, 1.7, 0.7 Hz, 1H), 4.85 − 4.81 (m, 1H), 4.04 (s, 3H), 3.88 (s, 6H), 3.72 (s, 1H), 3.14 − 3.07 (m, 2H), 2.97 (ddd, J = 13.0, 8.1, 2.4 Hz, 1H), 2.67 (m, 1H), 2.16 (ddd, J = 13.2, 6.3, 4.3 Hz, 1H), 2.08 (m, 1H), 2.05 − 1.98 (m, 2H), 1.93 (m, 1H); **^{13}C NMR** (176 MHz, MeOD): δ =162.70 (q, J = 34.6 Hz), 161.83, 147.24, 144.54, 141.47, 139.37, 137.90, 137.14, 129.63, 128.75, 125.30, 121.09, 117.74, 116.87, 109.17, 106.69, 102.50, 101.51, 72.55, 62.20, 56.40, 56.22, 56.01, 55.64, 55.58, 50.97, 48.48, 37.10, 27.62, 24.43, 23.71, 18.83; **HR-ESI-MS**: *m/z* = 461.2423 ([*M* + H]$^+$, calcd. for C$_{28}$H$_{33}$O$_4$N$_2$$^+$: 461.2435) – No TFA visible., (Δ = 2.48 ppm); $[\alpha]_{20}^{D}$= - 17° (c = 1.0, MeOH).
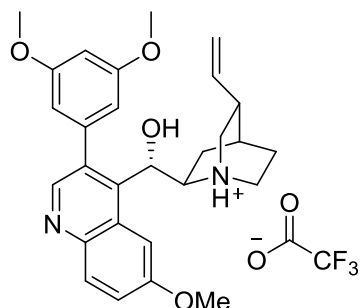
4.1.4.1.5.   Others Substitutions on the Quinidine Scaffold
4.1.4.1.5.1.   Compound with Reduced Double Bond

(S)-((1S,2S,4S,5R)-5-ethylquinuclidin-2-yl)(2-(4-fluorophenyl)-6-methoxyquinolin-4-yl)methanol- trifluoroacetate (134)
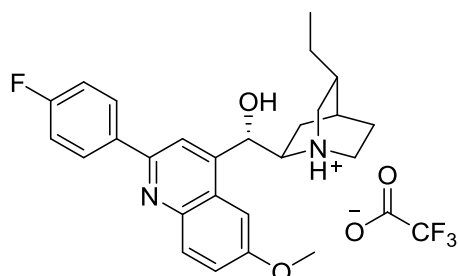
The compound was synthesized following **General Procedure IV** starting with dihydroquinidine (25.0 mg, 0.08 mmol, 1.0 eq). Crude was purified using preparative HPLC (ACN/H$_2$O + 0.1 % TFA) to afford the pure compound (31 mg, 48%).

^{1}H NMR (400 MHz, MeOD): δ = 8.23 − 8.15 (m, 3H), 8.12 (d, J = 9.3 Hz, 1H), 7.53 (dd, J = 9.3, 2.6 Hz, 1H), 7.36 (d, J = 2.6 Hz, 1H), 7.34 − 7.29 (m, 2H), 6.04 (s, 1H), 4.06 − 3.99 (m, 3H), 3.72 (t, J = 9.4 Hz, 1H), 3.55 (t, J = 11.2 Hz, 2H), 3.42 − 3.34 (m, 1H), 2.56 − 2.48 (m, 1H), 2.05 (s, 1H), 1.93 (dt, J = 12.7, 7.5 Hz, 3H), 1.77 − 1.60 (m, 2H), 1.38 − 1.29 (m, 2H), 1.00 (t, J = 7.4 Hz, 3H); **^{13}C NMR** (101 MHz, MeOD): δ = 166.56, 160.18, 154.96, 147.53, 144.91, 136.54, 132.12, 130.68 (d, J = 8.6 Hz), 126.22, 123.72, 117.97, 116.92, 116.71, 102.00, 69.18, 61.50, 56.48, 51.70, 50.61, 49.85, 36.23, 26.33, 25.38, 24.57, 18.92, 11.78; **^{19}F NMR** (377 MHz, MeOD): δ = -76.98, -114.25; **HR-ESI-MS**: *m/z* = 421.2274 ([*M* + H]$^+$, calcd. for C$_{26}$H$_{30}$O$_2$N$_2$F$^+$: 421.2286) (Δ = 2.77 ppm) − No TFA visible; $[\alpha]_{20}^{D}$ = + 79° (c = 1.0, MeOH).

(S)-((1S,2S,4S,5R)-5-ethylquinuclidin-2-yl)(5-(4-fluorophenyl)-6-methoxyquinolin-4-yl)methanol- trifluoroacetate (143)
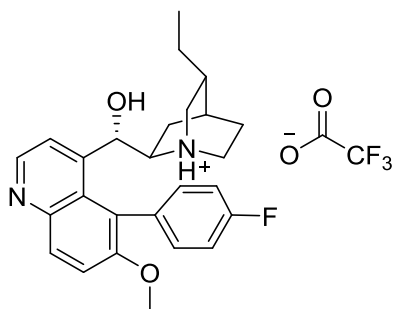
The compound was synthesized following **General Procedure IV** starting with dihydroquinidine (25.0 mg, 0.08 mmol, 1.0 eq). Crude was purified using preparative HPLC (ACN/H$_2$O + 0.1 % TFA) to afford the pure compound (6 mg, 10%).

^{1}H NMR (400 MHz, MeOD): δ = 8.87 (d, J = 4.9 Hz, 1H), 8.26 (d, J = 9.4 Hz, 1H), 8.14 (d, J = 4.8 Hz, 1H), 7.88 (dd, J = 9.4, 4.8 Hz, 1H), 7.76 − 7.70 (m, 1H), 7.37 (td, J = 8.6, 2.7 Hz, 1H), 7.26 (td, J = 8.6, 2.7 Hz, 1H), 7.20 − 7.14 (m, 1H), 5.08 (d, J = 3.6 Hz, 1H), 3.86 (s, 3H), 3.64 − 3.55 (m, 1H), 3.16 (ddd, J = 21.3, 17.3, 10.0 Hz, 2H), 1.88 − 1.71 (m, 5H), 1.43 (tt, J = 13.8, 6.8 Hz, 2H), 1.31 (d, J = 6.5 Hz, 2H), 0.89 (t, J = 7.4 Hz, 3H), 0.72 − 0.62 (m, 1H); **^{13}C NMR** (101 MHz, MeOD): δ = 163.12, 158.29, 152.59, 149.93, 146.82, 134.38 (dd, J = 3.6, 1.9 Hz), 134.07 (d, J = 8.0 Hz), 133.43 (d, J = 7.9 Hz), 130.70, 126.78, 123.97, 122.58, 119.03, 116.95 (dd, J = 38.8, 21.7 Hz), 69.00, 60.10, 57.20, 52.82, 50.65, 49.71, 35.92, 26.41, 25.07, 23.88, 19.69, 11.61; **^{19}F NMR** (377 MHz, MeOD): δ = -76.98, -114.05; **HR-ESI-MS**: *m/z* = 421.2274 ([*M* + H]$^+$, calcd. for C$_{26}$H$_{30}$O$_2$N$_2$F$^+$: 421.2286) (Δ = 2.77 ppm) − No TFA visible; $[\alpha]_{20}^{D}$ = + 79° (c = 1.0, MeOH).

(S)-((1S,2S,4S,5R)-5-ethylquinuclidin-2-yl)(2-(4-chlorophenyl)-6-methoxyquinolin-4-yl)methanol- trifluoroacetate (135)
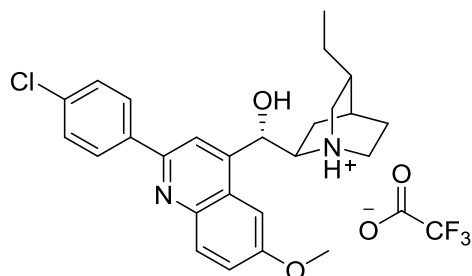
The compound was synthesized following **General Procedure IV** starting with dihydroquinidine (25.0 mg, 0.06 mmol, 1.0 eq). Crude was purified using preparative HPLC (ACN/H$_2$O + 0.1 % TFA) to afford the pure compound (28 mg, 42%).

^{1}H NMR (500 MHz, MeOD): δ = 8.28 (s, 1H), 8.15 (d, J = 9.3 Hz, 1H), 8.09 (d, J = 8.6 Hz, 2H), 7.63 – 7.59 (m, 3H), 7.51 (d, J = 2.4 Hz, 1H), 6.24 (s, 1H), 4.05 (s, 3H), 3.99 – 3.91 (m, 1H), 3.68 (t, J = 9.4 Hz, 1H), 3.50 (t, J = 11.2 Hz, 2H), 3.32 (d, J = 9.2 Hz, 1H), 2.52 – 2.44 (m, 1H), 1.99 (s, 1H), 1.95 – 1.81 (m, 3H), 1.65 (qd, J = 13.7, 7.3 Hz, 2H), 1.31 – 1.24 (m, 1H), 0.96 (t, J = 7.4 Hz, 3H); **^{13}C NMR** (126 MHz, MeOD): δ = 160.92, 153.38, 146.12, 130.51, 130.37, 129.22, 129.07, 126.80, 125.77, 122.10, 118.72, 102.42, 68.79, 61.07, 57.06, 53.59, 51.33, 50.61, 50.37, 36.03, 28.40, 26.19, 25.22, 24.38, 18.53, 11.63; **HR-ESI-MS**: *m/z* = 439.1967 ([*M* + H]$^+$, calcd. for C$_{26}$H$_{30}$O$_2$N$_2$ ^{37}Cl$^+$:439.1961) (Δ = 1.51 ppm) – No TFA visible; $[\alpha]_{20}^{D}$ = + 112° (c = 1.0, MeOH).

(S)-((1S,2S,4S,5R)-5-ethylquinuclidin-2-yl)(5-(4-chlorophenyl)-6-methoxyquinolin-4-yl)methanol- trifluoroacetate (144)
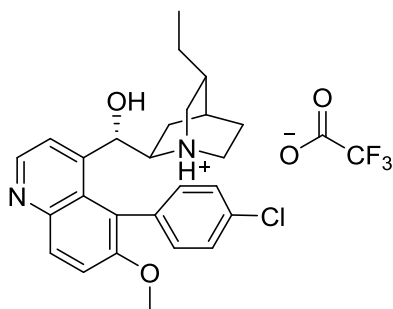
The compound was synthesized following **General Procedure IV** starting with dihydroquinidine (25.0 mg, 0.06 mmol, 1.0 eq). Crude was purified using preparative HPLC (ACN/H$_2$O + 0.1 % TFA) to afford the pure compound (4 mg, 6%).

^{1}H NMR (500 MHz, MeOD): δ = 8.92 (d, J = 5.1 Hz, 1H), 8.26 (dd, J = 18.0, 7.2 Hz, 2H), 7.96 (d, J = 9.4 Hz, 1H), 7.68 (dd, J = 8.2, 2.0 Hz, 1H), 7.61 (dd, J = 8.2, 2.2 Hz, 1H), 7.51 (dd, J = 8.2, 2.2 Hz, 1H), 7.11 (d, J = 8.2 Hz, 1H), 5.13 (d, J = 3.7 Hz, 1H), 3.85 (s, 2H), 3.57 – 3.49 (m, 1H), 3.23 – 3.01 (m, 3H), 1.84 – 1.65 (m, 5H), 1.39 (s, 2H), 1.25 (s, 2H), 0.85 (t, J = 7.4 Hz, 3H), 0.70 – 0.60 (m, 1H); **HR-ESI-MS**: *m/z* = 439.1967 ([*M* + H]$^+$, calcd. for C$_{26}$H$_{30}$O$_2$N$_2$Cl$^+$:) (Δ = 2.77 ppm) – No TFA visible; $[\alpha]_{20}^{D}$= ° (c = 1.0, MeOH).

4.1.4.1.5.2.   Modification of the Alcohol Functionality

(6-methoxyquinolin-4-yl)((1S,2S,4S,5R)-5-vinylquinuclidin-2-yl)methanone (136)
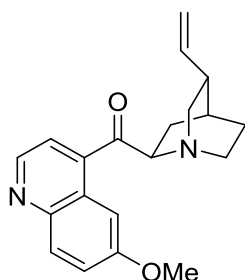
(+)-Quinidine (5.0 g, 15.4 mmol, 1.0 eq) was dissolved in anhydrous toluene (100 ml) and stirred for 5 min under an argon atmosphere. Then, benzophenone (5.59 g, 30.7 mmol, 2.0 eq) and potassium tert-butoxide (4.34 g, 38.7 mmol, 2.5 eq) were added to the solution. The mixture was stirred for 16 h at reflux. The resulting orange viscous mixture was cooled to 0°C and a 3M HCl (40 ml) was added slowly in order to keep the temperature below 30°C. The organic phase was separated, washed with 3 M HCl solution (3x30 ml). The combined aqueous extracts were cooled to 0°C and basified by dropwise addition of conc. ammonia solution (10 ml). The aqueous phase was saturated with brine (20 mL) and extracted with DCM (5x40 ml). The organic phases were recombined, dried over MgSO$_4$ and concentrated under vaccuo. The crude was purified by flash chromatography (EtOAc/acetone 9:1 -> 6:4, 25min) to afford the desired compound (2.8 g, 60%).

¹H NMR (700 MHz, MeOD): δ = 8.73 (t, J = 5.0 Hz, 1H), 7.93 (dd, J = 9.2, 2.3 Hz, 1H), 7.71 (t, J = 5.6 Hz, 1H), 7.56 (d, J = 2.6 Hz, 1H), 7.39 (dd, J = 9.2, 2.5 Hz, 1H), 5.88 – 5.80 (m, 1H), 5.09 – 4.96 (m, 2H), 3.86 (t, J = 7.3 Hz, 3H), 3.09 – 2.99 (m, 1H), 2.87 – 2.74 (m, 3H), 2.33 – 2.22 (m, 1H), 2.00 (t, J = 11.6 Hz, 1H), 1.86 (s, 1H), 1.76 – 1.71 (m, 1H), 1.69 (dt, J = 10.4, 5.2 Hz, 1H), 1.64 – 1.46 (m, 2H); **HR-ESI-MS**: *m/z* = 323.1751 ([*M* + H]$^+$, calcd. for C$_{20}$H$_{23}$O$_2$N$_2{}^+$: 323.1754) (Δ = 0.99 ppm) – No TFA visible; $[\alpha]_{20}^{D}$= - 99° (c = 1.0, MeOH). Data in accordance with the literature.[140]

(2-(4-fluorophenyl)-6-methoxyquinolin-4-yl)((1S,2S,4S,5R)-5-vinylquinuclidin-2-yl)methanone- trifluoroacetate (137)
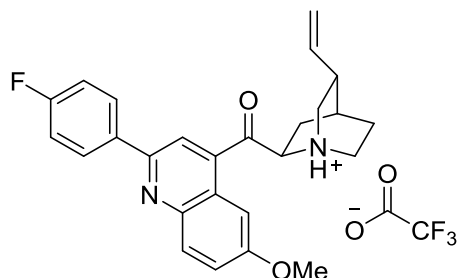
The compound **137** was synthesized following General Procedure I starting with compound **136** (100.0 mg, 0.32 mmol, 1.0 eq). Crude was purified using preparative HPLC (ACN/H$_2$O + 0.1 % TFA) to afford the pure compound (25 mg, 31%).

^{1}H NMR (400 MHz, MeOD): δ = 8.36 (s, 1H), 8.29 (m, 2H), 8.13 (d, J = 9.2 Hz, 1H), 7.87 – 7.79 (m, 1H), 7.55 (dt, J = 9.3, 2.2 Hz, 1H), 7.31 (m, 2H), 5.87 (ddd, J = 17.0, 10.6, 6.1 Hz, 1H), 5.42 – 5.33 (m, 1H), 5.26 – 5.19 (m, 2H), 4.11 (q, J = 7.1 Hz, 2H), 3.99 (s, 3H), 3.82 – 3.72 (m, 1H), 3.71 – 3.58 (m, 1H), 3.59 – 3.45 (m, 2H), 3.00 – 2.85 (m, 1H), 2.23 (m, 2H), 1.91 (m, 1H); **^{13}C NMR** (101 MHz, MeOD): δ = 203.46, 160.52, 147.94, 145.68, 142.71, 142.35, 141.12, 131.31, 126.99, 123.82, 123.64, 121.69, 121.19, 115.18, 103.93, 103.75, 55.96, 55.83, 49.98, 43.83, 40.61, 40.21, 28.75, 27.89, 27.13, 23.44; **^{19}F NMR** (377 MHz, MeOD): δ = -76.92, -114.02; **HR-ESI-MS**: *m/z* = 417.1963 ([*M* + H]$^+$, calcd. for C$_{26}$H$_{26}$O$_2$N$_2$F$^+$: 417.1973) (Δ = 2.33 ppm) – No TFA visible; $[\alpha]_{20}^{D}$ = + 11° (c = 1.0, MeOH).

(S)-(6-methoxyquinolin-4-yl)((1S,2S,4S,5R)-5-vinylquinuclidin-2-yl)methanamine (138)
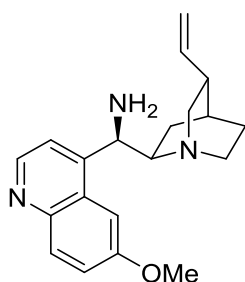
(+)-Quinidine (3.26 g, 10.0 mmol, 1.0 eq) and Triphenylphosphine (3.14 g, 12.0 mmol, 1.2 eq) were dissolved in 50 ml dry THF. The solution was cooled to 0°C. Then, Diisopropyl azodicarboxylate (2.42 g, 12.0 mmol, 1.2 eq) was added. A solution of diphenyl phosphoryl azide (3.30 g, 12.0 mmol, 1.2 eq) in dry THF (20 ml) was added dropwise to the mixture at 0°C and the reaction stirred for 12 h at rt. The mixture was heated to 50°C for 2 h and another portion of triphenylphosphine (3.41 g, 13.0 mmol, 1.3 eq) added at 50°C. The temperature was held until the evolution of gas stopped (approximately 2 h). Then, The reaction was allowed to cool to rt. Water (1 ml) was added and the reaction stirred for 3 hh. The solvent was removed and the crude reaction mixture was dissolved in a 100 ml solution of DCM/10% HCl (1:1) and the aqueous phase was extracted with DCM (4x50 ml). The aqueous phase was basified with excess cc. aqueous ammonia and extracted with DCM (4x50 ml). The combined organic phases were dried over $MgSO_4$ and concentrated under reduced pressure. The crude was purified with flash chromatography (EtOAc/MeOH/cc.aq.NH_4OH (50/50/1)) to afford the desired compound as an oil (1.9 g, 58%).

¹H NMR (500 MHz, MeOD): δ = 8.76 (d, J = 5.2 Hz, 1H), 7.95 (d, J = 9.3 Hz, 1H), 7.84 (d, J = 5.2 Hz, 1H), 7.56 (d, J = 2.2 Hz, 1H), 7.50 (dd, J = 9.3, 2.4 Hz, 1H), 5.71 − 5.62 (m, 1H), 5.59 (d, J = 10.6 Hz, 1H), 5.09 (dd, J = 31.8, 14.1 Hz, 2H), 4.23 (q, J = 9.6 Hz, 1H), 3.87 (s, 3H), 3.60 (m, 1H), 3.52 − 3.42 (m, 2H), 3.36 (dt, J = 12.7, 9.3 Hz, 1H), 2.69 − 2.61 (m, 1H), 1.88 − 1.75 (m, 3H), 1.33 − 1.26 (m, 1H), 1.10 (dd, J = 13.6, 9.5 Hz, 1H); **HR-ESI-MS**: *m/z* = 324.2062 ([*M* + H]$^+$, calcd. for $C_{20}H_{26}ON_3^+$: 324.2070) (Δ = 2.33 ppm) − No TFA visible; $[\alpha]_{20}^{D}= + 42°$ (c = 1.0, MeOH). Data in accordance with the literature.[139]

N^1,N^1-diethyl-N^4-(7-(4-fluorophenyl)quinolin-4-yl)pentane-1,4-diamine (157)
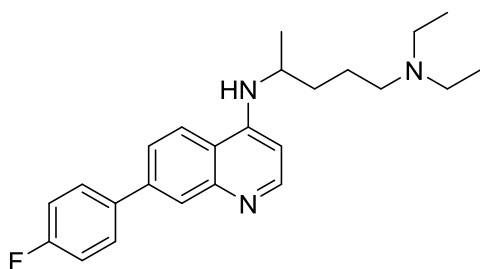
The compound was synthesized following **General Procedure V** starting with chloroquine (25.0 mg, mmol, 1.0 eq). Purified using preparative HPLC (ACN/H$_2$O + 0.1 % TFA) to afford the pure compound (21 mg, 35%).

^{1}H NMR (400 MHz, MeOD): δ = 8.58 (d, J = 8.8 Hz, 1H), 8.41 (d, J = 7.2 Hz, 1H), 8.02 (d, J = 1.5 Hz, 1H), 7.98 (dd, J = 8.9, 1.7 Hz, 1H), 7.84 (ddd, J = 8.3, 5.1, 2.5 Hz, 2H), 7.34 – 7.26 (m, 2H), 6.95 (d, J = 7.2 Hz, 1H), 4.19 (dd, J = 12.5, 6.2 Hz, 1H), 3.27 – 3.15 (m, 6H), 1.96 – 1.79 (m, 4H), 1.45 (t, J = 8.1 Hz, 3H), 1.30 (t, J = 7.2 Hz, 6H); **^{13}C NMR** (101 MHz, MeOD): δ = 166.25, 163.78, 162.52 (d, J = 34.4 Hz), 157.09, 146.67, 143.54, 139.97, 135.87, 135.84, 130.62, 130.53, 127.11, 124.87, 118.11, 117.35, 117.32, 117.13, 116.55, 99.46, 52.78, 50.99, 33.60, 22.06, 19.94, 9.08, 9.05; **^{19}F NMR** (377 MHz, MeOD): δ = -76.99, -114.70; **HR-ESI-MS**: *m/z* = 380.2500 ([*M* + H]$^+$, calcd. for C$_{24}$H$_{31}$N$_3$F$^+$: 380.2497) (Δ = 0.98 ppm) – No TFA visible.

(1S,2R,4S,5R)-2-((S)-((tert-butyldimethylsilyl)oxy)(6-methoxyquinolin-4-yl)methyl)-5-vinylquinuclidine (158)
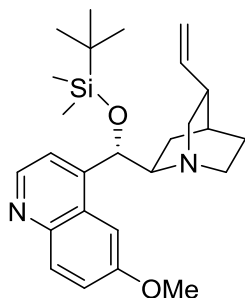
(+)-Quinidine (2.0 g, 6.21 mmol, 1.0 eq) was dissolved in dry DMF (10 mL). Then Et$_3$N (3.11g, 30.8 mmol, 5.0 eq), DMAP (75.3 mg, 0.62 mmol, 0.10 eq) and tert-butyldimethylsilyl chloride (1.40 g, 9.31 mmol, 1.5 eq) were added to the solution. The mixture was stirred at rt overnight. The mixture was diluted in toluene (15 mL). The organic phase was separated and washed with NaHCO$_3$ solution (3x10 mL). The organic phase were collected, dried over MgSO4 and concentrated under reduced pressure. The compound was used without further purification (2.4 g, 87%).

^{1}H NMR (500 MHz, MeOD): δ = 8.64 (d, J = 4.6 Hz, 1H, major rotamer), 8.54 (d, J = 4.4 Hz, 1H, minor rotamer), 7.92 (d, J = 8.9 Hz, 1H, major rotamer), 7.91 (d, J = 10.4 Hz, 1H, minor rotamer), 7.63 (d, J = 4.6 Hz, 1H, major rotamer), 7.41 (dd, J = 9.2, 2.6 Hz, 1H, major rotamer), 7.36 (d, J = 4.6 Hz, 1H, minor rotamer), 7.32 (dd, J = 9.2, 2.6 Hz, 1H, minor rotamer), 6.13 − 6.03 (m, 1H, major rotamer), 5.99 (ddd, J = 17.2, 10.5, 6.8 Hz, 1H, minor rotamer), 5.72 (d, J = 2.6 Hz, 1H, major rotamer), 5.16 − 5.10 (m, 2H, minor rotamer), 5.08 − 5.00 (m, 2H, major rotamer), 4.95 (d, J = 9.6 Hz, 1H, minor rotamer), 3.96 (s, 3H, major rotamer), 3.90 (s, 1H, minor rotamer), 3.58 (d, J = 8.9 Hz, 1H, minor rotamer), 3.36 − 3.29 (m, 1H, major rotamer), 2.96 − 2.84 (m, 1H, major rotamer), 2.82 − 2.66 (m, 1H, minor rotamer), 2.62 − 2.45 (m, 1H), 2.19 (dd, J = 12.1, 10.5 Hz, 1H), 1.88 − 1.23 (m, 5H), 0.94 (s, 9H, major rotamer), 0.87 (s, 3H, minor rotamer), 0.14 (s, 3H, major rotamer), 0.12 (s, 3H, minor rotamer), -0.34 (s, 3H, major rotamer), -0.42 (s, 3H, minor rotamer). Ratio of rotamers determined by NMR ≈ 3/1

$[\alpha]_{20}^{D}$= + 77° (c = 1.0, MeOH); **HR-ESI-MS**: *m/z* = 439.2773 ([*M* + H]$^+$, calcd. for C$_{26}$H$_{39}$N$_2$O$_2$Si$^+$: 439.2775). Data in accordance with the literature.[138]

4.2. Biology

4.2.1. Materials

4.2.1.1. Buffers and Solutions

- PBS   137 mM NaCl, 2.7 mM KCl, 10 mM Na_2HPO_4, 2.0 mM, KH_2PO_4, pH 7.4
- PBS/0.1% Triton-X   0.1% Triton-X in PBS
- PBS/0.1% Tween-20   0.1% Tween-20 in PBS
- Fixation buffer   3.7% Formaldehyde in PBS
- LICOR buffer   Used from commercial source

4.2.1.2. Antibodies for In Cell Western blot

Target	Host	Cat#	Manufacturer	Dilution	Incubation Conditions
Phospho-Src (Y416)	Mouse	2101	Cell Signaling	1:400	2 h in Odyssey Blocking Buffer
Src, clone GD11	Rabbit	05-184	Merck	1:400	2 h in Odyssey Blocking Buffer
Anti-rabbit IgG IRDye™ 800	Donkey	925-32213	LI-COR Biosciences	1:1000	1 h in in LICOR/0.05 % Tween-20
anti-mouse IgG IRDye™ 680	Goat	925-68070	LI-COR Biosciences	1:1000	1 h in in LICOR/0.05 % Tween-20

4.2.1.3. Software

- EnsoChemLab Version 5.0.8 Enso Software GmbH, Erbach, Germany
- Image Studio™ Version 5.2 LI-COR Biosciences GmbH, Bad Homburg vor der Höhe, Germany
- IncuCyte® ZOOM Version 2016A, Essen BioScience, Ann Arbor, USA
- Maestro Version 10.5, Schrödinger LLC, New York, USA
- MestReNova Version 6.0.3-5604, Mestrelab Research, Santiago de Compostela, Spain
- Tecan i-control Version 3.4.2.0 Tecan AG, Männedorf, CH

4.2.1.4. Laboratory Equipment

- Centrifuge, Minispin, Eppendorf, Hamburg, Germany
- IncuCyte® S3, Essen BioScience, Ann Arbor, USA
- Invitrogen™ Countess™ II Automated Cell Counter, Life TechnologiesTM, Darmstadt, Germany
- NanoDrop 2000c UV-Vis Spectrophotometer, Thermo Fisher Scientific, Waltham, USA
- Odyssey® Fc imaging System, LI-COR Biosciences, Bad Homburg, Germany
- pH-Meter, Mettler Toledo, Giessen, Germany
- Sterile Bench Microflow, NuncNalge, Rochester, USA
- Sterile Bench Nuaire, IBS tecnomara, Fernwald, Germany
- Waterbath (Memmert), Hettich AG, Bäch, Germany

4.2.2. Methods

4.2.2.1. Methods in Cell Biology

Mammalian Cell Culture

All the work involving living mammalian cells was performed with sterile equipment, media, and solutions in cell culture-approved benches. The generated waste was collected and sterilized by autoclaving at 134 °C for 15 min.

Thawing and Freezing of Cryo-Conserved Cells

Aliquots of mammalian cells stored in liquid nitrogen were thawed by transferring the vial containing the cells into a 37 °C-water bath. The cell suspension was diluted in 10 mL of the respective medium and the resulting suspension transferred into a 75 cm^2 tissue culture flask. The cells were incubated overnight. The DMSO-containing medium was replaced by fresh DMSO-free medium.

For cryo-conservation, mammalian cells were grown until reaching 80–95% confluence and then detached by trypsinization. The detached cells were suspended in the corresponding cell medium to inactivate the trypsin, and the cell number was determined. The suspension was centrifuged (r.t., 150 $x\,g$, 5 min) and the medium replaced by an appropriate volume of DMSO-containing medium (5% v/v) to reach a final concentration of ca. 1 x 10^6 per cryo-vial. The

vials were frozen in a cell freezing container (CoolCell® LX) at -80 °C overnight, to ensure a temperature decrease of 1 °C/min, and then stored in liquid nitrogen for long-term storage.

Passaging Mammalian Cells

MDA-MB-231 cells were grown until reaching a confluence of 80–90%. The medium was removed, the cells were washed with PBS (5 mL for 75 cm^2, 10 mL for 175 cm^2 tissue culture flasks) and then detached from the flasks by trypsinization (Trypsin/EDTA, 1 mL for 75 cm^2, 3 mL for 175 cm^2 tissue culture flasks, 1–5 min incubation at 37 °C and 5% CO$_2$). After full detachment, fresh medium was added to inactivate trypsin. 1/6 of the cell suspension was transferred into a new flask, containing 10 mL of pre-warmed (37 °C) fresh medium.

Determination of Cell Number

The cell number was determined using a Neubauer Counting Slide. The cell suspension was diluted with Trypan blue in a 1:1 ratio to distinguish between living and dead cells. The glass cover was moistened and placed on the Neubauer chamber's central area and 10 µL of the cell suspension prepared as described above were inserted into the chamber carefully. Cells in 4–5 quadrants were counted using a microscope, averaged and multiplied with the respective chamber factor (here 1 x 10^4) and dilution factor (here 2).

Alternatively, the Invitrogen™ Countess™ II Automated Cell Counter (Thermo Fisher Scientific, cat# AMQAX1000) together with Countess® Cell Counting Chamber Slides (Thermo Fisher Scientific, cat# C10228) was used according to the manufacturer's instructions. The sample was prepared as for the Neubauer chamber.

Routine Check for Mycoplasma Contaminations in Cell Culture

Cultured cells were routinely checked for mycoplasma contamination using the MycoAlert^{TM} Mycoplasma Detection Kit (Lonza) according to manufacturer's instructions.

Cell Treatment with Compounds

Compounds were dissolved in DMSO (Bioreagent, Sigma Aldrich, cat# D8418). Cells were plated into vessels in a cell number that allows 75–90% confluence at the end of the experiment. After 14–24 h incubation, the cells were treated with compounds pre-diluted in the given medium. The final DMSO concentration did not exceed 0.5% v/v.

4.2.2.2. Methods for the UNC119/Src Assay

Medium-Throughput High-Content Screening for UNC119/Myr-Src Inhibitors

This screen was performed by the Compound Management and Screening Center (COMAS).

A homogeneous time resolved fluorescence (HTRF) was used to screen our in-house library (c.a 200,000 compounds). In this assay, GST-tagged UNC119A protein together with an anti-GST antibody fused to an Eu3+ cryptate complex was used as a FRET donor. A myristoylated and biotinylated N-terminal peptide derived from the Src protein (see chapter **4.2.2**.) that binds to UNC119A with a K_D of 91 nM and streptavidin-d2 complex served as a FRET acceptor. In the presence of an inhibitor, the complex between the donor and the acceptor is destabilized, and the emission signal from the acceptor is abolished.

Viability and apoptosis assay

MDA-MB-231 cells were seeded in a 96-well plate ($3x10^3$ cells per well) in 100 µL DMEM. After incubation for 24 h, the tested compound or the controls (dasatinib or DMSO) were added at 6X the desired concentration in 20 µL DMEM containing the Essen Bioscience Apoptosis Reagent (final dilution 1:2000) to achieve the desired final concentrations. Plates were transferred to the IncuCyte and images were acquired in phase and green fluorescence mode with 10X magnification every hour over a period of 48-72 h. Images were analyzed using the confluence and fluorescence masks. Confluence data was normalized to the DMSO control in Excel and fluorescence data (Area/image or objects/image) was normalized to cell confluence (%) before plotting on Graphpad Prism.

Kinetic solubility

This experiment was performed by the Lead Discovery Center

DMSO stocks of the inhibitors **1** and **2** were diluted in aqueous Hepes buffer (50 mM pH 7.4) and incubated for 90 min while constantly stirring. Following filtration of the solution, the relative kinetic solubility of test compounds in aqueous buffer was calculated by measuring the spectrophotometric absorbance between 250 and 500 nm and comparing the recorded absorbance value to the absorbance of the compound in the 50% acetonitrile solution.

Selectivity towards UNC119 lipid binding cargo measurement

This experiment was performed by Dr. Eyad Fansa

For determining the ability of our designed molecules to displace lipidated cargo from different chaperones the following chaperone-lipidated peptide pairs were used: UNC119A-Src, PDE6δ-Rheb, AIPL1-Rheb, calmodulin-Rheb and RhoGDI-Rab. The peptides Src (Myr-GSNKSKPKFluorescein) and Rab1 (Fluorescein-SGGGSC(GerGer)-OMe) were prepared according to the previously reported method.[87] Rheb peptide (Fluorescein-SQGKSSC(Far)-OMe) was purchased from JPT. All the measurements were carried out at 20 °C in a buffer containing 30 mM Tris, pH 7.5, 150 mM NaCl, 3 mM DTE (for the measurements with calmodulin, 10 mM CaCl2 was added to the buffer). The fluorescently labelled lipidated peptides were placed in the cuvette. The corresponding chaperone proteins UNC119A (200 nM), PDE6δ (200 nM), AIPL1 (2 μM), calmodulin (5 μM) or RhoGDI (25 μM) were added. Increasing concentrations of inhibitor 1 or 2 (400 nM and 4 μM) were added to the protein-peptide complex and the changes in the fluorescence polarization were recorded at the excitation and emission wavelengths of 495 nm and 520 nm corresponding to the fluorescein-labeled peptides. Data analysis was done with GraFit 5.0 program (Erithracus Software).

In Cell Western (ICW) Assay for Src Y416 phosphorylation measurement

The ICW assay was performed using the Odyssey Imaging System (LI-COR,) according to the manufacturer's instructions. MDA-MB-231 cells grown in a 384-well plate (2×10^4 cells/well) were incubated with different inhibitors and concentrations for 30 min. Afterwards, cells were fixed using paraformaldehyde, washed, permeabilized with 0.1% Triton X-100 and blocked overnight at 4°C in LICOR buffer. The cells were stained for 2h at room temperature with mouse IgG antibody against Src (1:400, Merck) together with rabbit IgG antibody against phospho-Src (Tyr416) (1:400, Cell Signaling Technologies) in LICOR buffer. Subsequently,

the cells were washed and stained with donkey anti-rabbit IgG IRDye™ 800 antibody (1:1000, LI-COR Biosciences) and goat anti-mouse IgG IRDye™ 680 antibody (1:1000, LI-COR Biosciences). Protein expression was quantified using the Odyssey Imaging System. For statistical analyses, integrated intensities of fluorescence in wells were determined using software provided with the imager station (LI-COR). The relative amount of was obtained by normalizing to the amount of total Src in all experiments. All experiments were performed as quadruplicates and three biological replicates were carried out.

Western Blot Assay for Src Y416 phosphorylation quantification

This experiment was performed by Dr. Tom Mejuch

The cells were seeded in a 60-mm dish (6×10^5 cells per well) in 3 mL DMEM. After incubation for 24 h, the medium was removed and the cells washed with cold PBS (3 mL). Fresh DMEM medium (3 mL) containing the tested compound or the controls (dasatinib or DMSO) was added and the cells were incubated for 0.5 h. The medium was removed and the cells were washed with ice-cold PBS. RIPA lysis buffer containing protease inhibitor cocktail (cOmplete, EDTA-free) and phosphatase inhibitor cocktail (PhosSTOP) was added, the cells were harvested by scraping and kept on ice for 30 min. The lysates were centrifuged for 10 min at 12000 rpm at 4°C to remove any insoluble material. The total protein concentration was determined using the DC assay method. The lysates were separated by SDS-PAGE and transferred onto PVDF membranes. The membranes were blocked using Odyssey Blocking Buffer (PBS) (10 mL) over 1 h at the ambient temperature, incubated with primary antibody (5 mL, 1:700) in Odyssey Blocking Buffer (PBS) overnight at 4 °C. The membranes were washed with PBS-T (5 mL, x 3) and incubated with LI-Cor IRDye™ secondary antibody (5 mL, 1:3000) in using Odyssey Blocking Buffer (PBS) for 1 h at the ambient temperature. The signals were recorded using the Odyssey Imaging System. For statistical analyses, integrated intensities of fluorescence in wells were determined using software provided with the imager station (LI-COR). For re-probing, the membranes were incubated with the Odyssey NewBlot PVDF stripping buffer (5x, 1 mL diluted in 4 mL of water) for 20 min in the ambient temperature. Subsequently, the membranes were washed with PBS (5 mL, x 3), blocked and re-probed with another antibody as previously described.

In-Cell KD Measurement

This experiment was performed by Dr. Antonios Konitsiotis

FLIM experiments were carried out at 37 °C and 5% CO_2 on a Leica SP5 confocal microscope equipped with a Picoquant FLIM module (LSM Upgrade Kit/SMD Module, Picoquant). mCitrine fluorescence was excited at 514 nm with a pulsed supercontinuum laser with a repetition rate of 40 MHz.

Photons from the mCitrine channel were detected using avalanche photodiodes and arrival times processed by a time-correlated single-photon counting module (PicoHarp 300, Picoquant).

Intensity thresholds were applied to segment the cells from the background fluorescence. Global analysis of FLIM-FRET data was implemented using Matlab R2014A (The Mathworks Inc., MA, USA) to obtain images of the molar fraction (a) of interacting SFK-mCit with UNC119-mCh. Pixels with a total number of photons less than a pre-set threshold of 50 counts are excluded from the analysis.

4.2.2.3. Methods for the Autophagy Assay

Medium-Throughput High-Content Screening for Autophagy Inhibitors

This screen was performed by the Compound Management and Screening Center (COMAS).

The phenotypic autophagy screen utilizes MCF7-eGFP-LC3 cells. 4,000 cells per well were seeded in 25 µL medium in a 384 well Greiner µclear plate (cat# 781080, lid cat# 656191) and incubated overnight. Cells were then washed using a plate washer (Biotek, ELx405) three times with PBS followed by a final aspiration of the washing buffer. The addition of 25 nL of compound solution (10 mM stock solution in DMSO) was then carried out with an echo dispenser (Labcyte, Echo 520 dispenser). Addition of medium to induce autophagy was carried out with a Multidrop Combi (Thermo Scientific). 25 µL EBSS (Sigma Aldrich, cat# E3024-500mL) containing 50 µM chloroquine (Sigma Aldrich, cat# C6628-25g) was used for starvation-induced autophagy and 25 µL medium containing 50 µL chloroquine and 100 nM rapamycin (Biomol, cat# Cay13346-1) was used for rapamycin-induced autophagy screening. After incubation for 3 h, cells were fixed by addition of 25 µL 1:4 formaldehyde in PBS + 1:500 Hoechst (stock: 1 mg/mL, Sigma Aldrich cat# B2261) and incubation for 20 min at room temperature. Cells were then washed three times with PBS. Four images per well were taken with ImageXpress Micro XL (Molecular Devices) at 20x. Automated image analysis was

performed using the granularity setting of MetaXpress Software (Molecular Devices). The most significant analysis parameter was granule area, with resulting signal-to-background ratios around 40 and Z' values around 0.7.

4.2.2.4. External Services

In Vitro Pharmacology: Cellular and Nuclear Receptor Functional Assays

This experiment was performed by Eurofins®.

The assay was performed at Eurofins (France) and evaluated our top compound against agonist and antagonist CGRP receptors. Cellular agonist effect was calculated as a % of control response to a known reference agonist for each target and cellular antagonist effect was calculated as a % inhibition of control reference agonist response for each target.

Receptors	Source	Stimulis	Incubation	Measured Component	Detection Method
CGRP (h) Agonist effect	Human recombinant (CHO cells)	None (10 nM hCGRPα for control)	30 min r.t	1:400	HTRF
CGRP (h) Antagonist effect	Human recombinant (CHO cells)	hCGRPα (0.3 nM)	30 min r.t	1:400	HTRF

5. LIST OF ABBREVIATIONS

°C	degrees Celsius
β-ICD	β-isocupreidine
μM	micromolar
μW	microwave
Ac	acyl
ACD	acid ceramidase
aq.	aqueous
Ar	aryl
ASM	acid sphingomyelinase
BIOS	biology oriented synthesis
Boc	t-butyloxycarbonyl
BSA	bovine serum albumin
calcd.	calculated
CAS	Chemical Abstracts Service
cat.	catalytic
CETSA	cellular thermal shift assay
CGRP	calcitonin gene-related peptide
COMAS	Compound Management and Screening Center
COMU	(1-cyano-2-ethoxy-2-oxoethylidenaminooxy)dimethylaminomorpholino-carbenium hexafluorophosphate
CPA	cell painting assay
CQ	chloroquine
DCM	dichloromethane
DDQ	3-dichloro-5,6-dicyano-1,4-benzoquinone
DIPEA	N,N-diisopropylethylamine
DMAP	4-dimethylamino pyridine
DMF	dimethyl formamide
DMSO	dimethyl sulfoxide
eq.	equivalents
ER	endoplasmic reticulum
ESI-MS	electrospray ionization mass spectrometry

FCG	forward chemical genetics
FDA	Food and Drug Administration
FLIM	fluorescence lifetime imaging microscopy
FP	fluorescence polarization
FRET	Förster resonance energy transfer
GDP	guanosine diphosphate
GFP	green fluorescent protein
GPCR	G-protein coupled receptor
GTP	guanosine triphosphate
Fmoc	fluorenylmethyloxycarbonyl
HCTU	O-(1H-6-Chlorobenzotriazole-1-yl)-1,1,3,3-tetramethyluronium hexafluorophosphate
HPLC	high performance liquid chromatography
HR	high resolution
HTRF	homogeneous time resolved fluorescence
HTS	high throughput screening
Hz	Hertz
IC50	half maximal inhibitory concentration
ICW	in-cell western
J	coupling constant
LC	liquid chromatography
LC3	light chain 3
LDC	lead discovery center
Li	lithium
LOPAC	library of pharmaceutically active compounds
MS	mass spectrometry
mCh	mCherry
mCit	mCitrine
mTOR	mammalian target of rapamycin
NMM	N-Methylmorpholine
NMR	nuclear magnetic resonance
PAINs	pan-assay interference compounds
PBS	phosphate-buffered saline

Pd	palladium
PDB	protein data bank
PEG	polyethylene glycol
PI3K	phosphoinositide 3-kinase
PK	protein kinase
PTK	protein tyrosine kinase
PyBOP	benzotriazol-1-yl-oxytripyrrolidinophosphonium hexafluorophosphate
RAS	rat sarcoma
RCG	reverse chemical genetics
RNA	ribonucleic acid
rt	room temperature
SAR	structure–activity relationship
SH	Src homology
SPPS	solid phase peptide synthesis
TBDMS	t-butyldimethylsilyl
TFA	trifluoroacetic acid
THF	tetrahydrofuran
TMPMg.LiCl	2,2,6,6-Tetramethylpiperidinylmagnesium chloride lithium
UNC	uncoordinated
Y416	tyrosine 416

6. REFERENCES

1. O' Connor, C. J., Laraia, L. & Spring, D. R. Chemical genetics. Chem. Soc. Rev. 40, 4332 (2011).

2. Spring, D. R. Chemical genetics to chemical genomics: small molecules offer big insights. *Chem. Soc. Rev.* **34,** 472 (2005).

3. Lehár, J., Stockwell, B. R., Giaever, G. & Nislow, C. Combination chemical genetics. *Nat. Chem. Biol.* **4,** 674–681 (2008).

4. Stockwell, B. R. Frontiers in chemical genetics. *Trends Biotechnol.* **18,** 449–455 (2000).

5. Frye, S. V. Structure-activity relationship homology (SARAH): a conceptual framework for drug discovery in the genomic era. *Chem. Biol.* **6,** R3–R7 (1999).

6. Chaturvedi, P. R., Decker, C. J. & Odinecs, A. Prediction of pharmacokinetic properties using experimental approaches during early drug discovery. *Curr. Opin. Chem. Biol.* **5,** 452–463 (2001).

7. Korfmacher, W. A. Lead optimization strategies as part of a drug metabolism environment. *Curr. Opin. Drug Discov. Devel.* **6,** 481–485 (2003).

8. Cacace, E., Kritikos, G. & Typas, A. Chemical genetics in drug discovery. *Curr. Opin. Syst. Biol.* **4,** 35–42 (2017).

9. Haasen, D. *et al.* How Phenotypic Screening Influenced Drug Discovery: Lessons from Five Years of Practice. *ASSAY Drug Dev. Technol.* **15,** 239–246 (2017).

10. Barnash, K. D., James, L. I. & Frye, S. V. Target class drug discovery. *Nat. Chem. Biol.* **13,** 1053–1056 (2017).

11. Macarron, R. *et al.* Impact of high-throughput screening in biomedical research. *Nat. Rev. Drug Discov.* **10,** 188–195 (2011).

12.   Ziegler, S., Pries, V., Hedberg, C. & Waldmann, H. Target Identification for Small Bioactive Molecules: Finding the Needle in the Haystack. *Angew. Chem. Int. Ed.* **52,** 2744–2792 (2013).

13.   Kawasumi, M. & Nghiem, P. Chemical Genetics: Elucidating Biological Systems with Small-Molecule Compounds. *J. Invest. Dermatol.* **127,** 1577–1584 (2007).

14.   Hübel, K., Leßmann, T. & Waldmann, H. Chemical biology—identification of small molecule modulators of cellular activity by natural product inspired synthesis. *Chem. Soc. Rev.* **37,** 1361 (2008).

15.   Rishton, G. M. Reactive compounds and in vitro false positives in HTS. *Drug Discov. Today* **2,** 382–384 (1997).

16.   Sink, R., Gobec, S., Pečar, S. & Zega, A. False positives in the early stages of drug discovery. *Curr. Med. Chem.* **17,** 4231–4255 (2010).

17.   Ziegler, S. & Waldmann, H. Hunting the Targets of Natural Product-Inspired Compounds. in *Chembiomolecular Science* (eds. Shibasaki, M., Iino, M. & Osada, H.) 229–238 (Springer Japan, 2012).

18.   Stockwell, B. R. Chemical genetics: ligand-based discovery of gene function. *Nat. Rev. Genet.* **1,** 116–125 (2000).

19.   Bunnage, M. E., Chekler, E. L. P. & Jones, L. H. Target validation using chemical probes. *Nat. Chem. Biol.* **9,** 195–199 (2013).

20.   Eggeling, C., Brand, L., Ullmann, D. & Jäger, S. Highly sensitive fluorescence detection technology currently available for HTS. *Drug Discov. Today* **8,** 632–641 (2003).

21.   Gribbon, P. & Sewing, A. Fluorescence readouts in HTS: no gain without pain? *Drug Discov. Today* **8,** 1035–1043 (2003).

22.   Lea, W. A. & Simeonov, A. Fluorescence polarization assays in small molecule screening. *Expert Opin. Drug Discov.* **6,** 17–32 (2011).

23.   Baell, J. & Walters, M. A. Chemistry: Chemical con artists foil drug discovery. *Nature* **513,** 481–483 (2014).

24.   Baell, J. B. & Holloway, G. A. New Substructure Filters for Removal of Pan Assay Interference Compounds (PAINS) from Screening Libraries and for Their Exclusion in Bioassays. *J. Med. Chem.* **53,** 2719–2740 (2010).

25.   Hoelder, S., Clarke, P. A. & Workman, P. Discovery of small molecule cancer drugs: Successes, challenges and opportunities. *Mol. Oncol.* **6,** 155–176 (2012).

26.   Muegge, I. & Mukherjee, P. Performance of Dark Chemical Matter in High Throughput Screening. *J. Med. Chem.* **59,** 9806–9813 (2016).

27.   Yuan, W. *et al.* Chemical Space Mimicry for Drug Discovery. *J. Chem. Inf. Model.* **57,** 875–882 (2017).

28.   Reymond, J.-L. The Chemical Space Project. *Acc. Chem. Res.* **48,** 722–730 (2015).

29.   Reymond, J.-L. & Awale, M. Exploring Chemical Space for Drug Discovery Using the Chemical Universe Database. *ACS Chem. Neurosci.* **3,** 649–657 (2012).

30.   Wassermann, A. M. *et al.* Dark chemical matter as a promising starting point for drug lead discovery. *Nat. Chem. Biol.* **11,** 958–966 (2015).

31.   Das, J. *et al.* 2-Aminothiazole as a Novel Kinase Inhibitor Template. Structure−Activity Relationship Studies toward the Discovery of *N* -(2-Chloro-6-methylphenyl)-2-[[6-[4-(2-hydroxyethyl)-1- piperazinyl)]-2-methyl-4-pyrimidinyl]amino)]-1,3-thiazole-5-carboxamide (Dasatinib, BMS-354825) as a Potent *pan* -Src Kinase Inhibitor. *J. Med. Chem.* **49,** 6819–6832 (2006).

32.   Das, J. *et al.* Molecular design, synthesis, and structure–Activity relationships leading to the potent and selective p56lck inhibitor BMS-243117. *Bioorg. Med. Chem. Lett.* **13,** 2145–2149 (2003).

33.   Ciarcia, R. *et al.* Comparison of Dasatinib, Nilotinib, and Imatinib in the Treatment of Chronic Myeloid Leukemia: EFFECT OF TK INHIBITOR IN CML. *J. Cell. Physiol.* **231,** 680–687 (2016).

34.   Degorce, F. HTRF: A Technology Tailored for Drug Discovery - A Review of Theoretical Aspects and Recent Applications. *Curr. Chem. Genomics* **3,** 22–32 (2009).

35.   Jean, A. *et al.* Anorexia induced by activation of serotonin 5-HT4 receptors is mediated by increases in CART in the nucleus accumbens. *Proc. Natl. Acad. Sci. U. S. A.* **104,** 16335–16340 (2007).

36.   Romero, G. *et al.* Efficacy of selective 5-HT6 receptor ligands determined by monitoring 5-HT6 receptor-mediated cAMP signaling pathways. *Br. J. Pharmacol.* **148,** 1133–1143 (2006).

37.   Peres, C. M. *et al.* Specific leukotriene receptors couple to distinct G proteins to effect stimulation of alveolar macrophage host defense functions. *J. Immunol. Baltim. Md 1950* **179,** 5454–5461 (2007).

38.   Fantl, W. J., Johnson, D. E. & Williams, L. T. Signalling by receptor tyrosine kinases. *Annu. Rev. Biochem.* **62,** 453–481 (1993).

39.   Edelman, A. M., Blumenthal, D. K. & Krebs, E. G. Protein serine/threonine kinases. *Annu. Rev. Biochem.* **56,** 567–613 (1987).

40.   Maurel, D. *et al.* Cell surface detection of membrane protein interaction with homogeneous time-resolved fluorescence resonance energy transfer technology. *Anal. Biochem.* **329,** 253–262 (2004).

41.   Ferre, S. *et al.* G Protein-Coupled Receptor Oligomerization Revisited: Functional and Pharmacological Perspectives. *Pharmacol. Rev.* **66,** 413–434 (2014).

42.   Lopez-Crapez, E. *et al.* A homogeneous resonance energy transfer-based assay to monitor MutS/DNA interactions. *Anal. Biochem.* **383,** 301–306 (2008).

43.   Sicheri, F. & Kuriyan, J. Structures of Src-family tyrosine kinases. *Curr. Opin. Struct. Biol.* **7,** 777–785 (1997).

44.   Parsons, S. J. & Parsons, J. T. Src family kinases, key regulators of signal transduction. *Oncogene* **23,** 7906–7909 (2004).

45.   Thomas, S. M. & Brugge, J. S. Cellular functions regulated by Src family kinases. *Annu. Rev. Cell Dev. Biol.* **13,** 513–609 (1997).

46.   Lieu, C. & Kopetz, S. The Src Family of Protein Tyrosine Kinases: A New and Promising Target for Colorectal Cancer Therapy. *Clin. Colorectal Cancer* **9,** 89–94 (2010).

47.   Martin, G. S. The hunting of the Src. *Nat. Rev. Mol. Cell Biol.* **2,** 467–475 (2001).

48.   Chen, Q. *et al.* The importance of Src signaling in sarcoma (Review). *Oncol. Lett.* (2015). doi:10.3892/ol.2015.3184

49.   Kim, L. C., Song, L. & Haura, E. B. Src kinases as therapeutic targets for cancer. *Nat. Rev. Clin. Oncol.* **6,** 587–595 (2009).

50.   Resh, M. D. Fatty acylation of proteins: new insights into membrane targeting of myristoylated and palmitoylated proteins. *Biochim. Biophys. Acta BBA-Mol. Cell Res.* **1451,** 1–16 (1999).

51.   Farazi, T. A., Waksman, G. & Gordon, J. I. The Biology and Enzymology of Protein *N*-Myristoylation. *J. Biol. Chem.* **276,** 39501–39504 (2001).

52.   Desmeules, P., Penney, S.-É., Desbat, B. & Salesse, C. Determination of the Contribution of the Myristoyl Group and Hydrophobic Amino Acids of Recoverin on its Dynamics of Binding to Lipid Monolayers. *Biophys. J.* **93,** 2069–2082 (2007).

53.   Maduro, M. & Pilgrim, D. Identification and cloning of unc-119, a gene expressed in the Caenorhabditis elegans nervous system. *Genetics* **141,** 977–988 (1995).

54. Swanson, D. A., Chang, J. T., Campochiaro, P. A., Zack, D. J. & Valle, D. Mammalian orthologs of C. elegans unc-119 highly expressed in photoreceptors. *Invest. Ophthalmol. Vis. Sci.* **39,** 2085–2094 (1998).

55. Kobayashi, A. *et al.* HRG4 (UNC119) mutation found in cone–rod dystrophy causes retinal degeneration in a transgenic model. *Invest. Ophthalmol. Vis. Sci.* **41,** 3268–3277 (2000).

56. Ismail, S. A. *et al.* Arl2-GTP and Arl3-GTP regulate a GDI-like transport system for farnesylated cargo. *Nat. Chem. Biol.* **7,** 942–949 (2011).

57. Chandra, A. *et al.* The GDI-like solubilizing factor PDEδ sustains the spatial organization and signalling of Ras family proteins. *Nat. Cell Biol.* **14,** 148–158 (2011).

58. Chung, S., Kang, S., Paik, S. & Lee, J. NgUNC-119, Naegleria homologue of UNC-119, localizes to the flagellar rootlet. *Gene* **389,** 45–51 (2007).

59. Zhang, H. *et al.* UNC119 is required for G protein trafficking in sensory neurons. *Nat. Neurosci.* **14,** 874–880 (2011).

60. Keep, N. H. *et al.* A modulator of rho family G proteins, rhoGDI, binds these G proteins via an immunoglobulin-like domain and a flexible N-terminal arm. *Structure* **5,** 623–633 (1997).

61. Zhang, H. *et al.* Photoreceptor cGMP Phosphodiesterase δ Subunit (PDEδ) Functions as a Prenyl-binding Protein. *J. Biol. Chem.* **279,** 407–413 (2004).

62. Constantine, R., Zhang, H., Gerstner, C. D., Frederick, J. M. & Baehr, W. Uncoordinated (UNC)119: Coordinating the trafficking of myristoylated proteins. *Vision Res.* **75,** 26–32 (2012).

63. Wright, K. J. *et al.* An ARL3-UNC119-RP2 GTPase cycle targets myristoylated NPHP3 to the primary cilium. *Genes Dev.* **25,** 2347–2360 (2011).

64.   Kobayashi, A., Kubota, S., Mori, N., McLaren, M. J. & Inana, G. Photoreceptor synaptic protein HRG4 (UNC119) interacts with ARL2 via a putative conserved domain. *FEBS Lett.* **534,** 26–32 (2003).

65.   Veltel, S., Kravchenko, A., Ismail, S. & Wittinghofer, A. Specificity of Arl2/Arl3 signaling is mediated by a ternary Arl3-effector-GAP complex. *FEBS Lett.* **582,** 2501–2507 (2008).

66.   Haeseleer, F. Interaction and Colocalization of CaBP4 and Unc119 (MRG4) in Photoreceptors. *Investig. Opthalmology Vis. Sci.* **49,** 2366 (2008).

67.   Alpadi, K. *et al.* RIBEYE Recruits Munc119, a Mammalian Ortholog of the *Caenorhabditis elegans* Protein unc119, to Synaptic Ribbons of Photoreceptor Synapses. *J. Biol. Chem.* **283,** 26461–26467 (2008).

68.   Vepachedu, R. *et al.* Unc119 regulates myofibroblast differentiation through the activation of Fyn and the p38 MAPK pathway. *J. Immunol. Baltim. Md 1950* **179,** 682–690 (2007).

69.   Cen, O. Identification of UNC119 as a Novel Activator of SRC-type Tyrosine Kinases. *J. Biol. Chem.* **278,** 8837–8845 (2003).

70.   Gorska, M. M., Stafford, S. J., Cen, O., Sur, S. & Alam, R. Unc119, a novel activator of Lck/Fyn, is essential for T cell activation. *J. Exp. Med.* **199,** 369–379 (2004).

71.   Gorska, M. M., Liang, Q., Karim, Z. & Alam, R. Uncoordinated 119 Protein Controls Trafficking of Lck via the Rab11 Endosome and Is Critical for Immunological Synapse Formation. *J. Immunol.* **183,** 1675–1684 (2009).

72.   Ismail, S. A. *et al.* Structural basis for Arl3-specific release of myristoylated ciliary cargo from UNC119. *EMBO J.* **31,** 4085–4094 (2012).

73. Jaiswal, M. *et al.* Novel Biochemical and Structural Insights into the Interaction of Myristoylated Cargo with Unc119 Protein and Their Release by Arl2/3. *J. Biol. Chem.* **291,** 20766–20778 (2016).

74. Bos, J. L., Rehmann, H. & Wittinghofer, A. GEFs and GAPs: Critical Elements in the Control of Small G Proteins. *Cell* **129,** 865–877 (2007).

75. Gotthardt, K. *et al.* A G-protein activation cascade from Arl13B to Arl3 and implications for ciliary targeting of lipidated proteins. *eLife* **4,** (2015).

76. Nautiyal, J., Majumder, P., Patel, B. B., Lee, F. Y. & Majumdar, A. P. N. Src inhibitor dasatinib inhibits growth of breast cancer cells by modulating EGFR signaling. *Cancer Lett.* **283,** 143–151 (2009).

77. Vultur, A. *et al.* SKI-606 (bosutinib), a novel Src kinase inhibitor, suppresses migration and invasion of human breast cancer cells. *Mol. Cancer Ther.* **7,** 1185–1194 (2008).

78. Green, T. P. *et al.* Preclinical anticancer activity of the potent, oral Src inhibitor AZD0530. *Mol. Oncol.* **3,** 248–261 (2009).

79. Rajalingam, K., Schreck, R., Rapp, U. R. & Albert, Š. Ras oncogenes and their downstream targets. *Biochim. Biophys. Acta BBA - Mol. Cell Res.* **1773,** 1177–1195 (2007).

80. Cox, A. D., Fesik, S. W., Kimmelman, A. C., Luo, J. & Der, C. J. Drugging the undruggable RAS: Mission Possible? *Nat. Rev. Drug Discov.* **13,** 828–851 (2014).

81. Zimmermann, G. *et al.* Small molecule inhibition of the KRAS–PDEδ interaction impairs oncogenic KRAS signalling. *Nature* **497,** 638–642 (2013).

82. Papke, B. *et al.* Identification of pyrazolopyridazinones as PDEδ inhibitors. *Nat. Commun.* **7,** 11360 (2016).

83.   Martín-Gago, P. *et al.* A PDE6δ-KRas Inhibitor Chemotype with up to Seven H-Bonds and Picomolar Affinity that Prevents Efficient Inhibitor Release by Arl2. *Angew. Chem. Int. Ed.* **56,** 2423–2428 (2017).

84.   Martín-Gago, P. *et al.* Covalent Protein Labeling at Glutamic Acids. *Cell Chem. Biol.* **24,** 589–597.e5 (2017).

85.   Triola, G., Waldmann, H. & Hedberg, C. Chemical Biology of Lipidated Proteins. *ACS Chem. Biol.* **7,** 87–99 (2012).

86.   Rosi, F. & Triola, G. Synthesis of Lipidated Peptides. *Pept. Synth. Appl.* 161–189 (2013).

87.   Mejuch, T., van Hattum, H., Triola, G., Jaiswal, M. & Waldmann, H. Specificity of Lipoprotein Chaperones for the Characteristic Lipidated Structural Motifs of their Cognate Lipoproteins. *ChemBioChem* **16,** 2460–2465 (2015).

88.   Borror, A. L. *et al.* Regioselectivity of electrophilic aromatic substitution: syntheses of 6- and 7-sulfamoylindolines and -indoles. *J. Org. Chem.* **53,** 2047–2052 (1988).

89.   Burger, A. Isosterism and bioisosterism in drug design. *Prog. Drug Res. Fortschritte Arzneimittelforschung Progres Rech. Pharm.* **37,** 287–371 (1991).

90.   Sperlich, B., Kapoor, S., Waldmann, H., Winter, R. & Weise, K. Regulation of K-Ras4B Membrane Binding by Calmodulin. *Biophys. J.* **111,** 113–122 (2016).

91.   Majumder, A., Gopalakrishna, K. N., Cheguru, P., Gakhar, L. & Artemyev, N. O. Interaction of Aryl Hydrocarbon Receptor-interacting Protein-like 1 with the Farnesyl Moiety. *J. Biol. Chem.* **288,** 21320–21328 (2013).

92.   Chavez, K. J., Garimella, S. V. & Lipkowitz, S. Triple negative breast cancer cell lines: One tool in the search for better treatment of triple negative breast cancer. *Breast Dis.* **32,** 35–48 (2011).

93.   Franken, H. *et al.* Thermal proteome profiling for unbiased identification of direct and indirect drug targets using multiplexed quantitative mass spectrometry. *Nat. Protoc.* **10,** 1567–1593 (2015).

94.   Reinhard, F. B. M. *et al.* Thermal proteome profiling monitors ligand interactions with cellular membrane proteins. *Nat. Methods* **12,** 1129–1131 (2015).

95.   Egorina, E. M., Sovershaev, M. A. & Osterud, B. In-Cell Western assay: a new approach to visualize tissue factor in human monocytes. *J. Thromb. Haemost.* **4,** 614–620 (2006).

96.   Patwardhan, P. & Resh, M. D. Myristoylation and Membrane Binding Regulate c-Src Stability and Kinase Activity. *Mol. Cell. Biol.* **30,** 4094–4107 (2010).

97.   Pichot, C. S. *et al.* Dasatinib synergizes with doxorubicin to block growth, migration, and invasion of breast cancer cells. *Br. J. Cancer* **101,** 38–47 (2009).

98.   Sturani, E. *et al.* Kinetics and regulation of the tyrosine phosphorylation of epidermal growth factor receptor in intact A431 cells. *Mol. Cell. Biol.* **8,** 1345–1351 (1988).

99.   Brockmeyer, C. *et al.* T Cell Receptor (TCR)-induced Tyrosine Phosphorylation Dynamics Identifies THEMIS as a New TCR Signalosome Component. *J. Biol. Chem.* **286,** 7535–7547 (2011).

100.   Mejuch, T. *et al.* Small-Molecule Inhibition of the UNC119-Cargo Interaction. *Angew. Chem. Int. Ed.* **56,** 6181–6186 (2017).

101.   Cory, G. Scratch-wound assay. *Methods Mol. Biol. Clifton NJ* **769,** 25–30 (2011).

102.   Franken, N. A. P., Rodermond, H. M., Stap, J., Haveman, J. & van Bree, C. Clonogenic assay of cells in vitro. *Nat. Protoc.* **1,** 2315–2319 (2006).

103.   Sánchez-Bailón, M. P. *et al.* Src kinases catalytic activity regulates proliferation, migration and invasiveness of MDA-MB-231 breast cancer cells. *Cell. Signal.* **24,** 1276–1286 (2012).

104. Konitsiotis, A. D., Roßmannek, L., Stanoev, A., Schmick, M. & Bastiaens, P. I. H. Spatial cycles mediated by UNC119 solubilisation maintain Src family kinases plasma membrane localisation. *Nature Communications* (2017).

105. *Alkaloids*. (Springer US, 1998). doi:10.1007/978-1-4757-2905-4

106. Krishnamurti, C. & Rao, Sscc. The isolation of morphine by Serturner. *Indian J. Anaesth.* **60,** 861 (2016).

107. Amirkia, V. & Heinrich, M. Alkaloids as drug leads – A predictive structural and biodiversity-based analysis. *Phytochem. Lett.* **10,** xlviii–liii (2014).

108. *Concise encyclopedia biochemistry*. (de Gruyter, 1988).

109. Lipinski, C. A., Lombardo, F., Dominy, B. W. & Feeney, P. J. Experimental and computational approaches to estimate solubility and permeability in drug discovery and development settings. *Adv. Drug Deliv. Rev.* **23,** 3–25 (1997).

110. Wetzel, S., Bon, R. S., Kumar, K. & Waldmann, H. Biology-Oriented Synthesis. *Angew. Chem. Int. Ed.* **50,** 10800–10826 (2011).

111. Koch, M. A. *et al.* Charting biologically relevant chemical space: A structural classification of natural products (SCONP). *Proc. Natl. Acad. Sci.* **102,** 17272–17277 (2005).

112. Potowski, M., Bauer, J. O., Strohmann, C., Antonchick, A. P. & Waldmann, H. Highly Enantioselective Catalytic [6+3] Cycloadditions of Azomethine Ylides. *Angew. Chem. Int. Ed.* **51,** 9512–9516 (2012).

113. Over, B. *et al.* Natural-product-derived fragments for fragment-based ligand discovery. *Nat. Chem.* **5,** 21–28 (2012).

114. Welsch, M. E., Snyder, S. A. & Stockwell, B. R. Privileged scaffolds for library design and drug discovery. *Curr. Opin. Chem. Biol.* **14,** 347–361 (2010).

115.   Costantino, L. & Barlocco, D. Privileged Structures as Leads in Medicinal Chemistry. *Curr. Med. Chem.* **13,** 65–85 (2006).

116.   Maldonado, C. *et al.* Phylogeny Predicts the Quantity of Antimalarial Alkaloids within the Iconic Yellow Cinchona Bark (Rubiaceae: Cinchona calisaya). *Front. Plant Sci.* **8,** (2017).

117.   Foley, M. & Tilley, L. Quinoline antimalarials: mechanisms of action and resistance and prospects for new agents. *Pharmacol. Ther.* **79,** 55–87 (1998).

118.   Leete, E. Biosynthesis of quinine and related alkaloids. *Acc. Chem. Res.* **2,** 59–64 (1969).

119.   *Cinchona alkaloids in synthesis and catalysis: ligands, immobilization and organocatalysis*. (Wiley-VCH, 2009).

120.   Taggi, A. E. *et al.* The Development of the First Catalyzed Reaction of Ketenes and Imines: Catalytic, Asymmetric Synthesis of β-Lactams. *J. Am. Chem. Soc.* **124,** 6626–6635 (2002).

121.   Cortez, G. S., Tennyson, R. L. & Romo, D. Intramolecular, nucleophile-catalyzed aldol-lactonization (NCAL) reactions: catalytic, asymmetric synthesis of bicyclic β-lactones. *J. Am. Chem. Soc.* **123,** 7945–7946 (2001).

122.   Kolb, H. C., VanNieuwenhze, M. S. & Sharpless, K. B. Catalytic Asymmetric Dihydroxylation. *Chem. Rev.* **94,** 2483–2547 (1994).

123.   Armstrong, A. & Scutt, J. N. Stereocontrolled Synthesis of 3-(*trans* -2-Aminocyclopropyl)alanine, a Key Component of Belactosin A. *Org. Lett.* **5,** 2331–2334 (2003).

124.   Dijkstra, G. D. H., Kellogg, R. M. & Wynberg, H. Conformational analysis of some chiral catalysts of the cinchona1 and ephedra2 family. The alkaloid catalyzed addition of

aromatic thiols to cyclic α,β-unsaturated ketones. *Recl. Trav. Chim. Pays-Bas* **108,** 195–204 (2010).

125.   Li, H., Liu, X., Wu, F., Tang, L. & Deng, L. Elucidation of the active conformation of cinchona alkaloid catalyst and chemical mechanism of alcoholysis of meso anhydrides. *Proc. Natl. Acad. Sci.* **107,** 20625–20629 (2010).

126.   Bryant, L. A., Fanelli, R. & Cobb, A. J. A. Cupreines and cupreidines: an established class of bifunctional cinchona organocatalysts. *Beilstein J. Org. Chem.* **12,** 429–443 (2016).

127.   Iwabuchi, Y., Nakatani, M., Yokoyama, N. & Hatakeyama, S. Chiral Amine-Catalyzed Asymmetric Baylis − Hillman Reaction: A Reliable Route to Highly Enantiomerically Enriched (α-Methylene-β-hydroxy)esters. *J. Am. Chem. Soc.* **121,** 10219–10220 (1999).

128.   Ravanan, P., Srikumar, I. F. & Talwar, P. Autophagy: The spotlight for cellular stress responses. *Life Sci.* **188,** 53–67 (2017).

129.   Galluzzi, L. *et al.* Molecular definitions of autophagy and related processes. *EMBO J.* **36,** 1811–1836 (2017).

130.   Jung, C. H., Ro, S.-H., Cao, J., Otto, N. M. & Kim, D.-H. mTOR regulation of autophagy. *FEBS Lett.* **584,** 1287–1295 (2010).

131.   Noda, T. & Ohsumi, Y. Tor, a Phosphatidylinositol Kinase Homologue, Controls Autophagy in Yeast. *J. Biol. Chem.* **273,** 3963–3966 (1998).

132.   Rubinsztein, D. C., Codogno, P. & Levine, B. Autophagy modulation as a potential therapeutic target for diverse diseases. *Nat. Rev. Drug Discov.* **11,** 709–730 (2012).

133.   Mizushima, N. In Vivo Analysis of Autophagy in Response to Nutrient Starvation Using Transgenic Mice Expressing a Fluorescent Autophagosome Marker. *Mol. Biol. Cell* **15,** 1101–1111 (2003).

134. Balgi, A. D. *et al.* Screen for Chemical Modulators of Autophagy Reveals Novel Therapeutic Inhibitors of mTORC1 Signaling. *PLoS ONE* **4,** e7124 (2009).

135. Laraia, L. *et al.* Discovery of Novel Cinchona-Alkaloid-Inspired Oxazatwistane Autophagy Inhibitors. *Angew. Chem. Int. Ed.* **56,** 2145–2150 (2017).

136. Klionsky, D. J. *et al.* Guidelines for the use and interpretation of assays for monitoring autophagy. *Autophagy* **8,** 445–544 (2012).

137. Seiple, I. B. *et al.* Direct C−H Arylation of Electron-Deficient Heterocycles with Arylboronic Acids. *J. Am. Chem. Soc.* **132,** 13194–13196 (2010).

138. Jaric, M., Haag, B. A., Manolikakes, S. M. & Knochel, P. Selective and Multiple Functionalization of Pyridines and Alkaloids *via* Mg- and Zn-Organometallic Intermediates. *Org. Lett.* **13,** 2306–2309 (2011).

139. Cassani, C., Martín-Rapún, R., Arceo, E., Bravo, F. & Melchiorre, P. Synthesis of 9-amino(9-deoxy)epi cinchona alkaloids, general chiral organocatalysts for the stereoselective functionalization of carbonyl compounds. *Nat. Protoc.* **8,** 325–344 (2013).

140. SYNTHESIS OF cis-4a(S),8a(R)-PERHYDRO-6(2H)-ISOQUINOLINONES FROM QUININE: 4a(S), 8a(R)-2-BENZOYLOCTAHYDRO-6(2H)-ISOQUINOLINONE. *Org. Synth.* **75,** 223 (1998).

141. Bray, M.-A. *et al.* Cell Painting, a high-content image-based assay for morphological profiling using multiplexed fluorescent dyes. *Nat. Protoc.* **11,** 1757–1774 (2016).

142. Bickle, M. The beautiful cell: high-content screening in drug discovery. *Anal. Bioanal. Chem.* **398,** 219–226 (2010).

143. De Duve, C. *et al.* Lysosomotropic agents. *Biochem. Pharmacol.* **23,** 2495–2531 (1974).

144. Kitatani, K., Idkowiak-Baldys, J. & Hannun, Y. A. The sphingolipid salvage pathway in ceramide metabolism and signaling. *Cell. Signal.* **20,** 1010–1018 (2008).

145.   Amara, S. G. *et al.* Expression in brain of a messenger RNA encoding a novel

neuropeptide homologous to calcitonin gene-related peptide. *Science* **229,** 1094–1097

(1985).

146.   Durham, P. L. & Vause, C. V. Calcitonin Gene-Related Peptide (CGRP) Receptor

Antagonists in the Treatment of Migraine: *CNS Drugs* **24,** 539–548 (2010).

147.   Daines, R. A. *et al.* Quinine analogs as non-peptide calcitonin gene-related peptide

(CGRP) receptor antagonists. *Bioorg. Med. Chem. Lett.* **7,** 2673–2676 (1997).

148.   Rasmussen, H. Cellular calcium metabolism. *Ann. Intern. Med.* **98,** 809–816 (1983).

149.   Liu, C. & Hermann, T. E. Characterization of ionomycin as a calcium ionophore. *J.

Biol. Chem.* **253,** 5892–5894 (1978).

150.   Chen, Y.-X. *et al.* Synthesis of the Rheb and K-Ras4B GTPases. *Angew. Chem. Int.

Ed.* **49,** 6090–6095 (2010).

7. APPENDIX

Curriculum Vitae

PERSONAL INFORMATION

Surname:	Garivet
Name:	Guillaume, Michel, Jacques
Date of Birth:	16.07.1988
Place of Birth:	Mont-de-Marsan, France
Citizenship:	French

EDUCATION

Oct. 2013 - Dec. 2017

PhD student at the Max Planck Institute of Molecular Physiology (Germany)

Research topic: Small Molecule Inhibiting the UNC119/Src Cargo

Advisor: Prof. Dr. Dr. Herbert Waldmann

Sep. 2011 - Aug. 2013

Master's at University of Bordeaux (France)

Molecular and Macromolecular Chemistry (Bordeaux, France)

Master thesis, Wayne State University (Detroit, United States)

Research topic: Influence of Protecting Groups on the Reactivity of Glycosyl Donors

Advisor: Prof. Dr. David Crich

Additional research project

Research topic: Organic Synthesis of a Two-photon Absorption Molecule

Advisor: Dr. Mireille Blanchard-Desce

Sep. 2009 - Jul. 2011

Bachelor's at University of Bordeaux (France)

Organic Chemistry

Bachelor thesis, Imperial College London

(London, United Kingdom)

Research topic: Support Solid Synthesis of Peptide Nucleic Acid-Cy3 dye

Advisor: Dr. Sylvain Ladame

Eidesstattliche Versicherung (Affidavit)

Garivet Guillaume Michel Jacques____
Name, Vorname
(Surname, first name)

173416_____
Matrikel-Nr.
(Enrolment number)

Belehrung:
Wer vorsätzlich gegen eine die Täuschung über Prüfungsleistungen betreffende Regelung einer Hochschulprüfungsordnung verstößt, handelt ordnungswidrig. Die Ordnungswidrigkeit kann mit einer Geldbuße von bis zu 50.000,00 € geahndet werden. Zuständige Verwaltungsbehörde für die Verfolgung und Ahndung von Ordnungswidrigkeiten ist der Kanzler/die Kanzlerin der Techni-

schen Universität Dortmund. Im Falle eines mehrfachen oder sonstigen schwerwiegenden Täuschungsversu ches kann der Prüfling zudem exmatrikuliert werden, § 63 Abs. 5 Hochschulgesetz NRW.

Die Abgabe einer falschen Versicherung an Eides statt ist strafbar.

Wer vorsätzlich eine falsche Versicherung an Eides statt abgibt, kann mit einer Freiheitsstrafe bis zu drei Jahren oder mit Geldstrafe bestraft werden, § 156 StGB. Die fahrlässige Abgabe einer falschen Versicherung an Eides statt kann mit einer Freiheitsstrafe bis zu einem Jahr oder Geldstrafe bestraft werden, § 161 StGB.

Die oben stehende Belehrung habe ich zur Kenntnis genommen:

Official notification:
Any person who intentionally breaches any regulation of university examination regulations relating to deception in examination performance is acting improperly. This offence can be punished with a fine of up to EUR 50,000.00. The competent administrative authority for the pursuit and prosecution of offences of this type is the chancellor of the TU Dortmund University. In the case of multiple or other serious attempts at deception, the candidate can also be unenrolled, Section 63, paragraph 5 of the Universities Act of North Rhine-Westphalia.

The submission of a false affidavit is punishable.

Any person who intentionally submits a false affidavit can be punished with a prison sentence of up to three years or a fine, Section 156 of the Criminal Code. The negligent submission of a false affidavit can be punished with a prison sentence of up to one year or a fine, Section 161 of the Criminal Code.

I have taken note of the above official notification.

Dortmund, den 10.11.2017_____
Ort, Datum
(Place, date)

_____
Unterschrift
(Signature)

Titel der Dissertation:
(Title of the thesis):

Small Molecule Inhibition of Lipidated Proteins/Cargo Interaction and Synthesis of a

Cinchona Alkaloid-derived Library as potent Autophagy Inhibitors

Ich versichere hiermit an Eides statt, dass ich die vorliegende Dissertation mit dem Titel selbstständig und ohne unzulässige fremde Hilfe angefertigt habe. Ich habe keine anderen als die angegebenen Quellen und Hilfs mittel benutzt sowie wörtliche und sinngemäße Zitate kenntlich gemacht.
Die Arbeit hat in gegenwärtiger oder in einer anderen Fassung weder der TU Dortmund noch einer anderen Hochschule im Zusammenhang mit einer staatlichen oder akademischen Prüfung vorgelegen.

I hereby swear that I have completed the present dissertation independently and without inadmissible external support. I have not used any sources or tools other than those indicated and have identified literal and analogous quotations.

The thesis in its current version or another version has not been presented to the TU Dortmund University or another university in connection with a state or academic examination.*

*Pleasse be aware that solely the German version of the affidavit ("Eidesstattliche Versicherung") for the PhD thesis is the official and legally binding version.

Dortmund, den 10.11.2017_____
Ort, Datum
(Place, date)

_____
Unterschrift
(Signature)